IPP Max-Planck-Institut für Plasmaphysik

# Annual Report 1996

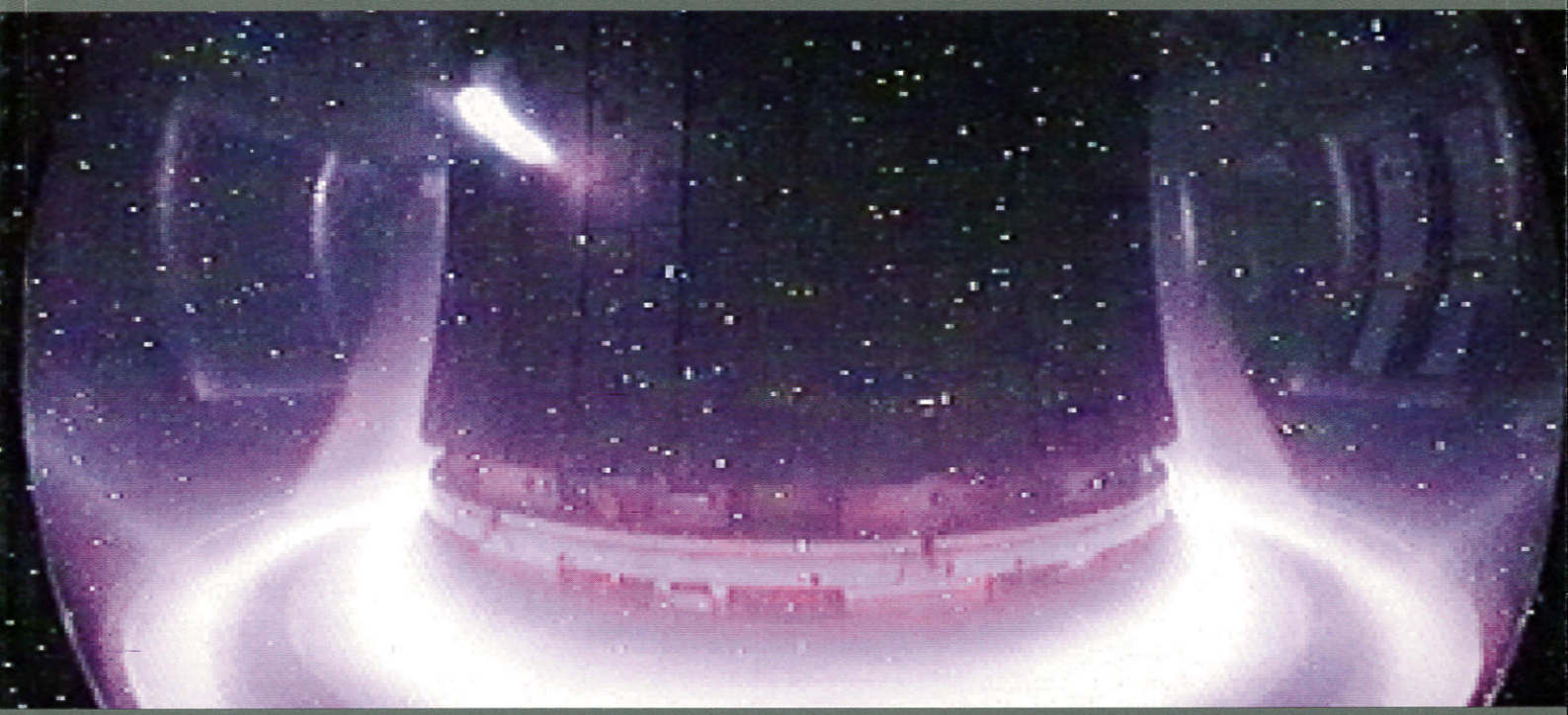

COVER ILLUSTRATION

Injection of a solid deuterium pellet from the high field side of the ASDEX Upgrade tokamak: This unconventional injection geometry was chosen for the first time in a tokamak since standart injection from the low field side suffers from very low refuelling efficiencies at high heating power. The adverse effect is exerted by the quick outward drift of a high-pressure plasmoid formed during pellet ablation. It can be turned to advantage by the new injection geometry, thus leading to strongly improved fuelling efficiencies.

IPP
Max-Planck-Institut
für Plasmaphysik

EURATOM Association

# Annual Report 1996

Max-Planck-Institut
für Plasmaphysik
EURATOM Association

## CONTENTS

# PREFACE

Two types of fusion experiments are being investigated at Max-Planck-Institut für Plasmaphysik: the tokamak and the stellarator. The aim of the ASDEX Upgrade divertor tokamak is to realize a reactor-compatible divertor and study reactor-relevant plasma edge physics. Experiments are strongly focused on preparations for ITER: In the last year ASDEX Upgrade could demonstrate effective helium control under ITER-relevant conditions and made major progress in the characterization and understanding of divertor properties, density limit and edge operating conditions. Studies with tungsten-covered divertor plates resulted in very tolerable core tungsten concentrations, even under high-power conditions. Especially successful were experiments with pellet injection from the high-field side. Thus the conventional problem of poor fuelling efficiency could be overcome. After the divertor has been converted to a closed configuration, ASDEX Upgrade will start operation with the new version in spring 1997.

The WENDELSTEIN 7-AS stellarator could demonstrate that radial electric fields reduce the neoclassical electron heat transport. Electron temperatures of up to 4 keV thus could be reached. The plasma edge studies were continued in preparation for later installation of the island divertor plates. The heating system was further improved, ICRH now allowing plasmas sustained by ICRH alone to be studied for the first time. Also two 140 GHz gyrotrons were successfully put into operation and the neutral beam heating power was increased by regapping the extraction grids of the ion sources.

The follow-up experiment for demonstrating the reactor relevance of the Advanced Stellarator principle, WENDELSTEIN 7-X, will be a 5-period Helias configuration with a helical divertor and a superconducting coil assembly. It will be built in the new branch institute at Greifswald. After final approval in 1996 the project organization was established and European associations were invited to contribute to WENDELSTEIN 7-X. Physics studies on WENDELSTEIN 7-X mainly dealt with divertor, diagnostics, heating and coil optimization. Technical development concentrated on testing of divertor elements, manufacture of an original-sized superconducting demonstration coil, development of an advanced conductor and manufacture of a section of the cryostat.

Work at the Berlin Division of IPP is concentrating on investigation of the plasma edge by experimental as well as theoretical methods. In 1996 the EBIT electron beam ion trap at Berlin started operation. This device - the first of its kind in Germany - produces and stores highly ionized ions up to the heaviest elements of the periodic system. The ion trap is intended for general atomic physics measurements and applications to fusion-relevant hot plasmas. The Berlin division also runs a linear plasma generator to study plasma-wall interaction and develop diagnostics.

On the national level, IPP coordinates its research effort with Forschungszentrum Karlsruhe within the "Entwicklungsgemeinschaft Kernfusion" and also with Forschungszentrum Jülich. IPP also closely cooperates with a number of German universities, the collaboration with the University of Stuttgart being particularly intensive.

The research conducted at IPP is part of the European fusion programme: IPP is involved in JET, the joint European experiment. The ASDEX Upgrade tokamak and the alternative stellarator concept of the WENDELSTEIN experiments provide essential information for preparing the next steps in the overall European programme. Furthermore, IPP acts as host to NET, the European reactor study group, which has been working at Garching since 1983.

Coordination of research activities also extends to the worldwide level. IPP is party to two Implementing Agreements: the one - with the USA - covering cooperation on the ASDEX Upgrade divertor tokamak; the other - with the USA, Japan, Australia and Russia - regulating cooperation in the joint stellarator programme, to which the WENDELSTEIN experiments make a major contribution. From April 1988 IPP provided the technical site for the American-European-Japanese-Soviet group responsible for the conceptual design activities of ITER, the International Thermonuclear Experimental Reactor. After completion of the conceptual design, IPP was also chosen in 1992 - together with the fusion laboratories in Naka and San Diego - as site for the ITER Engineering Design Phase.

Klaus Pinkau

# Projects

# TOKAMAKS

A large part of the capacity at IPP is devoted to investigating confinement in the tokamak configuration. IPP pioneered the divertor principle with the ASDEX tokamak, which demonstrated the favourable impurity control capabilities of this configuration and discovered the so-called H-regime of improved energy confinement. The divertor configuration has also been adopted for ITER, and ASDEX Upgrade, IPP's successor experiment to ASDEX, closely resembles a scaled-down version of ITER.

As a consequence, experiments on ASDEX Upgrade are strongly focused on the critical R&D tasks for ITER. Originally, this implied mainly studies of divertor behaviour and control issues relating to its ITER-like configuration and coil arrangement. With the enhancement and diversification of its heating and particle control systems and the extension of its diagnostic capabilities, ASDEX Upgrade is now also strongly contributing, however, to the basic understandig of magnetohydrodynamic instabilities and particle and energy transport in the bulk plasma. In all three areas this experimental work is accompanied by strong theoretical effort, with, in particular, IPP's divertor theory effort (carried out in close collaboration with KFA Jülich and New York University) also constituting the main modelling input to the ITER design. First-principle-based fluid turbulence studies for the understanding of transport in the outer regions of the bulk plasma are a further area of excellence of IPP, which in the coming years will benefit from the use of its 1/3 share of a powerful Cray-T3E parallel computer acquired by the Max Planck Society.

During 1996, ASDEX Upgrade routinely operated with plasma currents between 0.8 and 1.2 MA. NBI provided for heating powers of up to 10 MW, which, by feedback-controlled on-off modulation, could be fine-stepped for the sensitive power threshold and density limit studies. The ICRH system was working with powers of up to 3.5 MW, with two (out of four) antennas working in a configuration without Faraday screens, as envisaged for ITER. ECRH first became available with up to 500 kW used for heat pulse propagation studies of energy confinement. The available pellet centrifuge can reach injection velocities of up to 1200 m/s and injection rates of up to 80 pellets per second. Particularly successful was the installation of a high-field-side pellet injector system, which in spite of its hither to limited injection speed (<120 m/s) has achieved outstanding results. All heating and refuelling systems have profited from the continuous upgrading of the real-time control system, which now allows target plasma parameters for many scenarios to be specified and controlled. A particular feature of this operating period was the operation with tungsten-covered divertor target plates, which provided important, and generally encouraging, information for the use of high-Z materials in ITER.

Outstanding physics results of ASDEX Upgrade in 1996 were:

- experimental demonstration of the possibility of effective helium control under ITER-relevant conditions;
- quantitative understanding of critical divertor properties (e.g. pumping capability for different gaseous impurities, role of volume recombination in divertor detachment) through combined measurements and modelling efforts;
- successful operation with tungsten-covered divertor target plates (which, under high-power operating conditions, resulted in very tolerable core tungsten concentrations);
- clarification of the different nature of the density limit phenomenon in L- and H-mode plasmas;
- characterization of the different edge operating conditions (L-mode, type-I and type-III ELMs) through measurement of the local edge paramters, in particular Te and ne, including the role of the ballooning mode limit;
- significant progress in the clarification of the connection between core transport and edge behaviour;
- demonstration of the qualitatively different information on energy transport that can be extracted from (active and controllable) ECRH heat pulse experiments, compared with passive methods based on naturally occurring sawteeth;
- demonstration that pellet injection from the high-field side can overcome the problem of poor fuelling efficiency encountered in high-power H-mode discharges with conventional pellet refuelling from the low-field side (this extension of our fuelling system had been prompted by a theoretical explanation of the poor fuelling efficiency in the low-field-side case, which was thus verified);

- progress in the identification and theoretical understanding of a range of MHD phenomena (observation of TAE modes also in the absence of fast particles, quantitative agreement between predictions for neo-classical tearing modes with observed island structures and magnetic field signals, identification of type-III ELMs in L-mode discharges).

In summer 1996, ASDEX Upgrade started rebuilding converting its divertor structure to a closed divertor configuration, labelled divertor II whose first version is the Lyra. At the same time, the existing pumping system is being augmented by the addition of powerful cryopumps, and the magnetic field power supplies will be enhanced to allow better plasma shape control. ASDEX Upgrade will start operation, in its new configuration, in spring 1997. During 1997, the available ECRH heating power will also be raised to 2 MW, and, later in the year, a second beamline doubling the available NBI heating power will be added to the system.

ASDEX Upgrade maintains fruitful collaborations with the following institutions: KFA Jülich; KFK Karlsruhe; Inst. für Plasmaforschung, University of Stuttgart; University of Augsburg; Culham Lab., Abingdon, UK; Centro de Fusão Nuclear, Lisbon, Portugal; University College, Cork, Ireland; Inst. Allgemeine Physik, TU Vienna, Austria; NCSR Demokritos, Athens, Greece; CRPP, École Polytechnique, Lausanne, Switzerland; CREATE Group, Naples, Italy; University of Strathclyde, Scotland; FOM-Inst. voor Plasmafysica, Rijnhuizen, Netherlands; PPPL, Princeton, USA; GA, San Diego, USA; MIT, Cambridge, USA; Oak Ridge National Lab., Oak Ridge, USA; N.Y. University, Courant Institute, USA; Research Inst. for Particle and Nuclear Physics, Budapest, Hungary; Inst. of Applied Physics, Nizhni Novgorod, Russia; I.V.Kurchatov Institute of Atomic Energy, Moscow, Russia; Ioffe Institute, St. Petersburg, CIS; Technical University of Applied Physics, St. Petersburg, CIS; Landau Institute, Moscow, Russia; St.P.T.U., St. Petersburg, CIS.

Besides operating its own ASDEX Upgrade tokamak, IPP has been involved in JET, the joint European large-scale project at Culham (UK) for many years. IPP constructed and put into operation a large fraction of the JET diagnostics and also participates in exploitation of the JET experiment. During 1996 JET experimented with its MkII divertor configuration, which is a more closed divertor than the previous configurations. A particularity of its design is the compatibility for remote handling, which will allow replacement of its tile configuration also under activated machine conditions, following the DTE1 deuterium-tritium operation phase in early 1997. Experimental work on JET during 1996 was partly aimed at identifying optimum operating conditions for the upcoming DTE1 experiment, but was also focused on divertor studies, including the interrelation of edge conditions and global energy confinement. In this area, intensified collaboration between JET and ASDEX Upgrade was started, proceeding through a series of informal workshops. Advanced tokamak scenarios aiming at steady-state tokamak operation were investigated, too.

The results of JET, IPP and, in general, the world-wide tokamak programme formed the groundwork for planning an experimental reactor as a next step. The European Union, Japan, the USA and Russia have agreed to prepare this next step as a joint venture. The engineering design study (EDA) of this ITER experimental reactor is being carried out by a joint team of the four partners, working at three sites (San Diego/USA, Naka/Japan, Garching/EU). IPP has directed the major part of its experimental and theoretical effort to the scientific support of the ITER design. The results are fed into the system through three major channels: (i) direct participation of IPP scientists in the numerous expert meetings called together by ITER to deal with special subjects, (ii) handling of special tasks in support of NET/ITER, and (iii) participating in various NET/ITER committees. Important contributions included the analysis of the confinement data base and contributions to the development of a divertor model and to the design of diagnostic systems. In 1996, an independent panel of scientists and industry experts assessed the European Fusion Programme, including the economic and environmental aspects of energy production through nuclear fusion. The conclusions of this panel were very favourable and place the highest emphasis on the importance of producing with the ITER project.

# ASDEX UPGRADE PROJECT

(Head of Project: Dr. Walter Köppendörfer / Dr. Otto Gruber)

**Experimental Plasma Physics Division E1:** M. Albrecht, M. Alexander, Ch. Aubanel, K. Behler, M. Bessenrodt-Weberpals, H. deBlank, H.-S. Bosch, E. Buchelt, A. Buhler, Ch. Dorn, R. Drube, J. Engstler, J. Ernesti, U. Fahrbach, P. Franzen, J.C. Fuchs, O. Gehre, J. Gernhardt, O. Gruber, E. Gubanka, A. Gude, G. Haas, Th. Härtl, G. Herppich, W. Herrmann, M. Hoek, H. Hohenöcker, H. Hupfloher, D. Jacobi, W. Junker, E. Kaplan, Th. Kass, M. Kaufmann, G. Klement, G. Kölbl, H. Kollotzek, W. Köppendörfer, P. Krüger, B. Kurzan, P.T. Lang, R.S. Lang, M. Maraschek, F. Mast, K. Mattes, D. Meisel, R. Merkel, V. Mertens, H.W. Müller, M. Münch, H. Murmann, G. Neu, E. Oberlander, M. Oswald, M. Pflug, C.S. Pitcher, G. Raupp, G. Reichert, H. Röhr, H. Salzmann, W. Sandmann, H.-B. Schilling, M. Schittenhelm, H. Schneider, G. Schramm, G. Schrembs, S. Schweizer, U. Seidel, S. Sesnic, M. Sokoll, K.-H. Steuer, A. Stimmelmayer, J. Stober, B. Streibl, W. Suttrop, W. Treutterer, M. Troppmann, M. Ulrich, G. Weber, R. Wolf, D. Zasche, Th. Zehetbauer, G. Zimmermann, H. Zohm

Guests in Division E1: G. Fieg, Kernforschungszentrum Karlsruhe, Germany;
F. Hoenen, KFA Jülich, Germany;
B. Kuteev, Technical University, Plasma Physics Department, St. Petersburg, CIS;
I. Shustov, IOFFE Technical Institute, St. Petersburg, CIS;
T. Kiviniemi, VTT Energy, Finland;
A. Hatayama, Faculty of Science and Technology, Keio University, Yokohama, Japan;
A, Khuturetski, Kurchatov Institute, Moscow, CIS.
Q. Yu, Academia Sinica, Hefei, China

**Tokamak Physics Division:** G. Becker, A. Bergmann, K. Borrass, M. Brambilla, K. Büchl, A. Carlson, R. Chodura, D. Coster, O. Gruber, S. Günter, O. Kardaun, K. Lackner, P. Martin, J. Neuhauser, G. Pautasso, G. Pereverzev, K. Reinmüller, R. Schneider, W. Schneider, J. Schweinzer, B. Scott, M. Weinlich, R. Wunderlich, H.-P. Zehrfeld

Guests in Tokamak Physics Division: B. Braams, New York University, N.Y., USA;
G. Petravich, S. Kalvin, G. Veres, KFKI, Budapest, Hungary;
I. Veselova, V. Rozhansky, A. Ushakov, LPI. St. Petersburg, CIS;
P. Lalousis, IESL.Forth, Heraklion, Greece

**Technology Division:** B. Becker, F. Braun, H. Brinkschulte, H. Faugel, J.-H. Feist, R. Fritsch, J. Hartmann, B. Heinemann, F. Hofmeister, W. Kraus, F. Leuterer, F. Monaco, M. Münich, J.-M. Noterdaeme, S. Obermayer, A.G. Peeters, F. Probst, S. Puri, R. Riedl, F. Ryter, W. Schärich, E. Speth, A. Stäbler, Ph. Verplancke, O. Vollmer, F. Wesner, R. Wilhelm, K. Wittenbecher, S. Wukitch, M. Zouhar

**Experimental Plasma Physics Division E4:** K. Asmussen, A. Bard, K. Behringer, S. de Peña Hempel, R. Dux, W. Engelhardt, J. Fink, A. Kallenbach, H. Meister, B. Napiontek, R. Neu, D. Schlögl, A. Thoma

Guest in Division E4: Z. Wang, Southwestern Institute of Physics, Chengdu, China

**Berlin Division:** G. Fussmann, A. Herrmann, S. Hirsch, H. Kastelewicz, M. Laux, B. Napiontek, E. Pasch, V. Rohde, U. Wenzel

**Computer Science Division:** C. Brosig, H. Friedrich, K. Hallatschek, P. Heimann, F. Hertweck, J. Maier, M. Pacco-Düchs, I. Precht, U. Schneider, C. Tichmann, R. Tisma, M. Zilker

**Surface Physics Division:** R. Behrisch, E. Berger, V. Dose, K. Krieger, J. Roth, W. Poschenrieder, R. Schwörer, G. Venus, H. Verbeek

**Central Technical Services:** S. Deschka, R. Goihl, F. Gresser, E. Grois, H. Hofmann, S. Kamm, M. Kluger, A. Knallinger, H. Kosniowski, H.-J. Kutsch, H. Lohnert, W. Melkus, S. Mukherjee, J. Perchermeier, B. Sombach, M. Weissgerber, R. Zickert

**University of Cork, Ireland:** P. McCarthy

**IPF University of Stuttgart:** G. Dodel, W. Förster, J. Gafert, G. Gantenbein, K. Hirsch, E. Holzhauer, W. Kasparek, M. Niethammer, P.G. Schüller, U. Schumacher, H. Zohm

**Centro de Fusão Nuclear, Lisbon, Portugal:** E.-M. Manso, L. Cupido, Th. Grossmann, C. Loureiro, J. Santos, F. Serra, A. Silva, P. Varela

**NCSR Demokritos, Athens, Greece:** N. Tsois, N. Karakatsanis, M. Kakoulidis, G. Kyriakakis, M. Markoulaki, N. Xantopoulos

**University of Augsburg:** U. Fantz

# 1. OVERVIEW

The experimental programme of ASDEX Upgrade over the past years was (and still is) focused to a large extent on edge and divertor physics in high-power, high-confinement regimes, with the aim of identifying and optimizing methods of safe power exhaust and particle control for next-generation divertor tokamaks. In parallel, significant effort was placed on core physics and performence-related questions, such as disruptions and their avoidance and mitigation, the scaling an improvement of energy and particle transport with emphasis on the H-mode and MHD modes, and instabilities.

The edge and divertor physics programme culminated this year in the final divertor I phase with tungsten-clad target tiles in the inner and outer strike point regions. A comparison of low and high-Z target plate materials was therefore possible in the same machine and plasma configuration. No deleterious effects from tungsten were found; even under high-power operating conditions only tolerable core tungsten concentrations occurred. The new divertor II hardware, which allows several ITER-relevant divertor configurations to be realized on the same base structure, is currently being installed. The first version (LYRA including a roof baffle), which is rather similar to the present ITER reference design, will become operational in the spring of 1997 and should be investigated, with only minor modifications (e.g. baffle length), by the end of 1998. Depending on the results and the actual ITER R&D requirements at this time, changes of the baffle topology or the change to a gas bag configuration may follow as an integral part of this programme. It has reached a status of maturity (including advanced 2D codes such as B2-EIRENE) which should allow fairly reliable input for the ITER divertor on the desired time scale (as an integral part of the international ITER physics R&D programme).

Its similarity to ITER in plasma shape, in relative distance from the plasma to the poloidal field coils and in the divertor and performance studies, makes ASDEX Upgrade particularly suited to test control strategies for shape, plasma performance (including profile control) and mode stabilization. Finally, comparison with the other two European divertor tokamaks, Compass-D and JET, is important to determine size scalings for core and edge physics. this collaborative work has already started and will continue.

In addition, the physical and technical tasks at ASDEX Upgrade are embedded in a framework of national (IPF Stuttgart, University of Augsburg, KFK Karlsruhe, KFA Jülich (see also chapter University contributions to IPP programme)) and international (see Sec. International Cooperation) collaborations, including support of diagnostic developments.

## 1.1 Operational and Technical Systems

In the operation period 1996 (January till beginning of August) with tungsten-covered target plates of the divertor I configuration the routine operation was restricted to plasma currents between 0.6 and 1.2 MA, although 1.4 MA had already been reached in 1995. The toroidal field was varied up to 3.2 T using both directions compared with the plasma current. Flexible use of the auxiliary heating power was provided by the availability of three different heating methods (NBI / one beam line with up to 10 MW with deuterium; ICRH / two antennae with 2 db-couplers and two antennae without Faraday screens, and powers of up to 3.2 MB; ECRH / one gyratron with 0.5 MW). In this way the beam power could be feedback-controlled on-off modulated for sensitive power scans near the L-H (or H-L) transition or near the density limit. Pre-experiments for off-axis ICRF current drive (see Sec. 1.3) were performed using off-axis coupling to the electrons via mode conversion and different antenna phasings. The further extension of the heating systems in 1997 is described below.

Densities well above the Greenwald limit could be achieved in the L-mode both with gas puffing and pellet injection. A gas-pulse-driven repetitive pellet injector could be used for the first time for high-field-side pellet injection by installing a guiding tube and achieved remarkable results. The pumping system will be augmented by cryopumps in the divertor II phase. To exploit the tokamak plasma behaviour and its operational limits, our real-time control systems for the magnetics and the heating and refuellig systems were continuously upgraded. The prescription and control of shape and target plasma parameters is now provided together with the switching of the different control algorithms according to the real-time recognized plasma and discharge states. This is accomplished by constant effort to improve and refine the diagnostics of the plasma core, edge and divertor together with the extension of the data processing and storage capabilities and of the network enhacements.

"Advanced tokamak" equilibria (see Sec. 1.3) requiring plasma shapes with higher triangularities can already be run in the divertor II with the outer strike point on the roof baffle. To achieve higher triangularities and, additionally, precise positioning of the strike points in the divertor II configuration, the upper and lower OH-stray-field-compensating coils OH2 can now be additionally fed by using new thyristor bridges. But with the present in-vessel components (ICRH antennae, PSL) only equilibria with small triangularities of $d_{top} \geq 0.1$ and $d_{bottom} \geq 0.3$ can be investigated. Modest triangularities of $d_{top} \geq 0.2$ and $d_{bottom} \geq 0.4$ require modification of the ICRH antennae (envisaged in 1999), while going to even higher triangularities of $d_{top} \geq 0.5$ requires the construction of new ICRH antennae. In these configurations plasma currents of up to 1 MA are possible according to the poloidal field, power supply and heating capabilities available (see below).

## 1.2 Summary of the Main Results

The following important results were contributed by ASDEX Upgrade during this year to the understanding and development of the ITER physics:

- investigation of energy exhaust in combination with divertor detachment influenced by volume recombination and radiating scenarios (CDH-regime) combined with strong modelling support;
- exhaust measurements of gaseous impurities, where especially effective helium pumping could be demonstrated;

- operation of tungsten divertor targets showing no accumulation of the high-Z material at high powers and unchanged operational limits; erosion and migration studies of tungsten are governed by prompt local redepostion;
- operating conditions of the plasma edge parameters (L-mode and H-mode with different ELM types);
- interplay between edge and core physics, especially the roles of the edge density and power balance on the density limit and of the edge pressure gradient on confienment;
- exploration of the "cold" density limit in the L-mode (above the Greenwald density) and the "warm" limit in the H-mode connected with the transport barrier;
- influence of edge parameters and radial electric field on L-H and back-transition, including measurements of the fluctuations involved and development of first-principle theoretical models;
- comparable heat transport in ECRH heat wave and power balance studies, while the results from sawtooth propagation techniques are amplitude-dependent;
- gyro-Bohm scaling of the H-mode transport also at a high collisonality of $\nu^* \approx 0.1$;
- "deep" pellet refuelling with high fuelling efficiency from the high-field side compared with "shallow" penetration from the low-field side in high-power H-mode discharges, opening the route to increased density limits;
- understanding of MHD modes such as neo-classical tearing modes determining the $\beta$-limit in ITER-like discharges, TAE modes driven by transport in the absence of fast particles, and ELMs in both the H- and L-mode, including their identification with observed precursors.

## 1.3 Physics Programme and Technical Extensions

The edge and divertor programme at ASDEX Upgrade will continue at a high level in keeping with to its still crucial importance for any scheme. Core physics studies will be mainly concerned with the investigation of scaling and the improvement of global plasma performance (energy and particle transport, MHD instabilities and their stabilization). With respect to energy transoprt, the relation between core and edge and their reciprocal influences, attention is given to transoprt barrier physics, dimensionless scalings and heat wave studies. The studies on MHD modes such as the neoclassical tearing modes close to the $\beta$-limit or transport-induced toroidal Alfvén waves will be continued. Experiments on mode stabilization using ECRH and ECCD will start next year (the power will be raised to 2 MW / 2 s in 1997). Particle transport and the density limit remain a substantial part of our effort, including the promising refuelling by pellet injection from the high-field side.

While the ITER study seems to offer a viable solution for the next step despite some remaining uncertainties, e.g. with respect to the achievement and quality of the desired high-confinement regime, there are clear indications from recent experiments as well as from advanced theory that appropriate control of the plasma shape and radial profiles together with internally (bootstrap) and externally driven current might offer the chance of further optimization of the tokamak concept towards smaller steady-state machines. Following this line, a major part of the ASDEX Upgrade programme will be shifted to the investigation of "advanced tokamak" concepts characterized by, for example, some triangularity, a high fraction of bootstrap current and external current drive. The compatibility of these new ideas with stationary operation at high power and with simultaneously, cold divertor should be one of the key elements of the programme. Advanced tokamak equilibria can already be run in divertor II, though not with optimal performance.

For the above-mentioned physics programme and the ASDEX Upgrade parameters a heating power of about 20 MW is sufficient, which will be available in autumn 1997 with the second beam line (NBI / 20 MW; ICRH / 6 MW with four antennae using 3 db couplers; ECRH / four gyratrons with 2 MW). However, to achieve stationary flat or reversed shear profiles (at $q_0 > 1$) an off-axis current drive capability of about 250 kA is required at a plasma current of 1 MA (according to transport calculations). Options are

- ICCD using mode conversion (up to 150 KA off-axis, available in 1998),
- ECCD allowing a flexible current drive scheme, but with a low efficiency, and
- NBCD with tangential injection (100 keV $D^0$; turning of one existing injector or installation of a new tangential injector).

A long-term prospect for a third injector could be to replace the ion sources by negative ion sources and thereby provide a testbed for the technology of negative-ion beams.

Due to the limitation of the additional heating to 20 MW and the more effective generation of DN-like plasma configurations using the OH2 coils, the flywheel energy of the two generators EZ3 and EZ4 is sufficient for future AUG experiments. However, the flywheel energy of the generator EZ3 (500 MJ) can only be fully exploited by compensating the reactive power of the thyristor converters with capacitors. A study for a first 30 MVAr compensation unit has already been conducted.

The ASDEX Upgrade technical systems, including control and data processing, are described in Sec. 2. Section 3 deals with the results relating to the plasma core with regard to transport, operational regimes and MHD modes. Section 4 is manly devoted to the edge operating conditons and the core-edge interplay, while the tungsten divertor experiment is presented in Sec. 5. Section 6 describes results of the scrape-off layer properties and divertor physics, including modelling. The progress in diagnostic development and adaption to divertor II is given in Sec. 7.

# 2. TECHNICAL SYSTEMS

The Divertor I experiments with tungsten-coated strike point tiles were carried on until the summer opening in early August. Mounting of Divertor II then started with the cryo pump (CP), including the cryo feed and the resistor network for arcing protection /694/. This will be finished in late April 1997 with the target modules including the adapted and new diagnostics. Divertor II requires improved feedback control of the separatrix

position, independent control circuits for the OH transformer stray field compensation coils (OH2o,u) were provided. Operation of the second neutral beam injector (NI2) together with the additional control power for the OH2o,u coils will require compensation of reactive power to exploit the flywheel generator EZ3 to a larger extent. A study for a 30 MVAr compensation unit was therefore executed by SIEMENS. The generator EZ2 supplying the toroidal field magnet (TF) was overhauled and has got a new feedback control for the excitation circuit.

The feedback control of the plasma shape with the improved structure of the R2 controller was commissioned and the control of plasma parameters with the R4 controller was extended with respect to input signals and plasma scenarios. The change of the file system from AMOS to MR-AFS was completed in 1996 and the hardware and software of the data acquisition computer system were further extended.

For NI2 the foundations and iron yokes were erected in the experiment hall and the piping for the water supply was installed there. The new vacuum box for the injector will be flanged to the vacuum vessel in late February 1997. The ICRH group succsessfully tested two 3-db couplers borrowed from JET. Since these devices turned out to provide more power per transmitter with higher reliability, four new couplers optimied for AUG will be procured. Before the restart of the experiments all 8 vertical limbs of the ICRH antenna limiters will be hardened with CFC tiles against NBI losses by ripple diffusion. ECRH plasma heating with one gyrotron was successfully used for heat wave propagation measurements. The new long-pulse gyrotron (0.5 MW/2 s) will now be commissioned.

## 2.1 Machine

Mounting of Divertor II requires a 9-month shutdown of the experiment. A summary of machine performance starting with the first discharge on 21 March 1991 and ending with the last on the 1 August 1996 was therefore extracted from the AUG data archive.

### 2.1.1 Machine performance

The shot (#) counter stood at #8645 after 370 days of experimenting (shot days) over more than five years. The average values over the whole period are: 69 shot days/year and 23 shots with 10.5 plasma discharges per shot day. The low number of plasma shots per day is mainly due to the exploratory nature of experimenting, which lacks discharge series. This also led to a sizeable fraction (34%) of disruptive discharges. Fig. 2.1 shows the accumulation of plasma discharges versus the sequence of shot days. From April 1992 onwards, after hardening of the target plates, the rise in plasma discharges is fairly linear despite the increasing complexity of the experiment (rising plasma current and density, addition of auxiliary heating systems). The discharges with significant auxiliary heating by NBI (NBI > 4 MW) have now reached a fraction of about 25%. The discharges with significant auxiliary heating by ICRH (ICRH > 2 MW) are still few.

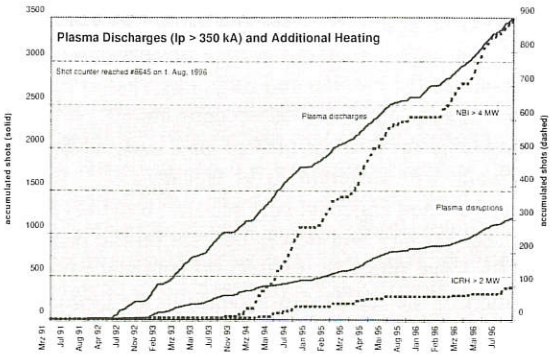


*FIG. 2.1: Total plasma discharges versus shot days.*

Fig. 2.2 shows the accumulation of typical plasma current values versus the sequence of shot days. Most discharges were run at 800 kA (0.7 - 0.9 MA curve). From mid-1994 onwards the 1 MA discharges become relevant. There are discharges with 1.2 MA up to now and only one ohmic discharge with 1.4 MA. During this discharge the TF magnet was stressed with 93% of the SN design load, Ip * Bo = 4.5 MA_T.

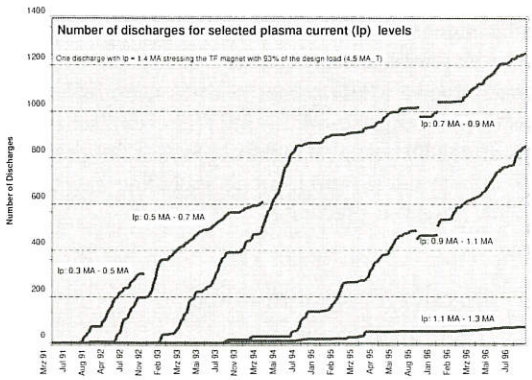


*FIG. 2.2: Number of discharges for selected Ip values.*

### 2.1.2 Power supplies

The OH circuit is basically a series connection of the central solenoid (OH1) and the upper (OH2o) and lower (OH2u) stray field compensation coils. Under unfavourable plasma conditions a high voltage is therefore also required during the flat top. The feeding thyristor, supplying current in two directions, was therefore upgraded. After current reversal the circulating current inside the twin thyristor bridge is now switched off to get the full voltage of an independent branch. To achieve this performance the thyristor control together with the protection system and the current transducers had to be changed.

Two parallel circuits have now been added to the series circuit of the OH transformer. The first additionally supplies the OH2o and OH2u coils in series and controls the triangularity of the plasma column in a very efficient way. The second circuit only supplies the OH2u with current in two directions via a new thyristor bridge with digital control. The new OH2u circuit, together with the divertor coil V2u, controls the location of the lower stagnation points on the inner and outer target plates.

Mainly the additional circuit current of the OH2u coil could lead to critical asymmetry forces on the central solenoid OH1. A new three-stage safety system has therefore been elaborated to keep the currents from leading to asymmetry forces on the OH system inside the allowed boundaries.

### 2.1.3 *Vacuum vessel*

The tungsten-coated divertor tiles had survived the high heat load (up to <7 MW/m2>) of ELMy plasma discharges without melting spots. Assessment of the tiles removed showed that noticeable tungsten erosion occurred only on the outer target plate, where a higher heat flux prevents early power detachment. Fine, mainly toroidally directed, cracks were also found on all target plates. These cracks are attributed to the significant difference in the thermal expansion coefficients between tungsten and the EK 98 carbon carrier. Closer matching by a more suitable carbon carrier could most likely considerably increased the fatigue strength and heat load. Additionally, tests had shown that a reduction of the layer thickness from 500 m to 200 m notably increases the fatigue strength. However, the addition of 10% rhenium to tungsten for achieving higher ductility of the coating gave no better results. Altogether, the past work indicates that a sizeable improvement of the coating technique for high heat flux components beyond the achieved state would require considerable effort. Alternatively, thin layers in the range of a few m are now assessed which could be useful for low heat flux components such as the heat shield.

The higher heat flux envisaged for Divertor II required new technologies for target diagnostics. Fig. 2.3 shows the ceramic coating of the strike point shunt tiles measuring halo currents locally via a resistor of 1 mW. The 0.2 mm AL2O3 coating insulates with a resistivity in the MW range and at the same time provides a good thermal heat transfer in combination with a compliant graphite layer. To measure the toroidal average of the halo currents, toroidally closed Rogowski coils are arranged at all locations where currents could flow from the target to the vacuum vessel.

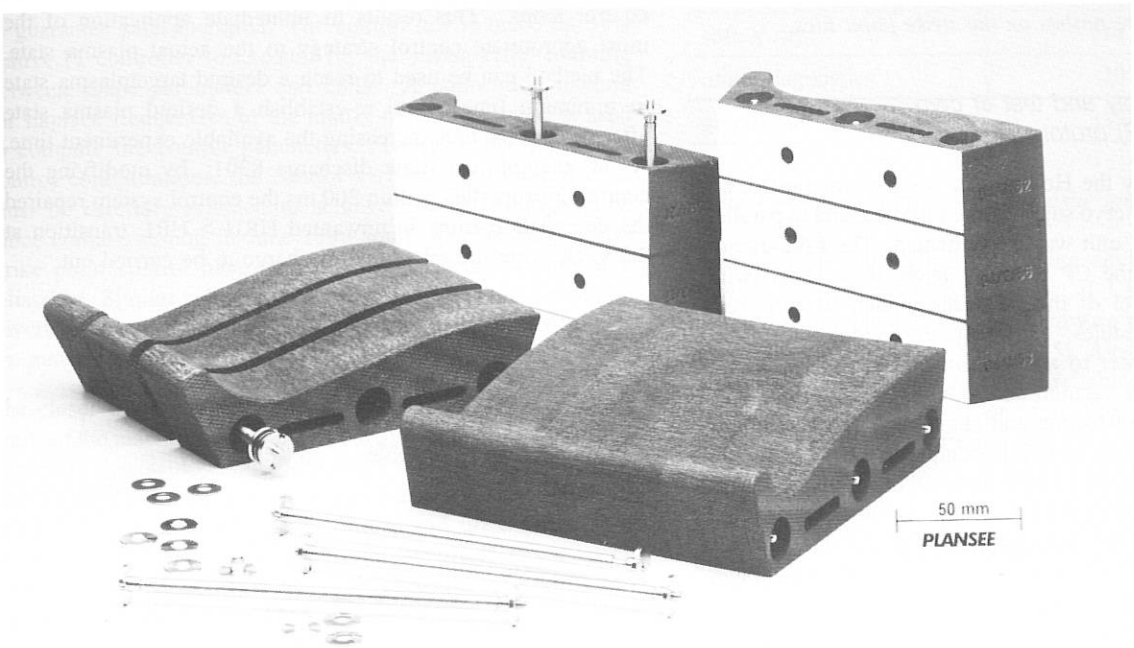


*FIG. 2.3: Ceramic-coated stike point shunt tiles.*

Up to 46 Langmuir probes measure in the poloidal circumference (Fig. 2.4) the target temperature and density. Also the probe cylinders are near the cooling plate insulated by a ceramic coating. On the strike point tiles the probes are arranged between adjacent elements (Fig. 2.5) and machined with the assembled tile to avoid hot spots.

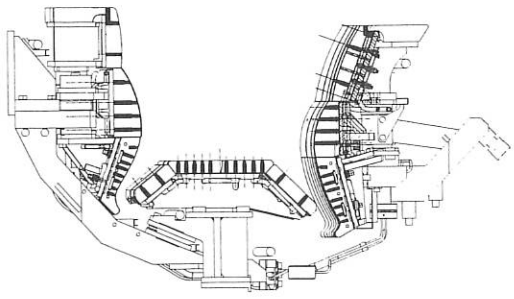

*FIG. 2.4: Poloidal arrangement of Langmuir probes.*

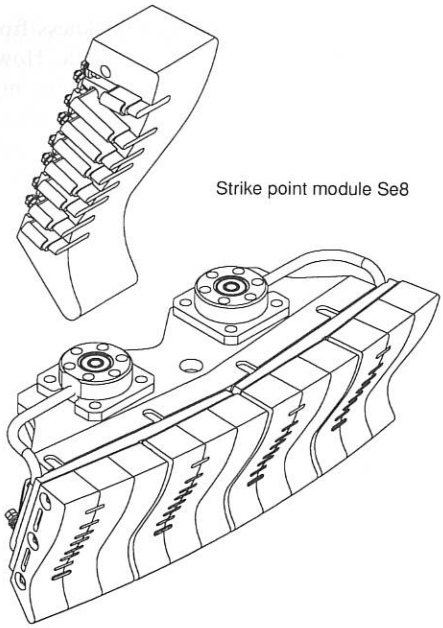


*FIG. 2.5: Langmuire probes on the strike point tiles.*

### 2.1.4 *Cryo supply and test of cryo pump (CP) prototype*

In the cryo laboratory the He-liquefier was commissioned, all components of the CP cryo supply were installed, and in parallel the SIMATIC control unit was implemented. The LN2 circuit and the function of the CP nitrogen shield were tested with a representative model of the CP. This model, like the real CP, consists of 7 modules. However, the modules were not toroidally bent, in order to allow them to be arranged inside an existing cylindrical vacuum tank. Only two of the modules have the original cross-section and chevron. The remaining 5 modules have the correct hydraulic conditions of the LN2 and LHe circuits and also the correct mass of the nitrogen shield but a reduced radiation-exposed surface. Up to now only the nitrogen circuit could be commissioned by a cool-down test of the CP model. The cool-down test was started with saturated nitrogen at a mass throughput of 12.5 g/s. With an electrical heat exchanger the mass ratio (mass of gas/total mass) was set to x = 0.7 in order to fill the 50 litres of the go transfer line with liquid nitrogen and also achieve a soft cool-down of the cryo pump (temperature gradient 20 K/m_length). While passing through the go transfer line of 42 m length (including the cryo feed), the nitrogen liquid-vapour mixture is first heated to ambient temperature gas. After 1 hour the gas temperature begins to drop at the CP entrance and the cool-down of the actively cooled part of the shield to 80 K is completed after a further 4 hours. Then the heater is switched off (x -> 0) and the LN2 throughput is reduced to 5 g/s, the value which covers just the steady-state heat input to the nitrogen shield of the CP and to the cryo transfer line. To reach steady-state conditions on the critical lids of the module connections, cooled only via heat conduction across their bolted joints, requires altogether about 16 hours. However, the final temperature reaches a satisfactorily low value of about 100 K. In the next step the LHe circuit will be commissioned by cooling down the cryo panel. Then the cryo plant and SIMATIC control will be transferred to the experiment /694/.

## 2.2 Control Systems

Current activities concern continuous improvement of real-time plasma control capabilities and further automation of experiment operation.

Improvements of real-time plasma control were achieved in conceptual design and implementation: A milestone in plasma control was the successful commissioning of plasma regime guided discharge control. Formerly, control loops had to be switched on or off at preset times that had to be known prior to a discharge. Problems degrading control quality resulted from inaccurate predictions of plasma state transitions, or from unexpected plasma behaviour. With the new plasma regime guided discharge control, the plasma regime state is calculated in real-time with a robust and reliable algorithm developed by Franzen /73/. Depending on the detected regime, i.e. currently OH, L, H, HRH, HRL, the control computers may switch control loops. This results in immediate application of the most appropriate control strategy to the actual plasma state. The method can be used to reach a desired targetplasma state in minimum time, or to re-establish a desired plasma state after deviations, thus increasing the available experiment time. As an example we show discharge 8301: by modifying the controller properties, within 200 ms the control system repaired the degradation from an unwanted HRH > HRL transition at 2.2 s, allowing the scheduled discharge to be carried out.

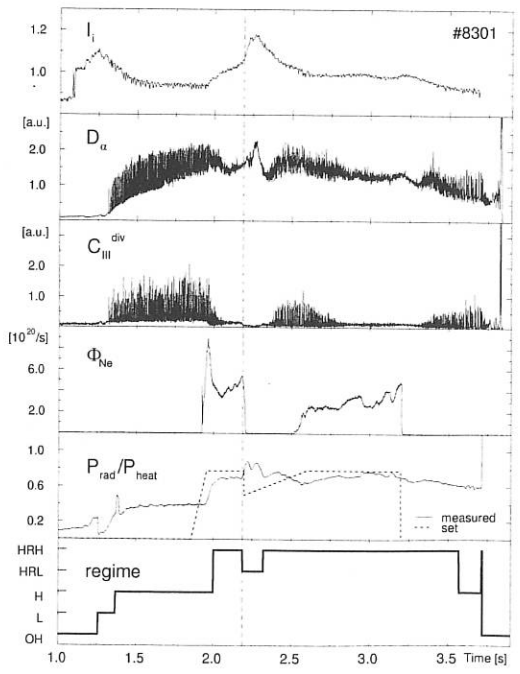


*FIG. 2.6: Example of a dynamically controlled discharge. The transition to the low confinement regime HRL is detected (at 2.19 s) and used to branch into a new segment.*

The real-time plasma parameter controller R4 was equipped

with additional sensor and actuator signals for refuelling and heating, and the feedback control algorithms were extended as scheduled. Integration of a set of automatic real-time protection functions similar to biologic reflex mechanisms is being prepared for fast counteraction of the occurrence of energy limit, MARFE and radiation collapse.

Plasma position control has been further improved to form the reliable backbone of discharge control. First experiments have been carried out with control of the ICRH antenna resistance by variation of the radial plasma position. The most significant progress, however, has been made with the implementation of full shape control. The goal of shape control is to optimize discharge performance by accurately adjusting the plasma cross-section. Shape control features:

- strike point control in the divertor region
- gap control and
- control of second-order geometrical moments such as triangularity or elongation using the distant vertical field coils.

The control algorithm offers high flexibility in the selection of controlled parameters combined with an intelligent control layer to guarantee safe operation. The control law is made up by a matrix PI controller to account for the strong cross-coupling between shape parameters and coils. A collocation method for Laplace frequencies of the matrix transfer function is used to compute the control parameters. To avoid ill-conditioned control configurations, the control variables and control coils must be carefully selected to achieve optimal orthogonality. Since commissioning in June 1996 some 100 discharges with strike point control have shown good performance and high reliability. Similar behaviour can be expected for the upcoming Divertor II campaign, which will impose even harder demands on control performance.

The closer the experiment programme approaches the design limits of the machine, components and power supplies, the more important does automation of experiment operation become. This obliges us to carefully configure the machine and individually check a number of side-conditions and stress limits prior to a discharge. Consequently, considerable effort was spent on preparing the required revision in the coupling of plasma and machine control systems and their interfaces to physicists and operators. From the physical discharge programme physical and technical key parameters are to be calculated. The required technical parameters must then be downloaded to configure the components, considering machine and operation limits. In parallel, complex calculations on electrical and mechanical stress limits are to be performed and, finally, maximum power requirements will be calculated. The entire automatic process execution for discharge preparation must be kept expandable to integrate experience and changes in operational procedures when preparing and executing discharges. A further measure in approaching the machine limits was the upgrading of the real-time control computers for monitoring the stress on poloidal and toroidal field coils. A substantial speed-up of the control algorithms could be achieved, allowing additional stress calculations. Full integration of the coil monitor controllers into the automatic experiment cycle operation and process protocol generation accounts for their increased significance for machine protection.

## 2.3 Data Processing

### 2.3.1 *Diagnostics*

As every year, the number of diagnostics was also significantly increased in 1996. A total of 67 level-0 diagnostics were delivering 333 MBytes of raw data per shot[1] during the last experiment campaign. Up to 202 MBytes per shot of evaluated data were calculated and stored by an additional 58 level-n diagnostics which are in fact data analysis codes started automatically or under the control of a physicist. Table 1 shows the diagnostic situation at the end of 1996. The implied continuous growth of the whole data processing environment was made possible by restriction to one type of UNIX workstation as an interchangeable and scalable hardware platform for all data processing purposes (see Sec. 2.3.5). Upgrading or replacing based on the chosen standard is a reliable method to achieve, for example, more memory or computing power (or both) for more detailed analysis of more data. With respect to future requirements, we are already working on towards real-time calculations for intelligent decisions on sampling time windows and sampling rate or to modify other parameters while measuring itself is in progress (see Sec. 2.3.6). This will probably be realized by using fast PCI data acquisition interfaces together with new powerful multiprocessor workstations conforming to the chosen standard.

| | amount of data | |
|---|---|---|
| type of diagnostic | raw [MB] | evaluated [MB] |
| electric and magnetic | 19 | 4 |
| density and temperature | 88 | 52 |
| spectroscopy | 32 | 1 |
| Mirnov probes | 51 | 32 |
| soft X-ray | 114 | 16 |
| other diagnostics | 29 | 82 |
| grand total | 333 | 187 |

*Table 1 Amount of data per diagnostic groups.*

### 2.3.2 *Data flow and data storage*

The measured data of a diagnostic are first stored as a file on the local workstation, then forwarded to the central evaluation workstation "ssl aug", where they are mapped into a globally shared memory area, and finally directed into the MR-AFS (Multiple Residence - Andrew File System) file space for archival. The ssl aug - a SUN SPARCserver 1000 - is equipped with 6 SuperSPARC CPU's having 60 MHz clock frequency and has 1GByte of solid-state memory and a local disk space of 40GBytes (32GBytes used as AFS foreground space). Another 50Gbytes of disk space is reserved for ASDEX Upgrade

[1] 333 MBytes is the averaged data amount for normal shots. A maximum of up to 610 MBytes is possible with extended inter-shot time gaps allowing completion of the data readout for the biggest diagnostics.

by the RZG (Computing Center Garching) as additional foreground space for the AFS archival system. The ss1aug is the main inter-shot evaluation platform for analysis requiring more than just the data of one diagnostic. It is to be upgraded to 8 processors in 1997 and finally replaced by a powerful new machine in early 1998.

### 2.3.3 *Moving from AMOS/2 to AFS*

The AMOS/2 archival system together with the old IBM 3090 mainframe was finally shut down in mid-1996. At that time about 341,000 files of ASDEX Upgrade diagnostics with 558 GBytes of data obtained from 8234 shots were stored in AMOS/2. The transition from AMOS/2 to AFS took place in several steps over the last two years. With the shutdown of the AMOS/2 system, all remaining components had to be ported to the UNIX server. These include the shot file monitor, the library of data access routines, and the Dependence Data Base DDB. Finally, a utility program was written which permits data to be recovered from the old AMOS/2 tapes in case of emergency.

### 2.3.4 *Dependence data base*

The Dependence Data Base DDB is now in full operation on the UNIX system. The DDB offers users a tool to keep track of the mutual dependences between data files and ensure consistency of these data. For each file registered in the EDTABLE (at present 28,000 entries), its predecessors are shown in the PRED table (at present 65,000 entries), and its successors in the SUCC table (at present 98,000 entries). Each main file entry in EDTABLE contains the parameters, status, verification, and quality. "Status" is set to valid when a file is produced. If a new addition of a file is computed, the status of the previous edition is set to "invalid" and this status value is automatically propagated to its successors. In order to set the parameters "quality" and "verification", automatically the (object-oriented) shot file structure was extended by a new object qualifier. This permits a signal vector in a level-n file to be marked section-wise section-wiseas acceptable or poor. The data access routines were extended accordingly to return that (optional) information, if available. The DDB system includes a command processor for both the users and the maintenance staff. It is possible to add new public diagnostics to the DDB while it is in operation.

### 2.3.5 *S-Bus CAMAC interface*

Already in 1995 the design of S-Bus CAMAC interfaces (equivalent to the Kinetic Systems controllers 3920 and 3922) was started. In 1996 the last twenty of them were commissioned, bringing their total number up to 55. With these interfaces it became possible to replace the old ISI workstations completely with SUN workstations to achieve a homogeneous SUN workstation environment as mentioned above.

### 2.3.6 *MULTITOP-MX*

During the first half of 1996 extensive measurements were made with the soft X-ray diagnostic with the newly developed prototype of the MULTITOP-MX computer system, consisting of two powerPC-boards with a Transputer interface (a design by Parsytec, Aachen), and two standard MULTITOP CPU1 cards (with 4 Transputers T800 each). In parallel to the established data acquisition with 128 channels on 16 × 4 Transputers, the new system was used on 20 of these channels to do real-time data analysis in order to determine the highest frequencies in the signals. This permitted a safer way of thinning out the mass of data without running into the aliasing problem of the old system. In many instances it was possible to reduce the data to 10 - 15% of the original amount. The favourable results of the new method (developed by Klaus Hallatschek as part of his Ph.D. thesis) encouraged us to upgrade the new system to four powerPC boards and establish that system as a separate diagnostic which will be connected to the existing one and will control the latter in real-time. Design and testing of the additional components has been completed.

### 2.3.7 *Network enhancements*

Being the medium for all data processing activities, the Internet-like computer network is one of the most important components of the ASDEX Upgrade infrastructure. To overcome recently encountered bottlenecks, two heavily loaded gateway workstations were replaced with FDDI/Ethernet network routers/switches of type 3Com LANplex 2500. So these formerly collisional, multibranched subnetworks were reconfigured into separately switched strings allowing much more efficient access to the backbone. It is planned to use the switching technology for tuning other subnetworks in 1997.

The ASDEX Upgrade project is part of the worldwide Internet via the RZG connection to WIN (WIssenschaftsNetz). A whole bandwidth of 32MBit/s is now available to the Max Planck Institutes at Garching. With WIN also having a strong link to the United States, our Internet connection allows moderate remote participation of national and international plasma physics groups collaborating on ASDEX Upgrade.

## 2.4 Neutral injection

During 1996 the work of the neutral beam group was concentrated on operating the first injector, still the workhorse among the ASDEX Upgrade auxiliary heating systems, as well as on preparing installation of the second injector, scheduled to become operational in autumn 1997. Teststand operation was devoted to optimizing those components which are new on the second injector: RF sources and their RF circuits. In addition, the qualification of a modified extraction system for 100 kV operation was demonstrated.

### 2.4.1 *Operation of the first beam line*

The various physics studies performed on ASDEX Upgrade derived benefit from the reliable operation of the neutral beam injection system. D0 beams of up to 10 MW at 60 kV or H0 beams of up to 7 MW at 55 kV were available for plasma heating. The maintained high level of reliability and availability

is the result of continuous effort in system maintenance and improvements with respect to operational safety and flexibility. A reduced high voltage holdoff capability of one of the ion sources towards the end of the recent experimental campaign was cured by carefully cleaning the PINI structure after removal. Meanwhile, a further ion source was conditioned to full parameters so that a spare source can be put into operation within a short time in case one of the sources fails. From the point of view of system control, further integration into the ASDEX Upgrade real-time control was characteristic of neutral beam operation, which was achieved in co-operation with the control group. Beam timing is now routinely incorporated into the ASDEX Upgrade shot programme. This allows neutral beam heating to be part of an event-triggered shot control. On the basis of the beam power signal as control input, the total power injected during one shot can be on-line monitored and limited, a feature which was introduced in order to prevent overloading of divertor plates during the recent W-coated divertor campaign. Further plans in this direction include compensation of dripped ion sources, i.e. a source which is lost due to too many breakdowns will be replaced by another source during a shot, as well as feedback control of the neutral beam power. A further characteristic of neutral beam operation during the last experimental period was a broad variation of beam parameters. Extraction voltages $U_{ex}$ = 30 - 60 kV were required in order to adjust the heating profile for the studies of dimensionless scaling. Changes from D0 to H0 beams were asked for on a shot-to-shot basis. Finally, on/off modulation of the beam voltage was widely used in order to vary the averaged beam power during one shot in much smaller steps than those given by the power per source. Beam operation with widely varying parameters is greatly facilitated by the shot library capability of the control system, which allows us to load all parameters of previous shots stored in this library.

### 2.4.2 *100 kV source tests*

The work at the teststand during the first half of the year was devoted to the 100 kV operation of a PINI with increased gap setting (8 -> 14 mm). This was necessary in order to qualify the otherwise unchanged grid support structure for the increased voltage and launch the manufacture. To prepare the teststand for this new level of high voltage, a number of components in the high-voltage cell have been replaced by parts already in house for the second injector. After the PINI was conditioned to the nominal parameters of 55 kV, 90 A, the gap setting was changed. Conditioning without beam from 55 kV to 100 kV was obtained within 100 pulses. The conditioning with beam was more complicated because only deuterium operation (which is not possible on the unshielded teststand) yields perveance match at 100 kV, 65 A (power supply limit) and acceptable power loading to the beam line components. Hydrogen beams at 100 kV with 40% off perveance, He beams with 100 kV, 65 A at perveance match but modulated to reduce the average power and H2/Ar beams at 100 kV, 30 A with perveance match were therefore produced for qualification. With all three mixtures reliable operation was obtained, sometimes even 5 s long pulses without breakdowns. It was therefore decided to launch manufacture of the second set of PINIs with unchanged grid support structure. During the second half of the year, a number of minor modifications were investigated for the preparation of the series RF sources for ASDEX Upgrade: Several options for the RF/HV transformer (type of ferrites and cooling, position on high potential or on earth, distance from the source), effect of the RF cable length on the matching, various types of Faraday shields, various snubber configurations etc. The results of these ongoing experiments will determine the configuration of the series sources, which will be put into operation starting in May 1997.

### 2.4.3 *Installation of the second beam line*

The preparations for the second injector proceeded well in 1996 and the installation of the auxiliary equipment is nearly complete: The main transformer is connected and the Ti evaporator power supplies are commissioned. The four cooling systems for the RF generators and the HV modulators were assembled and put into operation. The generators of the RF ion sources were delivered and installed. They have been successfully operated at the full specified RF power (125 kW regulated) into an ohmic test load. The HV circuits are complete and the commissioning of the four HV modulators is under way. A simplified air-core-coil based snubber (to suppress transients after HV breakdowns within the grid systems) was developed in co-operation with the University of Braunschweig. The results of tests will decide whether the small, lightweight air-core-coil snubber can be used instead of the more expensive and heavy iron-core-type snubbers of the first injector. The SIMATIC-based control system and the data acquisition of the injector were designed to be as identical as possible to the systems of the first injector and can be operated completely independently. Hard- and software to control the second injector with its subsystems and all bus connections are qualified to start commissioning of the injection system. All the hardware of the data acquisition system (workstation, CAMAC modules) is operational. The numerous modules for the frequency-based transmission of the diagnostic signals are tested and installed. The vacuum box was delivered to IPP in October 1996 and has been moved to a separate assembly site for preassembling to minimize the time for the activities in the torus hall with its restricted access. The box is meanwhile equipped with the main external and internal components (turbomolecular pumps, ion dumps, calorimeter, deflection magnet, Ti-pumps etc.). The conventional pumping system was put into operation and extensively used for leak-testing the box and its components. After completion of the external wiring, the box will be moved into the torus hall to its final position. The injector environment is complete and allows us to proceed immediately with the final cabling and piping of the box. Vacuum operation and cooling of the box provided by a low- and a high-pressure cooling system should be possible at the end of March 1997. Concerning the five series RF sources, all parts have been ordered and are partly delivered. The first RF source should be ready for conditioning and acceptance procedure on the teststand in May. The complete RF system of the injector (RF sources, generators, RF circuits) should be tested in July 1997. Beam operation is scheduled to start in late summer to get the system ready for first injection experiments in October 1997.

## 2.5 Ion Cyclotron Resonance Heating

The technical development work continued its main emphasis on methods to reduce the effect of plasma variations on the RF technical system:

The advantages of "3 dB hybrid" applications in ICRF systems were investigated in a test setup on ASDEX Upgrade. Such elements can reduce the effects of load variations by leading reflections into a dummy load. Two antennas and generators were combined with two hybrids, kindly loaned to us by JET. The first one combines the power of two gererators, the second one distributes this power to the two antennas. Since the different characteristic impedances of the systems (hybrids from JET 30 Ω, transmission lines at ASDEX Upgrade 50 Ω) had to be compensated by $\lambda/4$ transformers, the frequency range was limited to 30 MHz. The tests showed that a much larger heating power can be achieved more reliably: A generator power of $2\times1.8$ MW was reached with hybrids, corresponding to about $2\times1.6$ MW deposited in the plasma; without hybrids less than $2\times1$ MW would have been possible under similar matching conditions (VSWR of about 2). This corresponds to an increase of the power to the plasma, for the systems equipped with the hybrids, from 50% to 80% of the installed generator power. Furthermore, reflection peaks due to ELMs are largely compensated if the impedances of the two antennas are comparably matched /730/. On the basis of this success, it is planned for 1997 to equip all 4 ICRF systems with hybrids.

Arc protection systems have usually been triggered so far by high reflections, which also occur in the case of large antenna coupling variations, e.g. due to ELMs. On the other hand, the reduced reflection levels in hybrid circuits reduce the reliability of reflection-based safety systems. So the development of the alternative arc detection method using a frequency band below the ICRF /357/ has been intensified (it has already been described in the last annual report, Technology Division.). Successful tests allow its routine application in the next experimental period. In the event of failure, it will be backed-up by the former reflection-based system, only triggered with some delay if the power had not been cut off.

The power-reducing microcomputer circuitry (described in the last annual report), which allows stable operation to be maintained even during high reflections and ELMs, has been further improved and is being routinely applied. Even in hybrid circuits it may be further required in extreme conditions, e.g. with strong asymmetric mismatching. Its function has been extended to interrupt also the power triggerd by the new arc detection.

Frequency Sensitive Matching has been applied at limited heating power. These tests showed that all antenna impedances occurring in ASDEX Upgrade could in principle be matched by varying the frequency alone, and that this could be done fast enough to cope with ELMs /481/. But this was found to require not only a larger bandwidth of the generators but also prematching elements close to the antenna, in ASDEX Upgrade only possible at frequencies around 30 MHz due to the unavoidable antenna feeding length.

The first few tests with an antenna coupling feedback via the plasma condition showed that this method can simplify the ICRF operation, but that for some plasma conditions its influence is small. Further development work on this task is needed.

Frequency changes have so far requird typically one week due to a 25/50 Ω transition in the transmission line and a fixed stub near the antennas, which had been used for prematching and whose position had to be readjusted to a new frequency with great mechnical effort. Experience with matching and voltage strength now allowed us to remove both and use only one characteristic impedance of 25 Ω for the lines between the antennas and matching elements. This modification will be completed for the next experimental period, thereby allowing frequency changes within typically one day.

## 2.6 Electron Cyclotron Resonance Heating

An electron cyclotron resonance heating system with f = 140 GHz, P = 2 MW and T = 2 sec is under construction. The power will be generated by 4 gyrotrons and transmitted via 4 transmission lines to 4 ports of the vacuum chamber. The polarization can be changed, but the primary mode of operation will be the second-harmonic X-mode because of its highly localized absorption.

Up to now 2 transmission lines (partly mirrors and partly HE11 waveguides) are installed, of which one was used for preliminary experiments with a 0.5 MW/0.5 sec gyrotron. This gyrotron and its control system worked quite reliably. It was mainly used for heat wave experiments, described later in this report. The RF-beam is focused in order to achieve very localized power deposition even in cases with poloidal beam deflection.

Meanwhile 2 of the 4 final gyrotrons have been delivered and tested. One of them broke down during the acceptance tests at IPP (after successful factory acceptance tests) and had to be rejected. The other tube reached the design value of 0.5 MW in the Gaussian mode for 2 sec as its nominal regime of operation, as well as 0.7 MW for 1 sec as an optional regime at slightly increased cathode heating and beam current. The frequency of this gyrotron drops during the first 100 msec by about 500 MHz and then assumes a constant value of 139.5 GHz. Since this gyrotron is a diode-type tube, its power can be varied merely by changing the beam voltage. Stable operation is possible in the range from 50 to 500 kW. This allows modulation of the output power, which was verified for frequencies up to 20 kHz, as necessary for experiments on the stabilization of MHD modes.

The existing two transmission lines are now being modified to handle the longer pulse length. The subsidiary power supplies, the magnets and the control system are now being prepared to run two gyrotrons via one high-voltage modulator unit. Here, however, we still face the problem of avoiding an initial beam current peak while maintaining a sufficiently fast rise time for the modulation and keeping the beam overcurrent protection at a tolerable level.

Construction of the launching mirrors, transmission lines and gyrotron controls for the remaining two tubes is going on. The

second high-voltage modulator is ready for use. An automatic liquid-nitrogen filling system for the cryo magnets will be installed in the near future.

We expect to have two gyrotrons available for experiments in summer 1997 and install the next two tubes by the end of 1997.

# 3. CORE PLASMA PHYSICS

## 3.1 Operational Aspects

The rate of failure concerning the setup of an experimentally useful plasma could be drastically reduced during the reported operation period. The problems regarding this had arisen due to the additional currents in the Passive Stabilization Loops (PSL) necessary to avoid arcing across the PSL bridge, which on the other hand, strongly disturb the magnetic configuration for the initiation phase. To deal with these problems, an extended and systematic exploration of the early phase of the plasma current initiation and setup was carried out. Though the applicability of most standard diagnostics is limited during this early discharge phase, some notion of the essential processes could be gained and confirmed.

Due to the magnetic configurational conditions, which were identified in detail by the specially developed VAMP[2] identification code, the gas breakdown by the inductively applied loop voltage happens in the presence of a still substantial amount of vertical field opposite in direction to that required for an equilibrium. The plasma produced is therefore connected to the vessel wall along field lines and the initiating current follows these field lines many times around the torus. Finally, it passes, as measurable halo current, protruding parts of the inner vessel wall such as the divertor plates, which then act as electrodes for the discharge. The total plasma current reaches a sort of saturation at about 50 kA and the current density far exceeds the ion saturation current. An electron-yielding process on the cathode surfaces, known from other comparable plasma devices as "pre-arcing", must be assumed. This also becomes noticeable on video images of a high-speed CCD camera as an intense glow near the divertor plates serving as cathode .

The bolometer measurement of the total radiated power and the line density measurement by the DCN interferometer of the resulting discharge plasma in this phase indicate a power and particle balance which is dominated by recycling processes on the vessel walls and the divertor plates as electrodes. A substantial part of the power and particles involved seems to leave the plasma and reach the wall by or as atomic hydrogen. The initial wall conditions thus gain a decisive influence on the impurity and particle content of the early plasma and hence on the further fate of the discharge. The conditions established at the end of this phase, when the applied vertical magnetic field reaches its final sign and magnitude and provides a totally magnetic confinement will decide whether the supplied ohmic power will suffice to overcome the radiation barrier and the plasma current reaches its required growth rate.

The continuous recording of the gaseous inventory of the vessel wall (by observing the decay of the hydrogen content of the exhaust during the intershot glowing) and the corresponding choice of the prefill density and of the intershot glowing strategy, on the one hand, and minimizing the duration of the cri- tical discharge phase by a suitable gas filling programme on the other, finally led to the initially mentioned improvement of the plasma setup record.

## 3.2 Confinement and Transport Studies

### *3.2.1 Global confinement*

The L- and H- mode confinement properties were compared, in particular at high density, with and without radiative edge. Fig. 3.1 shows the reaction of the L- and H-modes to density increase by gas puffing. In such experiments, the neutral pressure in the divertor seems to be a useful technical parameter for the analyses. Whereas the L-mode is not influenced by the neutral gas pressure, the H-mode confinement is degraded. Physical reasons, which might be changes of density, temperature, $\beta$ and/or $\nu_*$ at the edge, are still under investigation. The highest H-mode points in Fig. 3.1 ($f_H$ = 2.0 - 2.2) are from discharges with somewhat higher averaged triangularity (0.2 instead of 0.1). However, the plasma shape in these cases simultaneously causes particularly low pressure and the influence of each effect could not be separated so far. The difference between L-and H-mode is attributed to the fact that the H-confinement is governed by the edge transport barrier, which is sensitive to conditions in this region.

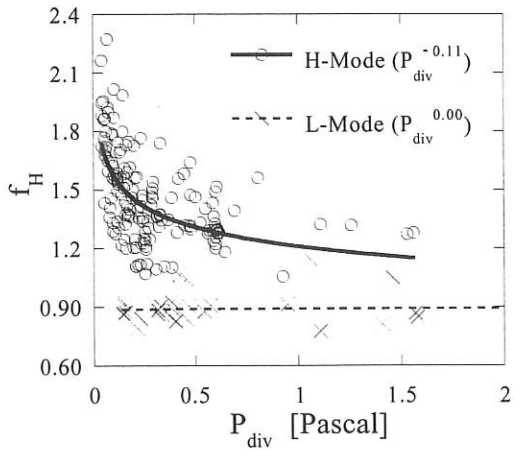


*FIG. 3.1: Enhancement factor relative to L-mode scaling ITER89-P versus divertor pressure (lines are fits).*

Operation at high density with radiative edge provided the

[2] The VAMP (VAcuum Magnetic field Prediction) code is a numerical procedure (without plasma current contribution) for vacuum magnetic field calculation in ASDEX Upgrade at discharge times between 10 ms and ≃ 80 ms. All external (V1, V2 and V3) and PSL currents contribute with their measurement value, whereas reactive currents in the vacuum chamber are optimized for best fit of an optional group of flux loop and magnetic coil measurements.

Completely Detached H-mode, in which $f_H$ reaches 1.6 because the degrading effect of the necessary high neutral pressure is compensated by peaking of the electron density profile. In L-modes with edge radiation density peaking also occurs and L-confinement approaches that of the H-mode.

### 3.2.2 Transport in dimensionlessly similar discharges

By the scale invariance approach to confinement scaling the thermal diffusivity can be expressed as a power law of the normalized gyro-radius $\rho_*$ in a dimensionally correct form as $\chi = \chi_B \rho_*^a F(\nu_*, \beta$, q shape, ... (Eq. 1),

$$\chi = \chi \rho_*^a F(\nu_*, \beta, q, \text{shape}, \ldots) \qquad (1),$$

$\chi_B \sim T/B_t$, collisionality $\nu_* \sim qn/T^2$ and normalized pressure $\beta \sim nT/B_t^2$ (minor radius a, safety factor q. plasma density n, electron or ion temperature T, magnetic field $B_t$). If the scaling with $\rho_*$ is known, then the transport behaviour of existing experiments can be scaled to larger ignition devices having similar q, $\nu_*$ and $\beta$, even without a complete understanding of the process of turbulent diffusion. The exponent $\alpha$ of $\rho_*$ can be interpreted as an indication of the characteristic turbulence wavelength $\lambda$: a) $\alpha$ = 1 ($\lambda \sim \rho_g$ gyro-Bohm); b) $\alpha$ = 0 ($\lambda \sim a$ Bohm); c) $\alpha$ = -1 ($\lambda \gg a$ stochastic); d) $\alpha$ = -1/2 (Goldston).

The confinement scaling with $\rho_*$ was examined in L and H "dimensionlessly similar" discharges by varying just $\rho_*$ while keeping all other dimensionless parameters fixed. To keep $q, \nu_*$ and $\beta$ constant, the relations $I_p \sim B_t, n_e \sim B_t^{4/3}$ and $T \sim B_t^{2/3}$ must be fulfilled and the power requirement scales as $B_t^{(5-2\alpha)/3}$, depending on the transport model.

The global analysis of the L-mode series showed $W \sim B_t^2$ with the power requirement of the Bohm model. The local analysis reveals the constancy of the $\beta$ and $\nu_*$ profiles ($\nu_* \approx$ 0.3 at r/a = 0.5) over a large part of the cross-section. The ratio of the local thermal diffusivities, $\chi_{eff}$, are in agreement with the Bohm model prediction for 0.3 $\leq$ r/a $\leq$0.8. Due to the high density, electron and ion channels could not be resolved and $\chi_{eff}$ was used. It can be clearly concluded that confinement scales as Bohm-like for this L-mode series, as observed in other tokamaks. The H-mode scans (steady-state with type-I ELMs) were performed in $H^+$ and $D^+$. It was not possible in any of these scans to achieve the $W_{th} \sim B_t^2$ dependence exactly by applying the power required by eeither gyro-Bohm, Bohm or Goldston assumptions.

The local demands on $\beta$ and $\nu_*$ for dimensionless similarity were achieved for only one pair (3T/2T) in $D^+$, out of 18 discharges. The local analysis of this pair reveals the constancy of $\beta$ and $\nu_*$ profiles ($\nu_* \approx 0.1$ at r/a = 0.5) in the region $0.3 \leq$ r/a $\leq 0.8$. Comparing $\chi_{eff}$ yields a gyro-Bohm behaviour of the local thermal transport. However, the heating power for this pair was between the Bohm and Goldston models.

This apparent discrepancy between the global and local results for this pair is caused by the differences in the heating profiles, despite the attempt to keep the heating profiles constant by varying the acceleration voltage. This was demonstrated in a transport simulation of the 3 T shot, taking as starting point the $\chi_{eff}$ profile of the 2 T shot and extrapolating it to 3 T under a gyro-Bohm assumption. Using the density and power deposition profiles at 3 T yields calculated temperature and $\chi_{eff}$ profiles in excellent agreement with the experimental ones.

The confinement deterioration caused by gas puffing described above also affects the $\rho_*$ experiments. When comparing discharges with $B_t$ = 2.5 T at the same heating power, line-averaged density and plasma current, distinct differences in confinement are found. No additional loss channels or other hidden parameters influencing the confinement in the whole set of scaling experiments could be identified. These shots, however, had different neutral gas pressures. The increasing neutral density causes lower temperature and higher density at the edge, which obviously leads to degraded confinement both at the edge and in the core. In the experiments, such behaviour s in conflict with the demands of dimensionless scaling.

### 3.2.3 Perturbative transport

#### 3.2.3.1 Temperature rise within the ECRH power deposition zone

The time evolution of the electron temperature inside the deposition zone and in the very close vicinity contains information on the width of the deposition profile, on the local electron heat conductivity and on the local damping. We assume a locally homogeneous plasma and fit the analytic result of the one-dimensional linearized electron heat diffusion equation to the experimentally measured time evolution of the electron temperature (ECE radiometer). This was done in ohmic phases when the plasma current reaches its flat top, so that sawtooth oscillations had not yet set in. The density in these shots was in the range 2.5 to 4 $10^{13}$ cm$^{-3}$. The location of the deposition was changed from r/a = 0.25 to r/a = 0.8 by poloidal deflection of the focused RF-beam. The deduced values of the electron heat conductivity are in the range 0.7 to 0.8 m$^2$/sec, lower than, but close to the values obtained from power balance or heat wave analysis outside the deposition zone. Higher values are obtained near the edge of the plasma. The damping term is in the range 0.05 to 0.1 msec$^{-1}$, as estimated on the basis of the decrease of the local ohmic heating and of the increasing electron-ion heat exchange.

#### 3.2.3.2 Heat pulse propagation for ECRH modulation and sawteeth

Comparison of transport coefficients obtained from power balance and perturbative experiments, which are per definition different, is expected to improve understanding of transport physics. We studied the electron heat conductivity ($\chi_e$) using sawtooth ($\chi_e^{ST}$) and ECRH modulation ($\chi_e^{ECRH}$) heat pulse propagation.

With the recently installed ECRH system we performed on/off power modulation with on-axis or off-axis deposition and frequencies between 10 Hz and 1 kHz. The sawtooth and ECRH modulation we studied were in ohmically and NBI-heated L-mode plasmas. The plasma current, magnetic field, density and working gas ($H^+$ or $D^+$) were varied to achieve a wide

range in $\chi_e$. The analyses were made with a Fourier transform interpreted in a slab model with geometrical corrections, for both sawtooth and ECRH modulation data. For our ECRH modulation scheme (50% duty cycle), the Fourier frequency spectrum of the temperature shows the odd harmonics and no even harmonics, suggesting the absence of nonlinear reaction of the plasma to the modulation. Both for sawteeth and ECRH, $\chi_e$ does not depend on the modulation frequency, excluding a temperature dependence of $\chi_e$. In Fig. 3.2 we compare $\chi_e^{ST}$ and $\chi_e^{ECRH}$ with $\chi_e^{PB}$. The analysis of sawteeth yields $\chi_e^{PB} \leq \chi_e^{ST} \leq 6\chi_e^{PB}$ and shows no correlation at all between $\chi_e^{ST}$ and $\chi_e^{PB}$. In contrast, for the ECRH modulation experiments Fig. 3.2 clearly shows that $\chi_e^{ECRH}$ is at most 2 times as large as $\chi_e^{PB}$. This is in agreement with the assumption $\chi_e \propto \nabla T_e^{\alpha}$ with $\alpha \leq 1$.

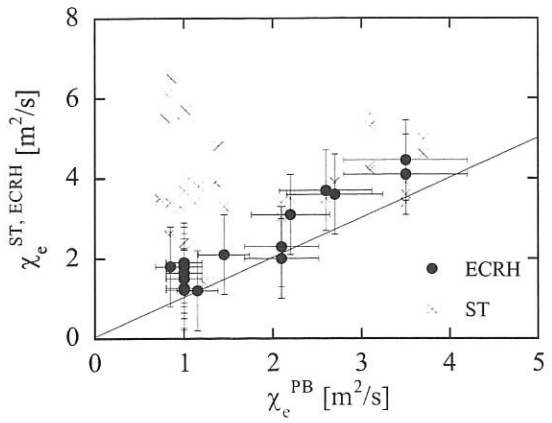


*FIG. 3.2: $\chi_e^{ST}$ or $\chi_e^{ECRH}$ versus $\chi_e^{PB}$ for ohmic and L-mode discharges. ($\chi_e^{PB} \geq 2$ m$^2$/s from discharges in hydrogen, the line is the 1-to-1 line).*

Generally, $\chi_e^{ST}$ is larger than $\chi_e^{ECRH}$. This is attributed to the size of the perturbation, which can be large (up to 400 eV) for sawteeth compared to at most 70 eV for ECRH modulation. This is related to the fact that the maximum modulated ECRH power was 400 KW, whereas the power liberated within a sawtooth crash (duration $\approx$100 $\mu$s) can reach 10 MW in NBI-heated plasmas, in which the largest $\chi_e^{ST}$ values are observed. We find a clear correlation between $\chi_e^{ST}$ and the amplitude of the perturbation for sawteeth, but no correlation for ECRH. We therefore conclude that the results from ECRH modulation are closely related to the steady-state transport. This is generally not the case for the sawteeth, for which other phenomena, seemingly linked with the sawtooth amplitude, probably play a role.

ECRH modulation experiments were modelled with the ASTRA transport code. For (r/a $\leq$ 0.7), good agreement with the data is obtained with $\chi_e$ profiles having values higher than $\chi_e^{PB}$. However, the power balance and ECRH modulation can be simultaneously well simulated by introducing a $\nabla T_e$ dependence of $\chi_e$. Agreement at the plasma edge (r/a $\geq$ 0.7) requires outward heat flux or a non-local transport model. It was, however, not possible so far to differentiate between the two possibilities.

#### 3.2.3.3 *Particle transport determined from density modulation experiments*

The particle transport coefficients are determined from Thomson scattering data through modulated gas puff experiments. The transport equation is solved for certain values of the transport coefficients, after which these coefficients are adapted by a nonlinear fitting procedure until the solution of the equation fits well to the data. The smoothest profile of the coefficients allowed by the measurements is found by a first-order regularization. The particle diffusion coefficient and pinch velocity increase towards the plasma edge.

The transport coefficients for shots in which the working gas is deuterium are much smaller than those with hydrogen. The observed temperature perturbation, which increases as it propagates towards the plasma centre, can be explained mostly by the convective heat flow connected with the particle flow.

### 3.2.4 *Transport modelling of ITER and ASDEX Upgrade*

A comprehensive scaling law for the effective heat diffusivity $\chi_{eff}$ in high-density ELMy H-mode plasmas has been developed which is compatible with the ITERH92-P ELMy scaling of the global energy confinement time. Model validation tests against three JET and three DIII-D discharges from the ITER Profile Database and against ASDEX Upgrade discharges were carried out. The scaling relation for $\chi_{eff}$ predicted the energy confinement time with an accuracy of about 10%. Moreover, the computed electron and ion temperature profiles were found to be close to the measured ones. The local scaling law was applied in simulations of high-density radiative mantle scenarios of the ITER IDA device with flat and peaked density profiles. It predicts an energy confinement time of 6.8 s compared with 6.0 s anticipated by the global scaling law. These confinement times have to be distinguished from the energy confinement time required for steady-state operation of ITER at the design parameters, which was found to be 4.8 s. A model of the neoclassical impurity transport was implemented in the code and was used in transport analyses of ASDEX Upgrade discharges with neon and argon puffing and in simulations of ITER.

### 3.2.5 *Linear $Z_{eff}$ scaling of the anomalous inward drift*

The origin of density profile peaking due to impurity puffing and the anomalous particle pinch were explored by computer simulations with special versions of the BALDUR 1.5-D predictive transport code. Transport analysis of high-density ASDEX Upgrade H-mode plasmas with strong neon puffing and density profile peaking yielded a new scaling law for the anomalous inward drift velocity, $v_{in}(x) = C_v 2x D(x)/(\rho_w x_s^2)$, with $C_v = F Z_{eff}(x)$, where $D$ is the diffusion coefficient. This scaling implies that $v_{in}/D \propto Z_{eff}$ and results in $v_{in} \propto Z_{eff}$, since $D$ is found to be independent of this parameter. The strong density profile peaking is caused by the increase in $Z_{eff}$ and by an enhanced factor $F$ discovered during neon puffing. The time evolution of $F$ correlates with the neon influx rate, but not with the neon content and the power losses due to line radiation and ionization. The factor $F$ was found to rise with growing influx

rate and depend non-locally on the region where inelastic collisions prevail. One plausible mechanism for the enhancement of $F$ is that inelastic collisions between fluctuating electrons and impurity ions change the dissipative part of the fluctuating electron distribution.

## 3.3 H-mode Threshold and Local Edge Parameters

As H-mode physics is strongly connected with the plasma boundary (by the creation of a confinement barrier connected with sheared poloidal rotation at the edge), it is natural to expect that the H-mode transition is governed by local edge parameters. The importance of $T_e$ at the edge as a key quantity was early recognized shortly after the discovery of H-mode[3]. Diagnostics development for edge profile measurements now makes it possible to derive local parameter scalings of the H-mode threshold. The influence of the electron density is demonstrated by a pair of discharges with different gas puffing but otherwise identical plasma parameters (Fig. 3.3).

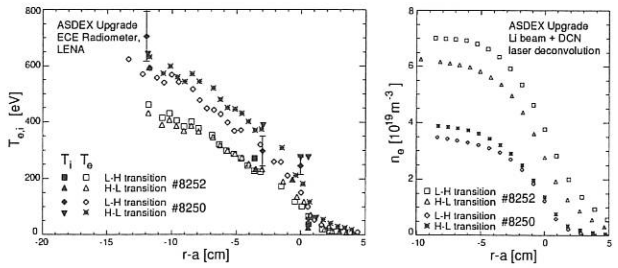


*FIG. 3.3: Electron density and temperature profiles at the time of the L-H and H-L transitions at two different densities. With increased $n_e$, the edge temperature at the transition decreases. No significant hysteresis between L-H and H-L transitions is observed in $T_e$.*

Duty-cycle-modulated NBI is used to increase the heating power in steps of 0.4 MW in order to achieve slow transitions with small power in excess over the H-mode power threshold. The electron density and temperature profiles shown in the figure are measured by the lithium beam method and an ECE heterodyne radiometer, respectively. LENA measurements of the edge $T_i$ profile, though having limited accuracy and spatial resolution, indicate that, at the edge, $T_i \approx T_e$ in the density range encountered. From this comparison it can be seen that the critical edge temperature for the H-mode transition decreases slightly but significantly with increasing edge density. No significant hysteresis in $T_e$ between the L-to-H and H-to-L transitions is seen, in contrast to the familiar hysteresis in heating power.

In order to find a local scaling of $T_e$ at the threshold, one has to select a radius at which the measurements are to be taken. We select a position of $r = a - 2$ cm near the boundary, which is inside the transport barrier region to be formed after the transition but sufficiently distant from the separatrix in order to avoid $T_e$ being solely determined by SOL transport. It is found that, apart from the dependence on $n_e$, $T_e^{\rm crit}$ depends on $B_t$ and, in contrast to the global power threshold scaling, on $I_p$ as well. From all well-diagnosed deuterium discharges with favourable grad-$B$ direction (grad-$B$ towards the X-point) conducted on ASDEX Upgrade during 1996, we can infer the dependences of $T_e^{\rm crit} = 145 \times n_e^{-0.3(+0.2-0.1)}\, B_t^{0.8(+0.2-0.1)}\, I_p^{0.5(\pm 0.2)}$ (see Fig. 3.4), where $T_e^{\rm crit} n_e, B_t, I_p$ are measured in units of eV, $10^{19}$ m$^{-3}$, T, and MA, respectively. Both $T_e^{\rm crit}$ and $n_e$ are measured at $r = a - 2$ cm. It is remarkable that type III-compound ELMs (type III ELMs followed by a brief L-mode phase, marked in the figure by asterisks) coincide with the $T_e$ threshold although originally not included in the analysis.

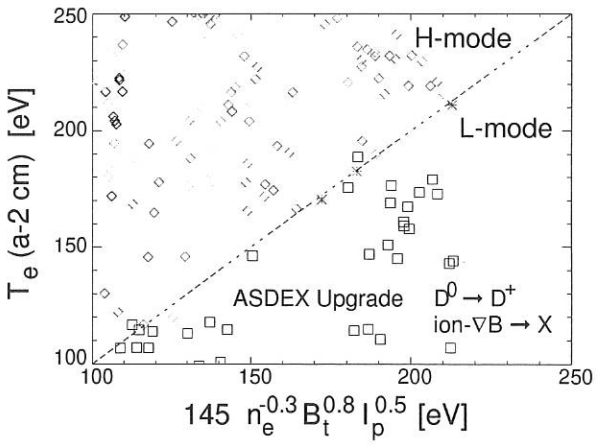


*FIG. 3.4: Scaling of $T_e^{\rm crit}$ ($r$ = $a$ - 2 cm)at the H-mode threshold for discharges in deuterium with favourable gradB direction.*

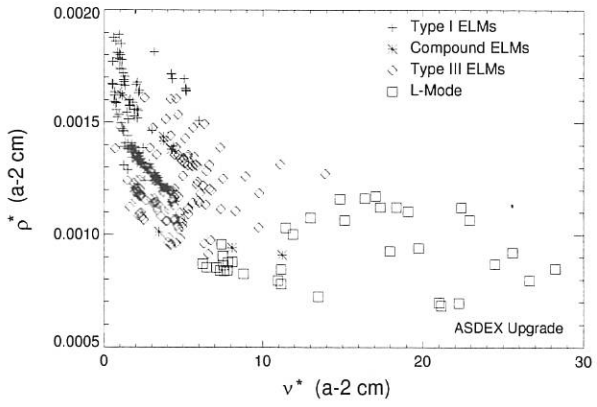


*FIG. 3.5: $\rho_*$ vs. $\nu_*$ at the plasma edge around the H-mode transition. Data are taken at r = a - 2 cm.*

For inter-machine comparisons as well as to test H-mode models, it is useful to express the threshold scaling in dimensionless parameters. We arrive at the relation $\beta^{-0.475}\nu_*^{0.175}\rho_*^{-0.35}$ const., where all dimensionless quantities are calculated using $T_e$ and $n_e$ at $r = a - 2$ cm and assuming $T_e = T_i$. This scaling is dimensionally correct in the sense that no explixit $R$-dependence of $T_e$ is required to obtain the dimensionless form. The size scaling can be checked only by inter-machine

[3] (Wagner, F. *et al.*, J. Nucl. Mater. **121**, 193 (1984))

comparisons. Note also the weak dependence of the H-mode threshold on edge collisionality $\nu_*$. We can plot edge $\rho_*$ vs. $\nu_*$ to characterize the range encountered (Fig. 3.5). While there is little variation in $\rho_*$ at the transition, the L-H transition is observed in a range of $\nu_* = 5 \ldots 15$. This observation indicates that most transitions take place in the Pfirsch-Schlüter or collisional regime (as $\nu_*$ increases towards the edge) and the threshold does not rely on a fixed value of $\nu_*$.

## 3.4 Impurity Transport in Highly Radiating Discharges

The key parameter for the efficiency of radiative cooling is the central $Z_{eff}$ increase for a given increase of radiated power. This parameter depends on the impurity transport in the plasma bulk which was investigated for H-mode discharges with high-power neutral beam injection and neon as radiating species. Impurity profiles observed in ASDEX Upgrade are typically flat and the above parameter is an accordance with a simple dependence found in a multi-machine comparison conducted at JET: $\delta P_{rad}/\delta Z_{eff} = S\bar{n}_e^2/7[MW, \mathrm{m}^2, 10^{20}\ \mathrm{m}^{-3}]$. However, CDH-mode discharges show a strong tendency to lose sawtooth activity, and in these cases impurity peaking in the plasma centre is observed.

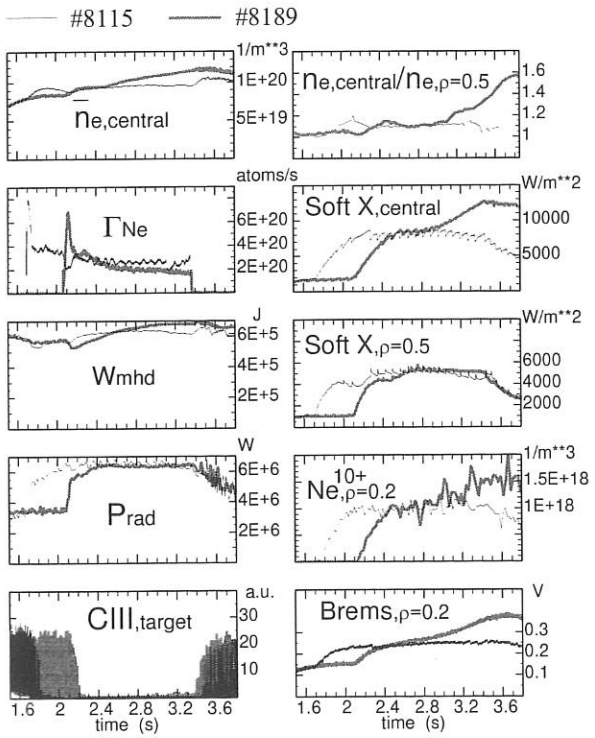


*FIG. 3.6: Comparison of two CDH-discharges with different central transport behaviour.*

This is demonstrated in Fig. 3.6, showing a comparison of two CDH-mode discharges. Both discharges have a safety factor $q_{95} = 4$, constant NBI heating with $P_{NI} = 7.5$ MW and feedback-controlled neon puff rate $\gamma_{Ne}$ to reach a constant power fraction $P_{rad}/P_{heat} \approx 0.9$. With the increase of $P_{rad}$ the plasma detaches from the target plates, as indicated by the CIII signal measured directly above the outer target plate (CDH-mode). About 0.4 s after the onset of the CDH-mode #8189 loses sawtooth activity and the bulk transport for the two discharges becomes very different. The electron density profile, represented by line-averaged values of a central line-of-sight and the density ratio $n_{e,central}/n_{e,\rho=0.5}$, remains constant for #8115, while it peaks for #8189. The soft X-ray time traces of a central chord and a chord with $\rho_{pol,tan} = 0.5$ stay nearly constant for #8115 and show strong peaking for #8189. Modelling with the STRAHL impurity transport code showed that this strong peaking of the soft X-ray profile for #8189 is caused by central accumulation of neon. Some indication of this is also given by the density of the fully ionized neon at $\rho_{pol} = 0.2$ measured by charge exchange recombination spectroscopy and by visible bremsstrahlung measurement on a chord with $\rho_{pol,tan} = 0.2$. The stored energy $W_{mhd}$ reaches higher values in the case of peaked electron and impurity density profiles (#8189).

In H-mode sawteeth are always found to suppress central peaking of the electron density and neon, while the lack of sawteeth always leads to peaked profiles. When reaching high levels of radiated power fraction the plasma is very close to the limit of sawtooth instability. For L-mode the database is not very large, but here sawteeth were always present. Triggering of sawteeth by central ICRH heating could not be clearly seen for the heating powers reached so far ($\approx 500$ kW). The bulk transport of neon in different H-mode regimes was determined from the evolution of measured $Ne^{10+}$ density profiles by analyzing the dependence of radial particle fluxes on radial density gradients. The analysis makes the assumption of zero sources and can only be applied to the inner part of the bulk up to a poloidal flux label of $\approx 0.8$.

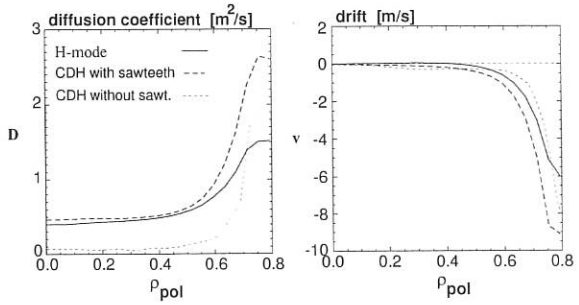


*FIG. 3.7: Impurity transport parameters for neon determined from CXRS measurements during gas puff experiments. In CDH-mode without sawteeth the central diffusion coefficient is strongly reduced. For the other two regimes D represents time-averaged values over sawteeth.*

In Fig. 3.7 the diffusion coefficient $D$ and drift velocity $v_d$ for three different regimes are plotted versus the poloidal flux label $\rho_{pol}$. The analysis gives time-averaged values for $D$ and $v_d$ including the effects of sawtooth crashes on the impurity profiles. For sawtooth-free CDH-mode discharges the central $D$ is strongly reduced. The peaking of the impurity density in these discharges occurred inside $\rho_{pol} \approx 0.5$ where $D$ is very low and even small inward drift velocities lead to a

large peaking factor. Analysis with STRAHL showed that the central transport parameters agree within ±50% with neoclassical predictions, which take only the friction of impurity with deuterium into account.

## 3.5 MHD Stability

### 3.5.1 $\beta$-limit studies

Future fusion reactors, to operate economically, require high stored energy and thus a high value of $\beta = 2\mu_0\langle p\rangle/B^2$. Assuming Troyon scaling, the MHD $\beta$-limit, expressed in terms of beta normalized $\beta_N = \frac{\beta}{I/(aB)}$, is independent of the safety factor q. In ASDEX Upgrade, for q≥3 the maximum achievable $\beta_N$ shows only a weak dependence on q, but for q≤3 drops from approximately 3 to 2 for q approaching 2. DIII-D proposed to extend the Troyon scaling by including the internal inductance $l_i$ to account for the dependence of the $\beta$-limit on the shape of the current profile. In ASDEX Upgrade more peaked current profiles have been obtained by current ramp-down, resulting in an increase of $l_i$ and transiently achieving values of $\beta_N$ as high as 4.5. As shown in Fig. 3.8, including $l_i$ in the Troyon scaling also accounts for the $\beta$-limit cases obtained in current ramp-down experiments.

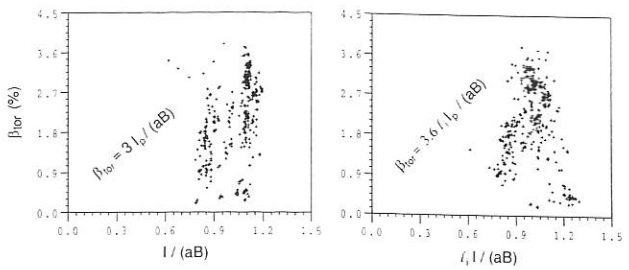


*FIG. 3.8: Plot of $\beta$ versus the normalization I/(aB) (left) and I/($l_i$aB) (right).*

MHD stability calculations with the ERATO code predict ideal kink stablility for $\beta_N \leq 4.3$ without, and $\beta_N \leq 3.7$ with wall stabilization. Since also the pressure gradients are usually below the ideal balooning limit, except at the plasma edge, where the balooning limit is linked to the occurrence of type I ELMs, ideal MHD cannot explain the limit of $\beta_N \leq 3.3$ usually observed in experiments without increased $l_i$. Thus resistive effects have to be considered.

There is strong evidence that q>1 tearing modes ((4/3) and (3/2)), which often develop at the $\beta$-limit, are of neoclassical origin, i.e. they grow nonlinearly due to the loss of bootstrap current in the islands. Firstly, $\delta$B grows linearly in time, which is typical of neoclassical tearing modes, in contrast to a $\Delta$'-driven mode, which grows quadratically. Secondly, the estimated loss of bootstrap current due to the flattening of the pressure profile at the (3/2) surface in a region of 5 cm, corresponding to the saturated island width from Mirnov analysis, is consistent with the helical current required to produce an (3/2) island of just that size. Thirdly, more centrally located tearing modes, such as the (4/3) mode, are usually $\Delta$'-stable for the measured pressure and estimated current profiles. Fourthly, the tearing modes are often triggered by ELMs and sawteeth, which is consistent with the need of a "seed island". Finally, the occurrence of these tearing modes agrees well with the theory of diamagnetic stabilization of neoclassical tearing modes, explaining the dependence on collisionality by taking the necessary seed island width into account.

In some cases $\beta$ is limited by q=1 mode activity only ((1/1) mode and fishbones), but increasing the heating power in these cases also leads to the occurrence of neoclassical tearing modes.

### 3.5.2 TAE modes

Toroidicity-induced Alfvén eigenmodes (TAE-modes) are a field of growing interest for future fusion devices, as they may have a deteriorating impact on the $\alpha$-particle heating. On the one hand, they are excited by the non-thermal fusion born $\alpha$'s by inverse ion Landau damping and, on the other, they can modify the distribution of resonant fast $\alpha$-particles and decrease the self-heating of the plasma. In today's experiments the excitation is mainly analyzed by non-thermal fast hydrogen or deuterium ions created by additional heating.

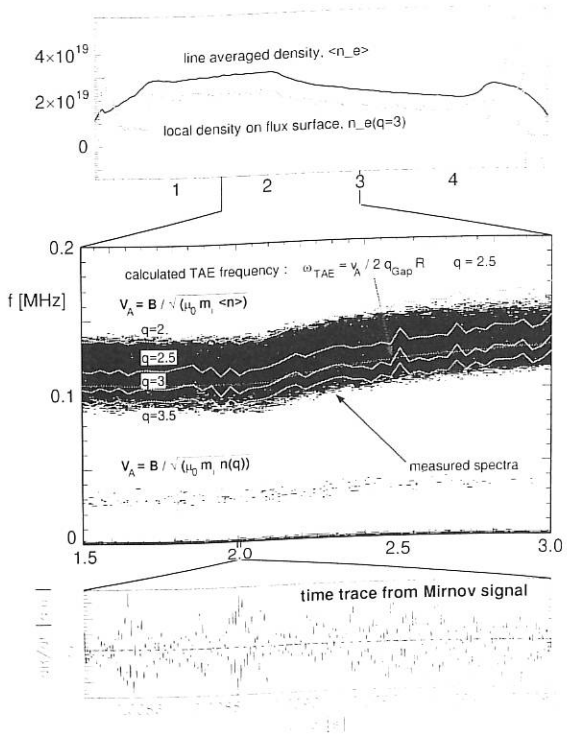


*FIG. 3.9: TAE-mode in an ohmic plasma. The dependence of the frequency spectrum on the density is illustrated. The mode frequencies agree with the TAE frequencies between q=2 and 3.5.*

Other excitation mechanisms for TAE-modes were investigated. The excitation via ICRH beat waves was the most promising approach. When the TAE frequency controlled by the density reaches the beat wave frequency a strong modification of the coupling of ICRH power to the plasma took place, which

may be caused by TAE-modes. However, the results of these experiments are not entirely conclusive.

In ohmic discharges TAE-modes could be observed on the Mirnov and soft-X-ray diagnostics without the presence of non-thermal fast particles (Fig. 3.9). Experimentally the frequencies scale of $f_{observed} \sim B/\sqrt{m_i n_e}$. Assuming TAE-modes in a plasma with $Z_{eff} \approx 1$, the expected frequency is $f_{TAE} = \frac{1}{2\pi}\frac{v_A}{2qR}$. They are observed consistently on both diagnostics in the vicinity of the q=2 surface. Theoretical calculations with the CASTOR resistive MHD code show that TAE-modes are expected in this radial region with the observed frequencies.

As fast non-thermal particles are not present and the modes propagate in the electron diamagnetic drift direction, it is clear that the driving mechanism of the modes has to be correlated with the electrons. Short-wavelength drift Alfvén wave turbulence can be excited if the parallel electric field $E_\parallel$ is determined not only by a scalar potential, as for electrostatic drift wave turbulence, but also by a vector potential $E_\parallel = -\frac{\partial A_\parallel}{\partial t} - \nabla_\parallel \Phi$. From these short-wavelength Alfvén modes the long-wavelength TAE-modes are excited by inverse cascading in three-dimensional MHD. Further theoretical and experimental investigations for understanding and confirming this mechanism are under way.

### 3.5.3 *ELM precursor*

Up to now, steady-state H-mode has been achieved only together with the occurrence of ELMs. To develop a deeper understanding of the destabilization of ELMs, the features of their precursor oscillation was investigated. In counter-injected discharges type I ELM precursors exhibit an oscillation frequency of the order of 20 kHz, whereas type III ELM precursors have an oscillation frequency of the order of 100 kHz. In co-injected discharges type III ELM precursors are shifted to lower oscillation frequencies of the order of 60 kHz, whereas type I ELM precursors can hardly be observed.

These characteristic differences in mode frequency can be explained by the distinctively different spatial mode structure of the ELM precursors. Type I precursors exhibit significantly lower (m,n)-numbers compared to type III ELM precursors. In the lab frame MHD modes roughly rotate with the sum of the diamagnetic frequency $\omega^*$ and the frequency due to fluid rotation $\omega_{\mathrm{rot}}$ driven by neutral beam injection. Thus, the detected signal frequency equals $\nu_{Mirnov} = (m \cdot \omega^* \pm n \cdot \omega_{rot})/2\pi$ (+/- for counter/co-injection). The fact that type I precursors are often hardly visible during co-injection is due to the resulting low frequency yielding a low Mirnov amplitude, as the contributions of $\omega^*$ and $\omega_{\mathrm{rot}}$ almost cancel. Actually, they may also become locked and therefore not be detected by magnetic probes at all.

Type III ELMs during the L-mode phase of counter-injected discharges were observed for the first time. They were identified unambiguously because of the features of the precursor oscillation.

## 3.6 L- and H-mode Density Limit

Next-step devices such as ITER envisage operating scenarios in the vicinity of the highest accessible density, i.e. the density limit. In addition, the H-mode is of particular interest owing to its good confinement characteristics. The density limit (DL),which is normally a disruptive limit, is empirically reasonably approximated by the Greenwald limit scaling $\bar{n}_e^{GW} \propto I_p$. A pronounced feature of this scaling is its heating power $P_{heat}$ insensitivity. In contrast, access to the H-mode, i.e. the H-mode threshold, depends on the heating power and is generally described by $P_{heat}^{L-H} \propto \bar{n}_e B_t$. Since the operational point of ITER is probably in the vicinity of this threshold, we directed a significant part of ourDL investigations, beside the efforts to surpass the Greenwald limit, to this area. Thestrategy here was to increase the density and heating power concomitantly in small steps to follow the threshold as close as possile. For the power, we intensively applied the NBI interruption technique here to change the duty cycle and correspondingly the effective heating power.

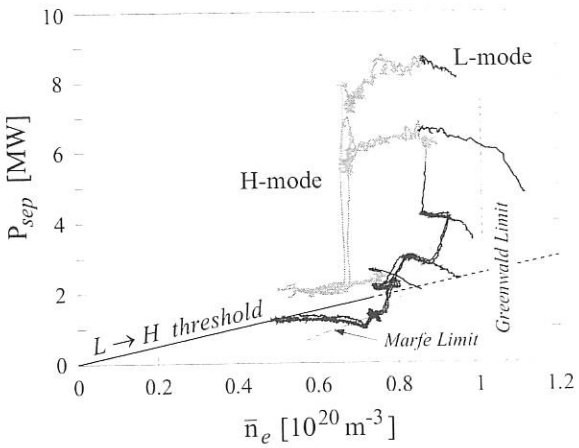


*FIG. 3.10: This figure exhibits typical trajectories for $I_p = 0.8$ MA,$q_{95} = 4$ discharges in deuterium. The grey area represents the experimentally realized L-mode operational space. The "Marfe limit" curve characterizes the start density for Marfe expansion into the bulk, i.e. full detachment.*

The resulting trajectories are demonstrated in the $P_{sep}$ versus $\bar{n}_e$ plane for $q_{95} \approx 4$. In the $P_{heat}$ versus $\bar{n}_e$ plane the behaviour looks very similar, but the power crossing the separatrix into the scrape-off layer, $P_{sep}$, is physically more decisive than the total heating power. The ''Marfe limit'' curve represents the establishment of complete detachment diagnosed by the strong suppression of $I_{sat}$ and the Marfe expansion. The figure exhibits that the usual threshold scaling describes the L/H-mode separation quite well up to medium densities and recycling fluxes. But just below the Greenwald limit the discharges always fall back into the L-mode despite their preceding confinement modes. In L-mode, maximum densities slightly above the Greenwald limit are achieved. The density limit in the H-mode, which is in principle the H—L back transition threshold, is at higher heating power nearly independent of the power, and the corresponding densities only approach $0.9\ \bar{n}_e^{GW}$ (Fig. 3.10). Moreover, the hysteresis has obviously vanished. The operational area close

to and beyond the Greenwald limit is apparently only accessible in the detached L-regime. The DL itself is not provoked by a radiation collapse (i.e. $P_{rad}^{tot}/P_{heat} \approx 1$) as in limiter discharges since up to the DL this fraction only rises to about 0.6 - 0.8.

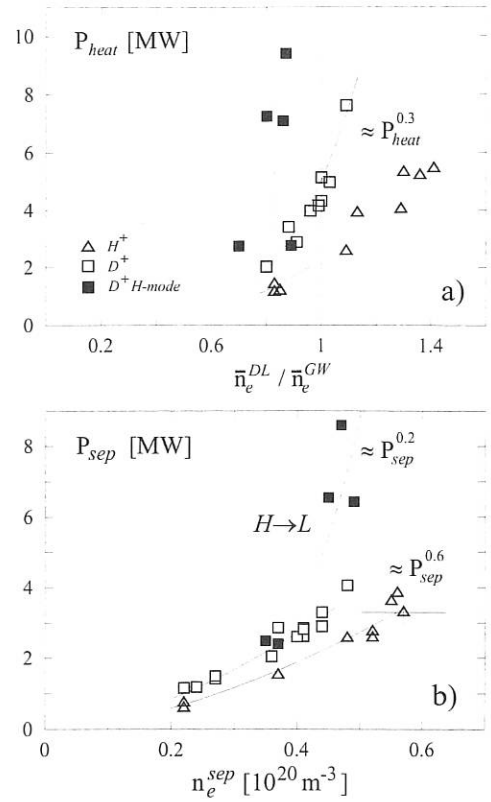


*FIG. 3.11: This figure shows global and local L- (blank symbols) and H-mode (solid symbols) DL data of hydrogen and deuterium discharges. The edge data in b) exhibit a significantly stronger power dependence than the averaged data in a). In contrast to the L-mode data, the H-mode densities show a very weak power dependence.*

To explore in more detail the heating power dependence and the possibility of exceeding the Greenwald limit, discharges with low plasma currents are performed to minimize the technical problems relating to high neutral particle pressure in the main chamber combined with NBI operation. The densities are ramped up so smoothly that the beams significantly contribute to the particle fuelling rate. Despite the high densities of the order of $\bar{n}_e \approx 10^{20}$ m$^{-3}$ the beams still provide a bulk particle source.

In contradiction to the Greenwald scaling, there is a moderate but clear increase of the DL with rising $P_{heat}$, as one would expect assuming the DL might becaused by thermal instabilities such as Marfes. The limit scales in the L-mode roughly as $\bar{n}_e^{DL} \propto P_{heat}^{0.3\pm0.1}$ for both hydrogen and deuterium. Furthermore, especially hydrogen discharges exceed the Greenwald limit by up to 40%. This is probably a consequence of the fact that discharges in hydrogen develop slighly lower $\bar{Z}_{eff}$ than those in deuterium and their total radiation is about 10% lower.

The present understanding of the DL as an edge density limit focusses attention on the boundary parameters. Plotting the edge densities as a function of $P_{heat}$ or, more instructively, as a function of $P_{sep}$ makes the power dependence even more pronounced (Fig. 3.11b). The data are taken just before the strong Marfe expansion slightly below the DL. For $H^+$ and $D^+$ the separatrix densities increase approximately as $n_e^{sep} \propto P_{sep}^{0.6\pm0.2}$. Moreover, the separatrix density grows as $n_e^{sep} \propto \bar{n}_e^2$, reflecting the strong broadening of the electron density profile towards high $\bar{n}_e$. This may help in a reactor to radiate enough power at the boundary at moderate $Z_{eff}$ values, since the additional radiation potential at a given $Z_{eff}$ rises strongly with density.

The H-mode DL behaviour is quite different. Neither the line-averaged density northe separatrix density exhibits a noticeable power dependence. This and other observations suggest that both density limits (L- and H-mode) originate from completely different physical mechanisms.

Finally, one can conclude that it may become difficult to obtain dischargeswith densities in excess of the Greenwald limit with improved confinement.

## 3.7 Particle Refuelling with Pellets

Efforts to develop scenarios allowing more flexible plasma density control by injecting solid deuterium pellets were mainly concentrated on ELMy H-mode discharges. The refuelling efficiency of pellets injected during ELMy H-mode phases was observed to decrease with increasing heating power and decreasing pellet penetration depths. For heating powers above 7 MW a plasma particle inventory increase of only up to 0.4 times the pellet particles was measured some ms after the injection took place when using the biggest (8 mm$^3$) and fastest (1200 m/s) pellets available. The efficiency was even lower when smaller and/or slower pellets were injected. To compensate for the decreasing efficiency, higher particle fluxes and hence pellet repetition rates had to be used. Thus, the centrifuge injector was upgraded to deliver now equivalent flow rates of up to $\Gamma = 3 \times 10^{22}$ deuterons/s and pellet rates of up to 80 Hz.

Density feedback controlling was achieved at levels well above the empirical Greenwald density limit $\bar{n}_e^{GW}$ by applying this hanced pellet refuelling rates. Thus, pellet refuelling gave access to operational conditions beyond the limits enfacedwith conventional gas puffing. An example of a feedback-controlled pellet-fuelled discharge with preprogrammed 1.5 $\bar{n}_e^{GW}$ is shown in Fig. 3.12. Pellet injection results in a stationary phase ($\gg \tau_E$) at a density level not to be realized by gas puffing. Strong pellet fuelling at presently available auxiliary heating powers, however, caused persistent cooling of the target plasma and gradually increasing pellet penetration depths, finally ending in a fuelling scenario with central pellet particle deposition, unreasonable for a fusion reactor. The problem of cooling the plasma too strongly by the pellets could be somewhat alleviated by injecting smaller pellets at less speed, at the expense of less fuelling efficiency and slower density increase.

The major problem faced when applying high pellet particle fluxes, however, turned out to be degradation of energy con-

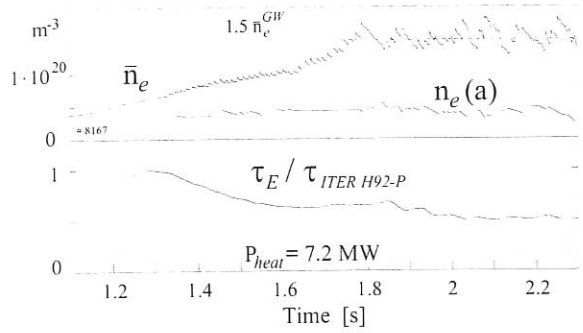


*FIG. 3.12: Discharge with feedback-controlled pellet refuelling with preprogrammed 1.5 $\bar{n}_e^{GW}$.*

finement time. In the discharge shown in Fig. 3.12 the plasma energy $W_{MHD}$ therefore gradually drops and a smooth H→L transition occurs at about 1.9 s. This is caused by the release of an ELM for each single pellet injected during H-mode phases. A pressure pulse is formed near the end of the pellet deposition profile, diffusing towards the plasma edge. Bottlenecking of the pressure at the H-mode transport barrier causes strongly increasing pressure gradients inside the barrier and hence triggers an ELM event. With the particles expelled by the pellet-triggered ELM, also the energy stored by these particles is lost from the plasma. This way, strong pellet refuelling at low fuelling efficiency can cause confinement degradation.

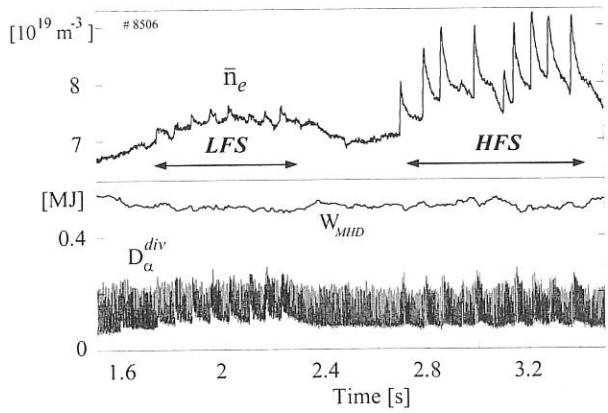


*FIG. 3.13: Pellet injection sequences into an ELMy H-mode plasma. The sequence injected from the magnetic low-field-side is followed by a high-field-side sequence once the plasma has returned to the initial conditions. Ablation of almost identical pellets results in strongly different density increase in both cases indicating much higher fuelling efficiency for the high-field-side pellets. The ITER normalized energy confinement time is approxomately one and show no significant reduction during the pellet sequence injected from the high-field-side.*

ELMs triggered by pellets are not the only particle losses faced when injecting pellets. Already during L-mode conditions with no ELMs present the fuelling efficiency in observed to decrease with increasing heating power. In hot plasmas, the material ablated by the pellets is rapidly shifted to the plasma edge and even partially expelled from the plasma when injecting from the magnetic low-field side of the torus. When a pellet is injected, its ablation cloud acts like an energy sponge and a localized plasmoid with high internal pressure is formed. This plasmoid represents an extremely localized perturbation and is subject to a curvature drift pushing it towards lower field. The drift force acting on the plasmoid strongly increases with plasma temperature. At plasma temperatures like those of auxiliary-heated discharges the acceleration of the plasmoid is too strong to allow its complete capture within the plasma column.

This particle loss can be avoided when injecting pellets via guiding tubes from the magnetic high-field side. In this novel injection scenario, the curvature drift force is directed into the plasma and nearly perfect absorption of the pellet material by the plasma takes place. This was clearly demonstrated by direct comparison of the two injection methods. Identical sequences of pellets at velocity 130 m/s were injected into almost the same target plasma during the flat-top phase of a type-I ELMy H-mode ($I_P = 0.8$ MA, $B_t = -1.9$ T, $q_{95} = 3.6$, $P_{NI} = 7.5$ MW; Fig. 3.13). The first sequence, injected from the magnetic low-field side, showed only little effect on the density, and the efficiency was quite small ($\approx 0.2$). Injection from the high-field side, however, caused strong density increase as the efficiency was much higher in this case (up to 0.7). Due to the reduced particle and energy losses, for the novel injection scenario no confinement degradation was observed although the density increase was significant. As a further advantage of pellet injection from the high-field side, deeper pellet penetration with respect to low-field-side pellets was observed. The origin of this finding is most probably pre-cooling of the plasma ahead of the pellet by the plasmoid moving much faster than the pellet.

Experiments based on the novel injection scheme are now under preparation with higher pellet repetition rates in order to allow feedback-controlled operation at plasma density levels well above the Greenwald limit without suffering from confinement degradation.

## 3.8 ICRF Experiments

The experiments concentrated on the comparison of antennas with and without Faraday screen, edge plasma-antenna interaction, heating of plasmas at high density, operation at $\pi$ and 0 phasing and direct e-heating off-axis using mode conversion. Also, by using a 3 dB coupler on two of the four systems we could increase the power to the plasma to 3.2 MW with only these two systems.

### 3.8.1 *Operation of antennas without Faraday screen*

The small difference (10% higher without screen) in the H-mode power level threshold in the H minority in D scenario was confirmed. The two antennas without screen were further operated successfully in a variety of other heating scenarios ($P_{RF} \approx 2$ MW): direct fast wave, $He_3$ minority in H and fast-wave mode conversion heating, with 0, $\pi$ phasing of the antenna straps.

In order to test the capability of the ICRF for off-axis current drive, we investigated the off-axis coupling to the electrons in the mode-conversion heating scenario, and the effect on the

plasma of operating the antennas at a phasing different from 0, $\pi$.

### 3.8.2 Mode conversion and off-axis power deposition

The $He_3$ in H-mode conversion scenario is a candidate for off-axis current drive. The profile of RF power deposition to the electrons in the heating mode of this scenario, with off-axis position of the conversion layer, was measured in ASDEX Upgrade. The experiment was performed in single-null L-mode plasmas ($B_T = 2.5$ T, $\bar{n}_e = 5 \times 10^{19}$ m$^{-3}$, $I_p = 0.8$ MA, and $T_e = 1$ keV, $f = 30$ MHz). The ICRF power was square wave modulated between 0 and 1.6 MW at 55 Hz. The sawtooth frequency was 63 Hz. The electron temperature was measured with a 45-channel ECE system with 30 $\mu$ sec time resolution. The data is Fourier analyzed and the fundamental Fourier coefficient is taken as being proportional to the power deposition profile. Inclusion of higher harmonics in the ECE data did not significantly modify the profile. The measured profile was then compared with the FELICE 1-D code (Fig. 3.14). The measurement and the FELICE results are shown in Fig. 3.14 as a function of the poloidal flux coordinate $\rho$. The results of the FELICE calculation with 6.5% $He_3$ minority is mapped from the high-field side, where direct ECE measurements are unavailable. The width of the profile is different for several reasons. First, the resonance layer is approximately a vertical line and cuts across several flux surfaces. This will lead to power absorption on the intersected flux surfaces, thereby broadening the absorption profile, while the FELICE code is a slab model. Second, the measurement includes direct absorption, heat wave propagation, and energy diffusion. The data clearly show, however, the off-axis power deposition on the electrons, thereby paving the way for off-axis current drive.

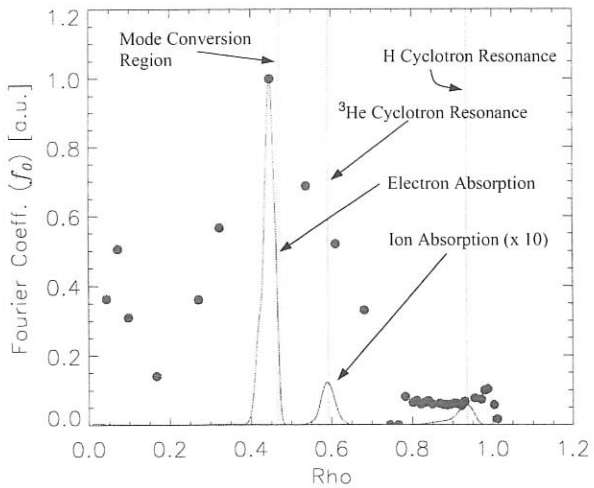


*FIG. 3.14: Comparison of the measured power deposition profile with that calculated by FELICE, mapped to flux surfaces.*

### 3.8.3 Comparing operation of the antenna loops in-phase and out-of-phase

Two antennas with Faraday screen were compared with 0 and $\pi$ phasings at powersof up to 1 MW. The conditions were $B_T = -2.1$ T, $I_p = 1$ MA $\bar{n}_e = 6 \times 10^{19}$ m$^{-3}$, $f = 31.6$ MHz (H minority in D). In the discharges (see Fig. 3.15), an antenna with 0 phasing and an antenna with $\pi$ phasing ($n_\phi$ peaking at 14, $k_\parallel \approx 6.5$ m$^{-1}$) were energized in sequence. The electron temperature, the sawtooth amplitude and the plasma energy increase were typically twice as high as for the in-phase case (Fig. 3.15) at the same generator power. The heating efficiency (increase of plasma energy vs total power increase - taking into account the reduced OH power because of the higher electron temperature increase in the out-of-phase case and a factor of 0.8 between the generator power and power in the plasma) is a factor 2 higher than for operation in-phase (incremental confinement time 58 m compared with 28 ms). Tungsten, the material of the divertor, stayed below the detection level in both phasings. Nor was there a significant difference between the increase of the carbon concentration as a function of the generator power. The increase of the O concentration vs generator power was somewhat higher (40%) in 0 phasing than in $\pi$ phasing. The absence of impurity problems even in 0 phasing indicates that current drive phasings will be possible.

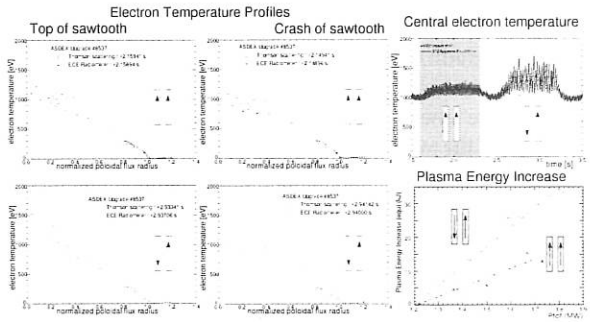


*FIG. 3.15: Operation of the antennas in-phase and out-of-phase. Shown are the electron temperature time trace for a generator power of 0.7 MW, as well as the electron temperature profiles at the top and the crash of the sawtooth. The increase in plasma energy (equ.) as a function of the total power shows the different heating efficiency.*

## 3.9 Disruption Investigations

The 1996 experimental period provided the most complete and better calibrated set of halo current measurements which document the Divertor I Phase of ASDEX Upgrade. The poloidal current flowing between the divertor plates and vessel was measured in six sectors equipped with shunts or Rogowski coils. The halo current in AUG can reach up to 50% of the pre-disruption plasma current; in addition, it exhibits significant toroidal and poloidal asymmetries, which impose undesirably large safety factors in the design of the divertor structures. Asymmetries of the halo current are reported from most machines but their origin has not yet been clarified.

The poloidal asymmetry (more current flowing at the outer divertor plate than at the inner one) is approximately of the same magnitude in every sector, thus excluding it as an error of calibration of the measurements and as being due to an n=1 radial displacement of the whole plasma. A plausible

explanation for the in-out asymmetry is the following: part of the halo region does not intersect the inner divertor but extends further between the two divertor plates and intersects the bottom side of the outer divertor. This fraction of the halo current therefore does not contribute to the vertical stability of the plasma but, nevertheless, enhances the mechanical load on the outer divertor.

Halo currents have also significant asymmetries in the toroidal direction. The toroidal peaking factor defined as (local maximum halo current)/(average halo current) can be as large as two. In many shots one can recognize an n=1 toroidal modulation of the halo current (Fig. 3.16). The remaining shots do not show any simple or systematic toroidal structure of the halo current. Unfortunately, we do not find any correlation between these structures and that of the MHD modes present before disruption.

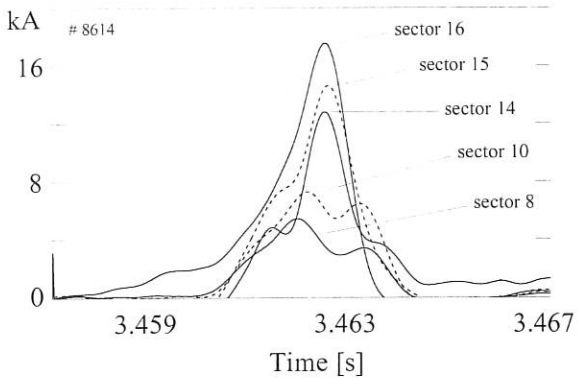


*FIG. 3.16: Time histories of the halo current (measured in different toroidal sectors) showing an n=1 toroidal structure.*

The investigation of load mitigation by means of killer pellets continued. SiC pellets were injected in to OH and NBI plasmas to collect data on radiation and ablation characteristics. Unfortunately, these pellets did not have a noticeable effect on the evolution of the current quench since they turned out to be too small for NBI plasmas and did not sufficiently ablate in OH plasmas. ASDEX Upgrade contributed further to the enrichment of the Disruption Database for ITER. Data on halo currents, current and thermal quenches were carefully selected and included in the international Database.

## 4. INTERPLAY BETWEEN EDGE AND CORE

In addition to core stability and power exhaust requirements, the tokamak operational space is limited by plasma edge related phenomena: the ideal ballooning limit,marked by the onset of type I ELMs, the H-mode threshold and the density limit, which requires a minimum edge temperature in order to avoid radiation instability onclosed flux surfaces. The accessible operation space can conveniently be describedin a single diagram (Fig. 4.1), showing the boundary electron temperature vs. electron density, both taken at a minor radius 2 cm inside the separatrix at the low-field side. This measurement position is chosen within the H-mode steep-gradient region but sufficiently far from the separatrix to ensure that $n_e(a-2\text{ cm})\ T_e(a-2\text{ cm}) \geq (7-10) \times n_e(a)\ T_e(a)$. Hence, the edge pressure gradient is represented in Fig. 4.1 as well as the absolute values of $T_e$ and $n_e$. Except for the radiation unstable cases, only discharges with $I_p = 1$ MA, $B_t = 2.5$ T (favourable grad$B$ direction) and deuterium neutral beam injection into a deuterium plasma are shown.

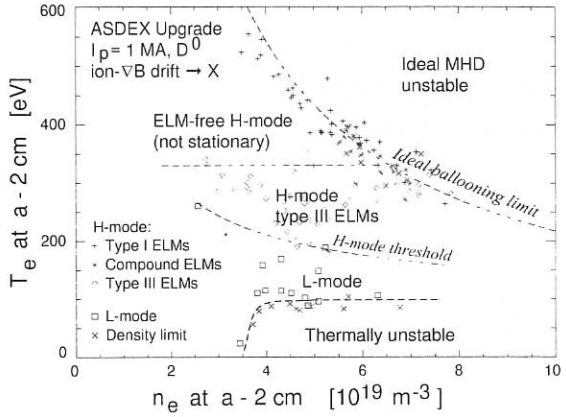


*FIG. 4.1: Edge operational diagram showing regime boundaries and experimental results of ASDEX Upgrade (discharges with $I_p = 1$ MA only).*

A lower limit for the edge temperature is defined by the thermal instability driven by radiation loss from low-Z impurities. This limit is associated with MARFE formation at $T_e(a-2\text{ cm}) < 70$ eV} above a certain edge density threshold, followed by rapid edge cooling, MHD activity and a disruption. The H-mode threshold edge temperature is consistently above the MARFE limit under all experimental conditions on ASDEX Upgrade. As a consequence, the wish or necessity to operatein H-mode puts a more severe restriction on the minimum separatrix power than thermal stability. Ideal ballooning stability associated with type I ELMs marks the upper limit for the edge temperature. As this is a pressure gradient limit, the maximum edge temperature is lowest for high edge densities and/or low plasma currents.However, for the entire range of parameters and equilibrium configurations encountered on ASDEX Upgrade so far ($n_e(a-2\text{ cm}) \leq 8 \times 10^{19}$ m$^{-3}$, $I_p = 0.6 \ldots 1.2$ MA), H-mode is found to be accessible.

Both type I and type III ELMs are found on ASDEX Upgrade. In addition, compound ELMs (short L-mode phases preceded by either type I or type III ELMs) and type I ELMs followed by a number of small type III ELMs are observed. As type III ELMs cause only a small $T_e$ modulation, type III-compound ELMs are naturally found in the vicinity of the H-mode threshold in Fig. 4.1. Type III ELMs exist only up to a maximum edge temperature (330 eV at $r = a - 2$ cm for the conditions shown), reflecting their resistive nature. Above this temperature, ELM-free H-mode is obtained at low edge densities. As no stationary ELM-free H-mode has been demonstrated as yet, ELM-free phases are generally short and usually terminated by the onset of type I ELMs. Long ELM-free H-modes, which

arerarely obtained on ASDEX Upgrade, are prone to impurity accumulation, causing edgecooling and a backtransition to L-mode. Note that for ASDEX Upgrade parameters theideal ballooning limit intersects the region of type III ELMs, i.e. on ASDEX Upgrade type III ELMy phases can have pressure gradients very close to the ideal limit.

There are no data points in Fig. 4.1 at highest edge densities ($n_e(a-2$ cm) > $6.5 \times 10^{19}$ m$^{-3}$) between the H-mode threshold and $T_e(a-2$ cm) = 250 eV. This area of H-modes with high edge densities is especially interesting for impurity-seeded high radiation scenarios (e.g. CDH-modes with Ne puff), which have restricted separatrix power ($P_{\rm sep} \leq 5$ MW during 1996 where $P_{\rm NBI} \leq 7.5$ MW) due to their significant power radiated from closely inside the separatrix. We can ask whether, in addition to the limitation of $P_{\rm sep}$, a degradation of confinement with increasing edge density exists which makes this region inaccessible. To this end, we compare the global confinement measured relatively to the ITER-92 ELMy (ITERH-92P(y), scaling with the behaviour of the local edge transport, represented by aneffective heat transport coefficient $\chi^* = (P_{\rm sep}/S)/(n_e(a-1$ cm) $T_e'(a-1$ cm)) (Fig. 4.2). We use the ancillary scalings given in[4] to account for $W_{\rm tot}/W_{th}$ and $P_{L'}/P_L$. Since we are concerned here merely with the density dependence, we normalize $\chi^*$ with respect to the power degradation expected in accordance with ITERH92-P(y)[1] and consider $\chi^*/P_{\rm sep}^{0.65}$. It can be seen that the global confinement of the best discharges reduces from a maximum at H-ITERH92-P(y) = 1.3 (type I ELMs) to values around 1.0 at high edge densities (type III ELMs).This degradation is not matched by $\chi^*/P_{\rm sep}^{0.65}$ (nor by $\chi^*$ itself), which exhibits favourable low values for high density type III ELMy discharges with high radiated power fraction. Note that the quantity $\chi^*/P_{\rm sep}^{0.65}$ has a weak dependence on $P_{\rm sep}$ and its low value is mainly a consequence of the high edge pressure gradient at high edge densities even for type III ELMy discharges.

The plasma edge is not only important for stability but can also be connected with global confinement properties. In this context, we have to distinguish cases at or below the ideal ballooning limit in the steep edge gradient region. Without having performed a ballooning stability analysis, we heuristically identify the ideal limit with edge electron pressure gradients $\alpha_e = 2\mu_0 Rq^2/B_t^2 \mathrm{grad}\ p_e = 1.6 \pm 20\%$, (i.e. the uppermost branch of data points in Fig. 4.1, where a saturation of grad $p_e$ is obtained), and lower values of grad $p_e$ as below the ideal limit. For those cases at the ideal limit, we find that edge(at $r = a - 2$ cm) and central electron temperatures (innermost Thomson scattering volume at $\rho_p \approx 0.15$) are approximately proportional (Fig. 4.3), and their ratio is unchanged for the entire range of $B_t, I_p, n_e$ covered. This finding might be indicative of profile self-similarity, e.g. as predicted by ITG turbulence simulations. However, we note that this proportionality holds only in the vicinity of ideal edge instability. L-mode discharges have significantly lower edge temperatures due to the lack of an edge pedestal. Also, CDH-modes[5] with type III ELMs highest radiation levels show particularly good confinement (and high central $T_e$) at low edge temperatures just above

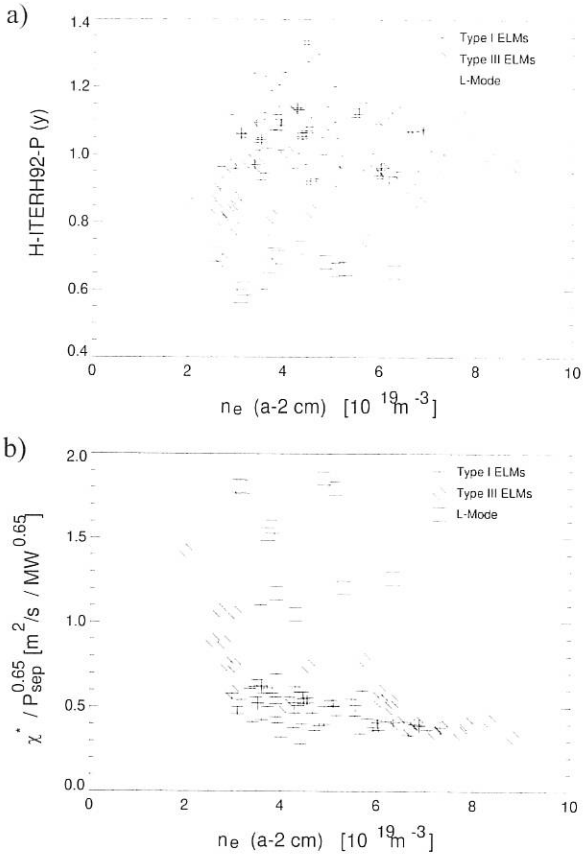


*FIG. 4.2: Confinement at high edge densities: a) global confinement measured relatively to ITERH92–P(y) scaling seems to degrade when compared with best low edge density discharges, b) no degradation is seen in the local transport at the edge, represented by the effective heat transport coefficient* $\chi^* = q_{\rm sep}/(n_e(a-1\ cm)\ T_e'(a-1\ cm))$.

the H-mode treshold. A similar proportionality of the edge and line-averaged electron densities is found for a broad range of discharges near the ideal limit, again with the exception of type III ELMy CDH-modes, where a significant peaking of the density profile is observed /120/,/13/.

A consequence of such profile self-similarity is the existence of a link between edge profiles and global confinement. In fact, it is experimentally found that the stored energy ($W_{\rm MHD}$) is approximately proportional to grad $p_e$ at the edge at the ideal limit. If core confinement is dictated by edge gradients near a stability limit, the confinement scaling must be expected to assume similar dependences on plasma parameters such as the edge pressure gradient at this limit. This is indeed found by making an independent power law regression analysis for grad $p_e$ and $\tau_E$. The dependences of grad $p_e$ and $\tau_E$ on the magnetic field and density at the ideal limit, $B_t^{-0.3}$ and $n_e^0$, respectively, are found to be practically identical. The $\tau_E \propto I_p^{1.6}$ dependence is much stronger than the ITERH-92P ELMy prediction, approaching the $I_p^2$ dependence of grad $p_e$, in line with the ideal ballooning limit. It must be noted that there is a limited $q_{95}$ variation ($q_{95} = 3 \ldots 5$ at $I_p = 0.8$ MA and varied less at other currents), so that the sum of the $B_t$ and $I_p$ exponents is somewhat more precisely determined than each exponent by itself.

[4] H-Mode Database Working Group, in: Plasma Physics and Controlled Nuclear Fusion Research 1992 (Proc. Int. Conf. Würzburg, 1992) Vol. 3, IAEA, Vienna (1993) 251

[5] O. Gruber et al., Phys. Rev. Lett. **74** (1995) 4217

Local transport analysis using the ASTRA 1-D code shows that the changes in confinement time correspond to a change of the effective heat transport coefficient $\chi_{eff}$ throughout the entire core up to 90% of the minor radius by about the same factor. Concluding, we can state that the effect of edge stability limits may go beyond mere changes of edge parameters such as the edge pedestal shape or transport across the edge barrier but can also influence global confinement. The favourable density dependence of the ITER H-mode scalings seems to disappear at highest edge pressure gradients attributed to the ideal ballooning limit, e.g. during type I ELMy phases. At the same time, no local edge confinement degradation with increasing density is observed. It remains task to find an expression for the confinement time valid for the various degrees of proximity to ideal edge instability.

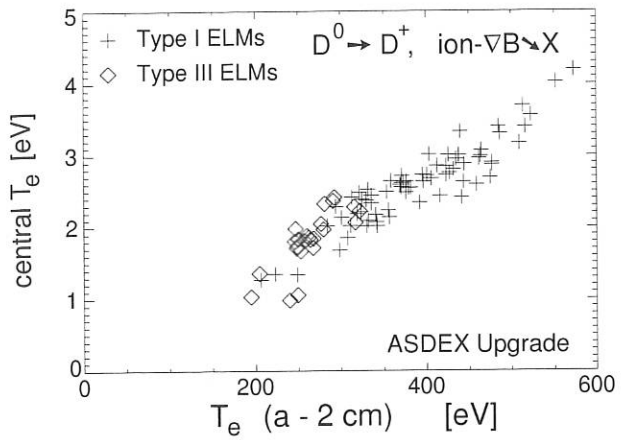


*FIG. 4.3: Correlation of edge and central electron temperature at the ideal stability limit.*

## 5. TUNGSTEN DIVERTOR EXPERIMENT

Tungsten-coated divertor tiles were mounted at the position of the strike zone in the ASDEX Upgrade divertor during the last experimental campaign, to investigate the suitability of W in a divertor tokamak under reactor-relevant conditions. The tiles consisted of a fine-grain graphite substrate coated with a 0.5 mm thick layer of tungsten.

Over 800 discharges with the tungsten divertor had been performed, with auxiliary heating powers up to 10 MW. The averaged power load on the target plates reached up to 6 $MWm^{-2}$; during ELMs power loads over 15 $MWm^{-2}$ were observed.

The W influx and the central W concentrations were monitored spectroscopically during the whole experimental campaign. Erosion and deposition measurements were made on long-term sample probes and single-exposure probes. The results of the spectroscopic measurements and the probe measurements were combined to establish a migration pattern for tungsten.

In the vast majority of discharges, where no accumulation of tungsten was observed, the influence of the W divertor on the main plasma was negligible. The carbon concentrations were barely reduced due to the large carbon source from the inner graphite heat shield. The density and the $\beta$-limits remained unchanged and no deterioration of the energy confinement occurred. The evaluation of a large number of discharges revealed a very similar result for the H-mode threshold with W divertor compared with previous investigations. There was also no influence on the radiating boundary scenarios.

### 5.1 Tungsten Flux Measurements

The tungsten erosion was measured by observing a WI spectral emission line at 400.9 nm. A spectral overview identified this line as the most prominent of the neutral tungsten spectrum. No WII emission lines except in the case of disruptions were found. The evaluation of the resulting tungsten influx depends on the ratio of ionization rate to excitation rate times the branching ratio S/XB, which was derived from a separate experiment on the Berlin plasma simulator. The W particle flux from the target plates in the divertor shows strong variation over the radial position. As an interesting feature, two distinct maxima in the tungsten emission profile were found. A maximum close to the strike point is caused by the electron temperature, while a second maximum in the SOL is due to the maximum of the particle flux. The results of probe erosion measurements (Fig. 5.5) also show a radial erosion pattern which correlates with the particle flux.

The dependence of the tungsten influx on the electron temperature in the divertor could easily be observed in density limit discharges. As the density is raised, the electron temperature in the divertor decreases and the plasma finally detaches. The WI emission follows this trend and continuously decreases, finally dropping below the detection limit as the detachment begins.

The sputtering yield for W was calculated for various divertor plasma conditions (Fig. 5.1). No strong dependence on the working gas was found. The lines in Fig. 5.1 represent the results from simulations based on ion beam measurements and taking into account the energy and angular distributions of an isotropic Maxwellian distribution accelerated in the sheath potential. The simulations for a pure deuterium plasma show a significantly lower erosion of tungsten than was observed. It is also remarkable that the measurements show a shift of the low-temperature onset of the sputtering to temperatures below 5 eV. These experimental results can be modelled by a divertor plasma with about 1% charged light impurities, which leads to the conclusion that the sputtering of tungsten is clearly dominated by the light plasma impurities.

Additionally to the spectroscopically measured yield for the tungsten erosion, Fig. 5.1 shows the results for the net erosion determined from probe measurements (Fig. 5.3). As expected, the determined net erosion yield lies below the overall tungsten erosion. The difference in these quantities can be interpreted as prompt redeposition due to the gyro motion of the W ions in the local magnetic field. For the measurement at 40 eV the divertor electron density is low ($n_{e,div} \approx 7 \cdot 10^{18}$ $m^{-3}$) and the net erosion is a factor of about 2 lower then the initially eroded tungsten. In the case of the low-temperature measurement the

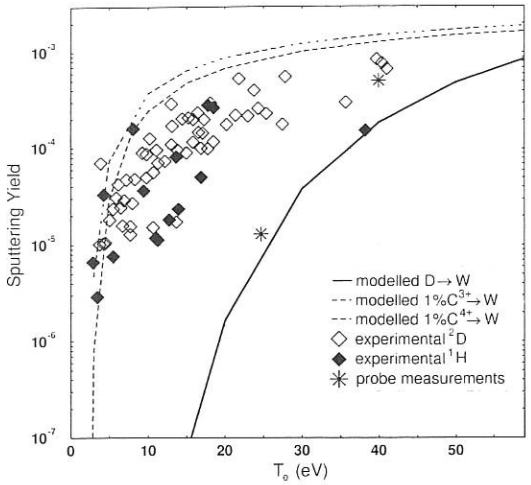


*FIG. 5.1: Measured sputtering yield of tungsten. The lines represent results from calculations assuming a pure deuterium plasma (solid line) or with contributions from carbon impurities in different charge states (dashed lines). The measured net erosion from probe measurements is shown as asteris.*

density was much higher ($n_{e,div} \approx 1 \cdot 10^{20}$ m$^{-3}$) and difference between gross and net erosion reaches a factor of 20. Both values are in excellent agreement with earlier simulations.

In ASDEX Upgrade neon is usually injected in radiative cooling scenarios. The increased radiative losses lead to lower electron temperatures at the plasma boundary and thus to lower erosion yields. On the other hand, the additional fraction of impurities with a higher net charge may cause additional erosion due to higher impact energies. Fig. 5.2 demonstrates both effects in attached discharges with neon puffs in the main chamber. The NeIV signal in the midplane gives an estimate of the time dependence of the neon concentration. In the cold divertor plasma of discharge #8026 the additional neon concentration did not lead to a tungsten influx above the detection limit, because the cooling of the plasma boundary was efficient enough to suppress erosion. In contrast to this observation, the tungsten influx of discharge #8025 clearly followed the time dependence of the NeIV emission because the divertor electron temperature was still high. However, in typical neon puff experiments the effect of the lowered temperature by radiative loss dominated by far the more effective erosion by additional impurities. In detached plasmas, such as the CDH-mode, the WI emission dropped below the background noise level.

As the plasma contains typically 0.5 to 2% carbon the deposition of carbon, on the tungsten tiles has also to be considered. The line emission of CD molecules measured above the tungsten tiles was nearly identical to that of graphite surfaces. Furthermore, new tungsten tiles immediately showed CD emission when they were exposed to the divertor plasma for the first time. From these observations it can be concluded that there is a significant carbon content in the sheath plasma from the first plasma contact. However, comparing the WI emission of standard discharges ($I_p = 600$ kA, $\bar{n}_e = 3 \cdot 10^{19}$ /m$^3$) reveals that there was no significant change in the tungsten erosion over the whole experimental period. This long-term stability shows that

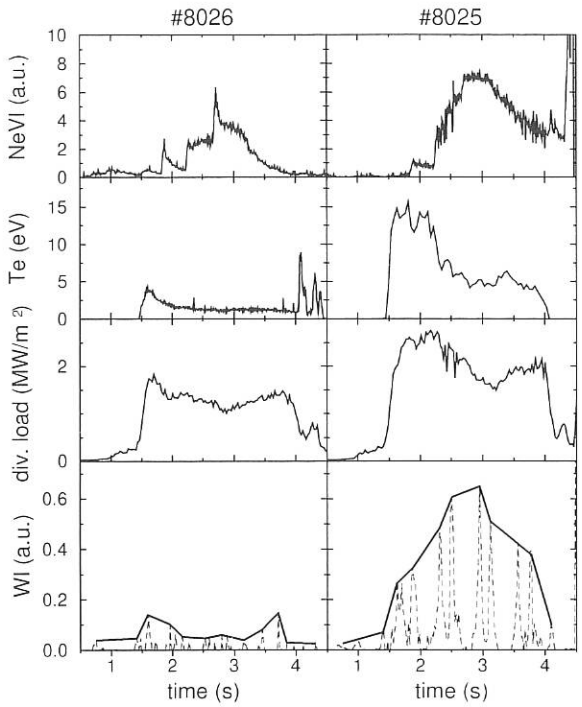


*FIG. 5.2: 1 MA attached ELMy H-mode plasma discharges with neon puffs. #8026 represents a typical discharge with a low electron temperature in the divertor. The tungsten influx is below the detection limit. In discharge #8025 the divertor electron temperature remains above 5 eV during the neon puff. The increased tungsten influx is clearly correlated to the NeVI emissivity in the core plasma.*

the carbon coverage did not reach a value where the W tiles are completely covered.

## 5.2 Tungsten Concentrations

In the plasma centre an array of spectral lines at 5 nm emitted by ionization states around W XXX was monitored with a VUV spectrometer. The spectrometer was cross-calibrated by comparison of the measured radiation with the theoretical radiation power after tungsten laser ablation. The accuracy of this method was estimated from W-laser ablation experiments to be within a factor of 2. The detection limit scales with the plasma density ($1/n_e^2$) and is about $0.5 \cdot 10^{-5}$ at $\bar{n}_e = 4 \cdot 10^{19}$ m$^{-3}$.

Over 90% of the investigated discharges - ohmic as well as L- and H-mode - exhibited concentrations in the range of or below $2 \cdot 10^{-5}$. Figure 5.3 shows the concentration of all investigated discharges of this experimental campaign as a function of the auxiliary heating power. Blank symbols represent discharges where the concentration was below the detection limit. The maximum concentration strongly decreases with increasing input power. This decrease might be explained partly by the well-known power degradation of the confinement and partly by the circumstance that the high-power discharges were preferentially run at higher densities, leading to shorter ionization lengths for W and therefore better shielding of the influx.

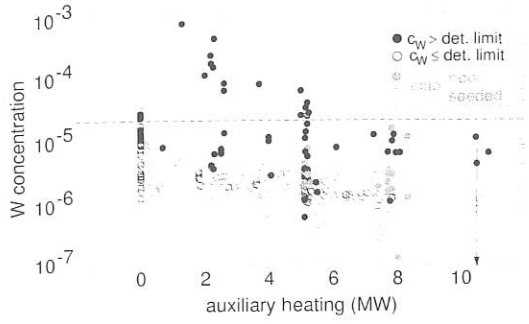


*FIG. 5.3: Concentrations of tungsten ($C_W$) deduced from the W line array at 5 nm plotted versus the auxiliary heating power. Blank circles represent dischargeswhere the concentration is below the detection limit, and gray circles (solid as well blank) represent neon-seeded discharges.*

At low auxiliary heating powers, as illustrated in Fig. 5.3, there exist conditions which can lead to tungsten accumulation. This was also found in previous experiments with laser ablation. The accumulation occurs preferentially at low central electron temperatures (≈1 keV) close to the maximum value of the radiative loss parameter. Figure 5.4a) shows a comparison of two almost identical 600 kA H-mode discharges withlow auxiliary heating power ($P_{aux} \approx 1.5$ MW). Whereas in discharge #8102 W accumulated after the disappearance of the sawteeth to concentrations of about $5 \cdot 10^{-4}$. the sawtooth activity continued in discharge #7560, keeping the W concentration at $\approx 10^{-4}$. The electron density and temperature profiles of discharge #8102 are shown in Fig. 5.4b) for time points before and during the accumulation.

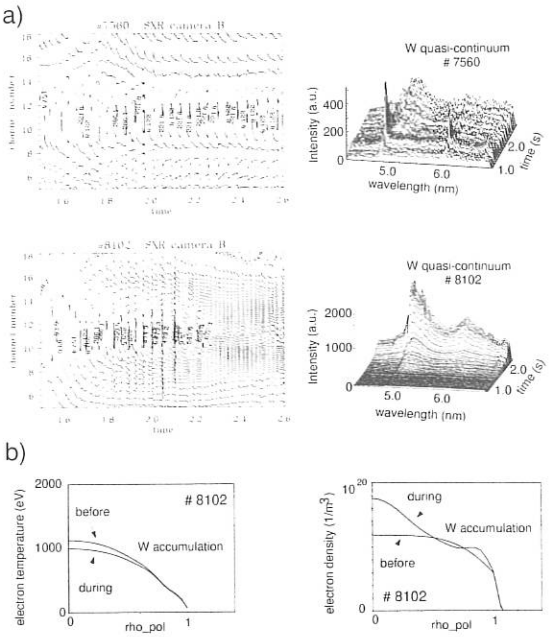


*FIG. 5.4: a) Temporal behaviour of the SXR radiation and the W quasicontinuum at 5 nm during two almost identical 600 kA auxiliary-heated discharges #7560 and #8102. The line-averaged density was about $6 \times 10^{19} m^{-3}$, the NBI heating power 1.5 MW. The intensity of the SXR radiation is shown as a contour plot; the channels 10 - 12 of the SXR cameras look through the plasma centre. Note the different scales for the W quasicontinuum radiation. b) Electron temperature and density profiles of discharge #8102 before and during the W accumulation.*

## 5.3 Erosion of Tungsten

Tungsten net erosion, i.e. the difference between erosion and subsequent redeposition, in the divertor was studied by exposure of material probes in the outer divertor plate. Thin tungsten marker strips (1-100 nm) were evaporated on graphite test target tiles. The test tiles were exposed in single discharges or in a set of a few similar successive discharges using a manipulator system which also allows the probes to be exchanged through an airlock system without breaking the machine and diagnostics vacuum.

Net erosion rates were determined by measuring the marker thickness before and after exposure by Rutherford backscattering analysis with $^4$He ions in the 0.7 - 2 MeV energy range. By combining these results with measurements of the particle flux to the target plates by a set of flush-mounted Langmuir probes, it was possible to calculate sputtering yields from the measured erosion rates. Figure 5.5 shows the spatial distribution of the tungsten marker erosion along the outer target plate surface for a series of low-density ohmic discharges. The erosion pattern is closely correlated to the plasma temperature and the spectral line emission of neutral tungsten atoms at the target plate, which are also plotted in Fig. 5.5. The effective erosion yield reaches a value of $Y_{eff} \simeq 5 \times 10^{-4}$ near the average location of the strike point. The experimental values for the tungsten net erosion were compared with results from ion beam sputtering experiments and TRIM simulations, taking into account the energy and angular distribution of an isotropic Maxwellian distribution accelerated in the sheath potential. The net erosion yields were a factor 5 - 40 lower than the predicted erosion yields. This is attributed to the effect of prompt local redeposition and is confirmed by the erosion yields obtained from analysis of the spectroscopic measurements of the W I spectral line (see Sec. 5.1).

## 5.4 Migration of Tungsten

Tungsten transport from the divertor region to the midplane scrape-off layer was studied by comparing the spectroscopically measured flux of tungsten atoms above the outer target plate with measurements of the tungsten flux to a collector probe exposed in the shadow of the ICRH antenna limiters. The cyclindrical probe was mounted under a shield with a slit aperture and could be rotated during a discharge to obtain time-resolved measurements of the tungsten deposition on the probe surface. From the measured tungsten deposition one can deduce the tungsten flux in the SOL, which is strongly correlated to the tungsten atom flux above the target plate (Fig. 5.6).

By combining the results of the erosion measurements described above with deposition measurements of the midplane

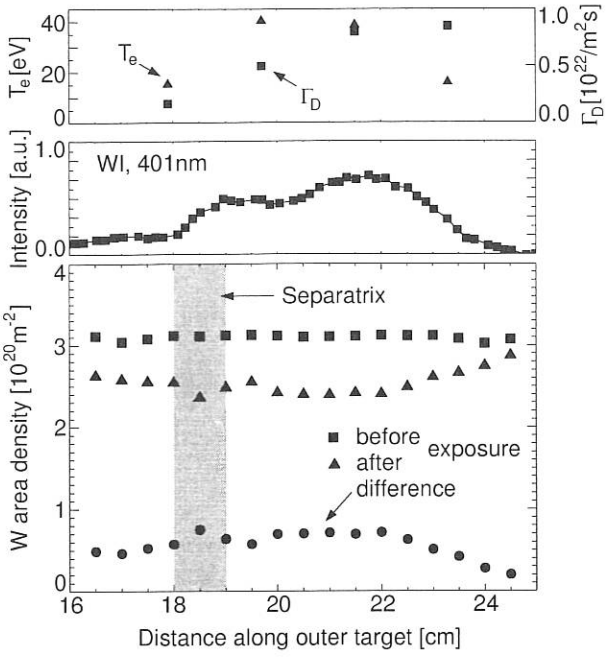


*FIG. 5.5: Radial profile of tungsten marker erosion along the outer target plate surface with W I spectral line emission above the target and $T_e$ and $\Gamma_D$ measurements by flush-mounted target Langmuir probes for a series of low-density ($\bar{n}_e = 2.5 \times 10^{19}$ m$^{-3}$) ohmic discharges with 18.7 s divertor plasma operation.*

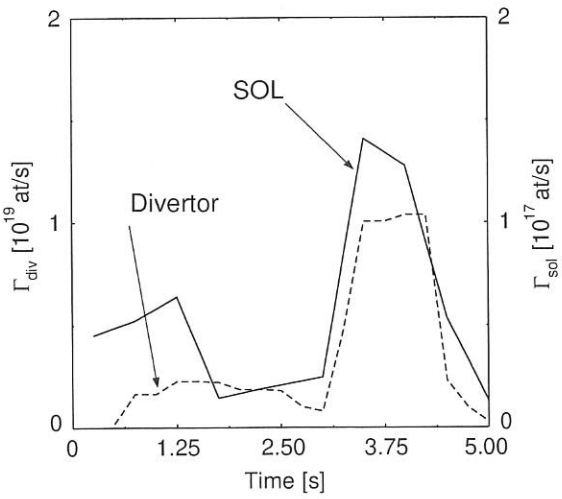


*FIG. 5.6: Spectroscopically measured flux of neutral tungsten atoms above the outer target plate (dashed line) and flux of tungsten ions in the midplane scape-off layer (solid line) estimated from collector probe measurements.*

collector probe and on long-term samples at various vessel locations and with spectroscopic measurements of the tungsten concentration in the confined plasma, it was possible to establish a global pattern for the migration of tungsten in ASDEX Upgrade.

Tungsten deposition at surfaces in the shadow of the ICRH antenna limiters was determined with probes exposed by a manipulator system in the midplane, similar to the system in the divertor. Wall deposition of tungsten was measured by analysis of long-term sample probes exposed for a whole experimental period, but no tungsten was found above the detection limit of 1/100 monolayers of W atoms. The ratio of inner target to outer target tungsten deposition was estimated by analysis of graphite tiles removed after the previous experimental period, where only a few tungsten test tiles were mounted in the graphite divertor.

Combining all these measurements, one obtains a migration pattern as shown in Fig. 5.7 for the low-density ohmic discharge type described above. Comparison of the W-flow pattern with results obtained previously for Cu on ASDEX shows as main difference the much better divertor retention of tungsten, which must, however, be largely attributed to the effect of prompt local redeposition.

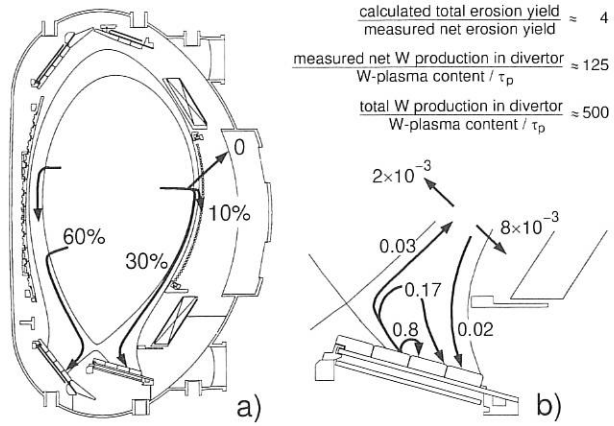


*FIG. 5.7: Migration pattern of tungsten in the ASDEX Upgrade vessel estimated for low-density ohmic discharges with a core W-concentration of $\simeq 10^{-5}$ and a tungsten confinement time of $\simeq 80$ ms determined in similar discharges by W-laser ablation. a) shows the fraction of tungsten from the confined plasma deposited on inner and outer target plates and on main chamber limiters and vessel walls. b) shows the migration pattern for tungsten eroded at the outer target plate.*

# 6. EDGE AND DIVERTOR PHYSICS

## 6.1 Divertor Characterization of the Scrape-off Layer (SOL) of Ohmic Discharges

The dependence of the divertor $n_e^{div}$ and separatrix density $n_e^{sep}$ on the neutral particle flux density $\Gamma_0^{div}$ measured at the outer divertor branch is shown in Fig. 6.1a). At low neutral flux densities, the separatrix density increases linearly. For higher values of $\Gamma_0^{div}$ a weaker dependence follows from a regression analysis: $n_e^{sep} \propto \Gamma_0^{div\ 0.5}$. The point where the separatrix density becomes nonlinear with the neutral flux marks the change from the low to the high-recycling divertor regime. Below this point, the divertor density is about half the separatrix

density, as is expected for pressure balance. The temperature ratio between midplane and divertor is found to be about unity. The electron temperature at the separatrix is between 50 and 100 eV and the heat transport is limited by the heat transport through the sheath. The change to the high-recycling divertor starts when the divertor region becomes dense for recycled particles, because the mean free path for neutrals attains the same order as the extent of the divertor region.

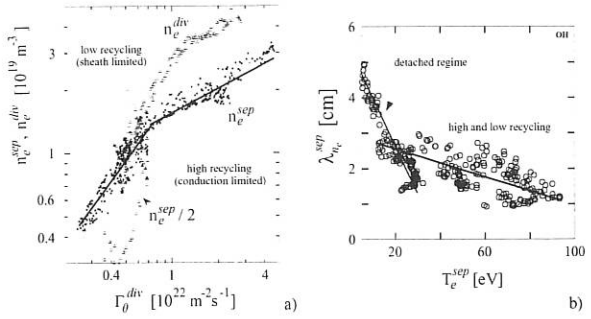


*FIG. 6.1: a) Dependence of the divertor and separatrix density on the neutral gas flux density for the low and high-recycling SOL regime in ohmic discharges. b) SOL density fall-off lengths vs. midplane separatrix temperature for different SOL regimes in ohmic discharges. Auxiliary-heated discharges show the same behaviour.*

At higher densities the separatrix temperature decreases and the heat transport is limited by the temperature gradient between the separatrix and divertor. This change from sheath-limited to conduction limited heat transport already occurs in ohmic discharges with moderate densities, so that for most of the discharges performed in ASDEX Upgrade the heat transport is conduction-limited. This is supported by a scaling of the H-mode electron temperature at the separatrix with the power crossing the separatrix, showing a $T_e^{sep} \propto P_{sep}^{0.4}$ dependence. A linear dependence is expected for convective heat transport and a 4/9 dependence for the conduction-limited case. For both regimes, the heat flux profile at the midplane and that measured at the divertor plate are comparable. The density fall-off lengths in the midplane measured by the lithium beam diagnostic and the reciprocating Langmuir probe show a moderate increase with decreasing midplane temperature (Fig. 6.1b)). At temperatures below about 30 eV the decay lengths strongly increase due to the fact that the divertor operates in the detached regime and the perpendicular momentum transport broadens the power-carrying sheath. In this regime the heat flux to the divertor is strongly reduced compared with midplane values and a significant pressure drop occurs.

## 6.2 Plasma Performance

The influence of the tungsten divertor on the other intrinsic impurities and on global plasma behavior was evaluated and compared with operation with complete graphite divertor.

In the vast majority of discharges, where no accumulation of tungsten is observed, the influence of the W divertor on the main plasma is negligible. The carbon concentrations are barely reduced due to the large carbon source from the inner graphite heat shield. The density and the $\beta$-limits remained unchanged and no deterioration of the energy confinement occurs. The evaluation of a large number of discharges reveals a very similar result for the H-mode threshold with W divertor compared with previous investigations. There is also no influence on the radiating boundary scenarios.

These results are encouraging for high-Z plasma facing components to be used in a future device. Lowest concentrations and negligible influence on the discharges were found at high heating power and high plasma density.

## 6.3 Volume Recombination in the Divertor Plasma

Spectroscopic measurements were performed in the divertor region usiong lines of sight parallel and close to the outer target plate. By this means we investigated the temporal evolution of hydrogen continuum radiation and Balmer series during ohmic and NBI-heated discharges with rising densities approaching the density limit. In such discharges the intensity of hydrogen radiation dramatically increased due to electron-proton recombination processes at the onset of detachment (Fig. 6.2).

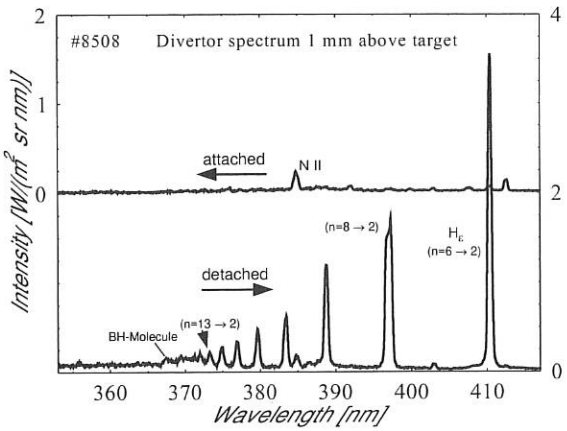


*FIG. 6.2: Spectra of Balmer series measured in the outer divertor in attached and detached phases.*

This indicates that volume recombination significantly contributes to the neutralization of incoming protons in front of the target plates. The Balmer and Paschen continuum radiation provides a sensitive method of determining $T_e$ and $n_e$ in the low-temperature region ($\leq$ 4 eV). At a distance of 1-50 mm above the outer target plate $T_e \geq 0.8$ eV and $n_e \leq 1 \times 10^{21}$ were found in the highest density phases.

## 6.4 Radiative Power Losses in the Divertor

Divertor emission was studied with an absolutely calibrated VUV spectrometer. Total losses were calculated by summing over the resonance lines of deuterium and the different ionization stages of carbon. Maximum power losses were obtained

at high densities when the divertor is detached. Then 1.4 MW is radiated, 29% by deuterium, 14% by CII, 36% by CIII, and 21% by CIV.

To increase the radiative losses nitrogen was puffed into the divertor. Fig. 6.3 shows the nitrogen power loss as a functiom of the flux rate. At maximum rate 2.4 MW was radiated. Also shown is the reduction of the target load. At the highest puffing rate the load is reduced by 1.8 MW. The difference is due to the reduction of the intrinsic divertor emission during the puff from 1.4 to 0.8 MW. With allowance for the intrinsic losses, a maximum radiative loss of 3.2 MW was obtained in the ASDEX Upgrade divertor.

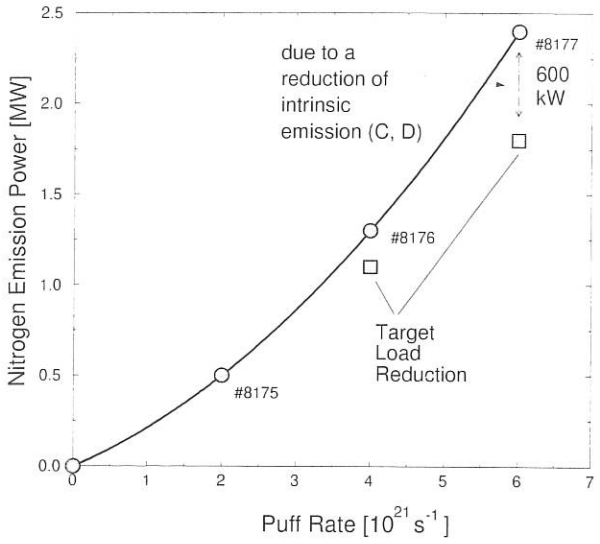


*FIG. 6.3: Radiated power losss during a nitrogen puff into the divertor. Also shown is the reduction of the target load (squares).*

## 6.5 Impurity Exhaust

To optimize particle exhaust, the neutral density in front of the pump duct has to be maximized. Also the concentration of the impurity gases (e.g. He or Ne) has to be high in order to keep the total gas throughput as low as possible. This requires compression of the impurities in the scrape-off layer and divertor plasma, i.e. a large ratio of He/Ne neutral gas density in the divertor region to the edge density of the respective species. In ASDEX Upgrade we find a strong increase of the compression of He and of Ne and Ar with increasing divertor neutral pressure (as described in the previous annual report). For detached discharges with high divertor neutral density He exhaust was achieved with $\rho = \tau^*_{He}/\tau_E \sim 5$. At constant pumping efficiency, an increasing divertor neutral pressure is achieved with increasing external gas throughput, which also increases the particle flow in the scrape-off layer. However, varying the pumping speed (number of active turbomolecular pumps) at constant neutral pressure at the pump duct, and hence the particle flux, demonstrates that the externally induced gas flow in ASDEX Upgrade does not play an important role. It is rather the much higher internal recycling fluxes which provide the divertor retention /30/. Experimentally, from the decay of short, external gas puffs one determines the effective particle confinement time $\tau^*_p$, which is determined both by the bulk plasma particle confinement time $\tau_p$ and by the recycling/pumping. Varying the pumping speed, however, under constant exhaust conditions (i.e. constant divertor parameters) allows separation of these different confinement times. An analytic model shows that $\tau^*_p$ is linear with the pumping time constant (inverse pumping efficiency) with the offset being $\tau_p$. Such an experiment in an H-mode discharge is shown in Fig. 6.4 for He and for Ne.

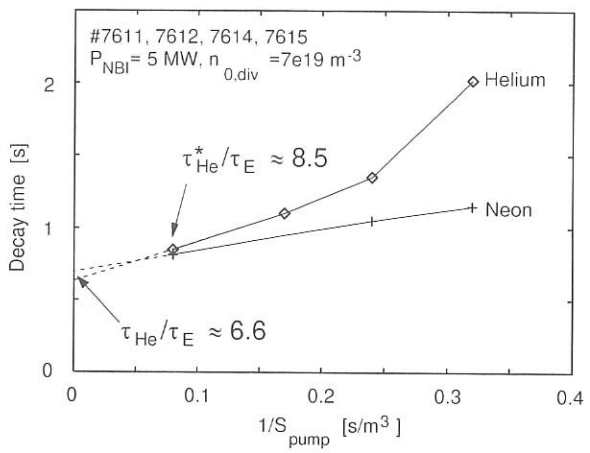


*FIG. 6.4: Extrapolation of HeII- and NeVII-line radiation decay rates, which are a measure of the global particle confinement time $\tau^*_p$ to infinite pumping speed allows the determination of $\tau_p$. The x-axis shows the inverse pumping speed, which is varied by switching off turbomolecular pumps via gate valves.*

There are, however, differences for He and the other noble gases. The He compression is lower than that of Ne for most conditions, and usually He is even de-enriched, i.e. the He fractional density in the pumped gas is smaller than at the plasma edge. But the compression improves with divertor neutral gas pressure, and in CDH-mode the enrichment factor of He is larger than about 0.3, which is consistent with the ITER requirement of a value of 0.2. For Ne the compression factor is always higher than for deuterium, i.e. Ne in the neutral gas is even enriched in the divertor volume compared with the plasma edge. Ne exhaust is therefore rather fast, as desired, and this eases control of the radiated power in the plasma edge by seeding it with Ne. Measurements of the He density in the bulk plasma were made by charge exchange spectroscopy. The He profiles and their decay after short He puffs show that the core transport of He is fast enough and the edge density is only limited by the exhaust.

## 6.6 Compression Analysis

Experimentally, the compression of neon and helium was measured as a function of the neutral gas flux density: the compression of neon and helium (neon is better compressed than helium) increases with higher neutral gas flux density in the divertor 6.5. Based on a transport model validated for CDH-mode conditions, this was reproduced by B2-Eirene calculations by

doing a midplane density scan. The basic mechanism for the compression is the recycling cycle in the outer SOL. For ASDEX Upgrade the existence of a pumping baffle in the outer divertor is quite important for the observed compression (Fig. 6.6). Integrating the modelling result over the SOL, this baffle affects the parallel particle flux of the deuterium background due to the effect of recirculation of neutrals in the pumping duct (limited leakage by the baffle) back to the SOL. The difference between neon and helium can be seen from the different distributions of the radially integrated ionization sources, where neon neutrals are kept more efficiently in the divertor compared with helium due to their smaller mean free paths.

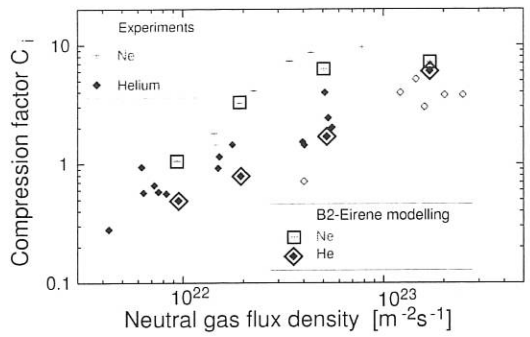


*FIG. 6.5: Experimental and modelling results for the compression of neon and helium as a function of divertor neutral gas flux density.*

The physics of the compression can be reduced to a rather simple model (Fig. 6.6) characterized by a layer the width of the mean free path of the impurity neutrals, from where they are able to feed the pump duct below the baffle, establishing a second particle flux maximum in the outer SOL at the plate. Doing a simple flux balance at the entrance of the box then shows that the compression is determined by the instreaming flow velocity of the impurity. In this outer SOL region there are no strong temperature gradients and the deuterium background has a relatively strong forward flow. The impurity flow velocity is therefore due to the dominant friction force of the deuterium background and is practically identical (at least for higher densities) to this background velocity. Enhancing the midplane separatrix density and therefore the neutral gas flux density in the divertor results in larger deuterium flows in this outer part due to stronger friction with CX neutrals. As a consequence, larger deuterium neutral gas flux density in the divertor gives larger compression. The difference between neon and helium is just a consequence of the mass difference (which is the dominant factor in the difference of the mean free paths of neutrals). From these considerations, the difference of deuterium and the other impurities is also clear: deuterium neutral transport is dominated by charge exchange, in contrast to the impurity neutrals. The deuterium recycling is well confined in this baffle region under conditions where the impurity neutrals leak out, because charge exchange in this outer part of the SOL with low densities and low temperatures very effectively trap the deuterium neutrals. The effect of the baffle is therefore less pronounced for deuterium than for impurities. The compression of deuterium therefore varies by only a factor of 2 to 3, in agreement with experiment.

This kind of concept offers very attractive potential for separation of power and particle exhaust: particle exhaust can be done just in the outer part of the SOL (allowing geometry optimization), whereas power exhaust is related to the region close to the separatrix.

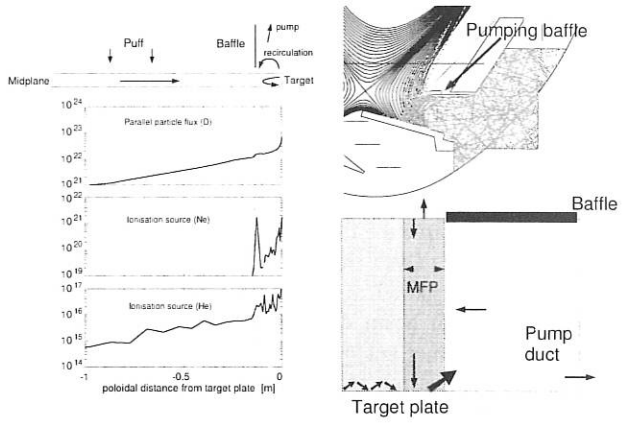


*FIG. 6.6: Radially integrated parallel particle flux (D) and ionization sources (Ne and He) for the outer divertor (left side). Trajectories of 100 neon neutrals from the outer target plate (right side top) and schematic model (right side bottom).*

## 7. DIAGNOSTICS

The main changes in diagnostics are caused by changing to Divertor II. At least about 10 diagnostics have to be modified to match the requirements of Divertor II.

### 7.1 DCN Interferometer

The 3 vertical DCN interferometer channels are replaced by combined $CO_2$/He-Ne channels (wavelength $\lambda$ = 10.6 $\mu$m/633 nm), because access to the main plasma is no longer possible for DCN in the new Divertor II geometry. The additional He-Ne wavelength is necessary for on-line compensation of vibrations in the interferometer. The shorter $CO_2$ wavelength will reduce the absolute density resolution ($\approx \lambda$) for these channels, but also has the advantage of being much less influenced by refraction effects in the plasma.

### 7.2 Magnetic Measurements

For Divertor II we had to replace the existing flux loops in the upper divertor region. Up to now we had a set of 12 differential toroidal flux loops. Divertor II will have 15 differential flux loops. To measure the halo currents during the disruptions we mounted 3 sets of toroidal Rogowsky coils in the lower divertor area. In segment 15 we installed an array of special Mirnov coils (printed circuit type) 60 mm in the shadow of the separatrix to measure ballooning modes. To measure locked modes before the disruption, we placed a saddle coil along the

high-field side of the torus, every 180 degrees of the toroidal angle. To measure the radial magnetic field, we mounted 10 Vespel coils on the lower field side of the torus.

## 7.3 Spectroscopy

The spectroscopic system for the Divertor II uses 120 lines of sight starting in the baffle. There are 20 successive lines of sight with a diameter of 10 mm viewing from the baffle to cover the whole outer target plate. An identical system is installed to observe the inner divertor. Two other sets with 20 lines of sight each view from the baffle to the midplane and will be used to observe the radially directed influx of impurities through diagnostic valves from the inner and outer wall. Such valves are also installed at the strike point region and will be used for helium beam diagnostic and other gas injection experiments. Another set of 40 lines of sight view from the outer side of the plasma through the divertor region in pairs along the magnetic field lines and in the opposite direction to measure flow velocities of ions. All lines of sight are variably fed to several spectrometers equipped with CCD cameras or a system of interference filters and photomultipliers.

## 7.4 Bolometry

The main modifications of the bolometric diagnostics for the new Divertor II configuration are:

- Replacement of the collimator cameras of Divertor I by two 8–channel pinhole cameras positioned under the roofbaffle to observe the inner and outer divertor leg.
- Modification of the 8–channel X-point camera and repositioning it behind the outer divertor plates.
- Fabrication of a new MICH bolometer specially designed for divertor measurements which is partly compensated against neutral gas pressure effects.

## 7.5 $H_\alpha$ Observations

Improvements by observation of inner and outer divertor with 8 channels each. Observation from the dome using quartz fibre bundles and microfibre plates as vacuum windows. By changing filters observation of $H_\alpha$ as well as CIII is possible. For ELM observation a spatially integrating channel for inner and outer divertor is envisaged.

## 7.6 Plasma Video Observation

Because of the changed geometry it is not possible to use the re-entry tube for observation of divertor plates. Image guides (670 × 500 fibres, resolution 50 lp/mm) are therefore used for radial as well as toroidal observation. The observation of the images is done by optical imaging via standard vacuum windows.

## 7.7 Langmuir Probes

Although the basic design of Divertor I was retained, the higher heat loads expected required construction with narrower gaps around the elements, special precautions to avoid an exposed edge in case of mechanical failure, and provision for conductive cooling between shots through a ceramic coating. The number of poloidal locations was expanded to 44, so that complete profiles should be available in every magnetic configuration. The number of tetra and penta probes was increased from 10 to 29. Outside the vessel, the measurement circuits were made more flexible, less perturbing, and less susceptible to offsets and drifts. The number of measurement channels was increased from 120 to 180.

## 7.8 Thomson Scattering

To measure $T_e$ and $n_e$ in Divertor II, a Nd-YAG-laser scattering diagnostic is under construction. The scattering volumes are nearly vertical in front of the outer divertor plate between strike point and roof baffle. For the time being only two local scattering volumes are available to find out the best signal-to-noise ratio (length of scattering volume ≈3 cm, rep. rate 20/sec, expected measuring range 0.3 eV $\leq T_e$ 30 eV, $n_e \geq 10_{18}$ m$^{-3}$).

## 7.9 Thermography

A new near-infrared thermography system monitors the surface temperature of the inner and outer strike point modules at three toroidal positions with a spatial resolution of 5 mm. The system will be primarily used for safety reasons for the NBI interlock system in order to prevent possible damage to the divertor tiles.

## 7.10 Fast-moving Langmuir Probes

The movement path of this probe system has to be changed. The new movement is a straight line about 400 mm long just above the roof baffle.

## 7.11 Divertor Manipulator

For the Divertor II phase the system is currently being modified for exposure of the front side of cylindrical probes in the vertical outer target. To fill the cylindrical hole left by the probes a special plug was developed. The exposure position was chosen such as to be right at the typical strike point position. Because of the high heat load the plug is actively cooled in its locked position. For probe exposure, the plug is removed and deposited in the probe storage magazine. Since the probes themselves are only exposed for single discharges, they do not need to be cooled.

# INTERNATIONAL COOPERATION

## 1. DOE – ASDEX Upgrade Activities

The main impetus was the establishment of the physics basis for the design of ITER. The key issues were: disruptions, dimensionlesly similar discharges, He ash transport and exhaust, and wall material.

In the field of transport, a start was made on the investigation of identical discharges in DIII-D and ASDEX Upgrade (current, field, shape, density, NBI heating power and voltage) and of dimensionlesly similar, ICRF (second harmonic) heated discharges (L-mode) in Alcator C-MOD and ASDEX Upgrade was started. In the first case the same plasma energy and confinement was found for the type-I H-mode discharges, demonstrating the reproducibility of tokamak discharges in different devices. Local transport analyses are now being done. Comparison of the ICRF heated L-mode discharges is under way.

High-Z materials are still an alternative candidate for all heat-loaded in-vessel structures. To compare the discharge behavior of the high-Z first-wall operation, experiments with molybdenum in Alcator C-MOD and tungsten-coated target plates in ASDEX Upgrade were performed. In ASDEX Upgrade sputtered tungsten could only be observed close to the strike point at the target plates. Small ionization length and gyroradius lead to redeposition in the immediate neighbourhood. To ensure the consistency of the results, comparative studies with different transport codes, MIST (Alcator C-MOD) and STRAHL (ASDEX Upgrade), are envisaged.

The Penning gauge for measuring the helium content in the exhaust gas was continuously operated. The physics of helium exhaust in ASDEX Upgrade and DIII-D was discussed.

The collaboration in the field of plasma-facing material development was continued. The aim of the experiments was to understand Be oxidation, carbidization and deuterium retention in oxides and carbides. In oxidation studies using $^{18}O$ it could be shown that the oxidation proceeds by surface oxidation of segregating Be layers. The carbidization of a-C:D films deposited on Be samples occurs at temperatures above 475 C with simultaneous release of the retained D.

ICRH: The use of a 3 dB coupler to reduce the effect of the load variations on the generators was implemented and proved to have significant advantages: 3.2 MW was achieved into the plasma. Experiments on ASDEX Upgrade using antennas without Faraday screen were extended to low single-pass aborption scenarios. No negative side-effects were seen. The $^{3}He$ in the H-mode conversion heating scenario, first tested on TFTR, was also investigated on ASDEX Upgrade.

## 2. DEMOKRITOS, Greece

The divertor Langmuir probe system (LPS) designed and built for ASDEX Upgrade by Demokritos (Athens, Greece) went into operation in 1996. The probe manipulator allows scanning of a large fraction of the divertor volume between the target plates and the x-point on a 100 ms timescale. The LPS was run in standard Langmuir characteristic mode to obtain the temperature and density, or, alternatively, as a Mach probe for plasma flow determination. A result of specific interest for divertor retention was the transient plasma flow reversal observed immediately after type-I ELMs and reproduced by B2–EIRENE modelling.

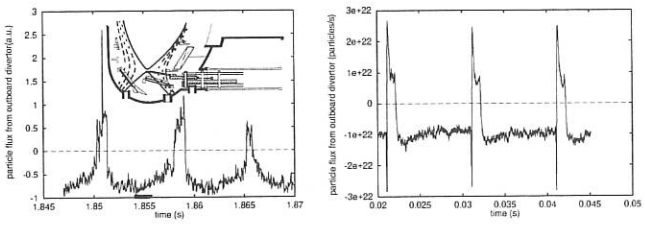


*FIG. 1 Particle fluxes at the outer divertor entrance as measured with a movable langmuir probe (left side) and modelled (right side). Positive fluxes are fluxes going from the divertor into the main chamber.*

## 3. Inst. of Electronics, Res. Found. Hellas, Heraklion, Greece

1.5–D and 2–D modelling of the vapour shield evolution dynamics over divertor plates during hard disruptions in large tokamaks show that in the case of graphite-coated plates electrostatic phenomena may play an important role in determining the erosion rate of the plates.

## 4. University of Cork, Ireland

The collaboration with the University of Cork concerning MHD equilibrium identification using magnetic measurements was continued. The routine application of FP to real-time recovery of geometric parameters for AUG feedback control was extended from 12 to 16 principal components to handle additional degrees of freedom due to two new OH2 poloidal field shaping currents. To reduce the statistical error bars of the FP results, a fifth FP category was introduced, consisting of lower single-null equilibria limited to a small volume in parameter space. Detailed studies between the different versions of FP

and an interpretative equilibrium package were started.

A comparative study was carried out to determine whether a FIR polarimeter using the existing DCN interferometer on AUG or a proposed MSE diagnostic would deliver more information on the safety factor profile in the plasma. Using realistic simulated errors for both diagnostics, the MSE diagnostic with four optimally positioned channels was superior to a six-channel FIR polarimeter.

## 5. TEKES (HUT and VTT), Finland

The Finnish group are concerned with modeling by Monte Carlo and Fokker-Planck techniques the energetic ion behaviour in the plasma under the influence of electromagnetic fields. In a first step the confinement of ripple-trapped ions by a radial electric field, as observed in the experiments, was verified and fast time constants were demonstrated to be possible in this measurement. Investigations were started to model ion loss orbits under the influence of radial electric fields.

## 6. Cooperation with Russian Institutes

Most of the collaborations are organized in the framework of WTZ, the Agreement between the Federal Ministry of Research and Technology of the FRG and the State Committee for the Use of Atomic Energy of the USSR on Scientific-Technological Cooperation for the Peaceful Use of Nuclear Energy.
1. Pellet injection – Technical University of St. Petersburg (SPU): The microwave detector for pellet masses delivered by SPU was installed at ASDEX Upgrade by a scientist from SPU.
2. ECRH – Institute of Applied Physics, Nizhni Novgorod (IAP): A gyrotron with 140 GHz/0.5 MW/0.5 sec and a corresponding torus vacuum window – on loan from IAP – were used for the ECRH experiments in ASDEX Upgrade. The electron beam deposition in the collector of a dummy tube (with magnetic beam sweeping) was studied under the influence of the adjacent iron floors and the tokamak stray magnetic field.
3. WTZ Project V.30 – State Technical University of St. Petersburg (SPU): a) Owing to the constraints imposed on the E-field components, lateral drift motion of the vapour layer may occur in the SOL. b) Numerical modelling of impurity pellet injection into tokamaks including the expansion of the ablated material and the effects of the traversing pellet motion.

Cooperation outside WTZ:
JOFFE Institute, St. Petersburg: The programme for maximum ion temperature evaluation from neutral particle analysis was improved for easy semi-automatic application.
Kurchatov Institute, Moscow: Splines were used in the ill-posed problem of ion temperature profile reconstruction from neutral particle spectra to investigate the influence of the number and position of nodes and different regularization methods (partly financed by the Volkswagen Foundation).

## 7. KFKI, Budapest, Hungary

One guest spent six months at IPP working on the optimization and design of the lithium beam diagnostic. New observation systems will be able to measure, besides the electron density, also the density of neutrals as well as concentrations of ionic impurities in the plasma edge of ASDEX Upgrade.

DFP Project 436 UNG 113/118: a) A collisional-radiative model computing the radiation emitted by low-temperature high-density impurity enclosures in hot plasmas without the usual equilibrium assumptions. b) A numerical model for the ablation rate of impurity pellets, the characteristics of the expansion of the ablated material along the magnetic field lines and its radiating characteristics.

## 8. Centro de Fusão Nuclear, EURATOM IST Association, Lisbon, Portugal

This cooperation is focused on the operation and extension of the microwave reflectometry diagnostics. By mid-1996 all waveguides and antennae installed in the vessel were insulated against the vessel wall preventing any further damage due to disruptions. New 200 MHz VME-bus acquisition boards were installed with a maximum of 10 channels now simultaneously available. Several methods of phase detection were compared with respect to their robustness against plasma fluctuation. In addition to routine density profile measurements, the system was used for the first time for fluctuation measurements near the plasma edge to monitor changes during the L- to H-mode transition.

## 9. UKAEA Culham, United Kingdom

The topics for personnel exchanges (2 visitors from UKAEA) were the ideal MHD stability of $\beta$-limit discharges w./w.o. walls using the CHEASE and ERATO codes and ELM identification and precursor investigations using a wavelet package. The ideal $\beta$-limit would be well above $\beta_N = 3.5$ compared with the experimental value of about 2.7 pointing to a resistive tearing mode limit.

## 10. Institut für Allgemeine Physik, TU Vienna, and Friedrich Schiedel Foundations

The collaboration concerns the development and operation of the lithium beam diagnostic methods. These activities are made possible by financial support of the Austrian Friedrich Schiedel Foundation für Energieforschung. The current project contributes to the extension of the diagnostic potential by enlarging and improving the necessary atomic data bases for raw data interpretation.

## 11. CREATE Group, Naples, Italy

The collaboration with the CREATE team concentrated on comparing numerical simulations using electromagnetic network codes (including passive structures) with magnetic measurements during the breakdown phase of ASDEX Upgrade discharges.

# JET COOPERATION

(Head of Project: Prof. Dr. Michael Kaufmann)

During the first three months of 1996 work continued on installing the new MKII divertor support structure together with the new MKIIA divertor modules . The design of this new divertor allows exchange of target modules by remote-handling operation and 33 modules were successfully installed using remote-handling tools. The MKII divertor structure succeeds the MKI divertor and was designed to improve plasma power handling and neutral particle retention. As in years before, three task forces were established to conduct experiments with high-performance plasmas, predominantly in the hot-ion H-mode regime, to study ICRH-heated discharges with emphasis on plasmas with optimized current profile, and to test the new divertor's power handling and neutral particle retention capability, particularly during steady-state H-mode discharges. JET's contribution to the ITER EDA included confinement scaling studies in relevant discharge configurations and H-mode power threshold investigations. Experimental work was briefly interrupted in November for three weeks to allow work to plug bypass leaks in the divertor structure which enabled neutral gas to escape from the sub-divertor volume into the torus main chamber volume. Performance results of hot-ion H-mode discharges with neutral beam heating only were very similar to previous MKI divertor results for similar plasma heating power inputs. As before, maximum performance, which is reached at the end of the ELM-free H-mode phase, is limited by a variety of termination events leading to loss of confinement. These events are either central MHD activities accompanied by sawtooth activity and giant ELMs, which in turn are observed when plasma edge pressure gradients are at the ballooning limit. Also outer modes at r/a = 0.8 have been identified and, by means of soft X-ray measurements, interpreted to be ideal kinks. Basically, the observations indicate that at higher heating powers termination events occur earlier, i.e. shorten the ELM-free H-mode phase. The use of the MKIIA divertor has facilitated particle control by allowing access to even lower plasma target density. Best performing hot-ion H-mode discharges were achieved with $3-4$ MA, $3 < q_{95} < 4$, triangularity $> 0.3$, and edge shear $S_{95} > 3.5$. Steady-state ELMy H-modes were reached with best triple products $nT\tau_E$ of $4-5 \times 10^{20}$ keV s/m$^3$ and stationary D-D neutron rate. In contrast to discharges with $q_{95} < 2.6$, ITER confinement requirements were fulfilled at higher $q_{95}$. Experiments to the machine-size-dependent scaling of H-mode confinement indicate the validity of the ITERH93-P scaling, suggesting a type of gyro-Bohm transport meachanism. However, attempts to radiate most of the power conducted onto the divertor target plates during H-modes by deuterium gas puffing and/or nitrogen puffing into the divertor resulted in loss of confinement or even back-transition into L-mode confinement. An important feature of the new divertor was (as expected) improved power-handling capability compared with the earlier MKI structure, preventing catastrophic surface temperature rises in high-power discharges even without plasma strike zone sweeping. Also, divertor plasma detachment occurred at roughly half the main plasma density compared with the MKI divertor and produced larger (factor of 2) neutral divertor pressure, indicating improved neutral particle retention. Plugging of bypasses leads to a further improvement, as was observed by a factor of 2 decrease of the main torus chamber neutral pressure. In the frame of three Task Agreements IPP contributes to the exploitation of JET scientific results.

## 1. TASK AGREEMENT NO. 1

The basic design of the JET pellet injection centrifuge closely follows that of the IPP injector. However, bigger pellet sizes and fuel inventories were provided to meet the higher particle flux required at JET. In 1996, IPP gave further advice during the final construction phase and supported commissioning and operation of the injector. First successful refuelling experiments were performed on the basis of experience gained at ASDEX Upgrade. After completion of the JET centrifuge hardware equipment, the second pellet extruder was finished early in 1996. Equipped with this extruder, the system is now capable of delivering deuterium pellets of 4.0 mm side length at velocities ranging from 50 to 600 m/s at repetition rates of up to 10 Hz for pellet sequences lasting up to 15 s. However, in order to achieve the highest possible efficiency and reliability during refuelling operation, only a 5 Hz pellet rate was applied. Various

refuelling scenarios were investigated with the aim of enhancing the flexibility in density control. Pellet trains, without and with additional gas puffing, were injected during quasi-stationary L- and H-mode phases of NI- and ICRH-heated discharges up to a level of 12 MW. Pellet refuelling was found to act faster and more efficiently than gas puffing. Combining the two methods proved more advantageous for fast density rises to values of hither to about 70% of the empirical Greenwald density limit. At the applied heating powers and fuelling rates, pellet-induced particle losses did not seem to contribute essentially to the bulk plasma losses connected with ELM activity. In high triangularity discharges without gas fuelling during the heating phase, where long ELM-free periods occurred without pellet injection, the controlled release of ELMs by pellet injection was demonstrated at moderate power levels. Pellet injection was applied with a frequency larger than that of the ELMs occurring without pellets. In this case, only pellet-triggered ELMs were obtained. With the time delay between pellets varying up to a factor 3, it was observed that the amount of energy and particles lost by each triggered ELM decreases with decreasing pellet delay.

## 2. TASK AGREEMENT NO. 2

Erosion at the JET vessel walls was investigated by means of carbon long-term samples (LTS) partly covered with 530 nm Al and 750 nm Ni films as well as implanted with Mo markers at a depth of 380 nm to measure the erosion of carbon. The samples were mounted directly at the vessel walls and exposed to JET plasmas in April-June 1995 (about 940 discharges). Upon removal, the surface layers of the LTS were analyzed with MeV ion beam techniques. On the inner torus walls, net erosion is found with an average of about $1.2 \times 10^{15}$ Al atoms/cm$^2$ and $9.4 \times 10^{14}$ Ni atoms/cm$^2$ per JET discharge. The observed erosion is due to sputtering by energetic charge-exchange neutrals emitted from the plasma during the discharges and He glow discharge cleaning between the discharges. From the observed erosion of the LTS one can deduce for a single JET discharge an upper bound of $1.6 \times 10^{17}$ D atoms/cm$^2$ for the total CX flux to the inner torus wall. The measured erosion of carbon on the LTS was $> 3.9 \times 10^{15}$ C atoms/cm$^2$ and per discharge. The main erosion mechanism for carbon is chemical erosion by formation of $CD_4$. The eroded wall material is partly redeposited at the outer wall and in the divertor. The composition of the surface layer of a poloidal cross-section of the carbon divertor of JET (tiles 1-22) was also analyzed with MeV ion beam techniques. Thick deposits of up to several mm were observed. The deposits consist mainly of C, Be, O, N, H, D and traces of Ni, Fe, Cr, S, Cl. The combined measurements of erosion and redeposition allow conclusions about the global transport of material in the JET torus.

In JET, as in other tokamaks, the confinement significantly varies with the neutral gas pressure in the midplane. The validation of physical models calls for neutral gas data of sufficient accuracy. In-vessel pressure gauges are available in JET only in the divertor region. The midplane pressure can be measured with Penning gauges only, which are installed outside the toroidal field. The Penning gauges were calibrated in the lower and upper pressure ranges and the pumping speeds of the cryopump were measured for $D_2$ and Ne (as model gas for impurities) in pure gases and gas mixtures as a function of the pressure. Surprisingly, not only an increase towards high $D_2$ pressure was found, but also a degradation towards low pressures, where the speed is expected to be constant. The interpretation of the latter is still open.

## 3. TASK AGREEMENT NO. 5

Tokamak detachment was investigated with a view to the potential role of volume recombination using the B2-EIRENE scrape-off layer simulation code package. A typical density ramp-up scenario was simulated by performing a sequence of B2-EIRENE runs to steady state, successively increasing the particle content with otherwise constant input parameters. A JET discharge which particularly clearly shows the drop of $J_{sat}$ at constant net input power was adopted as the study point. The main result of this study is that recombination indeed plays a significant role in the parameter range under consideration and is essential to reproduce the full set of detachment characteristics. A comparison of cases with and without volume recombination reveals that volume recombination basically affects the particle balance in the vicinity of the plate, while the solutions are otherwise virtually unchanged.

In current tokamaks the density limit is observed to be an edge density limit. It is also found that the maximum achievable edge density coincides with the achievement of complete detachment. Under these conditions the limit can be completely described by the SOL-based description of the completely detached state. Scaling relations for this limit were derived from simple two-point models and dimensional considerations. The main interest was in power-independent, $1/q$-type (Hugill-Greenwald type) scalings that are observed in most divertor tokamaks. It has been shown that this type of scaling results if the divertor is in the regime of intermediate transverse collisionality for neutrals. Extensive B2-EIRENE simulations for a typical JET configuration were performed to assess that this condition is actually achieved and the analytically predicted scaling is reproduced.

The SOL-One time-dependent 1-D scrape-off layer transport code was used to model the time evolution and magnitude of target plasma parameters during giant ELMs in JET $(n_{e,t}, T_{e,t}, T_{i,t}, n_0, q_t, \Gamma_t, etc.)$. Also investigated was the scaling of the peak $D_\alpha$ signal with energy and particle loss per ELM. The simulations give the observed time evolution of near-target quantities and the right order of magnitude for the measured variables. The nonlinear dependence of the particle flux and $D_\alpha$ intensities on the peak target load during an ELM is also reproduced. The detailed structure of the ELM (few $\mu$s timescale) is dominated by inertia effects and electron heat conduction.

# NET/ITER COOPERATION PROJECT

(Head of Project: Prof. Dr. Karl Lackner)

Since its foundation IPP has hosted the NET Team, a group of scientists and engineers from the European countries participating in the EURATOM programme. They were called together to prepare the design of NET, the Next European Torus. Since the initiation of ITER (International Thermonuclear Experimental Reactor) the primary function of the NET Team has been to carry out and coordinate the European contribution to the ITER design effort, in the areas of physics and, particularly, technology. IPP contributes to the NET activities both by direct secondment of personnel to the NET team and by performing NET supporting work.

Work on the ITER project started in 1988, as a joint project by EURATOM, Japan, Russia and USA. ITER aims at demonstrating the physical and technological feasibility of a fusion-based power station. IPP hosted the full ITER Team during the conceptual design activity (CAD) phase till the end of 1990. Since the initiation of the engineering design (EDA) phase, the strongly increased ITER Team resides at three locations (San Diego/USA, Naka/Japan, Garching/Germany). The work of the Garching branch covers the design of the in-vessel components and therefore fits very well to the scientific interests of IPP.

Through its scientific work, IPP Garching makes extensive and essential contributions to the ITER design activity. In particular, the programme of ASDEX Upgrade is directly aimed at the scientific support of ITER. The stellarator experiments at IPP also make significant contributions to ITER. The results of these efforts are described in the chapters dealing with the ASDEX Upgrade and W7-AS projects. The following sections therefore describe only additional, specific design effort projects.

## 1. ITER DIAGNOSTICS

H. Salzmann, A. Herrmann, H.-J. Hartfuß, G. Haas, F. Mast

LIDAR Thomson scattering (plasma core): The design study for this diagnostic is well advanced and has established its feasibility on ITER. The design concept for the critical optical front mirror in direct view of the plasma has been completed and detailed engineering can begin. Thermography for the divertor target plates: Front optics for the diagnostic divertor cassette was designed which wavelength multiplexes the collected thermal radiation from different points on the target plates into a single beam. This is achieved by using a low-frequency grating close to the front mirror, but shielded from the divertor plasma. Very complicated wide field-of-view borescope optics is thus avoided and the number of optical elements inside the vacuum vessel is drastically reduced. Pressure gauges: Special pressure gauges envisaged for ITER were tested in collaboration with JET and ITP Karlsruhe inside a superconducting magnet. The questions to be addressed were long-term stability of the filament, start-up in a high magnetic field and electron emission of the filament at fields up to 9 tesla. Filament deformation as observed at JET could be reliably avoided up to 9 T by modifying the filament. The start-up in the magnetic field poses no problem. A limitation of the attainable emission needs further investigations.
Bolometry of core and divertor region: At present miniaturized metal resistor MICA bolometers are regarded as the best choice for ITER. To investigate their performance under nuclear irradiation, various test samples of both 15 $\mu$m thick MICA foils and complete MICA bolometers with 250 $\Omega$ and 1.2 $k\Omega$ resistors were prepared. A first irradiation test of a pure MICA foil with a dose of up to $10^5$ dpa is to be performed in spring '97.
ECE: Activities comprised participation in the design of the front-end quasioptical antennas with subsequent transmission sections, design and cost estimates of the radiometer systems and discussion of the calibration procedure.

## 2. THERMAL STABILITY AND EROSION OF THE SILICON DOPED CFC MATERIAL NS31

M. Balden, J. Roth

The 3D silicon-doped CFC material NS31 with optimized ther-

mal conductivity was investigated. NS31 is reference material for the divertor plates. The sense of the dopant is to decrease the chemical erosion yield and the tritium retention of graphite. The morphology was viewed by scanning electron microscopy (SEM). The distribution and thermal stability of the silicon were controlled by backscattering spectroscopy (BS). Information about the erosion was obtained from of weight loss and $CD_4$ production measurements involving monoenergetic deuterium ions. The material consists of areas of pure graphite Si-covered fibres, and Si or SiC crystallites. The areas cover about $0.01 - 1\ mm^2$. Inside the BS information depth ($20\ \mu m$) the Si distribution is homogeneous, but the Si concentration varies drastically with the lateral position of the analyzing spot ($1\ mm^2$) around the average value of 8-10 at.%.
Heating to 1800 K for 2 hours reduces the mass of the initial material losses by $1 - 5\%$ and SiC crystallites a few $\mu m$ in size are created everywhere on the surface. Investigations of the Si distribution of heated samples show a depletion zone at the surface ($< 1\ \mu m$) followed by an enrichment layer ($6 - 8\ \mu m$). Deep inside the samples the average Si concentration of the initial material is restored. The average over the distribution of the crystallites of $\mu m$ size and the well-known depletion at the surface of the element with the lower sublimation temperature produce the shape of the observed profiles. Due to a second heating a cut face of a preheated sample does not show a Si enrichment layer, but the depletion layer is produced by the evaporation of silicon. The mass loss during a second heating could be neglected.
In both chemical erosion processes, thermally activated hydrocarbon emission ($Y_{therm}$) and kinetic ejection of surface hydrocarbon complexes from a collisional energy transfer ($Y_{surf}$), the chemical erosion is reduced compared with graphite for initial and heated samples. NS31 behaves as expected, with the sputtering yield being somewhere between the yield of graphite and silicon carbide, depending on the Si concentration of the individual surface. The highest reduction of the yield was found for a heated sample: a factor 2 at 40 eV and room temperature and a factor 3 at 1 keV and 800 K. Preliminary implantation and thermal desorption measurements do not point to changes in the implantation and trapping behaviour.

## 3. ITER-ACTIVITIES OF THE BERLIN DIVISION

Two-photon excitation of Lyman$_\alpha$-fluorescence as a diagnostic tool for atomic density of hydrogen isotopes was successfully demonstrated. This diagnostic - developed and tested in close cooperation with Physikalisch-Technische Bundesanstalt Berlin - was used for the first time to determine the density and kinetic temperature of hydrogen atoms in PSI-1. The search for long-term stable first mirrors for ITER is an outstanding problem. The stationary deuterium plasma of PSI-1 was used for studying the degradation of various mirror materials. The mirrors were bombarded with 200 eV $D^+$-ions using a total fluence of $1.5 \times 10^{21}$ D+/cm$^2$. Best results were obtained for rhodium and molybdenum. A number of graphite samples were compared in respect of chemical erosion. These investigations were performed with a constant ion flux density of$1.2 \times 10^{22}$ cm$^{-2}$s$^{-1}$; the target temperature was varied between 250 and 700°C. The maximum erosion yield of 1% was obtained for graphite type NS 31 xy whereas for concept II type we found about 2% at 550°C.

## 4. RUNAWAY ELECTRONS CAUSED BY DISRUPTION IN ITER

M. Schittenhelm

Due to the high loop voltage after the thermal quench during a disruption, a large number of runaway electrons can be generated, many of which can reach high energies. The impact of such a beam of runaways on a small area of a plasma-facing component can result in a high local heat load and damage due to melting. The development of the runaway population strongly depends on the plasma temperature and the contents of impurities. For typical conditions in ITER, the resulting runaway beam reaches energies up to 40 MJ. A high electron density strongly reduces the maximum beam energy, but results in a slow plasma current decay. The combination of a high electron density and high $Z_{eff}$ results in a moderate beam energy and fast plasma current decay. In the present mid-sized tokamak, the runaway energy is limited by the resonant interaction with the toroidal field ripple, but simulations predict that this effect will be insignificant in ITER, since most of the runaways generated will not reach the high energies at which the ripple resonance in this devise is strong enough to limit acceleration. Due to the low critical energy for runaway generation in ITER and the dominance of the secondary generation by close collisions, most of the generated runaways have a large perpendicular momentum compared with their momentum parallel to the magnetic field and are trapped in the magnetic mirror. In spite of detrapping due to pitch angle scattering, the secondary generation rate is reduced by a up to factor of three at the low-field side.

## 5. SURFACE VAPORIZATION DURING HARD DISRUPTION

L. Lengyel in cooperation with IESL.FORTH , Heraklion, and Tech. Univ. of St. Petersburg

Energetic plasma particles moving along the magnetic field lines and bombarding the solid surface are decelerated and in part stopped within the evolving vapour layer covering the surface. Balancing the net current carried by the hot plasma particles by the thermal current of the cold vapour particles, one can determine the strength of the local B-field-aligned component of the electric field. The resultant electric field is directed along

the normal to the solid surface and its strength is determined by the boundary conditions specified at the surface. Scenario calculations performed for graphite-coated divertor plates show that electric potentials of the order of keV may build up across the vapour layer, thus impairing the incident energy flux measured in the shielding clouds surrounding ablating pellets in the JIPP T-IIU tokamak. The resulting local drift velocities may be as high as $10^4 \mathrm{m/s}$. The existence of this lateral drift may impair the anticipated shielding characteristics of the vapour layer. Because of the relevance of pellet experiments in the validation of vapour shield codes, a numerical model is being developed for the global radiation characteristics of impurity pellets injected into hot plasmas ('killer pellets').

## 6. TRANSPORT MODELLING OF ITER WITH 1.5–D BALDUR CODE

G. Becker

A comprehensive scaling law for the effective heat diffusivity $\chi_{eff}$ in high-density ELMy H-mode plasmas has been developed which is compatible with the ITERH92-P ELMy scaling. Model validation tests against three JET and three DIII-D discharges from the ITER Profile Database and against ASDEX Upgrade discharges were carried out. The $\chi_{eff}$ scaling predicted the energy confinement time with an accuracy of about $10\%$ and electron and ion temperature profiles close to the measured ones. It was applied in simulations of high-density radiative mantle scenarios of the ITER IDA device with flat and peaked density profiles.

## 7. GLOBAL CONFINEMENT ANALYSIS

O. Kardaun, in cooperation with the ITER Database and Modelling Expert Group

The prediction of ITER energy confinement in H-mode is still an issue of vivid interest. Of the several approaches in this area, we discuss here only global confinement scalings. The presently most adequate simple power-law scalings are ITERH-93P for ELM-free and ITERH-92P(y) for ELMy H-mode confinement. Unlike the ELM-free data, within the class of simple power laws, the ELMy data do not statistically admit a dimensionally restricted scaling using 7 dimensionless physics variables. However, it is interesting to note that $\tau_{E,th}$ (ITERH-92P(y)) divided by $(n_e B_t)^{-0.05} R^{0.28}$ does so. The factor $R^{0.28}$ can be viewed as a reflection of the empirical fact that the influence of ELM's on confinement decreases with machine size. As already described in the previous annual report, several statistically significant non linear deviations (on log scale) from simple power laws have been detected during the last few years. For instance, the ELM-free dataset exhibits a definite curvature from an offset-linear scaling. This is far less so for the ELMy dataset, which can be explained by the fact that this dataset consists of a mixture of type III ELM's, which are close to the power threshold, and type I ELM's, which lead to a stronger confinement degradation and are usually well above the power threshold. As before, the simple power law scalings lead to a point estimate of 6 seconds and the nonlinear scalings contribute to the $95\%$ interval estimate of (3.5, 9) seconds for $\tau_{E,th}$ in ITER, provided H-mode is reached. Measured JET ELMy confinement times are within some $20\%$ of those predicted by a simple power law from ITERH.DB2, excluding the JET data. The standard ITER power law scalings, based on ITERH.DB2, predict the measured $\tau_{E,th}$ of ALC-CMOD and JT60-U within some $30 - 60\%$ and of
ASDEX Upgrade, except possibly at very high density, within some $15\%$. A further investigation of these differences and improvements of empirical scalings is expected with the assemblage, quality enhancement and analysis of ITERH.DB3, where data from these three machines are included.

## 8. ANALYSIS OF THE ITER DIVERTOR

A. Kukushkin, H. Pacher: ITER JCT, D. Reiter: Forschungszentrum Jülich, D. Coster, R. Schneider

The B2-Eirene code package was used to study the performance of the ITER divertor in the presence of radiating impurity. In these calculations, the total power coming to the edge with plasma was fixed at 200 MW (with allowance for 100 MW radiated from the core). The helium concentration at the core was always kept at $10\%$, and the neon density there was varied in order to see the trends. Three kinds of divertor operation regime - attached, shallow by detached and deeply detached plasma - are analyzed. Transition from one regime to another can be accomplished by changing the pumping rate. Although detached operation seems more attractive from the design point of view, current modelling indicates that the particular regimes shown here could be transient with a time scale of a fraction of a second to several seconds - that is, fast on the ITER operation time scale and extremely slow on the time scale of modelling capabilities. At the extremes of the range (in upstream density, impurity concentration or pumping rate), the plasma will either relax to the normal semi-attached state or collapse, forming an x-point MARFE. The size of the operating window and the possibility of stabilizing the operating point via feedback on the neutral pressure in the private flux region remains to be investigated. Even without full detachment, semi-attached operation with $0.7\%$ Ne is found to yield peak power levels of $5 \mathrm{MW/m^2}$, i.e. falls within the acceptable range with some further optimization. The efficiency of helium exhaust has also been addressed. Whenever the helium pressure of $0.01$ Pa at the entrance of the pump duct is attained, the pumping system of ITER as presently designed can remove the necessary amount of helium to ensure steady-state operation. The calculations indicate that this goal could be achieved even in the regime of semi-detached plasma, and that the helium exhaust conditions become more favourable with transition to detached operation.

# STELLARATORS

IPP's activities in the stellarator field are concentrated on developing the next-step facility in the WENDELSTEIN line, WENDELSTEIN 7-X, and on exploiting the WENDELSTEIN 7-AS experimental facility. Work on the first topic is split between the Experimental Division 2, headed by G. Grieger, for the scientific part, and the Project W 7-X Construction, headed by M. Wanner, for the construction of the W 7-X facility. Work on the second topic is done by Experimental Division 3, headed by F. Wagner. In addition, G. Grieger is responsible for the setting up of the new Institute at Greifswald to house the Greifswald branch of IPP.

Work on W 7-X concentrated on the divertor concept for W 7-X, the development of the various diagnostics and heating systems for W 7-X, W 7-X-related system studies on stellarator based power stations and general stellarator physics studies. The latter part coincides with the start of theoretical work at the Greifswald Branch Institute by the Stellarator Physics Group headed by J. Nührenberg.

Ground braking for the construction of the Greifswald Branch of IPP was done just before wintertime of 1996 with the start of construction of the institute buildings planned for spring 1997.

On W7-AS the ICRH heating system was technically further improved, thus allowing the extension of discharges up to 800 ms and for the first time the study of properties of plasmas sustained by ICRH alone. Two 140 GHz gyrotrons could be successfully operated at heating powers above 400 kW each and pulse lengths longer than 1 s. The neutral beam heating power was increased by regapping the extraction grids of the ion sources.

The neoclassical electron-root solution was observed experimentally for the first time in W7-AS in low-density ECRH plasmas. Theoretically expected and experimentally confirmed positive radial electric fields considerably reduce the neoclassical (electron) heat transport so that electron temperatures up to 4 keV could be reached. The impact of the radial electric field is similar to the negative electric fields found earlier in high-ion-temperature discharges (ion-root). The dependence of the anomalous electron heat transport on magnetic shear was investigated in ECRH plasmas with ohmic heating current drive. First results may indicate an improvement of confinement at high shear, independently of the sign of the shear. A 140 GHz gyrotron was used for collective Thomson scattering experiments in an improved experimental setup operated in collaboration with IAP, Nizhni Novgorod, and IPF Stuttgart. Ion temperatures in reasonable agreement with other diagnostics could be derived. The O-X-B mode conversion heating scenario was applied to an NBI sustained plasma using ECRH at 70 GHz above the cutoff density and at nonresonant magnetic field. A good heating effect was demonstrated. The heating process was theoretically investigated.

The plasma edge studies were continued in preparation for later installation of the island divertor plates in W7-AS. Measurements of the radial density profile across boundary islands with a fast-reciprocating probe indicate at least partial detachment of the plasma at high densities. These observations are quite well reproduced by 3D code calculations indicating high recycling as known from tokamak divertors.

# WENDELSTEIN 7-AS

(Head of Project: Prof. Dr. Friedrich Wagner)

Members of the W7-AS group: see section "Divisions and Groups, Experimental Plasma Physics Division 3".

## 1. OVERVIEW

In 1996 the work on W7-AS was roughly divided into two parts: a technical phase until early June and an experimental period continuing till the end of the year. During the technical phase new top and bottom limiters were installed. They can be drawn back further with respect to the inboard limiters and which are better instrumented. ECRH and NI were improved. Maintenance work at the large power supply in the second half of 1996 slightly impaired the technical conditions for running experiments.

Nevertheless, important new results were achieved and even a new record was established. The highest electron temperatures ever reached in stellarators (4 keV at $2 \times 10^{19}$ $m^{-3}$) could be obtained in W7-AS with evidence that the "electron root" has developed. The necessary radial electric field is possibly due to enhanced losses of trapped electrons. Operation at higher collisionality and with strong ion heating by NBI yields - as the neoclassical particle transport analysis shows - the "ion root" characterized by a negative radial electric field. Measurements of plasma rotation provide experimental access to the radial electric field and confirm the outcome of the analysis.

ICRH, which had its first success in the preceding year, could be improved so that self-sustained ICRH discharges were extended to 800 ms. Experiments with large co- and counter plasma currents may indicate an improvement of confinement at high shear. Concerning the recently detected resonant Electron Bernstein wave heating, clear evidence was found for the two conversion steps, O-mode to X-mode and X-mode to Bernstein waves. Appreciable and effective heating leading to plasma energy increases of 30% could be observed, thus allowing the cutoff density limit and the resonant magnetic field condition to be circumvented under certain conditions.

The scientific programme pursued so far - investigations of the energy and particle transport, plasma turbulence, MHD modes, edge physics and physics of heating and current drive - was continued. Some of these topics derive benefit from newly developed diagnostic instruments. For example, the 10×32-diode soft X-ray camera delivered impressive pictures of MHD modes. In investigations of the density limit in stellarators marfes were detected in W7–AS.

An increasing number of the activities performed at W7-AS are tests for the new experiment W7-X under construction. Examples are the island divertor being constructed for W7-AS and a provisional inboard ICRH antenna.

## 2. EXPERIMENTAL AND THEORETICAL RESULTS

### 2.1 Boundary Layer and Plasma-Wall Interaction Studies

#### *2.1.1 Island divertor studies*

In optimized stellarators with low to moderate shear it is planned to utilize the flux diversion properties of inherent magnetic islands at the boundary for plasma exhaust (e.g. W7-X). In W7-AS, studies (edge code development as well as first experiments) have been performed in order to assess crucial elements of this concept. They are part of an ongoing programme which will include further code completion and experiments with improved configurational control (by additional saddle coils) and more closed divertor geometry (1998).

The studies were performed at an edge rotational transform $\iota_a$ = 5/9, providing both sufficient main plasma cross-section and relatively large, "natural" magnetic islands at the boundary (Fig. 1). Furthermore, this configuration was proved to be sufficiently stable with respect to equilibrium plasma currents at finite plasma pressure. The islands are intersected by ten poloidal graphite targets (toroidal width 12 cm, tilted) at topologically equivalent positions (Fig. 1a).

The aim was to explore whether high recycling and related divertor scenarios can already be established with this extremely open divertor geometry.

*Modelling approaches.* The edge plasma was modelled for the 5/9 island topology by a two-dimensional (B2) and a three-dimensional fluid approach (EMC3), each coupled with the EIRENE neutral gas transport code. The B2/EIRENE approach allows basic divertor properties to be studied with sophisticated physics (proof of principle), but necessarily includes helical averaging of the 3D island configuration and, in particular, cannot treat the present target geometry and hence the interaction with neutrals in a fully realistic way. The EMC3 code utilizes the Monte Carlo technique and considers the full non-axisymmetric geometry, but is restricted, at present, to single-fluid plasma ($T_i = T_e$) only and embodies some simplification of the momentum balance. For these reasons the following gives only a kind of "complementary" picture: the EMC3/EIRENE results are directly referred to experimental data by adjusting free input parameters to match measured densities at certain positions, and the tendencies inferred are briefly compared with B2/EIRENE predictions.

*Experimental.* The analysis was made for net-current-free NBI discharges at B = 2.5 T. Line-averaged densities $\bar{n}_e$ were varied between $2 \times 10^{19}$ and $1.5 \times 10^{20}$ $m^{-3}$. Heating powers were 0.8 MW for $\bar{n}_e \leq 8 \times 10^{19}$ $m^{-3}$ and 2 MW for higher densities. Data were taken during flat-top phases of about 300 ms (low to moderate densities) or 150 - 200 ms (highest densities). In the latter case, density control was lost in general after that time and the discharges were radiatively terminated. Edge plasma parameters were mainly obtained from two Langmuir probes (CFC tips): a fast-reciprocating probe (FRLP) at the position shown in Fig. 1b and a second probe close to one of the targets (downstream probe, Fig. 1a). The measurements were completed by Thomson scattering, UV/VIS spectroscopy, bolometry, and target thermography.

*Experimental and EMC3/EIRENE code results.* Radial density profiles across the island (Fig. 2) are, up to $\bar{n}_e = 8 \times 10^{19}$ $m^{-3}$ ($n_{es} \approx 2 \times 10^{19}$ $m^{-3}$), rather flat inside the island but show steep gradients outside the outer island separatrix (private flux region). At $\bar{n}_e = 1.2 \times 10^{20}$ $m^{-3}$ ($n_{es} \approx 3 \times 10^{19}$ $m^{-3}$), a pronounced maximum close to the outer separatrix ("divertor fan") develops, and the downstream density (Fig. 3a) increases to about three times the upstream density. The downstream $T_e$ drops to about 10 eV in this case. $H_\alpha$ intensities from the target vicinity (Fig. 3b) show a strong increase similar to that of the downstream density. These features are quite well reproduced by the code and indicate high recycling as is known from tokamak divertors. Particle flux enhancement factors inferred reach up to 35, volumetric energy losses due to neutral hydrogen correspond to 50% of $P_s$ at $\bar{n}_e = 1.2 \times 10^{20}$ $m^{-3}$ (Fig. 3b). However, the data indicate significant total pressure drops of the plasma along field lines within the power-carrying island layer which shift, together with the extremely open target geometry, the onset of high recycling to very high density. With the exception of the highest densities, where momentum losses due to CX neutrals become effective, these drops are found to be predominantly balanced by cross-field transport of parallel momentum towards the private sector due to particle diffusion and viscosity.

At $\bar{n}_e = 1.5 \times 10^{20}$ $m^{-3}$ the peak of the cross-island density profile shifts inwards (Fig. 2) and the downstream density decreases ("roll over", Fig. 3a), indicating (at least partial) detachment. This latter interpretation is supported by data from time

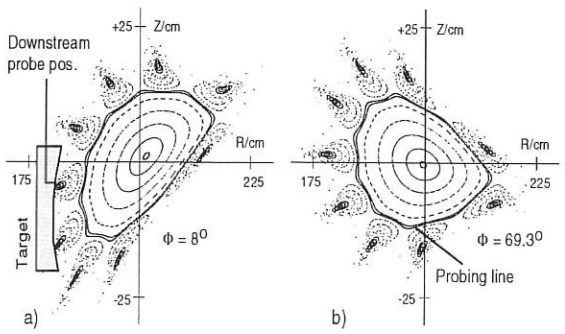


*FIG. 1: Cross-sections of the W7-AS vacuum magnetic field configuration with 5/9 boundary islands at (a) a target plane and (b) a plane with the FRLP probing line. The downstream probe position is indicated in Fig. a.*

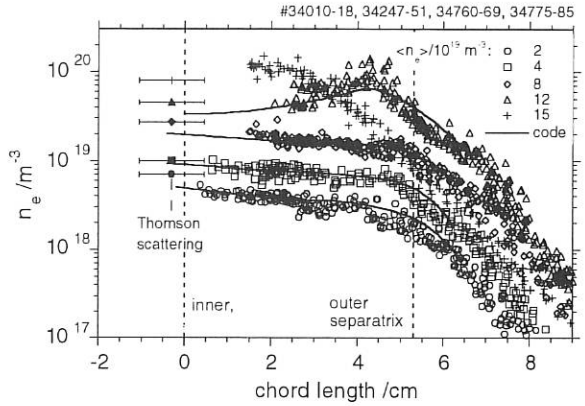


*FIG. 2: Electron density profiles measured by the FRLP across an island, Thomson scattering data measured close to the inner separatrix, and EMC3/EIRENE simulations of the probe data. Positions of the island vacuum field separatrix are indicated.*

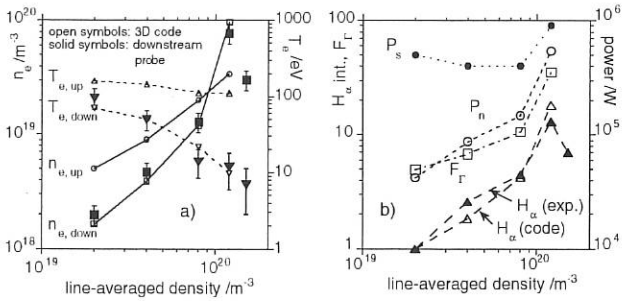


*FIG. 3: (a, left) Upstream and downstream $n_e$ and $T_e$ values from the EMC3/EIRENE code, and downstream probe data. (b, right) Powers $P_s$ crossing the inner separatrix, volumetric energy losses $P_n$ due to neutral hydrogen, particle flux enhancement factors $F_\Gamma$ and $H_\alpha$ intensities from the target. The latter are normalized to unity at the lowest density.*

and space-resolving spectroscopy, bolometry and target thermography. This scenario could, however, not yet be stably maintained. In parallel with the loss of density control, i.e. on a relatively slow time scale of about 100 ms, the hot plasma cross-section shrinks and the discharges become terminated (often via marfe formation at the inboard side).

*B2/EIRENE code predictions.* Time-dependent calculations with self-consistent treatment of carbon as main intrinsic impurity were performed until steady-state was reached. The upstream separatrix density was varied between $10^{19}$ and $5 \times 10^{19}$ $m^{-3}$; the power crossing the separatrix was kept fixed at 600 kW. As Fig. 4 shows, cold divertor conditions with high recycling are predicted for upstream separatrix densities above $2 \times 10^{19}$ $m^{-3}$, which is roughly in line with the above-mentioned experimental phenomenology. At the highest density considered, 85% of the input power is lost from the scrape-off layer volume by radiation (470 kW) and charge exchange (50 kW), but the plasma stays attached. In order to study the transition to detachment and marfe formation, calculations with higher density are under way.

*Progress on 3D edge modelling (EMC3/EIRENE code) since 1995.*

- Implementation of the present targets and momentum sources from the EIRENE code in the EMC3 code.
- Vectorization of the EMC3 code (factor 6 cpu-time global saving).
- Splitting of EIRENE code in two parts to make it available for large 3D plasma and installation structures and to increase flexibility: (a) atomic physics package (1D, no geometry, user-independent), and (b) geometric package (2D or 3D geometry, particle tracing and interaction with plasma-facing components, user-dependent).
- Parallelization of the EIRENE code. In a joint effort with KFA Jülich, the "stratified sampling" structure of the code was generalized for massive parallel processing and successfully tested first on the CRAY-T3D at Garching and then on the CRAY-T3E at Jülich. Performance studies are currently being done.

### 2.1.2 *Radiative boundary studies*

*Steady-state experiments.* The efficiency of radiative edge cooling and its influence on core plasma confinement were studied by injection of nitrogen gas into ECRH (140 GHz, 430 kW) heated, top/bottom limiter bounded discharges. Owing to a low recycling coefficient wall pumping of nitrogen is sufficient for feedback control of the radiation level (N IV, 765 Å). Steady-state plasma density ($4 \times 10^{19}$ $m^{-3}$) and nitrogen radiation can be simultaneously maintained for injection periods up to 0.7 s. At high injection rates density control becomes marginal with the radiation level remaining still controllable.

By increasing the nitrogen level the electron temperature at the LCFS can be reduced from 100 eV to 20 eV. The peak load at the top limiter decreases by a factor of 3. Due to profile narrowing the total power flow is even reduced by a factor of 5 (Fig. 5).

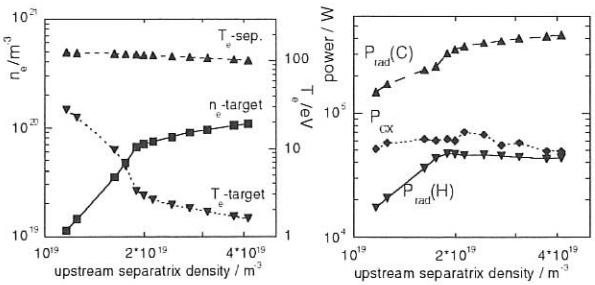


*FIG. 4: Predictions from the B2/EIRENE approach. Electron densities and temperatures (left), and volumetric power losses (right) by deuterium ($P_{rad}(H)$) and carbon ($P_{rad}(C)$) radiation and charge exchange ($P_{CX}$) versus the upstream separatrix density. The power flow across the separatrix is 600 kW.*

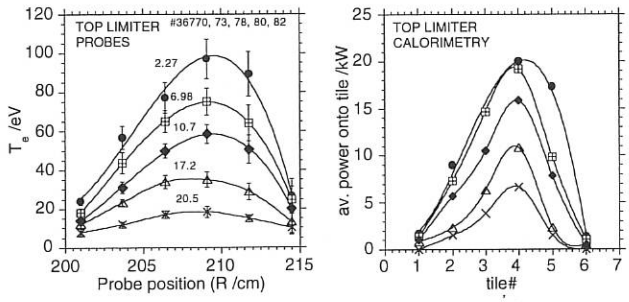


*FIG. 5: Profiles, along the major radius R across the top limiter, of the electron temperature (left, from limiter-integrated probes) and deposited power (right, from limiter calorimetry) for various nitrogen radiation levels (curve labels in arbitrary units). Profile peaks correspond to the LCFS.*

The edge density of about $1.5 \times 10^{19}$ $m^{-3}$ is only slightly affected. In spite of the significant reduction of the target load and edge temperature complete detachment from the limiter has not been reached in steady state. At high radiation levels and low edge temperatures an operational limit is set by a radiative instability propagating from the edge towards the centre. At the radiation limit the total radiation power reaches about 60% of the heating power. The central nitrogen concentration is estimated from CXRS measurements to be 3%. Safe and stationary operation is possible close to this limit. The attempt to exceed it leads to feedback-induced oscillations of the discharge parameters.

The stored plasma energy degrades approximately linearly with the radiation power because, due to the small size of W7-AS, the nitrogen radiation zone cannot be restricted to the very edge. It rather extends down to radii r/a = 0.4 deep in the confinement region and lowers the electron temperature $T_e$ there (Fig. 6). $T_e$ in the very centre is not affected, resulting in steepening of the $T_e$ gradient in the core. In the discharges under consideration neoclassical transport dominates in the core. The electrons are in the 1/ν lmfp collisionality regime, where transport sensitively depends on both the electron temperature and the radial electric field $E_r$. For comparison, in a discharge at a higher density of $8 \times 10^{19}$ $m^{-3}$ which was simultaneously heated by NBI

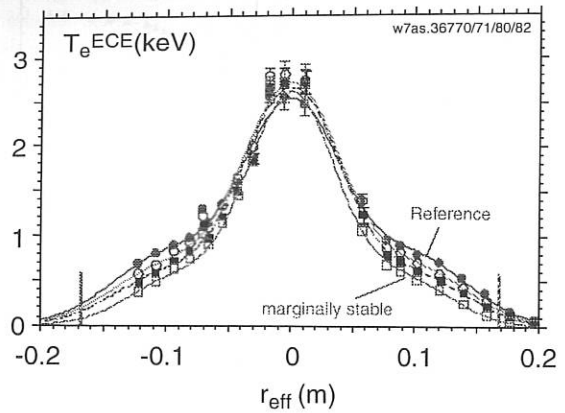


*FIG. 6: Radial electron temperature profiles for discharges with various nitrogen radiation levels.*

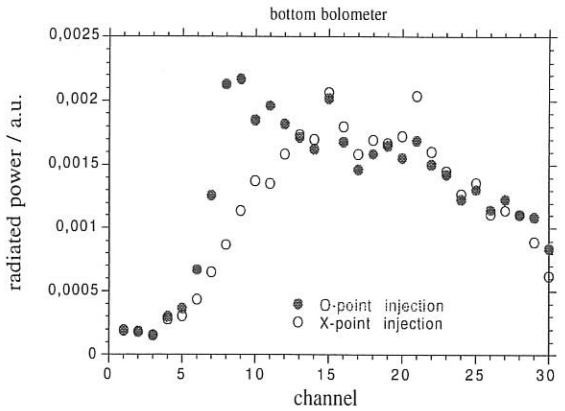


*FIG. 7: Line-integrated radiated power from different bolometer channels during injection into regions near the O-point or the X-point.*

and off-axis ECRH the central temperature significantly dropped from 1.2 keV to 1.0 keV when nitrogen was injected. The latter result can be explained on the assumption that electron heat transport is not affected by edge radiation.

*Transient experiments.* In order to study transport and radiation behaviour of impurities in magnetic islands, nitrogen was injected into natural islands at the plasma edge of separatrix-dominated discharges ($\iota$ about 0.568) by a reciprocating boron nitride erosion probe with a local accuracy of the injection of about 10 mm and a duration of about 10 ms. Due to the injection the electron temperature within the island measured by the probe itself decreased from values of up to 80 eV to about 10 eV. The disturbed region extends transiently far into the confinement region inside the separatrix. Besides the radiation from nitrogen, considerable enhancement of radiation from intrinsic impurity species occurred. This observation is explained by the increase of radiation with decreasing plasma edge temperature and a deeper penetration of the ion impurity species. Moreover, the impurity screening of the SOL plasma is strongly reduced at separatrix temperatures below 10 eV.

The spatial distribution of the radiation induced on injecting nitrogen in a magnetic island configuration of W7-AS was found to be only slightly dependent on the location of the injection (X- or O-point, see Fig. 7). In contrast, the radiation pattern is much more sensitive to the plasma density. Enhanced radiation mainly occurred on the inboard side. When the density was increased, plasma shrinking induced by the impurity injection was observed to start at densities of about $1 \times 10^{20}$ m$^{-3}$. Transient, complete limiter detachment was found together with strongly localized radiation at densities of $1.6 \times 10^{20}$ m$^{-3}$. The temporal evolution of the edge radiation on injecting the impurity within the island of W7-AS does not indicate significant impurity confinement within the islands.

## 2.2 Confinement and Transport

### 2.2.1 *Experimental observation of the neoclassical electron-root solution*

For the first time the neoclassical electron-root solution was observed experimentally in a stellarator for stationary discharge conditions. Active charge exchange recombination spectroscopy on helium was used to measure the toroidal and poloidal rotation velocity. The radial force balance equation is solved to obtain the experimental radial electric field $E_r$. The results are compared with neoclassical estimates obtained from the ambipolarity condition for the fluxes as determined by the DKES code. For the electron-root solution in W7-AS, strong positive values of up to 400 V/cm are expected for effective minor radii $\leq$4 cm. This agrees well with the experimentally observed values of more than 500 V/cm.

The diagnostic beam width was reduced to 2 cm to enhance the spatial resolution for the electric field measurement in the vicinity of the magnetic axis. Discharges with a relative He density of up to 30% are performed to increase the spectroscopic signal-to-noise ratio. Central electron densities below $2 \times 10^{19}$ m$^{-3}$ and high ECR heating power $\geq$400 kW in X-mode heating are necessary to attain the electron-root experimentally. Great care is taken to ensure that the ECR power deposition is exactly at the location of the magnetic axis. The appearance of the electron-root feature coincides with the location of a local magnetic field minimum in the ECRH resonance layer. This might indicate that enhanced $\nabla B$ drift of trapped electrons near the magnetic axis is a pre-requisite to drive $E_r$ towards the observed strong values.

### 2.2.2 *Magnetic shear and transport*

Net currents in the range -30 kA $\leq I_p \leq$ +30 kA were induced by the OH transformer in ECR-heated target plasmas. Radial profiles of the electron temperature and rotational transform are shown in Fig. 8 (left) for three cases with +30, 0, and -30 kA.

Two distinct effects are seen: i) Whereas strong temperature gradients exist within r/a < 0.3 for the case with zero net current and with positive currents, significantly lower central temperatures are measured in the negative-current cases. ii) Strong temperature gradients exist in the outer plasma region around

r/a = 0.8 for all cases with net currents >5 kA, independently of the sign of the current.

The ι profiles for negative currents indicate low central values, which may explain the central confinement degradation with increasing negative currents. The good confinement in the outer plasma region with both positive and negative net currents may be due to significant shear in this region.

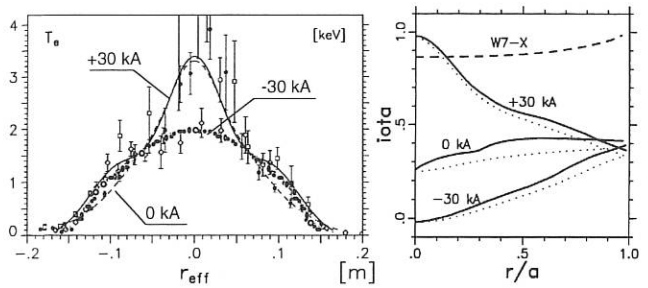


*FIG. 8: Radial profiles of the electron temperature (left) and the corresponding profiles of the rotational transform (right).*

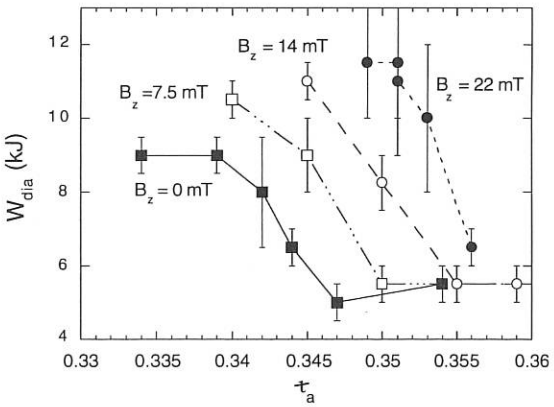


*FIG. 9: Diamagnetic energy content of ECH and NBI (solid circles) heated discharges at different $B_z$ and $\iota_a$ values. The error bars give the variation of the energy with time, large error bars indicate transitions between high and low confinement.*

### 2.2.3 *Confinement variations with small iota changes*

The energy confinement time in W7-AS is a complicated function of the rotational transform. The highest confinement is achieved in the vicinity of the major rational numbers ι ≈ 1/3 and 1/2. In between these regions of good confinement, degraded confinement is found and could be attributed to higher order rational ι values inside the plasma.

The degradation of confinement at ι values above 1/3 was investigated in a series of discharges at the same density of $n_e(0) \approx 1 \times 10^{20}$ m$^{-3}$ and ECH power of P ≈ 0.4 MW. In Fig. 9, the energy content of these discharges is plotted as a function of the systematically varied edge rotational transform $\iota_a$ (vacuum field configuration) and the vertical magnetic field $B_z$. The actual ι profile has to be calculated from the bootstrap and ohmic currents and including β effects as calculated by the VMEC MHD equilibrium code.

The critical $\iota_a$, at which the energy content drops, increases with increasing $B_z$. Preliminary calculations of the actual ι profile indicate, however, that the transition occurs at similar critical ι values. At lower plasma density, the relative change in confinement is less pronounced. Both the electron temperature and density profiles indicate that the degradation of confinement is introduced by the outer third of the plasma cross-section. The inner part seems to be much less affected.

An m=3 mode with a frequency of 15-18 kHz rotating in the electron diamagnetic drift direction can be identified for discharges with a rotational transform near the 'step' from high to low confinement. It is almost impossible to find a smooth dependence of the amplitude of the mode on the $\iota_a$ value; rather the mode is switched on when the confinement drops, and is turned off again with increasing values of the rotational transform, although the confinement remains low. The relative amplitude of the mode decreases with increasing $B_z$. A discharge with a density ramp and the 'critical' iota value also exhibits the m=3 mode. The mode appears at a line-averaged density of $3.5 \times 10^{19}$ m$^{-3}$. Its frequency drops with decreasing electron temperature from 25 kHz to 15 kHz. The possibility that the m=3 activity might be Alfvén mode driven by drift-wave turbulence is currently being investigated.

### 2.2.4 *High-confinement NBI discharges*

The longest energy confinement times in W7-AS were achieved in purely NBI-heated discharges under low wall-recycling conditions. Transport analyses show that at about 2/3 of the plasma radius a region with very low values of the heat diffusivity develops, where the experimental fluxes are comparable or even lower than the neoclassically predicted ones. The region of low transport is also characterized by strong gradients in the radial electric field and shear in the perpendicular flow. These features as well as the low edge density are also characteristic of the high ion temperature discharges previously reported, which were achieved with combined ECH and NBI heating.

The high confinement discharges can be distinguished by a low edge density and a, for W7-AS, high density peaking factor as well as by a gradual improvement of energy confinement. During a phase which can last up to three energy confinement times the electron temperature in the purely NBI-heated discharges rises at constant line-averaged density. At the same time, the edge density decreases and the density profile becomes increasingly narrow (see Fig. 10).

The discharge in Fig. 10 was heated by 330 kW of NBI, leading to a central electron and ion temperature of about 800 eV at a central density of $1 \times 10^{20}$ m$^{-3}$. The maximum energy content was above 13 kJ and the energy confinement time was improved by a factor of about 2 compared with the ISS95 scaling. During the phase of constant energy content, no strong impurity accumulation was observed and the discharge duration was not limited by radiative losses.

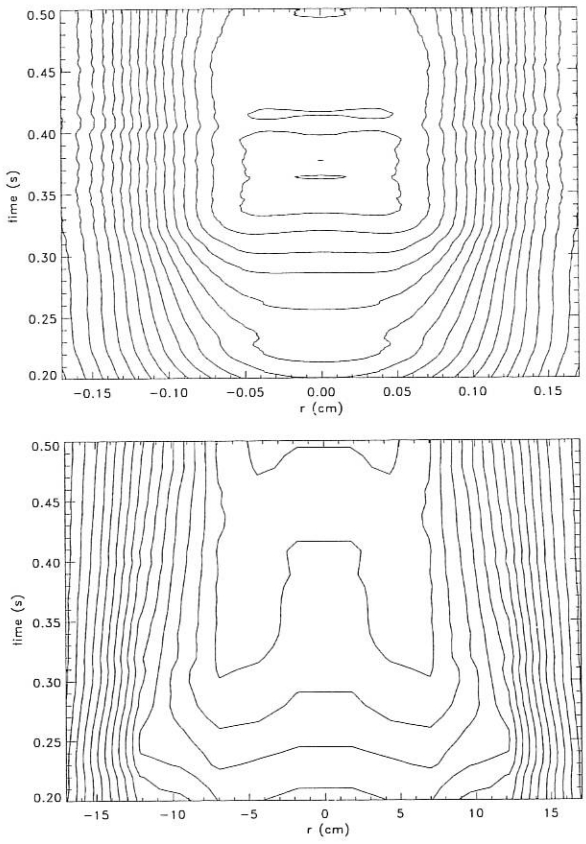


*FIG. 10: Electron temperature (top, max. 800 eV) and density (bottom, max. 1 × $10^{20}$ $m^{-3}$) profiles as a function of time for # 37553.*

### 2.2.5 *Impurity transport in high-confinement discharges*

To study the impurity transport in high-confinement discharges (see 2.2.4), during a nearly stationary phase of 100 ms aluminium laser blow-off experiments were performed.

Transport coefficients were derived by analysis of radially and temporally resolved radiation measured by the soft-X camera behind 25 µm beryllium filters during the penetration process of the injected aluminium into the plasma centre. The impurity density profiles were reconstructed for each time point, assuming coronal equilibrium in a first step, which is considered to be applicable in the high-density, high-confinement discharges under investigation. The transport coefficients were then derived from the analysis of impurity density fluxes calculated from the temporal and radial behaviour of the reconstructed impurity density profiles. Deviations from the coronal equilibrium due to non-negligible transport were taken into account by additional transport code calculations.

The transport coefficients could be measured only in the central half of the plasma and were linearly extrapolated to the minor plasma radius a. A rather low diffusion coefficient D(r) = 0.07 $m^2/s$ and an inward convection velocity of v(r) = 4(r/a) m/s were derived. With these values, the temporal evolution of spectral lines of Al X (33.3 nm) (measured by a grating spectrometer), of Al XII (0.778 nm) (measured by a crystal spectrometer) and of the radial soft-X profile itself could be simulated well by the SITAR transport code.

The results could not yet be compared with those from discharges at similar plasma parameters but without improved confinement.

### 2.2.6 *Investigation of the density limit*

Bolometer measurements of density limit discharges in a magnetic field scan on W7-AS were studied in detail. The first step towards using the ASTRA transport code with tokamak models, as proposed by Borrass (with stable thermal equilibrium in front of divertor/limiter plates and detachment at the density limit) or Stottler (radiation limit with corona equilibrium), was taken with the long-term aim of testing whether the physics used as the basis for these models can also describe the stellarator density limit. Experimentally, it was found that the maximum line-integrated density scales with the magnetic field to the power 0.75. Compared with ASDEX density limit discharges, the Greenwald limit for W7-AS in the large-aspect ratio, low-beta circular approximation appears to be a factor of 2 at least greater. Marfes in density limit discharges in W7-AS have been observed, as shown in Fig. 11. The marfes mostly occur well after the plasma energy content has begun to sink and the line-integrated density has reached its maximum. This is in contrast to JET limiter discharges, where the density limit coincides with marfe formation. The time scale for growth and decay of the marfe is 60 ms but it does not repeatedly grow and

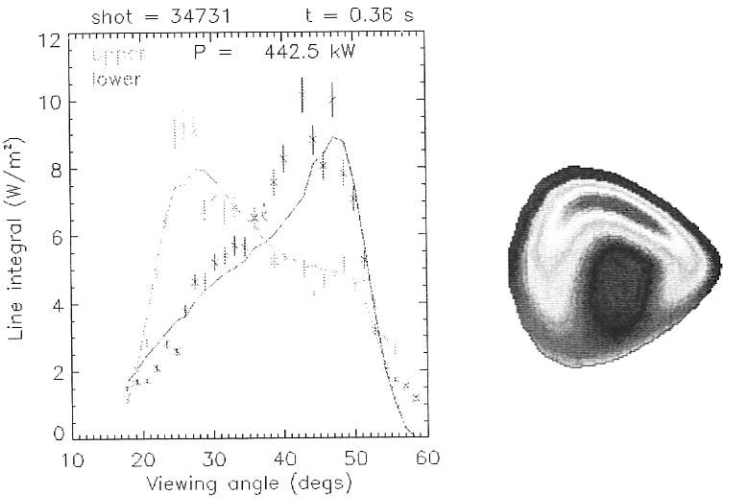


*FIG. 11: Marfe event in W7-AS. On the left, the line-integrated measurements from two bolometer cameras and on the right the tomographic reconstruction of the radiation power density. The marfe occurred after the peaks in diamagnetic energy and line-integrated density.*

collapse as observed in JET density limit discharges.

### 2.2.7 *Transient transport studies*

#### 2.2.7.1 *Density modulation experiments with multichannel microwave interferometer*

In order to determine the transient particle transport coefficients, density oscillations (see Fig. 12) were produced by injecting harmonic gas feed into the plasma.

A computer code was written to reconstruct the electron density profile from 10-channel microwave interferometer data. The electron density profile was chosen in the reconstruction algorithm such that the simulated line integrals fitted the data, and the information content of the profile was minimized by searching for an extremum for a regularization functional. On the basis of computer simulations, Fisher information was chosen to be used in practice as the regularization functional instead of the maximum entropy.

With the aid of the electron density reconstruction code, a phase shift of the density perturbation was detected, while the perturbation propagated from the plasma edge to the centre during density oscillation experiments. The multichannel microwave interferometer data will be analyzed by solving the transport equation and adjusting the transport coefficients in order to fit the Fourier coefficients of the measured line integrals.

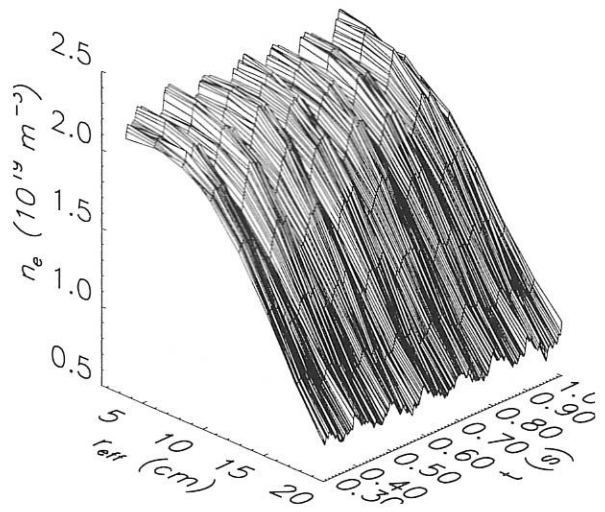


*FIG. 12: Temporal evolution of the density profile in # 36120. Density oscillations are produced by modulating the gas feed to the plasma*

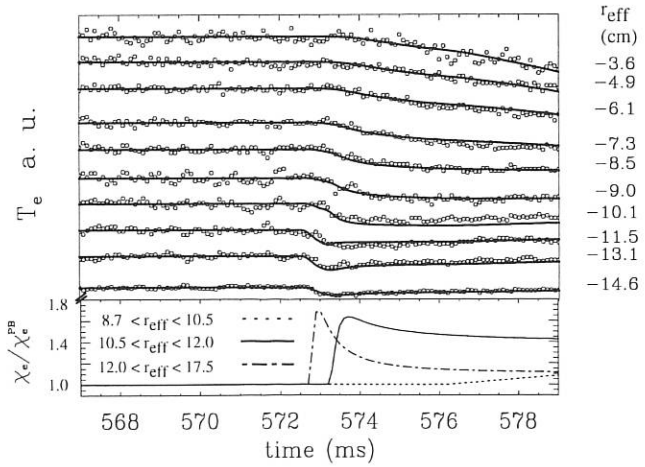


*FIG. 13: Cold-pulse propagation after injecting C-atoms in an ECRH discharge. The ECE electron temperatures are compared with the results form a time-dependent transport code (lines). In the lower part, the evolution of the diffusivity at different radii is described.*

#### 2.2.7.2 *Cold-pulse experiments*

Cold-pulse experiments were carried out by injecting aluminium or carbon atoms by laser blow-off. By radiative cooling a temperature perturbation is generated at the plasma edge. The propagation of the pulse to the centre is compared with model calculation.

The energy transport equation is solved and $\chi_e$ is varied in order to reproduce the measured electron temperature evolution. In Fig. 13 the time traces of the measured and simulated electron temperature are depicted at various radii. The heat diffusivity used in the simulation is described in the lower part of the figure. The value of the diffusivity in the stationary phase $\chi_e^{PB}$ of the discharge was evaluated prior to the impurity injection. In order to reproduce the data after the C-injection, the diffusivity had to be changed in time as follows: (i) The fast drop in the edge temperature can be simulated if $\chi_e$ increases abruptly in the region r > 12 cm. The radiation losses calculated with the STRAHL code are not large enough to account for the edge temperature drop. (ii) At r > 10.5 cm, the increase needed is delayed by 0.5 ms. (iii) In the inner region, a slower increase of the diffusivity is sufficient to fit the data. A diffusivity which depends on the local temperature does not fit the data.

### 2.2.8 *Plasma rotation and viscosity*

The dominating damping mechanism for plasma rotation is viscosity. In a strong magnetic field we distinguish parallel viscosity as a result of magnetic pumping and perpendicular viscosity due to sheared flow.

Parallel viscosity is the main damping mechanism for poloidal rotation in toroidal systems. Toroidal rotation, however, is usually damped by (anomalous) perpendicular viscosity as long as the toroidal variation of the magnetic field is small - as is the case in tokamaks.

For stellarators, the roles of neoclassical and anomalous damping mechanisms in toroidal rotation are studied as a function of the toroidal magnetic field ripple. While tokamaks exhibit no threshold for toroidal rotation due to their symmetry properties, in the case of stellarators the broken toroidal symmetry and strong variation of the magnetic field increase viscous damping

and introduce a threshold for rotation. Thus, viscous damping may be investigated in stellarators by maximizing these effects.

Previously it was found in W7-AS that in standard configurations anomalous viscous effects seem to dominate, whereas neoclassical viscosity is dominant in high mirror configurations.

Investigating the density dependence of toroidal rotation and its viscous damping, we find totally different behaviour in our standard (S) and high mirror (A) configurations. Due to improved beam coupling the ion temperature increases with density, see circles in Fig. 14. The rotation velocity in the high ripple case (A) slightly decreases with density, as expected from neoclassical calculations. However, in our standard case we find a strong increase with density.

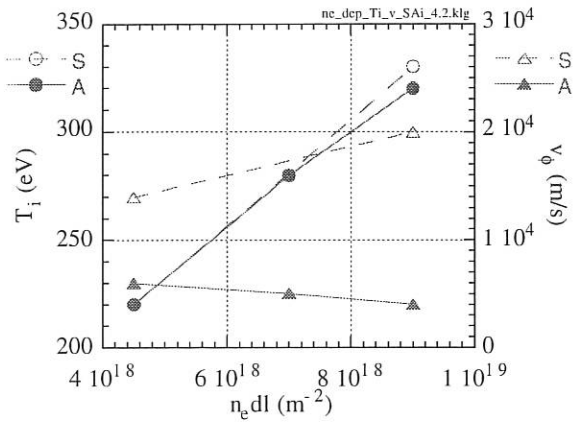


*FIG. 14: Ion temperatures and toroidal rotation velocities for standard (S) and high mirror (A) configurations as a function of plasma density.*

### 2.2.9 *Micropellet injection experiments*

Aluminium micropellets (40x40x10 μm) were accelerated by an intensive laser pulse using one of the blow-off injection devices of W7-AS. Several pellets, having velocities from 50 to 500 m/s, were injected into one plasma discharge. Micropellets contain not more than $10^{15}$ atoms and this way they do not perturb the plasma in a global sense. They penetrate to a maximum depth of 5 cm behind the Last Closed Flux Surface (LCFS) in low-density ECRH-heated discharges.

One aim of these experiments was to cross-check impurity transport measurements by an aluminium laser blow-off beam. As a certain time is required to heat the pellets to a temperature where ablation begins, the aluminium atoms contained in these pellets were all deposited inside the LCFS, which is not the case for laser blow-off beam injection. In contrast to the different injection techniques and impurity deposition depth, the decay time of highly ionized Al line radiation from the core plasma was found to be the same.

Recording the time history of visible line radiation emitted by low-ionization-stage aluminium ions during the micropellet ablation one can observe pronounced fluctuations (striation) similar to the case of millimetre-size pellet injection. As the origin of these fluctuations is not yet clear, comparative statistical investigations were done on the W7-AS stellarator and TEXTOR and MT-1M (Budapest, Hungary) tokamaks to compare the fluctuation frequency and amplitude as a function of the pellet velocity. As can be seen in Fig. 15, the mean fluctuation frequency does not depend on the pellet velocity, although the latter changes about an order of magnitude. This fact indicates that the process which generates the fluctuations does not depend on a characteristic length (e.g. pellet cloud diameter, structure scale in plasma) but rather on a characteristic time (e.g. pellet cloud instability growth time, repetition rate of short-lifetime plasma perturbations).

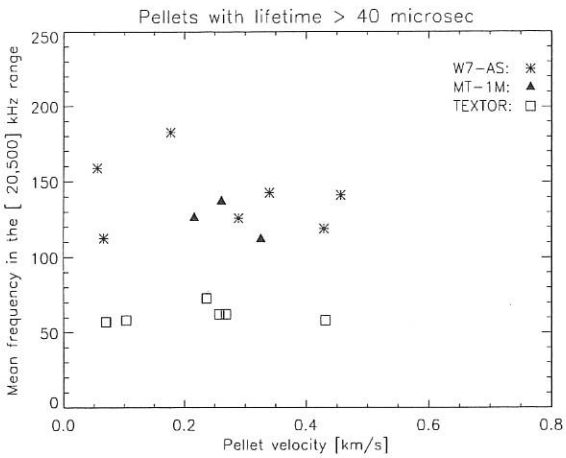


*FIG. 15: Mean frequency of fluctuations in Al III line radiation during micropellet ablation as a function of pellet velocity for different devices.*

### 2.2.10 *Fast-particle confinement*

To study the confinement of energetic ions we investigated the slowing-down of neutral beam particles. Active neutral particle analysis (NPA) is used to measure the velocity distribution of fast particles at two radial points.

In addition, neutron yield measurements were made in deuterium discharges with deuterium NBI at 50 keV. The neutron yield is dominated by beam target fusion reactions, and therefore is strongly related to the fast-particle velocity distribution. The absolute value of the volume-integrated neutron flux is measured with activation samples.

We use a time-dependent 2D Fokker-Planck code to simulate the measured neutral particle spectra and the neutron yield. The code takes into consideration the slowing-down of the fast ions, pitch-angle scattering and energy diffusion. It neglects additional particle losses induced for example, by neoclassical and turbulent transport or by particle-wave interactions.

The experimental values were taken at various plasma densities and temperatures. The energy-relaxation time thus varies between 5 and 50 ms at energy confinement times ranging from 20 to 5 ms, respectively. Figure 16 shows the ratio between simulation and measurement for the fast-particle densities and

neutron yields. At relaxation times longer than 20 ms systematic deviations of both the neutron rates and fast-particle fluxes from the calculated ones are observed. This indicates the importance of fast-particle losses if the slowing-down time becomes appreciably longer than the thermal confinement time.

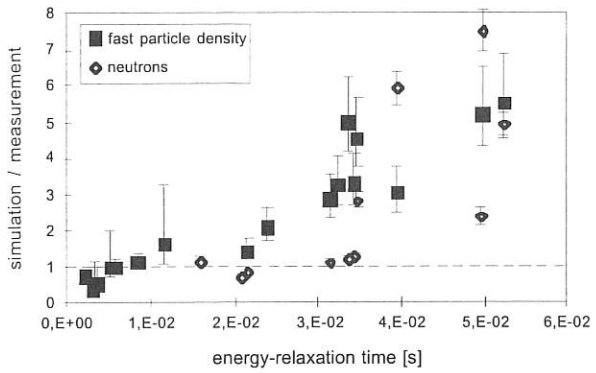


*FIG. 16: Ratio of simulated and measured fast-particle densities and neutron yields as a function of the energy relaxation time.*

## 2.3 Ion Cyclotron Resonance Heating

During the winter/spring 1996 opening of the vessel, the thin stainless-steel leads of the ICRH antenna were replaced by thick silver-plated copper leads in order to reduce the antenna inductance and increase the antenna voltage stand-off for long pulses. In order to avoid damage to the antenna and/or transmission line, the RF generator was equipped with a new fast switch that terminates the RF power within 50 μs in case of arcing. It was thus possible to condition the antenna and transmission line system so that voltages of up to 60 kV could be held. Self-oscillations of the transmitter limited the RF power to less than 600 kW.

This antenna was connected in π-phasing which leads to a narrow $k_{||}$-spectrum centred at $k_{||} = 6\ m^{-1}$. The vacuum loading of the antenna was about 0.65 Ω. The loading increased with plasma to about 1.2 Ω. It then follows that only one half of the generator power was radiated into the plasma and the other half was dissipated in the antenna by ohmic losses. Under these conditions it was possible to heat both helium and deuterium ECRH plasmas and sustain deuterium plasmas if the concentration of resonant hydrogen ions was 10% or less for both cases.

The dependence of the plasma loading on the distance between the antenna and fast wave cutoff agrees with an inverse decay length given by $2 \times k_{||}$. The absolute value of the plasma loading agrees with the value given by a theoretical model which assumes strong collisional absorption at the mode conversion layer.

Plasmas were sustained with ICRF alone under almost steady-state conditions for as long as 800 ms, i.e. >40 confinement times. No upper bound to the pulse length was found. The duration of the RF pulse was only limited to avoid warming-up of the uncooled antenna. The plasma density was predominantly determined by wall recycling and typically assumed values of about $\bar{n}_e \approx 4 \times 10^{-19}\ m^{-3}$. The maximum diamagnetic energy achieved was 4 kJ. The bolometric radiation stayed constant during the RF pulse and was comparable to ECRH plasmas of equal diamagnetic energy. The VUV diagnostic, however, observed a slow increase in iron and chromium radiation. The electron and ion temperature had flat profiles with equal central temperatures of about 450 eV. The electron density profile was slightly hollow with larger gradients at the plasma limiter radius than found in comparable ECRH plasmas. No fast minority ions were observed with active CX. If, however, the electron temperature was raised to $T_e \geq 2$ keV by an ECRH pulse, a tail in the minority ion distribution built up. Energetic ions with $E \geq 20$ keV could be detected by NPA at 45° to the magnetic field lines for 150 ms or more after the end of the ECRH pulse, although the electron temperature had dropped to its initial value with a decay time $\tau_E \geq 20$ ms.

ICRF heating increased the diamagnetic energy of an ECRH deuterium or helium plasma by about 25%. The central deuterium temperature increased from 450 eV to 600 eV. The central and edge electron temperature rose by about 200 eV. The bulk temperature of the minority hydrogen ions increased from 400 eV to 1.5 keV. A tail in the minority energy distribution function built up such that energetic ions with energies of up to 50 keV could be observed. An increase in the radial electric field was measured during ICRF heating. It was, however, not strong enough to confine the most energetic ions if they were generated in the local magnetic mirror in front of the antenna. It seems therefore likely that most the RF power was absorbed outside the local mirror, i.e. toroidally away from the antenna location. After ICRF heating was turned off the tail of the minority ion distribution function relaxed within 30 to 40 ms. The bolometric signal increased from 50 kW to 80 kW during the ICRF pulse.

From ICRF power switch-on/off and modulation experiments it was found that only about 50% of the radiated ICRF power was absorbed in the plasma. On the other hand, it was also found that the dependence of the confinement time on ICRF power agrees with the established stellarator confinement time scaling $\tau_E \sim P^{-0.54}$. From this scaling it would then follow that all of the RF power radiated from the antenna was absorbed in the plasma. Although many causes could be invoked for this discrepancy no definitive explanation has yet been found.

A second antenna, launching a broad $k_{||}$-spectrum centred around $k_{||} = 12\ m^{-1}$, was installed at the toroidal location where the plasma cross-section is triangular and has an almost constant magnetic field profile. The antenna has no Faraday shield. It was operated at low power (≤1 kW) and showed the high plasma loading expected at these power levels.

## 2.4 Electron Cyclotron Resonance Heating

### *2.4.1 EC heating via O-X-B mode conversion*

Mode conversion heating from an O-wave to an X-wave and, finally, to Electron Bernstein Waves (O-X-B), was investigated

and successfully demonstrated on the W7-AS stellarator. This scenario allows us to extend the experimentally accessible plasma densities with electron cyclotron heating (ECH) beyond the plasma cutoff density and removes the restriction to operate at resonant magnetic field. In addition to the heating effect, clear evidence for both mode conversion steps was detected. An example of the angular dependence of the O-X process is shown in Fig. 17.

Density fluctuations at the O-X-conversion layer can strongly reduce the O-X conversion efficiency, as was demonstrated experimentally. High heating efficiencies were achieved at target plasmas with a relative fluctuation level of less than 2% or with a very low density scale length ($L < 1$ cm), which compensates the influence of the high fluctuation level at the density gradient region. Both findings are consistent with a calculation of the conversion efficiency using a statistic description of the density fluctuation.

To explore the potential of the O-X-B heating for routine high-density operation the 70 GHz launching system was upgraded with two elliptical polarizers which now allow us to launch the full ECRH power of 330 kW with pure O-mode polarization and the optimal O-X-B launch angle into the plasma. The target plasma was sustained by 360 kW neutral beam injection (NBI). Additional O-X-B heating increases the plasma energy, i.e. the central plasma temperature, by 30% ($\Delta W = 2.5$ kJ, $\Delta T = 110$ eV) compared with a discharge with NBI only. Thus more than 80% of the power was found inside the plasma, taking into account the power scaling ($P^{-0.6}$) of the energy confinement time.

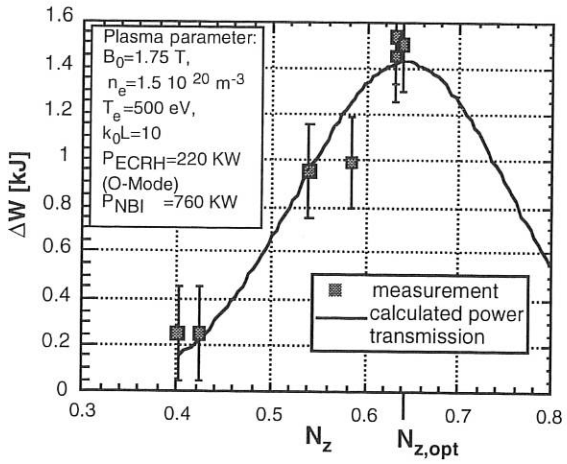


*FIG. 17: Increase of the plasma energy content $\Delta W$ by O-X-B-heating versus the longitudinal vacuum refractive index $N_z$ of the incident O-wave. The solid line is the calculated transmission function multiplied by the maximum energy increase.*

### 2.4.2 *Trapped-particle effects on the ECRH power deposition profile*

The ECRH power deposition in low-density, high-temperature plasmas has been analyzed at W7-AS for different magnetic configurations and heating scenarios (on-axis fundamental O-mode and second-harmonic X-mode).

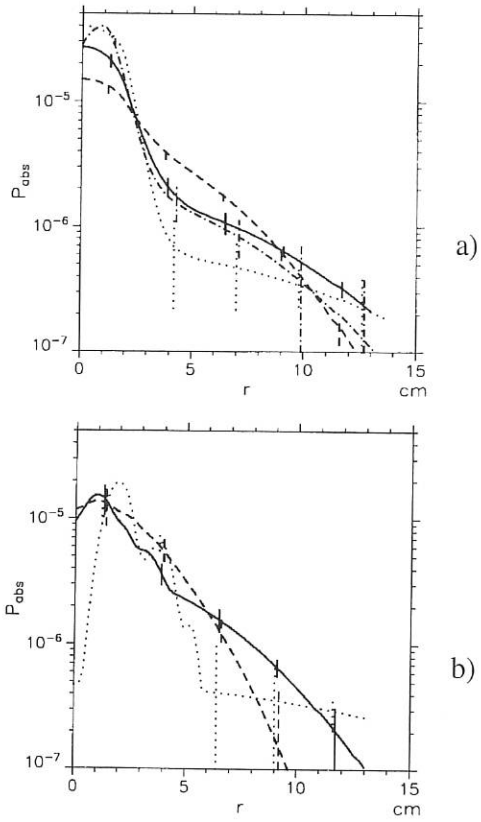


*FIG. 18: Power deposition versus effective radius. a) $B_0$ = 2.5 T. The solid and dashed lines refer to the fundamental O-mode heating (70 GHz), for $n_e = 2 \times 10^{-19}$ m$^{-3}$ and $n_e = 10^{-19}$ m$^{-3}$, respectively. The dotted and dash-dotted lines are the corresponding results for the second-harmonic X-mode heating (140 GHz). b) $B_0$ = 1.25 T, and $n_e = 2 \times 10^{-19}$ m$^{-3}$. The solid line refers to the "standard" configuration, the dashed and dotted lines to the configurations with a deeper minimum or a maximum of B in the ECRH injection plane, respectively.*

The absorption profile was evaluated from the propagation of heat waves generated by modulating the ECRH power at different modulation frequencies. The results present a much broader component in addition to a peaked component, which agrees with the deposition profile predicted by a 3D ray-tracing code. Taking the broader component into account, the total input power is recovered by the analysis, i.e. no indication of "missing power" was found.

This broadening of the power deposition profile was related to the radial transport (determined by the $\nabla$B-drift) of the locally trapped suprathermal electrons generated by the ECRH. The particles drift vertically, becoming passing particles by pitch angle scattering and contributing to the energy flux in the outer plasma region without direct ECRH deposition, through thermalization on the flux surfaces.

The results for the power deposition profile in the "standard" configuration of W7-AS are summarized in Fig. 18, while its dependence on the magnetic field configuration is shown in Fig. 18b. In agreement with the expectations based on the $\nabla$B-

drift of trapped electrons, the power deposition becomes broader with decreasing density or magnetic field strength. Moreover, in the case of a magnetic configuration with a local minimum of B in the ECRH injection plane (where a significant fraction of the injected power is deposited on trapped particles) the absorption profile is considerably broader than in the opposite case with a local maximum of B in the injection plane (where only passing particles are directly heated).

### 2.4.3 *Non-thermal electron energy distribution from vertical ECE measurements*

The appearance of suprathermal electrons during ECRH heating with high power density leads to a distortion of the Maxwellian electron energy distribution. By measuring the cyclotron emission of the electrons information about their energy distribution can be obtained, especially about characteristic parameters of suprathermal electrons such as their number and spatial distribution. While an antenna with a horizontal line of sight is used to get the local electron temperatures, which results in reabsorption of the main part of the relativistically down-shifted ECE radiation of the suprathermals by the thermal background, a vertical direction of observation with nearly constant magnetic field along the viewing line limits the reabsorption to a narrow frequency range and the line-averaged down-shifted suprathermal emission can be directly measured.

A new vertically viewing antenna system was constructed using Gaussian beam optics to get a high spatial resolution. The antenna is arranged in the ECRH deposition plane and is movable about 6 cm in the radial direction across the ECRH deposition zone, allowing us to change the parts of the thermal and suprathermal radiation components and localize in this way the suprathermal electrons. By measurements it was confirmed that the calculated beam waist in the plasma centre of about 17 mm

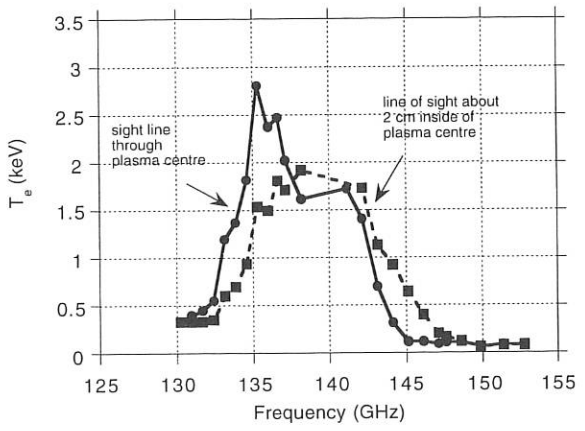


*FIG. 19: ECE spectra of an ECRH plasma (B = 2.5 T, P = 0.8 MW, ι = 1/3, $B_z$ = 250 G) as measured with the vertically viewing antenna using two different lines of sight with a distance of 2 cm. The spectrum with the sight line through the plasma centre (solid line) shows a suprathermal peak and is shifted to lower frequencies compared with the second one (dashed line) due to the lower magnetic field along the observation line.*

is reached very well. In addition, the exact vertical alignment of the line of sight was checked. An absorber at the opposite side suppresses contributions from multiple reflections which might significantly increase the radiation temperature of the detected radiation.

The second-harmonic ECE spectrum was measured in X-mode polarization in the frequency range of 130 - 155 GHz at $B_0$ = 2.5 T. The ECRH heating power and the plasma density were varied as well as the plasma position by changing the adjusted vertical field. Figure 19 shows as an example two measured spectra with the same plasma parameters, but different lines of sight of the vertically viewing antenna. Only in the vicinity of the plasma centre at about 136 GHz in Fig. 19, the suprathermal part appears indicated by an increase in radiation temperature. In the ECRH deposition plane the suprathermal population seems to be located in a small area around the plasma centre with a diameter of less than 4 cm. The comparison of measured ECE spectra with calculated ones shows that only about 1% of the electrons are suprathermal. It is planned to improve the simulation program to get more realistic calculations. Experiments with modulated ECRH heating shall show the time behaviour of the suprathermals.

## 2.5 MHD Activity and Fluctuations

### 2.5.1 *Tomographic reconstruction of MHD modes*

Since spring 1996, a small-size camera system (*MiniSoX*, miniature soft X-ray camera) for imaging of the plasma soft X-ray radiation is in operation. The camera system was introduced in IPP Annual Report 1995, page 64. Its main characteristic is the high number of cameras (10) with a total number of 320 viewing chords that are distributed almost uniformly over a poloidal cross-section. The actual position of the viewing chords was calibrated by a new method using experimental data for each individual camera that are Abel-inverted with the Maximum-Entropy algorithm.

The physical interest focuses firstly on MHD instabilities and, secondly, on plasma equilibrium effects. Examples concerning MHD modes are compiled in Fig. 20, which shows four reconstructions of modes with poloidal mode number m=3. Although a common (rather wide) m=3 structure is quite obvious in all cases, the mode structure differs in detail. This may be due to different physical origins: global Alfvén eigenmodes (GAE) , pressure-driven modes and tearing modes. In particular, comparing the two GAE cases (a,b) shows that the difference may be caused by different poloidal velocity shear in the plasma.

Furthermore (not shown here) multiple simultaneous GAE modes with different poloidal mode numbers and radial positions were reconstructed.

Concerning the reconstruction of equilibrium distributions, firstly the effect of the Shafranov shift and secondly the modification of the equilibrium by ohmic currents of both polarities were investigated. The tomographic reconstructions are in agreement with equilibrium calculations.

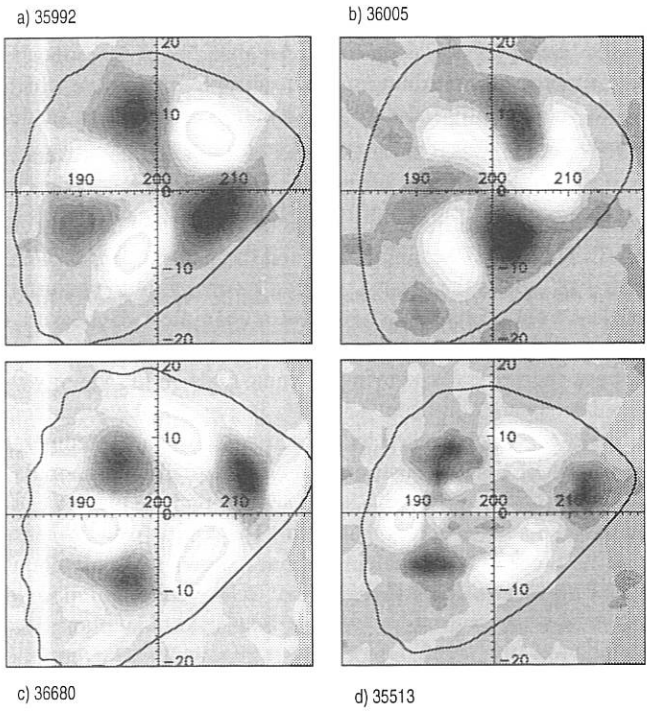


*FIG. 20: Mode structures in a poloidal cross-section near the triangular plane of W7-AS.*
*Spatial structure of m=3 modes: Global Alfvén eigenmodes (a, b), pressure-driven mode (c) and tearing mode (d). Each picture shows the result of tomographic reconstruction of about 50 consecutive time points. Additional post-processing with singular value decomposition is done to extract the mode structure from background radiation. A calculated flux contour (solid curve) is plotted at a normalized radius of 0.75.*

### 2.5.2 *Analysis of magnetic probe signals*

Some progress was made concerning the data analysis of Mirnov signals available from two arrays with eight and one array with sixteen probes.

Singular value decomposition (SVD) of a matrix containing the experimental data allows us to isolate and identify coherent phenomena such as MHD modes without the use of Fourier techniques. If the rows of the matrix contain time series of measurements of the different probes, SVD yields temporal and spatial 'eigenvectors'. The spatial eigenvectors allow us to identify the poloidal harmonic m (if present), whereas the temporal eigenvectors yield a time-resolved frequency.

Another technique to identify MHD modes is to calculate the cross-correlation function of the Mirnov signals. A contour plot of the cross-correlation function versus the time lag and probe position reveals the presence of a mode as well as its poloidal harmonic m, its frequency and its sense of rotation.

SVD and cross-correlation (see Fig. 21) as well as the standard techniques such as phase analysis of Fourier-decomposed signals were implemented as IDL functions and allowed us to identify a variety of MHD modes in different types of W7-AS discharges.

### 2.5.3 *Correlation between MHD activity and fast-particle behaviour*

The excitation of coherent global Alfvén eigenmodes (GAE) by resonant energetic particles of the NBI slowing-down distribution in W7-AS has previously been characterized. One of the important issues connected with this effect is whether the magnetic perturbations associated with the Alfvén instabilities lead to losses of fast particles and therefore reduced heating efficiency. Although usually the most prominent GAE activity occurs at low temperature and during degraded confinement, it was concluded that the deterioration was not caused by the modes but that the drive relative to the damping of the GAE modes was enhanced under these conditions. Particular investigations were made during deuterium injection experiments into a deuterium target plasma, since the neutron rate is mainly due to beam target reactions and therefore a measure of the fast particle content. Two neutron monitors were used in the experiment: firstly a calibrated $BF_3$-counter for the determination of the total neutron flux and secondly a NE213 liquid scintillator detector for fast correlation with MHD events. A particular new regime of strong bursting GAE activity was found during combined heating with ECRH and NBI where high temperatures ($T_e$ = 2 - 3 keV) are reached, and therefore the fraction of fast ions relative to the thermal bulk is expected to be high. In these discharges the slowing-down time, which reaches up to 40 ms, is well above the energy confinement time of <10 ms, and the fast-particle beta is expected to be comparable with the thermal beta. However, a significantly lower fast-ion content is found experimentally as deduced from the measured neutron rate. In correlation with the MHD bursts relaxations of the neutron rate corresponding to losses of fast ions are observed. The

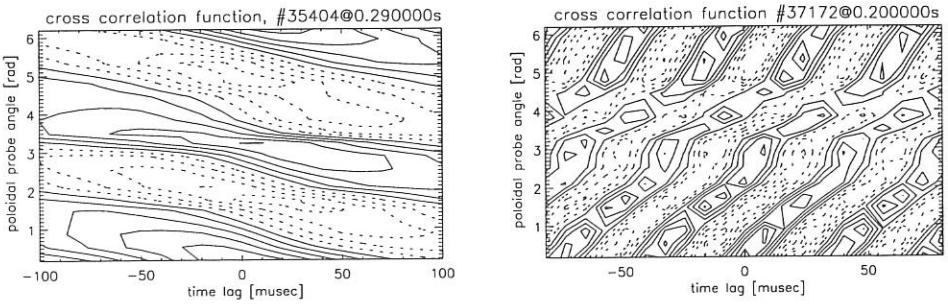


*FIG. 21: Two examples of cross-correlation functions indicating MHD mode activity are shown. Left: m=2 mode (tearing), rotating in the electron diamagnetic drift direction. Right: m=3 mode (GAE), rotating in the ion diamagnetic drift direction).*

fast-ion confinement time can be roughly estimated as $\tau_{fast} \approx \Delta t\,(\Delta\phi/\phi)^{-1}$, where $\Delta t$ and $\Delta\phi/\phi$ are the average time between bursts and the average relative drop of the neutron flux, respectively. However, in most cases the data do not allow a reliable quantitative analysis. In single large MHD events up to about 10% of the fast ions can be lost. These losses mainly occur at the edge of the hot central region, where the GAE modes are centred.

### 2.5.4 *Stability analysis*

The stability properties of the magnetic configurations of W7-AS were further investigated to cover strongly inward shifted configurations with and without negative toroidal field ripple. Consistently with previous results, inward shifting reduces the stabilizing vacuum magnetic well, leading to less stable configurations. In addition to previous studies at "moderate" vertical fields where only the stability of resistive interchange modes was destroyed, at high vertical fields the ideal (Mercier) stability criterion was also violated at low to medium $\beta$ values. The range of Mercier instability in $\beta$ was found to depend on the toroidal field ripple of the configuration just as in the case of resistive interchange stability. At higher $\beta$ values the ideal interchange modes were stabilized over the whole minor plasma radius due to finite $\beta$ effects.

The pressure profiles of the investigated free-boundary NEMEC equilibria were parabolic $(1-(r/a)^2)$ and bell-shaped $((1-(r/a)^2)^2)$. Within this variation the broader parabolic profile showed a smaller extent in the effective plasma radius of the resistive interchange unstable region at the same central $\beta_0$ (corresponding to a higher volume-averaged $<\beta>$). The main reason for this behaviour is the different radial well deepening due to finite $\beta$, which is more uniform over the effective plasma radius for the parabolic profile than for the bell-shaped one.

In the equilibrium calculations we assumed a vanishing toroidal current within each flux surface. The neglect of internal toroidal current densities modifying the profile of the rotational transform, thus introducing a different shear, could modify especially the ideal stability properties and has to be further investigated.

### 2.5.5 *ECE temperature fluctuations*

Fluctuations of the electron temperature measured in the plasma core ($\rho \sim 0.2$ - 0.5 at the high-field side) on W7-AS significantly depend on the plasma density, ECRH heating power, ECRH mode (i.e. O1, X2) and magnetic configuration (i.e. rotational transform and magnetic shear). Following kinetic drift wave simulations under development we are investigating these measurements as a function of the local electron temperature, density and their gradients. A dependence of the temperature fluctuations on the temperature gradient length is discussed. Fluctuations of series of discharges with different density and heating power can be summarized by the relation $\tilde{T} = \nabla T\, f(L_T)$. At W7-AS flat temperature profiles can be produced by off-axis ECRH deposition. This provides a large variety of temperature and temperature gradient values down to a vanishing gradient in the observed region where temperature fluctuations disappear. The density profile is usually flat in the observed radial region.

In this analysis only fluctuations above 10 kHz are taken into account, which are believed to be the ones relevant to turbulence- driven transport. The fluctuating component below 10 kHz seems to be generated outside ($\rho > 0.6$) the observed radial region. It propagates inwards on a diffusive time scale.

The measurements are carried out with a $2 \times 6$ channel ECE "crossed sightline correlation" radiometer as developed at W7-AS. It covers $r_{eff} \sim 5$-10 cm on the high-field side of the plasma core. Relative spectral fluctuation amplitudes down to $10^{-5}/\sqrt{\text{Hz}}$ are detected, with their spectral range extending up to 200 kHz. A newly designed focusing antenna system provides a sensitivity to poloidal wavenumbers of up to $k_\theta \leq 3.5\ \text{cm}^{-1}$.

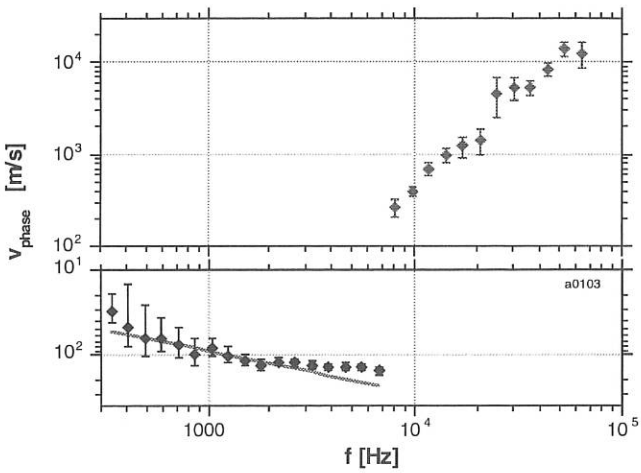


*FIG. 22: Phase velocity spectrum of ECE temperature fluctuations. Two components separated around 10 kHz propagate in opposite directions (solid line: diffusive propagation, $\chi = 1\ m^2/s$).*

### 2.5.6 *Reflectometer phase fluctuations and the propagation of density perturbations at the reflecting layer*

In mm-wave reflectometry the phase of the returned signal is used to monitor density fluctuations at the reflecting layer. However, under turbulent plasma conditions (e.g. in L-mode or during ELMs) the nominal coherent reflection is strongly modified by refraction, diffraction and scattering resulting from the turbulent density structures. As a consequence, the wave front of the reflected signal is distorted and the phase and amplitude measured at the antenna position cannot be related directly to the fluctuating density at the reflecting layer. Instead the observed fluctuations of the phase and amplitude can be explained as the result of interference of mm-wave components which return to the antenna with differing optical path lengths.

The line of sight of the antenna system in W7-AS is slightly tilted with respect to the normal to the reflecting surface, so that mm-wave components with finite poloidal wave vector exist. These components undergo a Doppler shift in the case of poloidal propagation of the reflecting structures with matching

wave vector. If the reflecting layer is sufficiently corrugated by these structures, the Doppler-shifted signal components dominate the measured phase fluctuations resulting in the so-called "runaway" phase. First results showed a fair agreement of the observed Doppler shift with poloidal plasma rotation obtained from spectroscopy and the diamagnetic drift. In parallel, numerical 2D code calculations were performed with results in good agreement with the measured behaviour of the phase. Experiments in which the tilt angle of the antenna could be varied showed that the observed Doppler shift should allow reflectometry to be used as diagnostics to measure the poloidal propagation of density turbulence.

### 2.5.7 *Edge fluctuation studies*

Fluctuations in the outer confinement zone and SOL are investigated because of their contribution to anomalous transport. Langmuir probe arrays provide high temporal and spatial resolution and can therefore be used for detailed analysis of the fluctuations in terms of their lifetimes, sizes and propagation velocities. Average properties of these fluctuations are obtained by means of correlation functions.

To characterize the behaviour of fluctuations along the magnetic field, two toroidally separated Langmuir probes were installed at W7-AS. By choosing the rotational transform such that two toroidally separated probes were connected by magnetic field lines, a very high correlation of about 90% over a connection length of 6 m was observed for both the ion saturation current and the floating potential fluctuations in the SOL and on closed flux surfaces. The experimental setup at W7-AS allows in addition a connection length of 40 m on a closed flux surface. In this case a field line connecting the two probes passes the inside of the torus, where fluctuations are known to be suppressed. Due to this suppression and the longer connection length the correlation is lowered to around 40%.

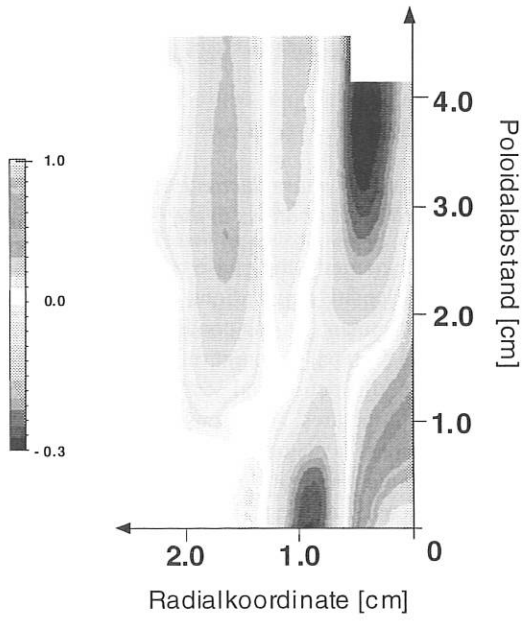


*FIG. 23: Typical 2D-correlation function derived from a floating potential measurement with the angled probe array. In this case the probe array was located in the SOL. The radial propagation velocity is 20 m/s outwards, while the fluctuations move poloidally with an average velocity of 120 m/s.*

Perpendicularly to the magnetic field the analysis must be two-dimensional in principle to obtain especially the radial velocities and sizes of the fluctuations correctly. For this reason an angled probe array was developed. A two-dimensional correlation function can be derived from the experimental data by assuming poloidal homogeneity of the turbulence. The results show correlation lengths of the order of centimetres in the perpendicular plane, while the poloidal size of the fluctuations is typically two to three times larger than the radial size.

To compare theoretical predictions with the experimental results both linear modelling and nonlinear simulation of the SOL and the confinement zone are being undertaken in collaboration with B. Scott, Tokamak Physics Division.

## 2.6 Analytic MHD Equilibria without Symmetry

### 2.6.1 *Explicit three-dimensional MHD equilibria without symmetries*

(in collaboration with R. Kaiser, University of Bayreuth)

The existence of ideal MHD equilibria without symmetry is uncertain although numerical approximations are used for, for example, stellarator configurations. It is therefore instructive to find exact solutions without symmetry, even if they are non-toroidal. Two such classes of exact analytic three-dimensional ideal MHD equilibria without symmetries were derived. The pressure is constant on smooth closed surfaces nested around a straight axis. The magnetic field has a finite rotational transform. Local shear is present in one of the configurations.

# 3. DIAGNOSTIC DEVELOPMENT

## 3.1 Periodic Multichannel Thomson Scattering

The periodic multichannel Thomson scattering diagnostic at W7-AS enables simultaneous measurement of electron temperature and density profiles at sixteen spatial points along the entire plasma diameter. A Nd:YAG laser with a pulse frequency of 20 Hz delivers profiles every 50 ms. The technical details of this diagnostic have already been reported (see Annual Reports 1992 to 1995).

At the beginning of this experimental campaign eight channels were added and successfully put into operation. The diagnostic is now completed, providing all sixteen spatial points arranged along the entire plasma diameter with six channels in the central region, six channels in the gradient region and four channels at the plasma edge. Their spectral ranges are adjusted to the scattering signals as expected from simulation calculations. The spatial resolution of all channels is about 1.4 cm.

Taking into account the different spectral ranges of the channels, measurements of temperatures down to about 100 eV were possible in the centre as well as in the gradient region. The channels at the edge yield temperatures in the range between about 50 eV and 2 keV. One of them with its spatial point at the very edge is able to detect temperatures in the range between a few eV up to about 300 eV. The installation of an automatic system to calibrate and control the relative spectral sensitivities of all channels will be finished at the beginning of 1997.

## 3.2 Multichannel Microwave Interferometer

A 10-channel microwave interferometer for measuring the line-integrated electron density at W7-AS was constructed. Each channel, consisting of a Gunn oscillator as signal source and a heterodyne receiver, runs on an individual frequency in the range 160-162 GHz.

Ten pairs of transmit and receive antennas polarized for O-mode propagation were installed inside the vacuum vessel during the shut-down period in spring of 1996. The antennas are located close to the elliptical plane ($\varphi = 36^{o}$) of W7-AS. The electronics for each channel consists of the microwave section, the intermediate frequency (IF) section operating at 100 - 200 MHz and 5 MHz and the phase measurement circuits operating at 5 MHz. An optical fibre link transmits the final IF signal from the experimental hall to the control room. Here the phase measurement is performed, offering a very short connection to the data acquisition system. The temporal resolution of each interferometer chord is 5 μs.

Eight chords of the interferometer are running routinely since June 1996. Two channels are still missed due to failure of frequency doublers from 80 to 160 GHz. During half a year of operation it turned out that the outermost edge chords fail due to probing beam refraction, if the central electron density exceeds the value of $7 \times 10^{19}$ $m^{-3}$. The most central chord operates up to a peak density of $10^{20}$ $m^{-3}$ (cut-off density at 160 GHz: $3 \times 10^{20}$ $m^{-3}$). This channel has successfully been incorporated into the density control loop.

To reconstruct the electron density profile from the line-integrated density, a computer code was established in collaboration with the Technical University of Helsinki. The results are in good agreement with those of other diagnostics measuring the electron density profile.

## 3.3 Electron Density Profiles of W7-AS Discharges

Since discharge #35042 a mm-wave, 8-channel interferometer has been in operation. It routinely delivers line integrals along horizontal lines of sight in the $\varphi \approx 30^{o}$ plane of module 5. There are therefore now five density diagnostics available: HCN and mm-wave interferometry, reflectometry, Li-beam and Thomson scattering. Three methods were developed to combine the data from interferometry and the Li-beam diagnostic:

1) Determination of an averaged plateau value by subtracting the contribution of the gradient region (measured by the Li-beam diagnostic) from the line integral of the centre HCN channel (vertical line of sight at R = 209 cm). In addition, a cubic spline representation of the density profile over the entire plasma radius is calculated by a NAG routine. The edge channels of the interferometer are used to check and eventually correct the plasma position calculated by the TRANS routines.

2) Taking into account the edge density profile (Li-beam) in the deconvolution process of the mm-wave interferometer diagnostic. For highest accuracy only the part of the edge profile up to the peak in the Li(2p)-profile is included. Again channels above and below the plasma centre permit us to check the plasma position.

Comparison of the density profiles obtained with Thomson scattering and reflectometry shows excellent agreement for discharges of the last experimental phase (closed main limiters).

3) The horizontal, vertical and sloped lines of sight of the diagnostics (mm-wave, HCN and Li-beam) allow determination of possible plasma displacement. It is assumed that the displacement is the same at all different toroidal positions. By means of this method radial and vertical displacements of less than 4 mm were found in the last experimental phase.

## 3.4 Line-integrated Electron Density Measurement with Cotton-Mouton Effect

The line-integrated electron density in a magnetized plasma can be measured by using its linear (Cotton-Mouton effect) and circular (Faraday effect) birefringent properties.

To examine the applicability of the Cotton-Mouton effect for diagnostic purposes two transmission lines for microwaves (~ 600 GHz) were installed at W7-AS: one for a beam with an orientation exactly perpendicular to the magnetic field for an unperturbed Cotton-Mouton effect, and another one where a small component of the magnetic field is parallel to the wave k-vector in order to examine the influence of misalignment of the beam orientation.

The phase difference between the horizontal and vertical components of the microwave beam is the quantity of interest and is directly proportional to the electron line density. To obtain a stable measurement, modulation techniques were applied by modulating the phase difference of the two polarization components of the launched beam (ellipticity modulation). The Faraday effect is being measured by a modulation technique in such a way that the plane of polarization rotates with the modulation frequency, resulting again in a measurable phase shift.

## 3.5 New Method of Measuring Fluctuating Plasma Parameters Using a Fast-Swept Langmuir Probe

In order to measure fluctuations of ion saturation current, floating potential and electron temperature of a plasma with a Lang-

muir probe, the frequency of the sweep voltage must be much higher than the bandwidth of the fluctuations. At the W7-AS stellarator a new electronic circuit was developed that makes it possible to measure the probe current directly and without distortions.

The circuit is mounted in the head of a reciprocating probe and can be extended from the presently installed 4 channels to 19 simultaneously swept probe tips. A 1 kW generator applies to all of them a sinusoidal voltage of up to ±300 V, 4 MHz. A common mode rejection ratio of 80 dB was achieved. Data sampling is done by 200 MHz transient recorders (256 k memory, 8 bit), allowing 1.3 ms of data acquisition. In 1997 it is planned to install new ADCs with 32 MB sample memory and 12 bit in order to increase both the time window and accuracy.

During the last experimental phase of W7-AS, the system went into operation and supplied first data. Analysis of this data was done on the assumption that the local plasma parameters remain constant during one sweep. If this is not the case, the measured characteristic would be distorted leading to incorrect results. So optimized data processing software must be based on realistic time slopes of the plasma parameters.

## 3.6 Comparison of Two Correlation Methods of Temperature Fluctuation Measurement

Fluctuations of the electron temperature in the plasma core (r/a ~ 0.2 - 0.5) are measured by ECE correlation radiometry. Two different correlation techniques are in use to suppress thermal noise and make fluctuations stand out. They are compared on W7-AS.

The "crossed sightline correlation" diagnostic developed at W7-AS is based on the spatial coherence properties of ECE. Corresponding signals of two identical heterodyne radiometers focusing a common plasma volume are correlated. An alternative approach based on the incoherence of ECE at different frequencies is the "single sightline correlation" technique as developed at TEXT. In this method the correlations of closely spaced but spectrally disjoint channels of a single radiometer sightline are taken. In both methods the Fourier transform of the cross-correlation function yields the fluctuation power spectrum.

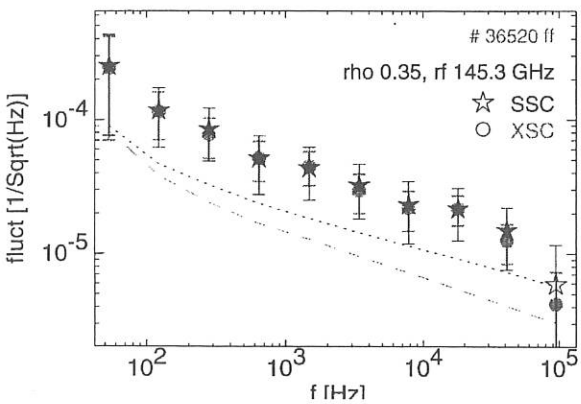


*FIG. 24: Two ECE temperature fluctuation spectra: "crossed sightline correlation" technique (o) compared with the "single sightline" technique (☆) (dotted lines indicate the noise limit).*

The "crossed sightline" double radiometer is extended by two additional pairs of "single sightline" channels installed in one sightline. This allows comparison at the same plasma volumes. Measurements at various discharge parameters (cf. 2.5.5) show both techniques matching within statistical errors all over the fluctuation spectra.

Though equivalent in the case of high fluctuation levels, the "crossed sightline" method is in advantage at low levels with respect to the signal-to-noise ratio determined by the spectral bandwidths of the radiometer channels. The bandwidth of the "single sightline" channels has to be significantly smaller compared with the "crossed sightline" channels, resulting in an up to 50% higher noise level limiting the sensitivity of the diagnostic.

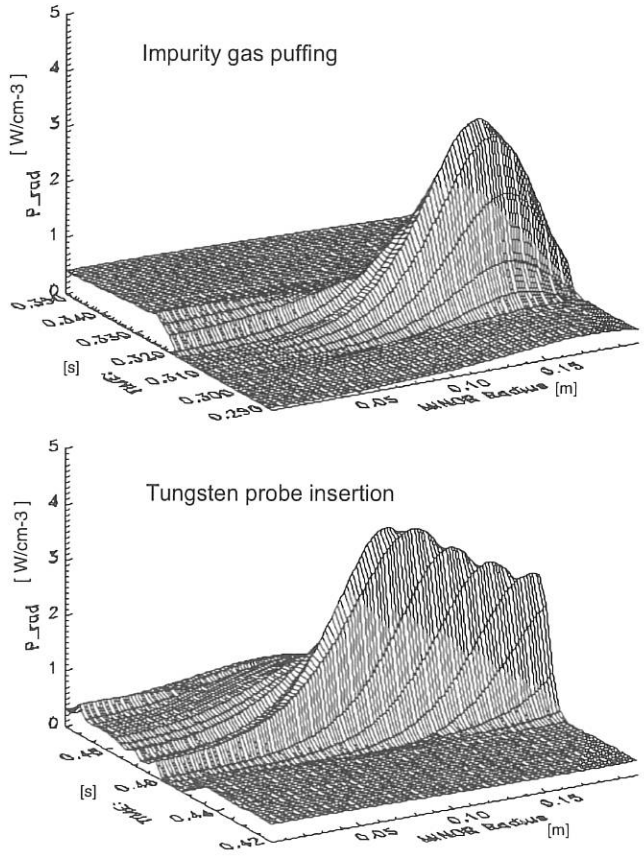


*FIG. 25: Time evolution of radiation power density with impurity gas puffing and tungsten probe insertion (#37640).*

## 3.7 12-channel Bolometer

A 12-channel array of the minituarized gold foil bolometers developed at IPP by F. Mast were installed on W7-AS. The camera is mounted in a manipulator and can be moved in the radial direction and tilted in the poloidal direction. The AC bridge excitation at 20 kHz and synchronized demodulation of

the bolometer bridge output is carried out with electronics allowing computer control of gains and offset adjust. It is envisaged that the electronics will be further developed for W7-X into a PC-based system and used in conjunction with standard PC analogue to digital conversion cards. A PC-based calibration unit is currently under development. In this case a DC voltage will be applied to 8 foils concurrently and the ohmic heating and cooling yield the desired calibration constants.

With a 3 db frequency of 4 kHz the bolometer camera provides time resolution sufficient to follow transient events instigated by impurity gas puffing (nitrogen) or insertion of a tungsten probe into the plasma, as shown in Fig. 25.

The installation of a divertor in W7-AS has necessitated planning for wall-mounted bolometer heads. Such a development is necessary to access good lines of sight.

## 3.8 Collective Thomson Scattering at W7-AS

In 1996, the collective Thomson scattering (CTS) experiments using 140 GHz ECRH gyrotrons were continued in collaboration with IAP (Institute for Applied Physics), Nizhni Novgorod and IPF Stuttgart.

Successful experiments were performed with a newly developed antenna in a 90° scattering geometry, which provide a spatial resolution of 4 cm and a very low stray radiation level of $< 2 \times 10^{-7}$.

With a slightly inward shifted resonant magnetic field (2.4 T on axis) where the resonance zone lies outside the line-of-sight of the receiver antenna, scattering spectra could be measured down to the thermal level. An example is given in Fig. 26, where the scattered spectrum of a deuterium discharge heated with a neutral hydrogen beam is shown. Assuming that the plasma is composed of an H/D ion mixture, fit procedures yield ion temperatures in reasonable agreement with independent diagnostic methods. Further details can be found in the contribution of IPF Stuttgart to this report.

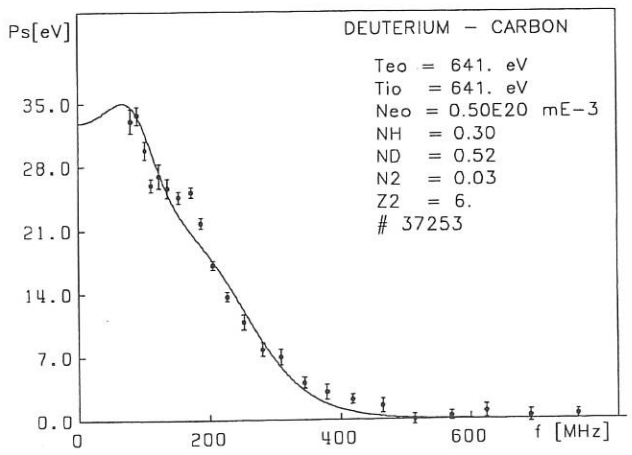


*FIG. 26: Thermal ion spectrum of a NBI-heated discharge (solid curve: theoretical fit).*

## 3.9 Impurity Pellet Injector

The impurity pellet injector was assembled in the laboratory and its technical data were checked. The compact gas gun injector uses helium as propellent gas to accelerate solid diagnostic pellets (0.15 - 0.7 mm Δ) up to 600 m/s. Four fast valves (opening times <10 ms) and a two metre long gun barrel minimize the propellent gas throughput to less than $10^{16}$ gas particles.

During the last experimental period the impurity pellet injector was moved to W7-AS. First test shots into W7-AS plasmas using middle sized carbon pellets exhibited moderate effects on global plasma parameters and accordingly demonstrated its applicability to perturbation experiments and transport investigations. As a second impurity material LiD was injected into eight successive plasma discharges. A shot-to-shot accumulation of the implanted lithium - an element of interest for wall conditioning experiments - was observed. Within few shots without injection no more intrinsic lithium could be measured.

To investigate the behaviour of the ablating pellet along its flight path through the plasma two optical observations were built up. The temporal evolution of the visible radiation is recorded by a fast sampled (≤ 2 MHz) diode. Spatial information can be achieved by a fast gateable CCD camera (integration time ≥1 ms) which images the pellet path inside the poloidal plane. Both units can be supplied with bandpath filters to choose spectral line radiation of low ionization stages of the pellet material. This allows investigation of the ablation process with high temporal and spatial resolution.

## 3.10 Sniffer Probe Measurements at the W7-AS Stellarator

Mass-spectroscopic measurements at and near the plasma edge with the so-called 'sniffer probe' were carried on during the spring measurement campaign. With this probe the gas composition could be studied with a time resolution down to 10 ms/u during scans across a preset mass range, its position relative to the plasma edge being determined by its additional Langmuir probes. This means that measurements concerning the H/D isotope ratio could be made with a time resolution down to 40 ms before, during and after the discharges. These measurements showed that even in discharges shortly after boronization with deuterated diborane an H/D isotope ratio of up to 0.17 could be observed though only deuterium was blown in. An example of the time development for the mean of a number of ICRH test discharges is given in Fig. 27.

The studies of the mass range above m/e = 4 showed the development of large amounts of hydrocarbons in some of the discharges that turned out to originate locally near the probe by a shine-through of the neutral beam injection heating in their beginning. But in many cases the hydrocarbon concentration was below the detection limit of the probe. The old sniffer probe at port 8 in section 3 was dismantled and the erection of a new sniffer probe at port 8' in section 4 was started during the summer shut-down and finished in the middle of December. For this probe the mechanical stability was improved, allowing a

sufficient screening of the magnetic field. This makes the use of the secondary electron multiplier possible, leading to substantially higher sensitivity. Apart from that the sniffer head is better adapted to the plasma shape and can now be changed without disintegration of the probe. The response time constant was also lowered (60-80 ms, depending on probe position).

To evaluate the large amount of data gained during the measurement campaign (order of 10,000 mass spectra over 1,000 discharges), the data should be pooled to gain valuable mean values for typical time developments of the partial pressures from which further conclusions may be drawn. For this purpose the method of group analysis was used and it was shown that it helps to classify the various discharges and find outliers that do not fit into the groups. In a second step a mathematical theory was developed to determine probabilities for a proposed grouping. On the basis of this theory a search for the optimum grouping of the data was started.

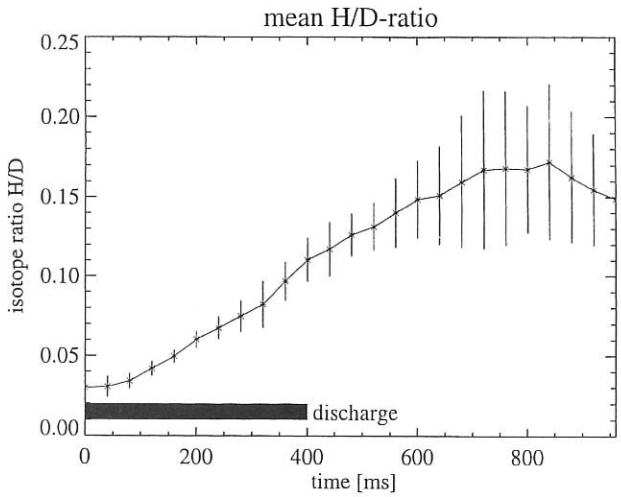


*FIG. 27: Mean H/D ratio at z = 35.5 cm (distance below horizontal middle plane of W7-AS) for the similar discharges #34330 - #34353. Similarity is guaranteed by group analysis. The error bars denote the statistical error of the used discharges.*

# 4. NEUTRAL INJECTION INTO W7-AS

## 4.1 Upgraded injection power

By regapping the extraction grids of the ion sources, the acceleration voltage could be raised from 45 kV to 50 kV for hydrogen, keeping the ion current constant at 25 A. The beam divergences decreased from 1.3° to 1.15° so that a larger fraction of the beam was transmitted into the torus. The total injection power could be increased in this way from 3 MW to 3.5 MW.

Species measurements via beam spectroscopy in the torus gave power fractions of full-energy particles of 38 ... 47% for hydrogen at 50 kV and 52 ... 60% for deuterium at 55 kV, varying from source to source.

## 4.2 Numerical work

The FAFNER NI code was extended to high-β targets. With increasing β the plasma moves outwards and its cross-section becomes larger. New data sets created with VMEC (J. Geiger) were used and the β range was extended to $\langle\beta\rangle = 2\%$. The changes of the limiter configuration were also introduced into the FAFNER code. The correct wall configuration is important because of its influence on the fast-ion losses. Many FAFNER runs were necessary to provide the heating profiles and beam-driven currents which are used as inputs for transport and GAE mode theory. Furthermore, the velocity distributions of slowing-down ions were calculated for comparison with measurements.

## 4.3 Radial injector

Preparations for an additional injector were continued. The new beams will be aimed at such an angle that most ions are created on lost orbits. It is expected that the charge of the electrons left behind produces beneficial electric fields which improve plasma confinement. There will be a longer shut-down for the installation of a divertor, during which the new injector shall be put in place. Like the existing two injectors, also the third one will be of the type originally developed for ASDEX. The major difference will be the use of HF ion sources instead of periplasmatrons.

# WENDELSTEIN 7-X

(Head of Project: Prof. Dr. Günter Grieger)

## 1. W7-X DIVERTOR STUDIES

H. Greuner, A. Herrmann+, F.-W. Hoffmann, J. Kißlinger, H. Renner, E. Strumberger, W. Bitter*, F. Kerl*, R. Holzthüm*, O. Jandl*( +IPP Berlin, * ZTE )

### 1.1 Physics and Modelling

A divertor system capable of stationary operation with a heating power of 10 MW has been developed for the new W 7-X stellarator. The five-fold symmetry of the magnetic configuration calls for 10 divertor units (2 units per period). To achieve effective particle and energy exhaust for a wide range of operating magnetic parameters of W7-X, an "open divertor structure" has to be chosen. The optimization of the geometry of the divertor was based on field line tracing for the vacuum configurations and simulation of perpendicular transport by "field line diffusion" (Monte Carlo code) to calculate the power deposition on the targets[1], whereas the pumping efficiency was estimated by means of the EIRENE code taking into account reasonable boundary parameters. The intersection angles of the flux bundles on the targets are typically 0 - 3°. Local power densities of up to 8 MW/m$^2$ at the target plates were obtained in a wide range of magnetic parameters for the worst case with low-density and high-temperature plasma. With neutrals and impurities taken into account, it is possible to achieve significant unloading of the target plates already at moderate separatrix densities[2].

#### *1.1.1 W7-X modular coil system*

In 1996 the divertor target geometry was adjusted and optimised to the new HS5V10T configuration with the larger plasma radius in the high-ι case compared to the HS5V10N configuration of the phase 2 proposal. During this work it was found that a local enlargement of the vacuum vessel is necessary to protect the vessel by target plates located at the same toroidal position as in the former HS5V10N configuration. As a consequence, the modular coils for the new HS5V10U configuration, mainly coils 4 and 5, and also the ancillary coils, have to be locally enlarged in the radial direction. These small modifications of the coil shapes could be made without significant change of other magnetic parameters, e.g. the plasma radius and the shear, the magnetic well and the low-harmonic Fourier components of the magnetic field.

#### *1.1.2 Finite-ß magnetic fields of W7-X*

In order to optimize the divertor geometry for various plasma equilibria and improve SOL studies, a detailed knowledge of the corresponding magnetic field structures is necessary. For this purpose, magnetic fields are calculated for ß equilibria of up to $\langle ß \rangle = 5\%$ and rotational transform values of $\iota = 5/5, 5/6, 5/4$ in the edge region. For these first computations a system of numerical codes is used that allows us to calculate vacuum magnetic fields and trace field lines (GOURDON code), determine free-boundary equilibria (NEMEC code[3]; it assumes nested flux surfaces) and determine the topology of the magnetic fields of these equilibria (MFBE code[4]).

Comparisons of the finite-ß magnetic fields with the corresponding vacuum fields confirm the properties expected for optimized Helias configurations, namely small outward shift of the plasma column, slight decrease of the rotational transform and almost stationary positions of the X- and 0-points of the macroscopic islands.

### 1.2 Divertor Components

An almost complete description and 3D CAD studies of the main divertor components are now available which integrate

- target plates and baffles (FIG. 1), including water-cooling circuits, feed troughs on the vessel
- control coils, operational diagnostics ( thermography )
- pumping system, consisting of TM pumps.

---

1) H. Greuner et al., Proc. of 18th SOFT , Karlsruhe (1994), Vol. 1, p. 323

2) J. Kißlinger et al., 22nd EPS, Bournemouth (1995), Vol. 19C-III, p. 149

3) S.P. Hirshman, W.I. Van Rij, P. Merkel, Comput. Phys. Comm. 43 (1986), p. 143

4) E. Strumberger, Nuclear Fusion 37 (1997), p. 19

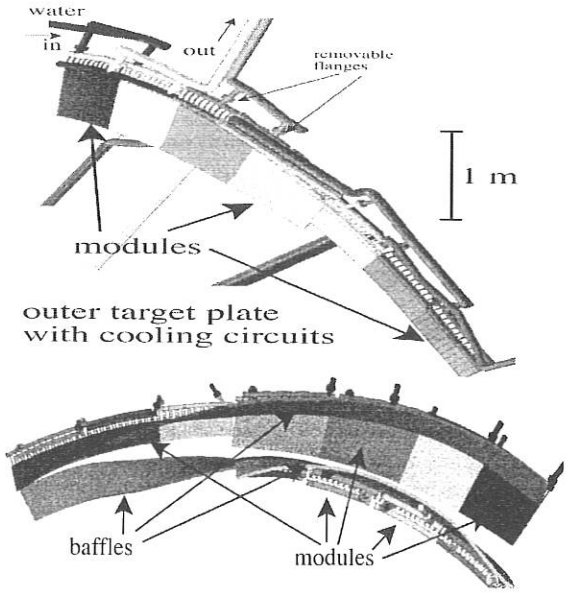


*FIG. 1 : CAD drawing of the outer target plate of one divertor unit. Target elements are combined to modules (marked by different grey intensity). The lower part shows the two target plates and baffles of one divertor unit as seen from the magnetic axis. Note the gap for pumping.*

#### *1.2.1 Target elements*

An R&D programme has been started for the target element as the most critical component of the divertor. For the prototypes the favourable fin design was selected. The internal fin structure needs the lowest water flow rate and lowest pumping power. The material combination TZM/CFC was chosen to integrate the brazing technique as developed for application of the NET/ITER team. The prototype elements were successfully manufactured by PLANSEE AG and ANSALDO Richerce .

The thermal heat test using the JUDITH electron beam facility of the KFA Jülich (Drs. Bolt, Duwe, Kühnlein) showed that the measured temperatures agree very well with results of 3D FEM modelling. Two elements were tested with a stationary power load of 10 MW/m$^2$ , leading to a surface temperature of 1000° C for up to 1000 cycles.

## 2. DIAGNOSTICS AND HEATING

### 2.1 Diagnostics Strategy of W7-X

Efforts are being made to equip the experiment with those diagnostics necessary to measure the quantities directly relating to the optimization of the machine. A main goal of W7-X is the experimental verification of the major design elements, selection of iota = 1 with moderate shear, improved equilibrium, particle drift optimization, energetic particle confinement, negligible bootstrap current, and the investigation of the role of the drift optimization on anomalous transport. The diagnostic set must also be capable of providing the necessary information in experiments demonstrating the high performance of the machine in various confinement scenarios, making use of stellarator-specific properties such as long-pulse operation, under operation conditions with and without ECCD-driven currents for MHD measurements and all studies on the tokamak-stellarator comparison. The inherent property of a stellarator for steady-state operation has implications on the diagnostics too. This scenario may not require a basically new diagnostic approach, but intelligent event recognition will be required. Despite the complex coil set and 3-dimensional geometry, a large number of ports is available for diagnostic access to the plasma. The final design of the ports, their orientation and location is being done simultaneously with the basic definition of the diagnostic instrumentation and the required sightlines through the plasma to ensure optimum conditions concerning the scientific issues to be diagnosed.

### 2.2 ECRH for W7-X

The ECRH system for W7-X consists of 10 gyrotrons with 1 MW power per unit at 140 GHz and has CW capability. Such sources have to be developed for W7-X. For the development of the gyrotrons with the required performance an R&D contract will be placed with industry, which will include the consulting collaboration of the experienced European laboratories. FZ Karlsruhe will, on behalf of IPP, supervise the R&D programme and provide its own test facilities. The microwaves will be transmitted from the ECRH hall to the stellarator ports by a purely optical transmission system. A set of plug-in-launchers will provide the necessary flexibility to meet the relevant physics goals of W7-X. The conceptual design, the engineering design and the supervision of the construction of the entire transmission system will be handled by IPF Stuttgart.

### 2.3 Neutral Injection into W7-X

Neutral beam injection on W7-X is envisaged for bulk heating of the plasma in the high-density, high-ß regime. Up to now, stage I has been approved, delivering 5 MW at 60 kV from two injector boxes, each equipped with only one ion source. It can be upgraded to 20 MW by using 4 sources per box (stage II). The operation range of the plasma density $n_e(0)$ will be $0.3...1.5 \cdot 10^{20}$ m$^{-3}$ for centrally peaked heating profiles. This range could be extended to $n_e(0) = 3 \cdot 10^{20}$ m$^{-3}$ if beams with 250 keV/amu atoms were used. The application of a negative-ion-based injector is therefore under investigation (stage III).

### 2.4 ICRH for W7-X

Personnel, cost and time expenditure and the requirements for vessel ports, technical infrastructure, control etc., and for the intended housing of ICRH in the assembly hall were specified in more detail and implemented in the W7-X planning. Rough outlines of the RF generators and switchgear arrangement and of the premises required for mechanical and electronic engineering and ICRH control showed that these can be installed in the southern half of the hall.

# 3. STELLARATOR SYSTEM STUDIES

C.D. Beidler, E. Harmeyer, F. Herrnegger, N. Jakšić,[1] J. Junker, N. Karulin,[2] J. Kißlinger, H. Maaßberg, F. Rau, H. Renner, J. Simon-Weidner,[1] H. Wobig, A.V. Zolotukhin

## 3.1 Wendelstein 7–X Studies

In 1996 Wendelstein 7-X studies were focussed on special questions of the configuration, mainly the issues of the divertor design and the plasma boundary layer. For the coil system a local computation on stresses and strains was made. Plasma physics issues, neoclassical transport, electric fields and plasma rotation were investigated. Aspects of a Helias reactor were considered, especially the coil system and its mechanical support, the start-up scenario, and the $\alpha$-particle behaviour in such a device. The results of the investigations were presented at the EPS conference in Kiev, Ukraine, and the SOFT conference in Lisbon, Portugal.

### *3.1.1 Configuration development*

Configuration development for Wendelstein 7-X was mainly carried out in view of the divertor design, see chapter 1. The divertor target geometry was modified, which led to a local expansion of the vacuum vessel in order to protect the vessel by the target plates. In this connection, the modular coils, mainly coils 4 and 5, and also the auxiliary coils were locally expanded in the radial direction. The result of these investigations was the configuration designated HS5V10U. The modifications of the coil shapes were rather small, consequently no significant change of other magnetic parameters e.g. the shear, the magnetic well, the plasma radius, was found.

### *3.1.2 Force and stress calculations*

Force and stress calculations of the Wendelstein 7-X coil system were continued, using the EFFI code to compute the magnetic forces, and the ADINA code to analyze mechanical stresses. The effects of the cooling-down of the coil module and the influence of sliding on stresses were included in these investigations. The calculations were based on the standard case at an axis magnetic field of 3 T. Each coil winding pack, consisting of 120 windings of a cable-in-conduit conductor with a co-extruded aluminium jacket, is embedded in a stainless-steel coil housing. A local stress computation was made on the cross-section of the modular coil 3, that applied a fine subdivision of the windings, the insulation and voids, and specified the magnetic force distribution of each individual conductor [489]. The results of these calculations showed a good agreement of the extreme values of the stress components and their location with former global analyses. Furthermore, a sufficient safety value was found. These investigations are being done by members of the ZTE Division.

[1] ZTE Division

[2] Nuclear Fusion Institute, Moscow

### *3.1.3 Neoclassical transport*

Neoclassical transport studies investigated the role of a large toroidal mirror term in the magnetic-field spectrum of advanced stellarators. In the plateau regime, the toroidal mirror is capable of substantially altering the usual resonance conditions, making large reductions of the neoclassical transport coefficients possible. In the long-mean-free-path regime, an accurate description of the neoclassical transport based on solutions of the bounce-averaged kinetic equation has been made possible by extending the theory to allow for effects due to non-zero rotational transform per field period and the non-symmetry of local ripples.

### *3.1.4 Plasma rotation in stellarators*

Plasma rotation in stellarators was investigated on the basis of a fluid model. For this purpose the general plasma equilibrium was taken into account by adopting the Hamada coordinate system. The rotational instability of a toroidal plasma is caused by various mechanisms: Stringer spin-up, turbulent Reynolds stresses and lost orbits. Starting from a general stellarator equilibrium, a set of momentum balance equations is established which balance the driving forces of plasma rotation against the damping forces. Plasma rotation is damped by magnetic pumping, which strongly depends on the geometry of the magnetic surfaces. The geometrical coefficient was evaluated for various stellarator configurations. The results show a considerably lower damping rate in Helias configurations than in standard stellarators. In parallel to the optimization of drift orbits and the reduction of Pfirsch-Schlüter currents the poloidal damping rate is reduced in Helias configurations. It was found that in the neighbourhood of magnetic islands the damping rate increases. In particular in Wendelstein 7-AS, where magnetic islands exist on rational magnetic surfaces, this effect may inhibit poloidal rotation and the achievement of H-mode confinement. Low poloidal damping rates occur in the regime slightly below $\iota = 1/2$ and above $\iota = 1/2$, which may be correlated to the H-mode observed in this regime. Extrapolating these results to Wendelstein 7-X shows that in the standard configuration with $\iota < 1$ low poloidal damping rates are also expected.

## 3.2 Helias Reactor Studies

To determine the prospects of a future stellarator fusion reactor, the investigations on a Helias Stellarator Reactor (HSR) were continued. The modular coil system, the divertor, the behaviour of $\alpha$-particles, and the start-up scenario of HSR were investigated, and the questions of blanket, shield, etc. were considered.

### *3.2.1 Coil system of HSR*

The coil system of HSR is a scaled-up version of the magnetic configuration of Wendelstein 7-X. The magnetic field is generated by a single set of modular non-planar coils. Sufficient space for the blanket and shield is provided between the coils and plasma. These specify a minimum reactor size, which provides sufficient plasma confinement to

reach ignition. In Fig. 2.1 two poloidal cross-sections of the configuration are shown. The maximum magnetic field at the coils is about 10.6 T, which allows to remain within the existing NbTi-technology. The main data of HSR are listed in Table I.

| | |
|---|---|
| Average major radius [m] | 22. |
| Average coil radius [m] | 5.0 |
| Number of coils | 50 |
| Induction on axis [T] | 5.0 |
| Max. induction on coils [T] | 10.6 |
| Total magnetic energy [GJ] | 110. |
| Virial stress [MPa] | 153. |
| Average plasma radius [m] | 1.8 |
| Plasma volume [$m^3$] | $1.4 \times 10^3$ |
| Total weight [t] | $\approx 3.5 \times 10^4$ |

*TABLE I: Main data of the Helias reactor HSR.*

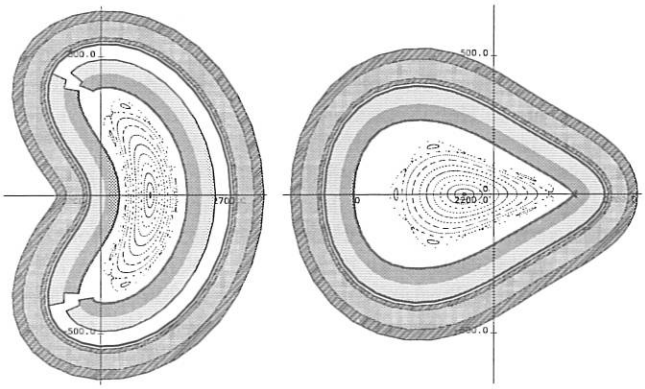

*FIG. 2.1: Cross-sections of the two symmetry planes of HSR showing the vacuum magnetic surfaces, blanket, shield, and the radial coil domain.*

The magnetic forces on the modular coils were calculated with the EFFI code, using a refined subdivision of $4 \times 4$ elements over the coil winding pack cross-section [459]. The coils of HSR were surrounded by a strong stainless-steel housing, with thicknesses of 30 cm at the outer coil face and 15 cm at the other three sides. For the nonlinear FE calculations, the ADINA code was used, covering half a field period and employing the stellarator symmetry. 'Contact elements' derived from a nonlinear stress-strain characteristic were introduced between the coil winding pack and the coil housing. As a first step, the intercoil structure was modelled uniformly between the coils as a toroidal shell. Using the material data of a conductor developed earlier as input for the winding pack, the FE computations show that the values obtained are within the technical limits. Further iteration steps need to be done, with the geometry of the coil support structure being varied in order to minimize the amount of structural material, equalize the stress distributions, and take the necessary ports of HSR into account.

Critical parameters of HSR determining the major radius and the superconducting coils are the minimum distance between the plasma and field-generating coils and the distance between these coils. In order to improve these two distance values, the coil set for the Helias reactor was modified. Keeping the major radius at 22 m, the new coil system enlarges the radial space for the blanket and shield by about 11 cm. The minimun distance between the central filaments of the coils is increased from 82 to 96 cm. This modification provides the space necessary for the coil case by a simultaneous reduction of the current density in the superconductor and the maximum field at the conductor surface.

### 3.2.2 *Collisionless α-particle motion in HSR*

The guiding-centre motion of collisionless $\alpha$-particles is studied for the HSR (Report IPP 2/330) in the vacuum field and in a finite-$\beta$ configuration ($\beta_0 = 3\%$, major radius $R = 22$ m, minor radius of a last closed magnetic surface $a = 1.7$ m, average on-axis magnetic field $B = 5$ T, 10 coils per field period; mirror ratio 10% on the axis and 18% at the boundary). The fusion $\alpha$-particles have a normalized Larmor radius of $\rho/a \approx 1/30$. Effects due to the electric field are neglected, while effects of the modular ripple are taken into account.

The interaction of thermonuclear particles with the first wall of the device is of interest for fusion reactors. Trapped $\alpha$-particles are characterized by a pitch parameter value $\gamma \geq 0.9$ ($\gamma = v_\perp/v$, where $v$ and $v_\perp$ are the total particle velocity and the velocity perpendicular to the magnetic field). To obtain a map of the intersection points of lost $\alpha$-particles orbits with the vacuum chamber in HSR, the particles were launched from randomly distributed positions at various cross-sections of the magnetic surfaces with average radii $r/a = 0.2$ and $r/a = 0.4$. Hot spots on the wall were found, these being due to $\alpha$-particles which are trapped in the modular ripple and satisfy $\gamma \geq 0.95$.

### 3.2.3 *Start-up calculations*

An improved version of the ASTRA code has been utilized to simulate the start-up phase of a Helias reactor. These improvements comprise computation of the density profile, computation of particle sources from pellet ablation, and self-consistent calculation of the radial electric field. Ablation of the pellets is modelled according to the model of Kuteev (Kuteev, B.V., Report NIFS-260, 1993), typical parameters of the pellets being: velocity 6 km/s, radius of pellets 0.4 cm, repetition rate 4-10 $s^{-1}$. The startup of the reactor plasma requires a net heating power of 60-80 MW, which can be realized by ECRH heating from the high-field side. Ignition in the Helias reactor can be achieved with L-mode confinement, the required confinement time being about the same as predicted by the Lackner-Gottardi scaling. The plasma parameters stay below the expected stability limit of $< \beta > = 4.5\%$.

# 4. STELLARATOR PHYSICS STUDIES

S. Arndt, M. Drevlak, S. Gori, Ch. Hennig, A. Könies, C. Nührenberg, J. Nührenberg, P. Merkel, U. Schwenn, E. Strumberger, S. Weber, R. Zille
Guests: K. Matsuoka [1], S. Okamura [1]

## 4.1 Introduction

In 1996, the work of the Stellarator Physics Group was concentrated on the start of the theoretical work at the Greifswald Branch Institute, on advanced theoretical descriptions of stellarators /217/, and on further development of the stellarator concept [2], e.g. the property of quasi-isodynamicity /420/.

## 4.2 Stellarator Equilibria Including Magnetic Islands

In contrast to the variational VMEC code by S. P. Hirshman assuming nested magnetic surfaces, the iterative, nonvariational PIES code by A. H. Reiman and H. S. Greenside is able to deal with magnetic fields having islands and stochastic regions. Since this code exhibits rather slow convergence rates, it is essential to improve the initial conditions. The way chosen here is to use equilibrium solutions obtained with the VMEC code as such initial guesses in the PIES code. W7-X configurations with values of $\langle\beta\rangle$ of about 0.03 and 0.05 were considered. Compared with corresponding PIES runs without VMEC input, the number of necessary iterations was considerably reduced. For instance, in an $\langle\beta\rangle \approx 0.03$ case without islands, convergence was reached after around 40 iterations, compared with several hundred iterations without VMEC input. For the W7-X fixed-boundary equilibrium including islands shown in Fig. 1, about 100 PIES iterations were required.

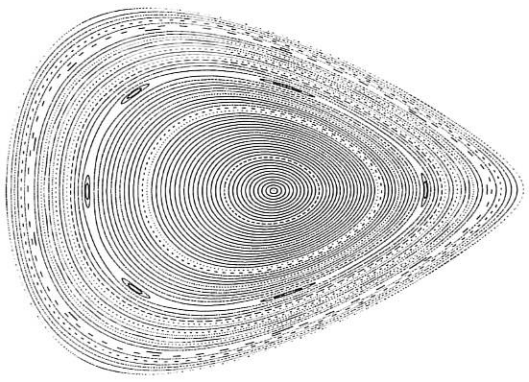

*FIG. 1: Flux surfaces of a W7-X equilibrium with $\langle\beta\rangle = 0.05$ obtained from the PIES code with the corresponding VMEC equilibrium as input. Number of radial grid surfaces $k = 65$, $0 \leq m \leq 16$ poloidal and $-8 \leq n \leq 8$ toroidal Fourier modes.*

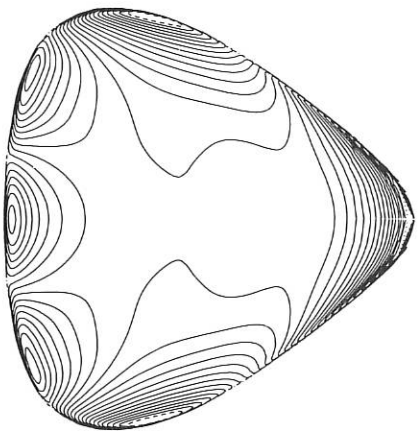

*FIG. 2: Perturbed pressure contours on the $\varphi = 180^{\circ}$ plane for a W7-AS equilibrium, which is unstable with respect to global ideal MHD free-boundary modes (essentially $M = 3$, $N = -1$), but stable with respect to the local Mercier criterion ($B_Z/B_0 = 0.015$, $\iota = 1/3$ on the plasma boundary, $\langle\beta\rangle \approx 0.013$).*

## 4.3 Ideal MHD Modes

The CAS3D stability code may now be used to analyze the ideal MHD energy principle for three-dimensional plasmas surrounded by a vacuum region, i.e. for free-boundary perturbations which may deform the plasma-vacuum interface. For a first application of the free-boundary CAS3D code a one-parametric series of finite-$\beta$ W7-AS plasma configurations was computationally generated from the W7-AS coil data, with the sequence parameter being the relative magnitude of a vertical field, which yields an *inward shift* of the plasma column. The specific free-boundary modes investigated /571/ shift the fixed-boundary mode stability limit by 0.006 in the series parameter (see Fig. 2).

A second focus of the applications of the CAS3D code /175, 176/ was the investigation of the MHD stability properties of the quasi-axisymmetric configuration MHH2 [3] which was proposed by P. Garabedian. Equilibria with $\langle\beta\rangle \approx 0.018$ were found to be unstable with respect to medium-node-number fixed-boundary ballooning-type modes ($N \sim 11$).

## 4.4 Kinetic MHD Stability Analysis

Fast $\alpha$-particles from fusion may destabilize the toroidal Alfvén eigenmodes and ballooning modes in tokamaks. Especially the contributions of the reflected energetic particles have been found to be destabilizing. In a 3D plasma there are reflected particles which are restricted to the period of the magnetic field. Thus, a stability analysis from the kinetic point of view is also necessary for the 3D case and the development of a kinetic generalization of the CAS3D code was started. The new energy functional results from the guiding center description of a plasma and differs only in its kinetic term from the MHD result. It is equivalent to the adiabatic conservation of the magnetic moment and the

[1] National Institute for Fusion Science, Nagoya, Japan.

[2] K. Matsuoka et al., Post-CHS Project, US/Japan Stellarator Workshop, 1996, in press.

[3] A. H. Reiman et al., MHD Calculations for MHH2, US/Japan Stellarator Workshop, 1996, in press.

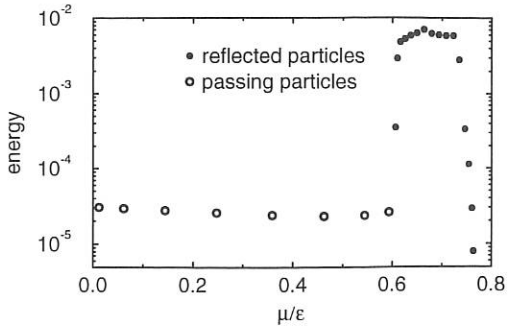


*FIG. 3: Contributions of passing and reflected particles to the kinetic energy term versus the ratio of magnetic moment and particle energy at the radial position $s \approx 0.34$.*

longitudinal action invariant. This kinetic energy principle is investigated for an optimized W7-X type field configuration (see Fig. 3).

Furthermore, it was found that the toroidal periodicity of the problem and the special magnetic field structure of W7-X like configurations allow a categorization of reflected particles according to similar values of their longitudinal invariants in not more than three groups.

## 4.5 Optimization of Stellarator Coils

An extended version of the NESCOIL code by P. Merkel was used to produce alternative coil configurations increasing the space inside the W7-X device. This code performs a simultaneous optimization of both the properties of the magnetic field and the geometrical properties of the coils themselves.

Of the new coil configurations found, one was designed to increase the space available inside the coils rather uniformly, making it attractive for consideration in a HELIAS power plant /177, 329/, where considerable additional space is required for shield and breeding blanket. The second design increases machine space selectively in the regions close to the divertor. An inner view of one period of the latter design is shown in Fig. 4.

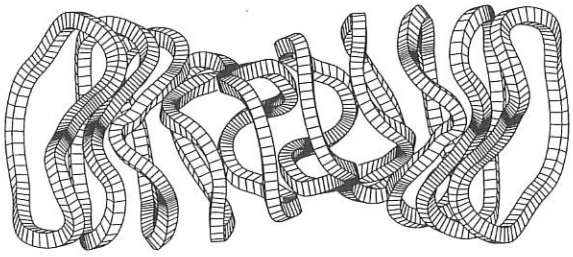

*FIG. 4: Inner view of one period of an alternative coil design for W7-X offering more space for installation of the divertor system.*

## 4.6 Initiative for the Development of a 3-dimensional Plasma Edge Code for W7-X

It is envisaged to develop a fully 3-dimensional plasma edge code (based on the standard Braginskii equations) for W7-X. The inherent 3-dimensionality of the advanced stellarator requires the code to have the same dimension. The code should eventually reach the same level of sophistication as the corresponding tokamak codes.

A first step is the construction of a computational mesh which follows as closely as possible the magnetic topology and preserves the magnetic field line parallelism, i.e. one of the coordinate lines has to be the magnetic field line which winds around the torus. The periodicity allows to model just one field period or even half of it if the stellarator symmetry is taken into account. The idea is to construct the computational mesh by starting long field lines on the divertor surface and follow them for many toroidal circuits around the torus till they again intersect the divertor plates. The periodicity is exploited to fold the traces into one segment. This should provide a natural way of covering the SOL with a mesh. The basic ingredient is the magnetic field line which is followed, irrespective of the possible presence of stochasticity or magnetic islands. These should only play a role for the transport coefficients perpendicular to the field line. Nevertheless the presence of islands and/or stochasticity in the SOL might complicate the construction of a reasonable mesh.

## 4.7 High-$\iota$ High-mirror W7-X Configurations

The coil system HS5V10T was investigated with respect to its suitability for the attainment of stable, high-$\iota$, high-mirror, low-shear, high-$\beta$ plasma equilibria. For this purpose the coil currents of the modular and auxiliary coils were varied individually, and a suitable current configuration was iteratively determined with the help of a system of numerical codes /196, 229 - 231, 651, IPP 2/333 /. Figure 5 shows the resulting magnetic field for $\langle\beta\rangle = 0.04$, which fulfills the required MHD and neoclassical properties.

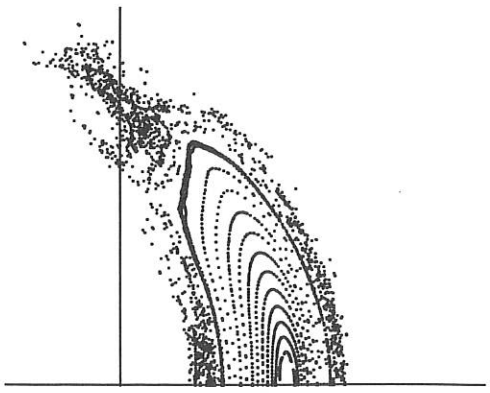

*FIG. 5: Poincaré plot of the upper half of the symmetric bean-shaped cross-section for $\langle\beta\rangle = 0.04$.*

# WENDELSTEIN 7-X Construction

(Head of Project: Dr. Manfred Wanner)

Members of the W7-X-Team and contributors to the project: see section "Divisions and Groups, Wendelstein 7-X Construction".

## 1. INTRODUCTION

The WENDELSTEIN 7-X (W7-X) project comprises the establishment of a new institute at the Greifswald site and installation of the stellarator experiment. Following governmental approval of the whole project in May 1996 the responsibilities within IPP were reallocated. Prof. Grieger, the founding director of Greifswald Branch Institute will be responsible for the building, the local infrastructure, the energy-supply and cooling systems and will supervise the scientific objectives of the project.

In addition, a new division "W7-X Construction", headed by Project Director Dr. Wanner, was established. This division is responsible for the engineering, design, manufacture and installation of the W7-X device. The whole stellarator system will consist of 70 superconducting magnet coils and a plasma vessel in a common cryostat, the in-vessel components, the ECR, ICR and NBI heating systems and the operation and control systems.

A project organization appropriate to the size and complexity of the project was established. Special emphasis was placed on the cross functions project control, system engineering and quality assurance, which will support the activities of the technical departments. European associations have been invited to contribute to W7-X.

The technical work is still focused on the R&D activities. These activities comprise the testing of divertor target elements (see W7-X Physics), the manufacture of an original-sized superconducting coil, the development of an advanced conductor and the manufacture of a section of the cryostat.

## 2. MAGNET SYSTEM

### 2.1 R & D Work

#### *2.1.1 Superconductor*

IPP placed an order with the SWISS METAL company to produce a test length of 200 metres of the "advanced conductor" with improved stability properties /211/, following the results from former development work and the recommendations of the "ad hoc group". After some trials an optimized cabling law could be fixed. The order will be completed with major delay at the beginning of 1997. A test coil will be manufactured in the first half of 1997 and then undergo tests (STAR test bed at FZK).

A further test-coil from a W7-X conductor length was produced at FZK. Sophisticated investigations on this coil are under way with the goal of making quench propagation measurements (pressure and temperature distributions).

#### *2.1.2 DEMO coil*

The work on the DEMO coil (ordered from NOELL, with ANSALDO as sub-supplier) is entering its essential phase. The winding work is 50 % complete, with encouraging results concerning the workability of the conductor and the accuracy achievable. Completion of the winding pack is expected to be in August 1997. The manufacture of the coil casing was interrupted because the foundry went bankrupt. A new sub-supplier had to be taken under contract by NOELL and will start production in February 1997. As the winding work at ANSALDO has been delayed more than one year because of unexpected problems with details, the casing is not yet a critical issue. The delivery of the whole coil is expected at the end of 1997 with more than a one-year delay.

The test bed (TOSKA plant) at FZK is under preparation for the DEMO coil after the successful 1.8 K test on the LCT coil.

## 2.2 Basic Machine

### *2.2.1 Magnet design*

Final and detailed design of the confinement system of W7-X is under preparation. A powerful CAD system with full 3D qualities and included 2D drafting is in the implementing and testing phase at IPP in conjunction with Computer Vision, a systems consultant. The complete organization of the document and drawing records will be done with an integrated data system which can also be used for schedule and status reports. The coil set underwent final optimization of the geometry for better divertor properties of the machine. The design of the coil system will follow the incoming results of experience with the DEMO coil. Furthermore an improved FE-model of the structural design was generated.

### *2.2.2 Power supply design*

The electrical power supply for W7-X comprises three essential components:
i) The 50 Hz plant for an installed power of approx. 50 MVA, supplied by a 110 kV overhead line and a 20 kV ground cable. The power is distributed by a 20 kV bus bar system in the institute, equipped with phase compensation and harmonic filters.
ii) The HV-DC modules for the heating supply with 100 kV. This system is modularized in 5.6 MW-units and essentially depends on the gyrotron requirements under study.
iii) The high-current DC modules for the magnet supply. The nominal data for these units will be 15 V, 20 kA with highest precision current control. These rectifiers will be designed on the basis of know-how acquired jointly with industry.

# 3. CRYOGENIC SYSTEMS

## 3.1 Demonstration cryostat

Construction of the DEMO cryostat is progressing well at BALCKE-DÜRR company. All model coils are finished and covered with the 4 K copper shield (= housing cooling). About half of the most challenging plasma vessel components as well as the plasma vessel thermal shield (part of it being shown in Fig. 1) are completed, and the manufacture of the coil support structure has started. Design of the ports, the outer vessel and the rest of the thermal insulation is practically finished and the instrumentation is specified in detail.

The 110 W refrigerator for operating the DEMO cryostat was delivered in April. Some damage during transport had to be repaired. It was installed, tested and commissioned, and is now operating as a He liquefier for the institute.

The distribution box, serving as an interface between the refrigerator and the DEMO cryostat, was installed and acceptance tests are under way.

## 3.2 W7-X refrigerator

In order to detail the W7-X refrigerator system layout /210/ and prepare the specification, two conceptual design study contracts were placed with two competent and competing companies (AIR LIQUIDE and LINDE). First results are already available.

## 3.3 W7-X cryostat

A gas-permeable, detachable and economic high-voltage insulation was developed for the coil conductor connections which are situated within the cryostat vacuum /IPP/2/332/. Such an insulation is required in case of vacuum failure occurring simultaneously with a fast coil discharge, which would result in voltages of several kilovolts between coil connections and between the latter and ground. During such an event the gas pressure within the cryostat could reach conditions of the Paschen minimum with its low breakdown voltage of ≈160 V. The demonstration cryostat dummy conductor connections will be equipped with such insulations.

## 3.4 W7-X component cooling

The temperature distribution within the superconducting coil winding pack was studied /668/. Not only is the cable temperature determined by the helium state and mass flow, housing cooling and losses due to heat influx as well as magnetic field changes, it is also significantly affected by heat exchange between conductor windings. Both winding layers of one conductor length (= cooling length) represent a counterflow heat exchanger which causes temperature increase at the coil side opposite the helium inlets and outlets. This heat exchanger effect has to be taken into account in choosing the helium conditions for a certain superconductor temperature safety margin.

*FIG. 1: Part of the plasma vessel heat radiation shield*

# IEA IMPLEMENTING AGREEMENT
## for Cooperation in Development of the Stellarator Concept
## EUROPEAN ATOMIC ENERGY COMMUNITY / US DEPARTMENT OF ENERGY

### 1. OBJECTIVES OF THE AGREEMENT

The objective of the Implementing Agreement, first concluded in 1985, is to "improve the physics base of the Stellarator concept and to enhance the effectiveness and productivity of research and development efforts related to the Stellarator concept by strengthening co-operation among Agency member countries". To achieve this, it was agreed to exchange information, conduct workshops, exchange scientists, do joint theoretical, design and system studies, coordinate experimental programmes in selected areas, exchange computer codes, and perform joint experiments. In 1995 the Agreement was extended until June 2000. The contracting parties are EURATOM, the U.S. DoE, Japan (since October 1992), and Australia (since October 1993). In September 1994, Russia became an Associate Contracting Party.

### 2. STATUS OF THE AGREEMENT

In 1996, there were two meetings of the Executive Committee. A special meeting on possible collaboration on Stellarator Power Plant Studies took place at La Jolla (CA), USA, on March 11. As a result it was agreed that successful collaboration requires the following: a) exchange of personnel, including all stellarator and systems study groups with stellarator experience, b) regular meetings (once a year) of the groups active and experienced, c) a powerful communication system by using the possibilities offered by Internet. The 22nd meeting was held at Montreal, Canada, in conjunction with the IAEA International Conference on Fusion Research, which took place from October 7 to 11. The main points of this meeting were Stellarator Power Plant Studies, the IEA Workshop on Remote Participation in Experiments, the IAEA Third World Plasma Physics Meeting, collaboration between LHD and W 7-X, possible non-member countries´ association to the IEA Implementing Agreements, status of the experiments, and meetings and personnel exchanges.

### 3. REPORT ON 1996 ACTIVITIES

In 1996, seven physicists participated in the exchange of scientists. Staying from May 24 to September 2, J.F. Lyon from Oak Ridge cooperated in ICRH and pellet experiments on W 7-AS. L.R. Baylor, also from Oak Ridge, assisted in improving the pellet injection technology during his visit to IPP from July 8 to August 6.

Three scientists from the National Institute for Fusion Science (NIFS), Nagoya, paid short visits to IPP in 1996. During his stay from March 18 to 27, R. Kanno discussed the calculation of neoclassical transport in stellarator plasmas. S. Okamura and K. Matsuoka were concerned with the optimization of stellarators, in particular low-aspect-ratio stellarators with quasi-axisymmetry, during their two-week visit to IPP from May 11 to 24.

U. Gasparino from IPP spent about two years in Japan, from March 1994 to June 1996, to study neoclassical treatment of RF-induced transport, the kinetic description of RF heating, heating and current drive in 3D geometry, and the bootstrap current in 3D geometry. P. Merkel from IPP stayed two weeks in March and two weeks in June at Princeton to continue the cooperation with PPPL on developing the combined PIES-NESTOR code for computing 3D plasma equilibria with free boundary.

# Divisions and Groups

# THE SCIENTIFIC DIVISIONS OF IPP

**Experimental Plasma Physics Division 1**
Director: Prof. M. Kaufmann

ASDEX Upgrade
- divertor experiment for investigating the ITER/NET plasma boundary in a reactor-relevant divertor configuration and parameter regime, especially under good confinement conditions
- investigation of disruptions, betalimit and the densitylimit in an ITER-type plasma
- advanced tokamak studies

JET collaboration
- operation of diagnostics at JET and general collaboration

**Experimental Plasma Physics Division 2**
Director: Prof. G. Grieger

WENDELSTEIN 7-X
- divertor development
- contributions to stellarator power plant systems studies
- preparation of Greifswald site

**Experimental Plasma Physics Division 3**
Director: Prof. F. Wagner

WENDELSTEIN 7-AS (Advanced Stellarator)
- stellarator with improved confinement conditions
- toroidal plasma confinement in the stellarator
- net-current-free plasmas, plasma production and heating by neutral injection, and high-frequency waves
- plasma stability and impurity effects
- development of an island divertor

Preparation of the WENDELSTEIN 7-X diagnostics

**Experimental Plasma Physics Division 4**
Director: Prof. K. Behringer

Experimental and theoretical investigations of plasma boundary and divertor physics, impurity transport, chemical impurity production and plasma radiation in ASDEX Upgrade and WENDELSTEIN 7-AS
- Spectroscopic diagnostics on ASDEX Upgrade
- Spectroscopic diagnostics on WENDELSTEIN 7-AS
- Laboratory experiments at the University of Augsburg, Department of Experimental Plasma Physics

**Surface Physics Division**
Directors: Prof. V. Dose, Prof. J. Küppers

Surface physics
- atomistic characterization of surfaces

Plasma-wall interactions (analytical)
- interactions of atoms, ions and electrons with solid surfaces
- wall fluxes in the boundary layer of plasma devices
- limiter and wall analyses

Plasma-wall interaction (preparative) (see also Technology Division)
- preparation and characterization of thin-film coatings for plasma devices

**WENDELSTEIN 7-X Construction**
Director: Dr. M. Wanner

WENDELSTEIN 7-X R&D programme
WENDELSTEIN 7-X Construction
- Engineering, construction and installation of the WENDELSTEIN 7-X device incl. plasma heating and in-vessel components
- Project control and quality management

**Technology Division**
Director: Prof. R. Wilhelm

Neutral injection
- development and construction of the injection systems for WENDELSTEIN 7-AS, ASDEX Upgrade and WENDELSTEIN 7-X
- implementation of injection experiments

Electron cyclotron resonance heating
- construction and operation of an ECRH system for ASDEX Upgrade

Ion cyclotron resonance heating
- preparation and implementation of ICRH experiments for WENDELSTEIN 7-AS, ASDEX Upgrade and WENDELSTEIN 7-X

Plasma technology (see also Surface Physics Division)
- development, characterization and modelling of low-pressure plasma processes for thin-film formation

**Theory Division**
Acting director: Prof. K. Pinkau

General fusion-oriented plasma theory
- MHD equilibrium and stability
- analytical theory of drift instabilities

**Tokamak Physics**
Director: Prof. K. Lackner

General tokamak physics
- experiment-oriented theoretical work for the design and interpretation of tokamak experiments

Plasma edge physics
- experimental and theoretical work on plasma edge physics

Nonlinear Plasma Dynamics
- numerical simulation of turbulent transport and MHD reconnection phenomena

ITER collaboration

**Computer Science Division**
Director: Prof. F. Hertweck

Development of the AMOS/D system
Development of data acquisition systems for experiments at IPP
Studies in parallel computer architectures
Studies in neural networks

**Berlin Division**
Director: Prof. G. Fußmann

Edge plasma physics
- experimental and theoretical work relating to fusion devices

Plasma generator PSI-1
- basic plasma physics
- plasma interaction with solid surfaces
- development and testing of plasma diagnostics

Electron Beam Ion Trap (EBIT)
- production of highly charged ions
- X-ray spectroscopy and atomic physics measurements

UHV laboratory, arc physics, ITER collaboration

**Greifswald Branch of IPP**
Director: Prof. G. Grieger

Construction of institute and infrastructure

**Stellarator Physics Division**
Director: Prof. J. Nührenberg

Numerical and analytical methods of investigating equilibrium, stability and transport in three-dimensional toroidal configurations incl. plasma heating, particle and power exhaust.

# EXPERIMENTAL PLASMA PHYSICS DIVISION 1

(Prof. Dr. Michael Kaufmann)

The division E1 comprises

1. 4 diagnostic groups

   a. pellet injection, electromagnetic measurements, DCN interferometer, plasma control, MSE, halo current measurements, calorimetry
   b. Thomson scattering, bremsstrahlung, bolometer, SXR
   c. He measurements, neutral gas, neutron measurements, HXR, mass spectrometer
   d. ECE, microwave reflectometry, SABA, charge exchange, LENA

   which are responsible for the development of plasma diagnostics as well as for plasma physics exploitation;
2. 3 machine groups

   a. operation
   b. mechanical design
   c. assembly,

   which are concerned with the operation and engineering developments of the tokamak experiment ASDEX Upgrade and its peripheral installation;
   as well as groups for

   a. real-time control of the ASDEX Upgrade plasma,
   b. data acquisition and data evaluation.

These groups are supported by 3 workshops: mechanical, electrical, and electronical.

Divison E1 is also devoted to support diagnostics on JET and to continue studies for ITER.

# EXPERIMENTAL PLASMA PHYSICS DIVISION 2

(Prof. Dr. Günter Grieger)

The activity of the Experimental Plasma Physics Division 2 is concentrated mainly on the WENDELSTEIN 7-X Project (see Sec. WENDELSTEIN 7-X Project).

The relevant team is:

**W 7-X-Team**

S. Arndt, C.D. Beidler, R. Bünde, M. Drevlak, S. Gori, H. Greuner, G. Grieger, E. Harmeyer, Ch. Hennig, F. Herrnegger, F.-W. Hoffmann, J. Junker, J. Kißlinger, A. Könies, P. Merkel, H. Münch, A. Nitsche, C. Nührenberg, J. Nührenberg, I. Ott, M. Pillsticker, F. Rau, H. Renner, J. Sapper, F. Schauer, I. Schoenewolf, U. Schwenn, H. Strobel, E. Strumberger, M. Wanner, S. Weber, H. Wobig, R. Zille, A.V. Zolotukhin.

The team is supported by contributions from Forschungszentrum Karlsruhe (FZK - Institut für Technische Physik), Forschungszentrum Jülich and by the Central Technical Services of IPP.

# WENDELSTEIN 7-X CONSTRUCTION

(Dr. Manfred Wanner)

The work of the division is fully reported in section WENDELSTEIN 7-X Construction. Since November 15, 1996 the division has comprised the following members:

R. Bünde, M. Pillsticker, J. Sapper, F. Schauer, I. Schoenewolf, M. Wanner, F. Werner.

The team was supported by contributions from the Central Technical Services of IPP (W. Bitter, B. Fleischer, R. Holzthüm, N. Jaksic, F. Kerl, J. Simon-Weidner, B. Sombach) and from Forschungszentrum Karlsruhe (FZK: R. Heller, H. P. Jüngst, W. Maurer).

# EXPERIMENTAL PLASMA PHYSICS DIVISION 3 (W7-AS)

(Prof. Dr. Friedrich Wagner)

The W7-AS group comprises Experimental Plasma Physics Division 3. The work is fully reported in the section "STELLARATOR Project", of which the members are as follows:

*Experimental Plasma Physics Division 3:* M. Anton, R. Balbin[11], G. Beikert[13], E. Bellido[14], J. Bleuel[13], R. Brakel, G. Cattanei, Ch. Christou, R. Croci, D. Dorst, O. Dumbrajs[4], S. Egorov[10], M. Ellmauer[14], A. Elsner, M. Endler, K. Engelhardt, V. Erckmann, B. Ernst[14], Y. Feng, S. Fiedler, M. Francés[11], C. Fuchs[13] U. Gasparino, A. Geier[14], J. Geiger, T. Geist, S. Geißler, L. Giannone, C. Goerner[13], P. Grigull, H. Hacker, M. Haese[13], H.J. Hartfuss, O. Heinrich, G. Herre[14], M. Hirsch, J. Hofmann, F. Hoffmann, E. Holzhauer[3], J. K. Huebner[2], K. Ida[6], R. Jaenicke, F. Karger, M. Kick, A. Kislyakov[9], J. Knauer, C. Konrad[13], J.P. Koponen[4], H. Kroiss, G. Kuehner, A. Kus, H. Laqua, L. Ledl[13], H. Maassberg, C. Mahn, J.L. Malaquias[7], N. Marushchenko[12], K. McCormick, H. Niedermeyer, W. Ohlendorf, W. Pernreiter[13], U. Pfeiffer[14], S. Reimbold[13], M. Romé, N. Ruhs, A. Runov[8], N. Rust[13], J. Saffert, M. Saffmann[1], A. Salat, F. Sardei, Ch. Scheiba[14], F. Schneider, U. Siart[14], E. Simmet, M. Smirnova[12], U. Stroth, W. Svendsen[1], A. Chih Yao Teo[13], G. Theimer[13], F. Wagner, H. Walter[13], Ch. Watts, A. Weller, E. Würsching, X. Zhang, D. Zimmermann, M. Zippe, S. Zoletnik[5]

1) Guest from RISØ, Roskilde (Denmark)
2) Guest from IAP/University Heidelberg (Germany)
3) Guest from IPF Stuttgart (Germany)
4) Guest from University of Helsinki, Espoo (Finland)
5) Guest from KFKI Research Inst., Budapest (Hungary)
6) Guest from NIFS, Nagoya (Japan)
7) Guest from IST, Lisbon (Portugal)
8) Guest from Kurchatov, Moscow (Russia)
9) Guest from IOFFE Institute, St. Petersburg (Russia)
10) Guest from TUAP, St. Petersburg (Russia)
11) Guest from CIEMAT, Madrid (Spain)
12) Guest from IPT-NSC Kharkov (Ukraine)
13) Doctoral fellow
14) Undergraduate

*Technical Team W7-AS:* G. Abele, W. Andres, W. Bendak, M. Bergbauer, P. Böhm, J. Bömerl, K.H. Brumm, H. Czich, S. Eder, A. Eschlwech, J. Fink, M. Fusseder, D. Gonda, G. Grünwald, M. Heckmeier, T. Henningsen, J. Hofner, F.W. Hoffmann, H. Holitzner, R. Horn, G. Hussong, H. Ibbach, K. Iraschko, E. Katzmarek, K.H. Knauer, J. Littwin, R. Mulzer, R. Neuner, F. Offenbächer, J. Prechtl, S. Ravichandran, M. Richter-Gloetzl, H. Rixner, H. Schmid, L. Schmid, A. Schmidtmeier, H. Scholz, S. Schraub, R. Semler, H. Speer, J. Stadlbauer, B. Stajminger, P. Voigt, H. Volkenandt, K.H. Wagner, U. Weber, H. Wolf, G. Zangl, W.v. Zeppelin, Do. Zimmermann

*Experimental Plasma Physics Division 2:* K. Kisslinger, F. Rau, J. Sapper, H. Wobig and the workshop of Exp. Div. 2.

*Experimental Plasma Physics Division 4:* J. Baldzuhn, K. Behringer, R. Burhenn, J.V. Hofmann, A. Weghorn

*ECRH (Electr. Cycl. Resonance Heating):* W. Kasparek, L. Empacher, W. Förster, G. Gantenbein, P.G. Schüller, K. Schwörer (IPF Stuttgart)
A. Borshegovsky, L. Lubyako, V. Malygin, V.N. Sigalaev (GYCOM Nizhny Novgorod, Russia)
A. Burov, N. Skalyga, E. Suvorov (IAP Nizhny Novgorod, Russia)

*ICRH (Ion Cycl. Resonance Heating):* W. Becker, F. Braun, H. Faugel, R. Fritsch, D.A. Hartmann, F. Hofmeister, J.M. Noterdaeme, F. Wesner (Technology Div.)
J.F. Lyon, D.A. Rasmussen (ORNL, USA)
V. Plyusnin (IPP Kharkov, Ukraine)

*NBI (Neutral Beam Injection):* W. Ott, F.-P. Penningsfeld, F. Probst, E. Speth, R. Süss, (Technology Div.), W. Melkus (Central Technical Services)

*Plasma Surface Interaction Group:* R. Behrisch, V. Dose, K. Ertl, W.v.d. Linden, H. Verbeek, J. Roth, E. Taglauer, P. Zebisch

*Division Berlin:* A. Herrmann, D. Hildebrandt, B. Jüttner, D. Naujoks, H.-D. Reiner

*Computer Centre:* S. Heinzel, H. Lederer

*Central Technical Services:* B. Brucker, B. Fleischer, W. Melchior, J. Perchermeier and the workshop.

# EXPERIMENTAL PLASMA PHYSICS DIVISION 4

(Head of Division: Prof. Dr. Kurt Behringer)

Experimental Plasma Physics Division 4 (E4) consists of the groups ASDEX Upgrade, W7-AS and ITER Diagnostics. Their work is described in the ASDEX Upgrade and W7-AS project reports as well as the ITER Diagnostics contribution. Experimental Plasma Physics at the University of Augsburg is closely linked to E4, allowing physics students to participate in IPP's scientific programme or do basic research at Augsburg. Recent results are given under University Contributions to IPP Programme.

ASDEX Upgrade: K. Asmussen, A. Bard, S. De Peña Hempel, R. Dux, B. Endras, W. Engelhardt, J. Gafert, A. Kallenbach, B. Napiontek, R. Neu, H. Meister, D. Schlögl, A. Thoma
W7-AS: J. Baldzuhn, R. Burhenn, J. Hofmann
University of Augsburg: U. Fantz, H. Paulin
ITER Diagnostics: H. Salzmann
Guest: Z. Wang, Southwestern Inst. of Physics, Chengdu, Sichuan
Co-operation: IPP Berlin, JET, KFA Jülich, TU München, University of Strathclyde, Stuttgart University

The E4 scientific programme is concerned with understanding plasma boundary and divertor physics, studying impurity transport and plasma radiation, and investigating low- and high-Z wall materials with respect to performance and impurity problems. Spectroscopic diagnostics and analysis methods are being used for studying the plasma response. Recent topics in ASDEX Upgrade were edge cooling by impurity radiation, plasma recombination and ion dynamics in the divertor, and tungsten as high-Z wall or divertor material. The interest in W7-AS is focused on measurements of toroidal rotation and electric fields, on impurity and neo-classical transport, and on magnetic field topology .

A particular problem in the analysis of plasma radiation is the large amount of atomic data required. This knowledge is being acquired in an international co-operation creating a constantly growing data base, which is also of importance for plasma simulation codes. The main activities for low- and medium-Z ions are organized in the ADAS project (Atomic Data Analysis Structure, H.P. Summers, Strathclyde, Scotland). Present activities deal with cooling rates for many elements, with diagnostic line data for spectroscopy and with opacity effects in high-density divertor plasmas. As an example, Fig. 1 shows E4 ADAS calculations of the hydrogen ionization balance in high-density, low-temperature divertor plasmas. Opacity of the resonance lines is taken into account for neutral hydrogen densities of $10^{19}$ (moderately thick) and $5 \cdot 10^{19}$ $m^{-3}$ (optically thick). ADAS optically thin standard data ("93" data) are also presented. Fig. 2 presents carbon and neon cooling rates calculated on the following basis: purely theoretical atomic data; detailed analysis of each ionization stage ("93" data, W.J. Dickson, Ph.D. thesis, Strathclyde University, 1993), and zero-density results of earlier simple estimates (default "89" data, K. Behringer).

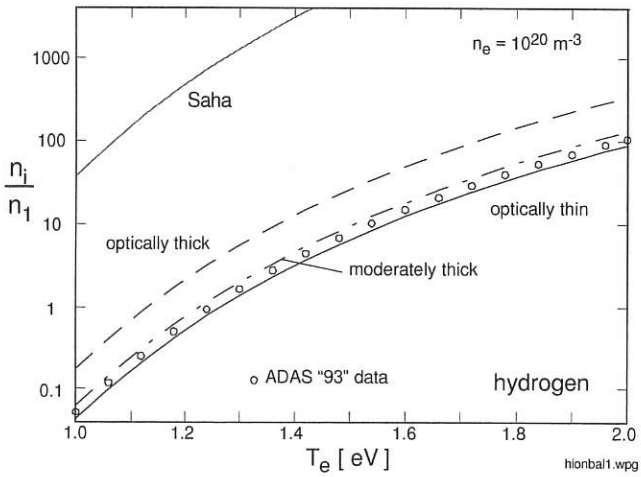


*FIG. 1: Hydrogen ionization balance for optically thin and thick plasma conditions.*

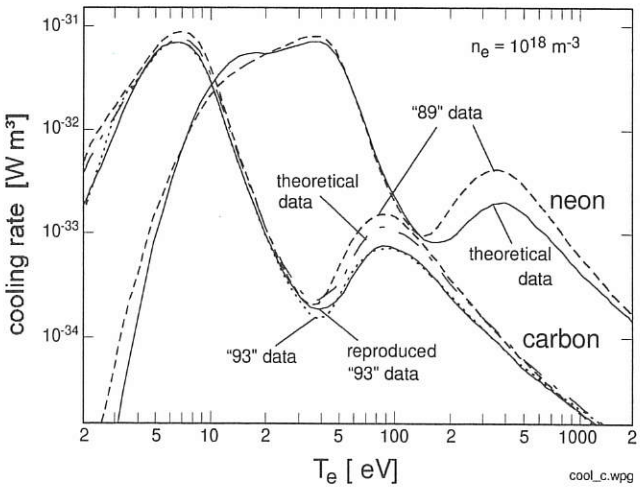


*FIG. 2: Cooling rates for carbon and neon from simple theories and from detailed data sets for each ionization stage.*

# GREIFSWALD BRANCH OF IPP

(Prof. Dr. Günter Grieger)

The Greifswald Branch of IPP is planned to house practically all the stellarator activities of IPP. At present, the activity is concentrated on the construction of the institute and its infrastructure. But also the Stellarator Physics Division (see below) under Prof. Dr. J. Nührenberg moved to Greifswald some time ago.

The relevant team is:

G. Grieger, J. Junker, W. König.

The team is supported by the construction division of IPP and MPG.

# STELLARATOR PHYSICS DIVISION

(Prof. Dr. Jürgen Nührenberg)

The activity of the Stellarator Physics Division is concentrated on further development of numerical and analytical methods to investigate equilibrium, stability and transport problems in three-dimensional toroidal configurations including plasma heating, particle and power exhaust.

The relevant team is:

S. Arndt, M. Drevlak, Ch. Hennig, A. Könies, P. Merkel, C. Nührenberg, J. Nührenberg, S. Weber.

# GENERAL THEORY

(Acting Head: Prof. Dr. Klaus Pinkau)

Contributions by D. Correa-Restrepo, R. Croci, D. F. Düchs, D. Lortz, R. Meyer-Spasche, D. Pfirsch, F. Pohl, M. Schiegl, G. O. Spies, H. Tasso (all IPP),
and by K. Grote (Technische Universität München), G. Kamelander (Österreichisches Forschungszentrum Seibersdorf), M. Rilee and R. N. Sudan (Cornell University, Ithaca, USA), and G. N. Throumoulopoulos (University of Ioannina, Greece)

## 1. OVERVIEW

After the retirement of Prof. Pfirsch in October 1995 part of the staff of the previous General Theory Division have been transferred to other IPP divisions. The work of the remaining theoreticians comprises the subjects of fusion plasma equilibria with flow, of macroscopic and microscopic plasma stability, of drift–wave turbulence, of propagation, absorption and conversion of waves under ICH conditions, and of anomalous plasma transport mechanisms.
These topics are treated by using the various levels of plasma description: Ideal MHD, resistive MHD, drift–fluid, as well as kinetic theory in form of Vlasov–Maxwell or test particle approximation.
New improved basic equations have been developed, namely small scale averaged MHD ("AMHD") for field reconnection problems, and drift–fluid equations deduced in such a way as to automatically satisfy the basic conservation laws. Under the heading of new mathematical resources, the structure of Burgers hierarchy and numerical schemes for nonlinear differential equations have been studied. Finally, the advantages of fusion energy have been reviewed in the light of the present status of research.

## 2. IDEAL MHD THEORY

Realistic fusion plasmas practically always exhibit flows. Therefore, stationary rather than the customary static equilibria are to be investigated.

### 2.1 Magnetized parallel flows (Tasso)

The nonlinear 2-D stability of magnetized parallel flows is proved for all Reynolds numbers. Three-dimensional ideal equilibria with flow aligned with the magnetic field are investigated. It is proved that incompressible flows with isothermal magnetic surfaces lead necessarily to Palumbo's solution.

### 2.2 Cylindrical ideal MHD equilibra with flow (Throumoulopoulos, Tasso)

An elliptic equation is derived for MHD equilibria with general incompressible flows. Several classes of analytic solutions can be explicitly found. For isothermal magnetic surfaces the cross section must be circular.

## 3. RESISTIVE MHD THEORY

Resistivity can change magnetic field topology (e.g. reconnection) and thus strongly affect the stability of plasma/field equilibria. The basic equations for this resistive MHD have been extended and adapted for tearing modes. Resistive MHD also has been applied to predict the stability of a plasma/vacuum interface.

### 3.1 Averaged MHD (AMHD) Technique (Rilee, Sudan, and Pfirsch)

For tearing modes only topological changes are important but not dissipation. The AMHD equations are obtained from a Langrangian, which in turn allows one to construct an energy principle. The latter affords the luxury of employing trial functions and in this way extremely simplifies the algebra. The results obtained with this technique agree very well with those found in the numerical treatment. The new theory has been applied to tearing instability in solar coronal loops.

### 3.2 Singular inertial operator in resistive MHD (Tasso)

The stability conditions are qualitatively similar to the case of nonsingular operators, but suggest more optimism quantitatively. The 2 by 2 matrices of this exercise do not, however, reflect the full problem related to a continuous fluid.

### 3.3 Extended theory of interface localized modes (Lortz, Spies)

In a previous paper, resistive interface localized modes (ILMs) were considered in a plane plasma-vacuum slab. Attention was restricted to wavelengths much smaller than the plasma diameter, but still much larger than some length proportional to the square root of resistivity. It was then shown that resistive ILMs are unstable unless

the current density vector and the magnetic field vector are perpendicular to each other in the plasma-vacuum interface, and that the growth rates are much smaller than the Alfvén frequency. It is shown that the ratio of growth rate and Alfvén frequency becomes independent of the resistivity and proportional to the inverse of the square root of the wavelength as the latter approaches zero.

## 4. DRIFT-FLUID PLASMA MODEL

In this plasma model, particle drifts approximate the full flow velocities. It is widely used for extensive numerical plasma turbulence studies. The validity range of its basic equations is investigated.

### 4.1 Lagrangian for plasmas in drift-fluid approximation (Pfirsch, Correa-Restrepo)

For drift waves and related instabilities, conservation laws can play a crucial role. In an ideal theory these conservation laws are guaranteed when a Lagrangian can be found from which the equations for the various quantities result upon application of Hamilton's principle. Such a Lagrangian for plasmas in the drift-fluid approximation was obtained by a heuristic method in a recent paper by Pfirsch and Correa-Restrepo. The same Lagrangian has now been derived from the exact multi-fluid Lagrangian via an iterative approximation procedure that resembles the standard method usually applied to the equations of motion. That method, however, does not guarantee that all conservation laws will hold.

### 4.2 A nonlinear equation for drift waves (Tasso)

In the long wave-length approximation and in the presence of an electron temperature gradient, drift waves obey in the electrostatic approximation the 2-D Korteweg-de Vries equation. The modified form of this equation leads to the 2-D Ginzburg-Landau Hamiltonian previously used by the author to compute the fluctuations spectrum of drift waves.

## 5. MAXWELL-VLASOV PLASMA MODEL

Velocity distribution functions, often non-Maxwellian, are needed to describe sub-fluid properties of fusion plasmas. The simplified kinetic plasma description of the Maxwell-Vlasov model is used to predict plasma stability and is, in particular, necessary for the description of wave propagation and absorption (ICH and ECH).

### 5.1 Negative-energy perturbations in general axisymmetric and helical Maxwell-Vlasov equilibria (Correa-Restrepo, Pfirsch)

The expression for the free energy of arbitrary perturbations of general Vlasov-Maxwell equilibria derived by Morrison and Pfirsch was transformed and put in a concise form, which was subsequently evaluated for general equilibria with one ignorable coordinate, e.g. axisymmetric and helical equilibria, in the case of internal perturbations, i.e. perturbations which vanish outside the plasma, and on its boundary. In order to generate the electric currents necessary for equilibrium in the presence of pressure gradients, the equilibrium distribution function of at least one particle species must be anisotropic. Related to this anisotropy there are gradients in velocity space which are a source of free energy. As a consequence, these equilibria always allow negative-energy perturbations, without requiring a large spatial variation of the perturbation across the equilibrium magnetic field.

### 5.2 Nonlocal effects of ICRH on the singularities of the e.m. field (Croci)

The system of the Maxwell and Vlasov equations is singular (at $v_{th} = 0$, it then yields $k_\perp^2 \to \infty$ in a local approximation) for some finite values of the dielectric tensor (say, on the curve $f(r, \Theta) = 0$), or when the dielectric tensor becomes infinite in the presence of a resonance, e.g. for ICRH. At finite temperature, the form of the solution in the neighbourhood of $f(r, \Theta) = 0$ is changed both by the local finite Larmor radius effect and because ICRH modifies the dielectric tensor also far from the resonance region. The study of the second effect requires a new approach to the determination of the singularities at zero temperature. The electric field is not written as a series with a given first singular term, but is determined in the relevant two-dimensional strip by requiring that the components of the electric field parallel and perpendicular to the curve $f(r, \Theta) = 0$ (not yet known) satisfy some inequalities. The solution shows that the non-local effect of ICRH on the field singularities is limited to a narrow region about the ICRH resonance zone and to a narrow interval of $k_z$. However, it dominates over the finite Larmor radius effect where the field is not singular and should not be neglected as is generally done. The e.m. energy flux does not cross the curve $f(r, \Theta | v_{th} = 0)$, even when the non-local ICRH effect is taken into account.

### 5.3 Correct asymptotic treatment of a group of cut-offs and mode conversion points in a Vlasov plasma (Croci)

An asymptotic method of solution of the Maxwell and Vlasov equations is being developed for a region $S$ in a tokamak plasma with a group of "relevant points" (cut-offs and mode conversion points). The region $S$ is treated as a slab in the $x$-direction. The cornerstones of the method are: The dispersion relation in the regions of $S$ where the WKB approximation is valid (i.e., sufficiently far from the relevant points) is not limited by the assumption $kp \ll 1$. For the sake of a clear description, an example has been chosen that corresponds to ICRH in a deuterium plasma with minority protons.
Non-linear Riccati equations for the functions $k(x)$ in the neighbourhood of the relevant points are deduced and solved. On the two sides of a relevant point, different Riccati solutions have to be chosen (although the solutions are continuous there) and have to be connected by continuity relations. The Riccati solutions are connected with the WKB solutions by a "matched asymptotic procedure". The transmission and reflection coefficients for an incoming e.m. energy flux are derived.

## 6. KINETIC THEORY WITH TEST PARTICLE ORBITS

Another approximation to a kinetic plasma description is the test–particle approach where statistical samples of particle orbits are calculated. Here the assumptions for orbit computations are questioned, and the models are applied to study mechanisms of anomalous transport.

### 6.1 Quantitative validity of drift approximation (Düchs, Pohl, Kamelander)

The drift approximation for particle orbits is deduced for $\rho/l \ll 1$, with gyroradius $\rho$ and gradient length $l$. For $\rho/l$ close to 1 corrections to the gyroradius seem to be more necessary than to the drift velocities.

### 6.2 Transport across magnetic islands (Schiegl, Düchs)

When magnetic surfaces are perturbed and form chains of islands, plasma transport can become "anomalous", especially for overlapping islands. Both through analytical models and with Monte-Carlo numerical codes the modifications in particle transport are being studied and estimated.

### 6.3 Transport effects due to finite ion gyroradii (Düchs)

In plasmas with local gradients in (average) ion gyroradius, charge separation occurs. The resulting drifts can lead to important and rather complex non-linear transport properties.

## 7. DEVELOPMENT OF MATHEMATICAL RESOURCES

Nonlinearity and complexity are basic characteristics of fusion plasma theory. The appropriate mathematical tools are often not yet available and must be developed.

### 7.1 Hamiltonian formulation of odd Burgers Hierarchy (Tasso)

A bi-Hamiltonian formulation is derived for the prime member of the odd Burgers hierarchy:
$u_t = (u^3)_x + 3/2 \cdot (u^2)_{xx} + u_{xxx}$.
This property permits, as usual, the construction of the complete hierarchy. It is also related to the integrability of the equation.

### 7.2 Dynamical properties of one-step-methods (Meyer-Spasche, Grote)

To understand the behavior of difference schemes on nonlinear differential equations, it seems desirable to develop a nonlinear stability theory that extends the standard linear theory. As a step in that direction, we investigated the stability properties of Euler-related difference schemes by checking how they preserve and violate the dynamical structure of (a) the logistic differential equations and (b) a Lotka-Volterra predator-prey system. We found in case (a) that the linearly implicit self-adjoint scheme is dynamically faithful in an Euler-typical range of step sizes and gives correct stability for all step sizes, as long as the blow-up time (depending on the initial value) has not passed (IPP 6/330; to appear). In case (b) this same scheme still has very good properties (it is symplectic with respect to a non-standard Hamiltonian), but it does turn unstable on periodic orbits for "too large"step sizes. The results of these case studies are now investigated in a more general theoretical frame.

### 7.3 Linearly implicit schemes for quasilinear diffusion equations (Meyer-Spasche, Pohl)

The dynamical behavior of linearly implicit difference schemes was investigated on quasilinear diffusion equations with one space dimension. As test equation we mostly used a Burgers-type equation

$$u_t = 1/R \cdot u_{xx} - uu_x + u,$$

$$u(0,t) = u(1,t) = 0$$

with several different initial conditions. Depending on the value of the parameter $R$, this equation has one or more steady states. Different initial values can thus lead to qualitatively different trajectories and the differential equation and its discrete models can behave differently in this respect. The linearly implicit scheme mostly investigated is dynamically faithful in neighborhoods of stationary states of ordinary initial value problems for step sizes not exceeding the blow-up time. On equations of the type of our parabolic test equation, however, it has a more limited range of faithfulness.

## 8. FOUNDATIONS OF FUSION ENERGY RESEARCH

Controlled thermonuclear fusion is a field of long term research of general importance and thus needs constant substantiating.

### 8.1 Comparison of long term energy sources (Düchs)

The advantages of energy from thermonuclear fusion in comparison to other long term energy sources (solar, fission breeder, etc.) are collected and assessed in the light of presently available research results.

# TOKAMAK PHYSICS

(Head of Project: Prof. Dr. Karl Lackner)

The main task of this division is theoretical and experimental support of IPP tokamak activities. Consequently, the major part of its work is reported in the sections on ASDEX Upgrade, JET, and ITER/NET. The activities described below concern either more basic aspects of fusion plasma physics or the development of models and codes not exclusively linked to one particular experiment.

Head: K. Lackner, Deputy: J. Neuhauser
Team: G. Becker, A. Bergmann, D. Biskamp, K. Borrass, M. Brambilla, K. Büchl, A. Carlson, R. Chodura, D. Correa-Restrepo, D. Coster, W. Feneberg, S. Günter, F. Jenko, O. Kardaun, L. Lengyel, P. Martin, J. Neuhauser, G. Pautasso, K. Reinmüller, R. Schneider, W. Schneider, E. Schwarz, J. Schweinzer, B. Scott, H. Tasso, M. Weinlich, R. Wunderlich, H.-P. Zehrfeld, A. Zeiler

Guests: C. Atanasiu, Central Inst. of Physics, Bucharest, A. Boozer, Columbia University, New York, B. Braams, New York University, E. Kakoulidis, G. Kyriakakis, N. Tsois, Demokritos, Athens, P. Lalousis, IESF.FORTH, Heraklion, P. McCarthy, H. Callaghan, University of Cork, A. Ushakov, I. Veselova, V. Rozhansky, Technical University, St. Petersburg, A. Hatayama, Keio University, Japan

## 1. NONLINEAR PLASMA DYNAMICS

### 1.1 Three-dimensional Nonlinear Simulations of Plasma-edge Turbulence

Electron and ion temperature fluctuations $\widetilde{T}_e$ and $\widetilde{\mathrm{T}}_\mathrm{i}$ and magnetic field fluctuations $\widetilde{B}_\perp$ were included. The effect of $\widetilde{T}_e$ is found to be relatively weak. Parallel thermal conduction strongly suppresses the ability of the electron temperature gradient to drive the turbulence and transport. Over most of the resistive ballooning regime only the density gradient drives the turbulence, and the temperature fluctuations are convected as a passive scalar. In the drift wave regime only the density gradient acts to drive the nonlinear instability, and the temperature fluctuations have a relatively strong stabilizing influence on the resulting turbulence. From the numerical results we obtain expressions for the anomalous particle and electron thermal transport coefficients D and $\chi_e$, which are independent of the electron temperature gradient. $\widetilde{T}_i$ and $\widetilde{B}_\perp$ are included by deriving a more general set of nonlinear reduced Braginskii equations combining resistive ballooning/drift wave equations with ion pressure dynamics, thus introducing the $\eta_i$ mode. Ion temperature fluctuations strongly affect the turbulence for $\eta_\mathrm{i} \gtrsim 2$. At low temperature $\nabla T_i$ enhances the ballooning drive. In contrast to the density-gradient-driven resistive ballooning mode, it is only weakly affected by electron diamagnetic effects. At high temperature the resistive ballooning mode converts into the toroidal $\eta_i$ mode. Magnetic fluctuations become important for $\beta > 0.1\beta_{ball}$ ($\beta_{ball} = q_a^2 \beta R/L_n$ = ideal ballooning limit), leading to strongly enhanced transport.

### 1.2 Two-fluid Theory of Magnetic Reconnection

In the high-$\beta$ case ($\beta \gtrsim 1$) reconnection is controlled by the Whistler mode, which leads to a decoupling of ions and electrons on scales $l < c/\omega_{pi}$. Though reconnection requires finite electron inertia, the reconnection rate is independent thereof, being controlled only by ion inertia, and is hence much faster than in the absence of the Hall term. In the presence of a strong axial field (low-$\beta$) the Whistler mode is suppressed. Hence ions have to follow the electrons into the narrow reconnection layer $\delta \sim c/\omega_{pe}$, which strongly reduces the reconnection rate. A three-dimensional EMHD code for a periodic box has been developed. Studies of EMHD turbulence, which plays an important role in high-$\beta$ collisionless reconnection, were conducted with high spatial resolution ($128^3$ and $256^3$ modes). Dominant structures of the current density are filaments with the diameter of the dissipation scale, similar to the vorticity structures in Navier-Stokes turbulence and different from the sheets seen in MHD turbulence.

## 2. AB-INITIO TRANSPORT MODELLING

### 2.1 Fluid and Kinetic Drift Alfvén Turbulence

An extended fluid model can treat shear Alfvén dynamics, and collisional and Landau dissipation with arbitrary ordering. The principal electromagnetic effect was found to be purely linear

magnetic induction, which acts to slow down the parallel dynamics through the inverse dependence of the shear Alfvén transit frequency with beta. Both ballooning and magnetic flutter were found to be of secondary importance; although they have a strong effect on the overall level of turbulence and transport, the character of the internal dynamics and the scaling with beta were unaffected when the terms representing ballooning and magnetic flutter were removed from the computations. In all cases, moreover, the transport itself is predominantly ExB transport. This shows that the fundamental dynamics behind fluid electron drift turbulence at relevant edge parameters is drift Alfvén turbulence. The principal ingredient is the nonlinear drift wave instability, modified by the effect of magnetic induction on the parallel dynamic time scale.

In tandem with the extended fluid model, a companion one with drift kinetic electrons was constructed. The principal new effect studied with this model is the velocity space nonlinearity, which accounts for trapping of slower particles in fluctuating electric potential wells along the magnetic field. The turbulence is of the collisionless universal-mode type; collisions and magnetic fluctuations are still to be incorporated. Since the main parameter controlling the thermal electron transit frequency is proportional to the electron/ion mass ratio, the model produces an isotope mass scaling with the same trend as that observed in experiments. The velocity space nonlinearity leads to slightly weakened transport by smoothing out the details of the Landau wave-particle resonance, but so far we observe no effect on the qualitative mode structure. That mode structure itself is very similar to that produced by the extended fluid model, confirming earlier calculations showing the same thing in two-dimensional slab geometry.

### 2.2 Neoclassical Temperature Screening

The numerical solution for the temperature screening term calculated with the same pitch angle scattering model as used in the analytic theory exceeds the predicted values of Hirshman-Sigmar by a factor between 2 and 4. Including energy scattering reduces these values by about 40%, but leaves the temp. screening term high enough to prevent neoclassical impurity accumulation.

## 3. LINEAR MHD STABILITY

The CASTOR (Complex Alfvén Spectrum in Toroidal geometry) linearized resistive MHD code and the corresponding HELENA equilibrium code have been installed at IPP. The HELENA code was used to perform a ballooning stability analysis for ASDEX Upgrade plasmas. It was shown that the often applied relation between the critical normalized pressure gradient $\alpha_{crit}$ and the shear s $\alpha_{crit} = 0.6\ s$ which has been developed for circular plasmas and large aspect ratio is not valid for toroidal and shaped plasmas. For ASDEX Upgrade geometry approximately the relation $\alpha_{crit} = 0.95\ s$, with $\alpha_{\mathrm{crit}} = -\frac{-2\mu_0 q^2}{\varepsilon B_0^2}\frac{\mathrm{dp}}{\mathrm{d}\sqrt{\Psi}}$, $\mathrm{s} = \frac{\sqrt{\Psi}}{\mathrm{q}}\frac{\mathrm{dq}}{\mathrm{d}\sqrt{\Psi}}$ holds. Experimental observations of TAE modes which are localized near q=3 were confirmed theoretically for ohmically heated plasmas. The calculated frequencies and damping rates agree very well with the experimental results.

The critical values for the kinetic-energy beta-poloidal (the ratio of poloidal rotational to poloidal magnetic energy density) as a function of the total plasma beta were reconsidered. It was found that the first elliptic regime is limited by a kinetic-energy beta-poloidal of the order of beta. It turns out that the intermediate (hyperbolic) regime between the first and second elliptic regions is very small.

For finite aspect-ratio the parameters $\alpha$ and shear appear as generalized quantities in the ballooning mode equations and vary on magnetic surfaces. Taking their flux surface averages it was found that these are of only limited importance because of the large variation of their local definitions. For ASDEX Upgrade it turns out that the region of unfavourable normal curvature is considerably extended towards the (lower) X-point.

## 4. THEORY OF HIGH FREQUENCY PLASMA HEATING

Several improvements were made to the FISIC code, which solves the Finite Larmor Radius wave equations in tokamaks in the ion cyclotron range of frequencies. The most important is a new formulation of the Galerkin discretization in the vacuum region between the plasma and vessel, which explicitly guarantees that the wave electric field in this region is divergence-free. This eliminates numerically produced oscillations on the radial mesh scale, which with the usual discretization often spoils the solution in situations with weak absorption in the plasma.

## 5. 2D PARTICLE SIMULATION

The non-saturation of the ion current collected by a flat Langmuir probe oriented almost parallel to a strong magnetic field was studied by two-dimensional particle simulations. The influence of the ExB drift on the electron and ion flows towards the probe was studied. A reduction of the electron current to strongly positive by biased probes occurs which extends over about half a poloidal gyro radius. The flow of current across the magnetic field back to the wall adjacent to the probe was studied: A current of the order of the ion saturation current can flow back to the wall.

Emissive Langmuir probes are used as a diagnostic tool to measure the plasma potential. In the case of strong emission a double layer is formed in front of the probe which limits the emission current into the plasma. The floating potential of an emissive probe is lower than the plasma potential, depending on the emission current and the ratio between the wall and plasma temperatures.

# SURFACE PHYSICS DIVISION

(Prof. Dr. Volker Dose
Prof. Dr. Jürgen Küppers)

Scientific activities in the Surface Physics Division proceed via three routes, which we call plasma wall interaction (analytical), plasma wall interaction (preparative) and surface science. Our work on analytical problems of plasma wall interaction is for the purpose of this report further divided into two categories. Those activities which take place in intimate collaboration with fusion devices are included in the respective chapters on tokamaks and stellarators. Additional laboratory work described in this chapter is grouped under the title plasma wall interaction processes. Contributions to the field of plasma wall interaction (preparative) are described in a separate section entitled plasma technology. This project is a joint venture with the IPP Technology Division. More fundamental studies, summarized under the heading of surface science, comprise a continuation of previous activities in magnetism and contributions to the Sonderforschungsbereich 338. The latter concentrates on adsorption at solid surfaces and integrates work at the Munich Universities and IPP and MPQ.

Head: V. Dose, Deputy Head: E. Taglauer,

Scientific Staff:
A. Annen[1], F.-P. Bach[2], M. Balden[3], U. Bauernschmitt[2], R. Behrisch, E. Berger[1], E. Bertel, J. Biener[3], M. Donath, H. Ebert[15], W. Eckstein, K. Ertl, Th. Fauster, R. Fischer, M. Friedrich[14], C. García-Rosales[13], St. Grigull[1], R. Grötzschel[14], B. Gubanka[1], P. Hanesch[1], A. Horn[1], W. Jacob, A. v. Keudell[3], H. Knözinger[15], U. Kreißig[14], K. Krieger, M. Küstner[1], S. Labich[1], B. Landkammer[1], J. Lehmann[1], W. von der Linden, Ch. Linsmeier[3], C. Lutterloh[1], K. Maruyama[4], M. Mayer[3], N. Memmel[3], S. Miller[1], W. Möller[14], U. Murtfeld[2], J. Onsgaard[5], F. Passek[3], P. Pecher[1], K. Plamann[3], H. Plank[3], W. Poschenrieder, R. Preuss[3], V. Prozesky[6], A. Ramaswami[7], G. Rangelov[3], J. Reinmuth[1], S. Reiter[3], Ch. Reuß[1], J. Roth, R. Ruggieri[8], M. Saß[2], B. Scherzer, Th. Schwarz-Selinger[1], R. Schwörer[3], A. Starke[9], G. Staudenmaier, A. Steltenpohl[1], J. Stober[12], G. Sun[14], K. Swamy[1], U. Thomann[1], P. Valášek[1], G. Venus, H. Verbeek, W. Wang[10], W. Weiß[9], M. Wittmann[3], S. Wolf[1], G.N. van Wyk[11], P. Zebisch[3].

Technical Staff:
S. Bassen, L. Beck, M. Ben Hamdane, S. Figge, Ch. Fritsch, K. Gehringer, R. Hippele, A. Holzer, M. Hunger, P. Matern, J. Mauermair, M. Nagy, W. Ottenberger, M. Roppelt, J. Schäftner, A. Schlamp, H. Schmidl, F. Schuster, I. Zeising.

1 Doctoral Candidate
2 Undergraduate Student
3 Post Doc

Guests:

4 Nagaoka University of Technology, Japan
5 Universität Odense, Denmark
6 National Accelerator Laboratory, SA
7 Washington University, St. Louis, MO, USA
8 Tore-Supra, Cadarache, France
9 Universität Erlangen-Nürnberg, Germany
10 Shanghai Institute of Nuclear Research, China
11 University of Bloemfontein, SA

Collaboration with:

12 IPP, Experimental Division E1
13 Centro de Estudios e Investigaciones Técnicas de Guipúzcoa, San Sebastián, Spain
14 Forschungszentrum Rossendorf, Germany
15 Ludwig-Maximilians-Universität, Munich, Germany

## 1. PLASMA-WALL INTERACTION

### 1.1 Hydrogen Inventory in Plasma-facing Materials (PFM)

In fusion experiments using D/T as fuel gas the T inventory in the vessel walls is a critical issue for the choice of the PFM. For carbon-based materials the codeposition of hydrogen isotopes with eroded carbon atoms has been identified as dominant source for a permanent inventory. The search for alternative materials with low permanent codeposition as well as methods of outgassing or removal of deposited layers are of major interest.

#### *1.1.1 Codeposition of deuterium with BeO at elevated temperatures*

The codeposition process of hydrogen isotopes with beryllium oxide as occurring at deposition-dominated wall areas of fusion experiments has been simulated at the Garching high-current sputtering device in the temperature range between room temperature and 800 K. During sputtering with 2 keV $D^+$ ions Be atoms are deposited as BeO on silicon collectors. Reflected deuterium codeposits with BeO at room temperature in a ratio of 0.36 D/BeO, which is comparable to the amount of deuterium codeposited with carbon (about 0.42 D/C). At elevated temperatures the amount of codeposited deuterium

decreases. At 573 K the ratio D/BeO is 0.17 and decreases to 0.07 at 773 K. The thermal release of deuterium codeposited at room temperature begins at 400 K. At temperatures above 800 K all deuterium is released. It is assumed that the deuterium is trapped at damage sites with a spectrum of different activation energies. From the viewpoint of tritium inventory trapped in codeposited layers in next-step fusion experiments such as ITER beryllium has only minor advantages compared with carbon.

### *1.1.2 Hydrogen isotope exchange and oxidation of hydrogenated carbon layers*

Another aim of the investigation is to identify methods of routine removal of codeposited carbon layers. The isotope exchange and oxidative removal of a-C:D layers were therefore investigated by heating in air at temperatures between 300 and 800 K. The layer thickness and composition were determined by MeV ion beam analysis. It could be shown that hard a-C:D layers can be completely removed at heating temperatures between 600 and 700 K due to chemical erosion with oxygen. Also, in the remaining layer isotope exchange occurs where D is released and O and H are incorporated in the layer. In addition to hard a-C:D layers, soft codeposited layers from the walls of ASDEX Upgrade were also investigated.

Fig. 1 shows the time dependence of deuterium release and carbon removal from both layers at 650 K. While hard layers can be removed within about 15 h, codeposited layers from ASDEX Upgrade show much higher chemical reactivity and are completely removed in less than 3 h. Further studies on deposited layers of different hardness show the importance of the microstructure for oxidative layer removal.

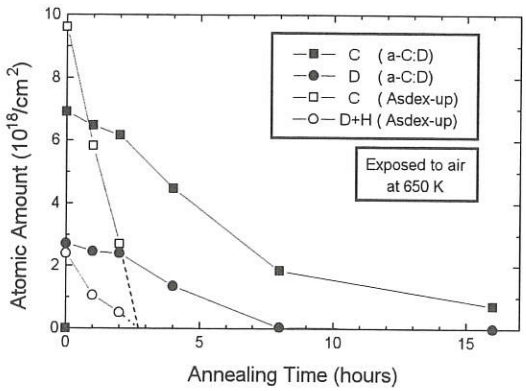


*FIG.1: Comparison of the erosion rate between the ASDEX Upgrade sample and an a-C:D film for air exposure at 650 K.*

## 1.2 Erosion of Plasma-facing Materials (PFM)

Erosion of PFM's strongly influences the design of advanced divertors for ITER. Erosion is important for estimates of both plasma contamination and the lifetime of plasma-limiting components. Physical sputtering due to light plasma ions was investigated in detail and erosion yields obtained from computer simulations are provided in tabulated form for external users in / afs / ipp / u / wge / trim.data / sputter.data.

Most newly developed PFM's are compounds of different elements. In these materials compositional changes of the surface layer occur due to ion-induced diffusion and segregation, preferential sputtering of components as well as deposition or implantation of incident ions. These processes are difficult to study by computer simulation and constitute the emphasis of the experimental investigations.

### *1.2.1 Influence of surface roughness on the sputtering yield*

Earlier measurements of different graphites have shown that the increase of sputtering yield with angle of incidence is reduced with increasing roughness. Only best-polished surfaces exhibited the steep angular dependence calculated for flat surfaces (TRIM.SP). On artificial test surfaces, it could be shown that two parameters determine the angular dependence: the distribution of the local angle of incidence on the tilted surface, and the shadowing and redeposition of sputtered particles on neighboring surface structures.

The model has been tested with two different graphite samples sputtered with high $D^+$ fluence at different angles of incidence. Surfaces of pyrolytic and isotropic porous graphite (EK98) are sputtered until dynamic equilibrium is reached, which means constant yield with ion fluence. After sputtering, surfaces are monitored using Scanning Tunneling Microscopy (STM) and the distributions of local incidence angles are determined. The distributions are used as input to the TRIM.SP simulation code. The results of the simulation of rough surfaces are compared with the measured yields. The simulation and the measurements are in good agreement within the error bars for both graphite surfaces.

### *1.2.2 TiC phase formation and its influence on chemical erosion*

In previous X-ray Photoelectron Spectroscopy (XPS) measurements it was shown that the interaction of Ti layers on graphite substrates leads to the formation of $TiC_x$ carbides with x values depending linearly on the annealing temperature between 700 and 1200 °K. At higher temperatures, a stable $TiC_{0.93}$ phase was formed. However, it has not been possible to determine definite phases at annealing temperatures below 700 °K due to surface contamination, mainly by oxygen.

The carbidisation of thin Ti films on natural diamond was therefore investigated in the temperature range between room temperature and 1000 °K. It is possible to separate chemical phases in Ti $2p_{3/2}$ electron peaks after deconvolution of the spectrometer's broadening function with Bayesian reasoning, using Maximum Entropy (ME) prior information. The broadening function is calculated by deconvoluting measured spectra of the Fermi edge of a silver sample with its theoretical form. Data analysis of reconstructed Ti $2p_{3/2}$ core level spectra shows that, with increasing temperature, Ti films are

transformed from metallic Ti to a mixed phase consisting of metallic Ti and $TiC_{0.59}$. No carbidic phase is found with a ratio of carbidic C to Ti smaller than 0.59. The metallic layer is fully transformed to $TiC_{0.59}$ at 700 °K. At higher temperatures, the concentration value of carbidic C to Ti depends nearly linearly on temperature. At temperatures above 1200 °K graphitic carbon precipitates within the $TiC_{0.93}$ layer.

For carbidic layers prepared at different temperatures formation of hydrocarbons during the interaction with 1 keV D ions was investigated. Fig. 2 shows the chemical sputtering yield as a function of temperature for layers containing various degrees of carbon. It can be seen that hydrocarbon formation is strongly suppressed as long as all carbon is bound in carbidic form. Only for carbon contents above $TiC_{0.93}$ is a drastic increase of chemical erosion found.

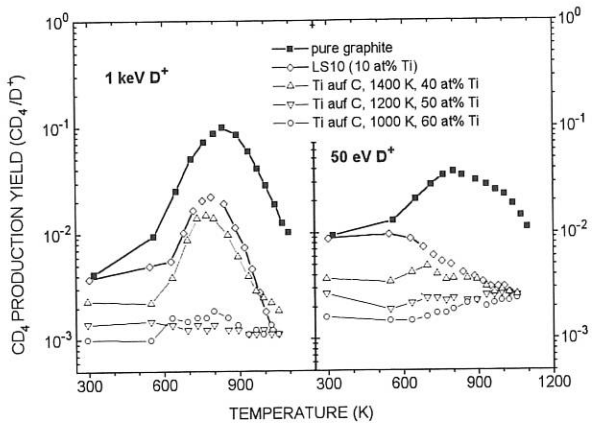


*FIG.2: Chemical sputtering yield for Ti films on graphite reacted to $TiC_x$ at 1000, 1200 and 1400 °K compared with pure graphite and LT10 (10 at% Ti).*

### *1.2.3 Preferential sputtering of carbides under deuterium irradiation - comparison between experiment and computer simulation*

Recently, it was shown that doping of graphite with appropriate elements such as B, Si, Ti yields an effective reduction of chemical erosion. The erosion behavior and surface composition changes of doped graphites can be understood from the microstructure of the material and the erosion behavior of corresponding carbides. Changes of surface composition due to deuterium irradiation at room temperature in the energy range between 20 eV and 1.5 keV were therefore investigated for SiC, TiC and WC. Results of surface composition measurements obtained by Auger Electron Spectroscopy (AES) are compared with preferential sputtering calculated from experimental sputtering yields of pure elements, or computer simulations with the TRIDYN Monte Carlo code.

TRIDYN calculations for SiC and TiC show a moderate enrichment of the metallic component at energies above 100 eV, while for WC the enrichment reaches 100% due to the high threshold energy for sputtering of W. At 20 eV neither W nor carbon can be physically sputtered and the concentration remains unchanged.

The measured erosion behavior of SiC and TiC at ion energies above 100 eV and 200 eV, respectively, can be accounted for by physical sputtering as seen from the good agreement between AES measurements of surface compositions and TRIDYN results. Decreasing the ion energy causes the formation of an altered surface layer enriched in Si or Ti. For SiC, the measured surface concentrations tend towards the values expected from the sputtering yields of pure elements. This is caused by preferential sputtering of C, mainly due to chemical erosion. The measured surface concentrations of TiC differ from both TRIDYN results, and the values expected from experimental sputtering yields. The surface compositions of TiC at ion energies below 200 eV thus cannot be explained only in terms of preferential erosion of C. We believe that radiation-enhanced segregation of C and a solid-state reaction between Ti and C forming TiC take place, which hinders a higher Ti surface enrichment. For WC, the measured surface concentrations in the investigated energy range from 20 eV to 1.5 keV agree more with TRIDYN results than with concentrations expected from sputtering yields of pure elements. Thus, chemical processes are of minor influence. The erosion behavior can be understood in terms of preferential erosion of carbon due to threshold effects caused by the large mass ratio of W to C.

## 1.3 Plasma Edge Studies in Fusion Experiments

The investigations of the plasma-wall interaction group in direct collaboration with the ASDEX Upgrade, W7-AS, JET and NET/ITER plasma experiments are treated in the respective sections. Only examples of general applications and new techniques are presented here.

### *1.3.1 Erosion of the main chamber walls of ASDEX Upgrade by CX neutrals*

Investigations on wall erosion have been mainly concentrated on the divertors of plasma machines. However, the erosion in the main chamber still needs to be considered because of the limited lifetime of the wall and impurity influxes to the plasma.

At AUG the CX fluxes and energy distributions have routinely been measured in the most relevant energy range of 20 to 1000 eV by the Low-Energy Neutral particle Analyzer (LENA) at one particular location on the outside wall. The CX intensities and the shapes of the corresponding energy distributions, which can be characterized by the total fluxes $\Gamma$ and the mean energies ($E_{mean}$), largely depend on the discharge conditions. For ohmic discharges $E_{mean}$ decreases with $n_e$, while the flux increases. For heated discharges the flux increases with the heating power but $E_{mean}$ shows no simple dependences.

LENA is located where there are no strong neutral gas sources nearby. But the CX fluxes are toroidally very different and are

very large especially near areas with strong recycling such as antenna limiters. For the poloidal plane of the LENA location the CX fluxes and energy distributions were simulated by the EIRENE code taking the experimental CX fluxes and $H\alpha$ intensities into account. This allowed us to extrapolate the energy distribution down to 1 eV and determine the angular distributions. Furthermore, the same calculation for different wall positions showed that not only the fluxes but also the energy distributions are poloidally very different. In the case of a particular discharge, one has $E_{mean}$ = 25 eV at the upper inner wall (a location where the flux surfaces have large separations), while it is 150 eV at the LENA location.

By multiplying the energy distribution of the CX fluxes by the energy dependence of monoenergetic sputtering yields an effective sputtering $Y_{eff}$ can be calculated as a function of $E_{mean}$. Due to the chemical erosion of carbon $Y_{eff}$ varies by a factor of only 1.4 for all measured CX spectra, independently of $E_{mean}$. The erosion of a C wall can therefore be estimated from the local fluxes, which are roughly proportional to $H\alpha$ signals. However, if metal walls are considered, $Y_{eff}$ increases with $E_{mean}$. For a W wall $Y_{eff}$ would be 50 times smaller at the upper inner wall than at the LENA location. For Be the factor would be 2.

The evaluation of $Y_{eff}$ for various discharge conditions and wall materials is important in choosing the proper materials for future machine applications. For comparing different materials use is often made of a figure of merit given by the ratio of the maximum tolerable impurity concentration and the sputtering yield, $c_{max}/Y_{eff}$. In Fig. 3 the materials C, Be and W are compared. It can be shown that W has better values than C only at very low values of $E_{mean}$, i.e. very high density plasmas. In typical ASDEX Upgrade discharges W is an order of magnitude worse than the low-Z materials.

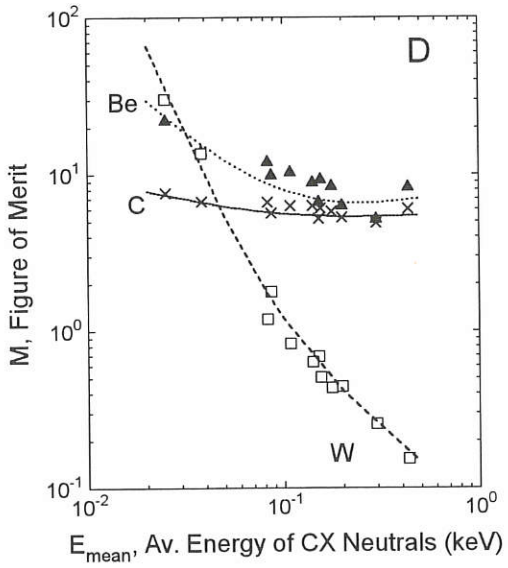


*FIG.3: Figure of merit of different potential first-wall materials for sputtering by a flux of CX neutrals characterized by its average energy <E>.*

### *1.3.2 Measurements of the extremely small amount of T trapped in carbon tiles at the vessel walls of ASDEX Upgrade*

The Accelerator Mass Spectroscopy Technique (AMS) was applied to measure the very small amounts of T originating from DD reactions in the plasma and being implanted in the surface layers of the vessel walls. The measured T concentrations are about 3 $10^{10}$ to 3 $10^{12}$/cm$^2$. The integrated amount is in good agreement with the total number of 2.5 MeV neutrons, indicating that the major part of the produced T is trapped in the carbon tiles at the vessel walls.

### *1.3.3 Trapping of N implanted in carbon*

To cool the boundary plasma, especially in the divertor, injection of nitrogen is used in ASDEX Upgrade and JET, and good "wall pumping of the nitrogen" was observed. For an understanding of this wall pumping, the trapping of nitrogen injected in carbon was investigated by the ERDA technique. The nitrogen ions are initially trapped within the implantation range up to a concentration of about 0.35 N/C at room temperature and about 0.2 N/C at 700 °K. This corresponds to about 1 to 2 $10^{17}$ N/cm$^2$ at an implantation energy of 20 keV.

## 2. SURFACE SCIENCE

The cooperation of the surface science group within the Sonderforschungsbereich (SFB 338: Adsorption on Solid Surfaces) is continuing. Recent contributions include the exploration and manipulation of electronic surface states on metal surfaces, the dynamics of diffusion and growth, and the investigation of model catalysts. Additionally, the magnetic properties of thin-film systems are being studied.

### 2.1 SFB 338

The interaction of xenon with metal surfaces was studied by high-resolution photoemission. It could be demonstrated that Shockley surface states yield an essential contribution to the energy budget of the rare-gas metal interaction. This explains in particular the clustering of Xe on terraces and the Xe decoration of upper step edges on Pt(111) as well as the absence of these effects on Pd(111).

Quantum size effects on Shockley-type surface states were investigated on the notorious O/Cu(110) striped surface oxide phase. The transition from the extended periodic system to isolated one-dimensional quantum well states (a surface Mott transition) was followed by high-resolution photoemission.

A scanning tunneling microscopy (STM) study of Pt(110) and Pt(110)-c(2x2)Br revealed a mesoscopic island structure on clean Pt(110). It is attributed to elastic relaxation of the intrinsic surface stress. A quantitative analysis of such mesoscopic surface structures may for the first time provide

experimental access to measurements of the absolute surface stress.

The homoepitaxial growth of Pd on Pd(111) was studied by STM. At 400 K growth of 3-dimensional islands occurs, while at 300 K a much flatter film morphology is observed. This unexpected temperature dependence can be explained by energy barriers for step-down diffusion which depend on the step orientation and thus on the island shape: At 400 K the islands are triangular, while at 300 K islands are almost circular.

The reconstruction of stepped vicinal copper surfaces due to oxygen adsorption was further investigated by ion scattering (ISS) and STM in UHV. It had been shown that the development of energetically favored Cu-O-Cu chains results in the formation of two kinds of {104}-type facets that intersect in a {118}-oriented ridge. The orientation of the third type of facet which is necessary to maintain the macroscopic orientation of the surface was supposed to depend on the orientation of the macroscopic Cu(11n) surface (n<15) relative to the {118} direction. This was demonstrated for Cu(115) and could be confirmed for Cu(119). Atomically resolved STM images demonstrate that this surface reconstructs into two types of {104} facets terminated by a (001) facet, see Fig. 4.

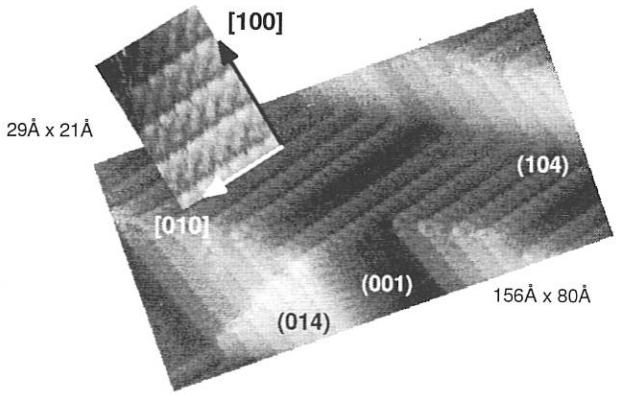


*FIG.4: STM image of a Cu(119) surface after oxygen adsorption at 500 K. The insert shows enlarged the atomically resolved (104) facet.*

The previously developed $Rh/TiO_2/Mo$ model catalyst was used to investigate the occurrence of strong metal-support interactions (SMSI) by various surface analytical methods, i.e. ISS, TDS, XPS, and AES. The surface composition and morphology and their changes under relevant reaction conditions can thus be studied. After temperature treatments in UHV above 730 K all SMSI effects which have been postulated for real catalysts were observed. The rhodium clusters agglomerate and are encapsulated by a reduced $TiO_{2-x}$ species. Oxidation at 570 K and subsequent reduction with CO restores the original state of the model catalyst. As a model for promoted catalysts a $V_2O_x/SiO_2/Mo$ system was prepared in a similar way by chemical vapor deposition and characterized. The original $V_2O_5$ oxide is reduced to a mixture of $V_2O_4$ and $V_2O_3$ by heating up to 820 K in UHV.

## 2.2 Surface Magnetism

The spin-dependent electronic structure of Gd films deposited on W(110) was the subject of a spin-resolved inverse-photoemission study. One focus of interest was the temperature-dependent spin polarization of a magnetic surface state (SS) at Gd(0001), which is held to be responsible for exceptional surface magnetic properties. While at low temperature the SS consists of an empty minority and a partially empty majority part, the spin splitting vanishes upon approaching the bulk Curie temperature (Fig. 5). The same collapsing band behavior is observed for bulklike *d* bands (BS). No indication of enhanced surface magnetic order was found on flat and well-ordered 100 Å thick Gd films. The observed temperature behavior is an important result for any theoretical description of surface magnetism at Gd(0001).

The local magnetization at the Fe and Ni sites in $FeNi_3$ was studied with spin-resolved appearance potential spectroscopy. The influence of matrix-element effects on the partial spin intensities of the spectra was investigated in collaboration with H. Ebert (LMU Munich). The measured temperature dependences of the local magnetizations are identical for the two elements in the alloy and give no indication of surface magnetic properties different from the bulk.

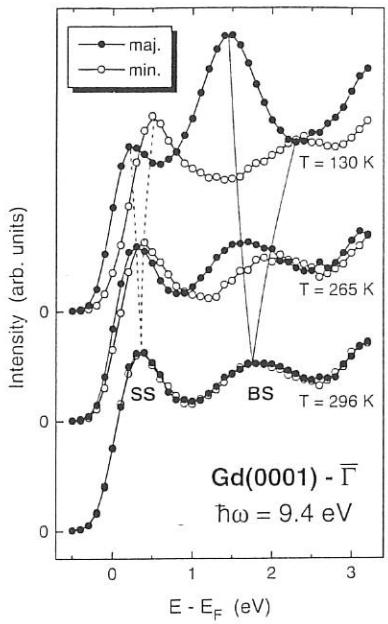


*FIG.5: Spin-resolved inverse-photoemission spectra for normal electron incidence on Gd(0001) as a function of temperature. The temperature-dependent spin splittings are emphasized by solid and dashed lines for transitions into bulk (BS) and surface states (SS), respectively.*

# TECHNOLOGY DIVISION

(Prof. Dr. Rolf Wilhelm)

The main task of the Technology Division is the development and operation of the various plasma heating systems at IPP's two major facilities. For a more detailed description of these projects (viz. neutral beam injection and ion cyclotron heating on ASDEX Upgrade and W7-AS, and electron cyclotron heating on AUG) the reader is referred to the respective sections of this report. The following sections present some further information on specific technical developments and experimental and theoretical work within the plasma heating programme or in connection with general reactor aspects.

## 1. NEUTRAL INJECTION HEATING

NI Group

### 1.1 Collaboration CEA/IPP on Negative Ions

M. Ciric, J.-H. Feist, P. Frank, B. Heinemann, W. Kraus, F. Probst, E. Speth

Work in the frame of the CEA/IPP collaboration on production of negative ions, mentioned in the last annual report, was continued. The old testbed, mothballed for the last two years, was completely renovated. The different power supplies for extraction (9 kV, 8 A; produced by 4 old power supplies connected in series and in parallel), beam acceleration (conversion of the former positive polarity into negative), RF power (old 150 kW generator), and plasma grid biasing (truck batteries) were installed. The originally envisaged RF source of the old type with the quartz wall, the internal Faraday shield, and the protection vacuum (RIG-HEX) was replaced by a new type of source. This source has no quartz vessel and the Faraday shield is integrated in the vacuum wall. The vacuum vessel now has 92 slits which are individually sealed by O-rings, pressed into specially formed grooves. The RF coil, which is a cable with high-voltage insulation, is simply wound around the vacuum vessel. The extraction system (3 grids with 48 holes, 11.3 mm diameter on a 6 · 20 $cm^2$ area, produced by CEA) was installed on a newly designed support structure inside the standard PINI insulator. For beam diagnostics, a simple, moveable calorimeter (flat copper plate with a number of thermocouples and water cooling) with an electron deflection system in front of it (Helmholtz coils and separate electron dump) was installed in the vacuum chamber.

First plasma operation was started in August, with RF powers of up to 80 kW and pulse lengths of up to 3 s, showing very reliable source behaviour. Beam extraction, without any means of electron suppression, was also carried out up to 2 kV, 8 A to test the electrical integrity of the testbed. It turned out that protection against breakdowns in the extraction gap was not sufficient in the present arrangement. For more reliable operation, the extraction power supply was therefore replaced by the acceleration power supply, which has the fast switch tube. With this arrangement and a magnetic filter in front of the plasma grid (strength appr. 700 G · cm), negative ion extraction was clearly demonstrated up to an RF power of 115 kW and an extraction voltage of 6 kV. Figure 1 shows the calorimetrically measured negative ion current as a function of the RF power for the optimum extraction voltage in each case. The source operating pressure is 1.6 Pa. From these values a maximum current density at the source of 3 mA/$cm^2$ can be calculated, with due allowance for the rather bad beam quality (beam divergence around 4 deg.). The next steps will be installation of a Cs-oven, already delivered by CEA, hardening of the extraction power supply, to allow acceleration, and increase of the magnetic filter strength.

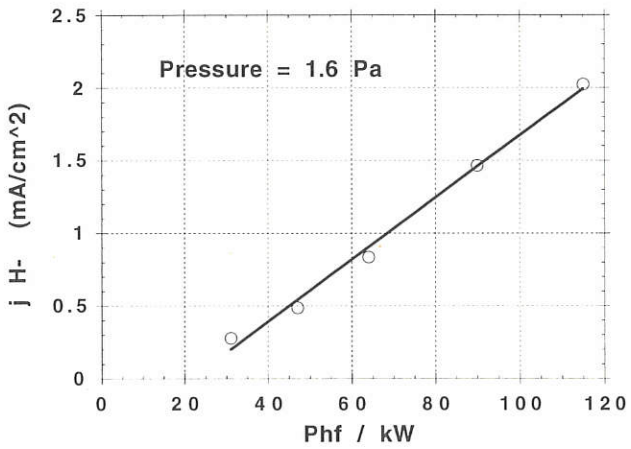


*FIG. 1: Calometrically measured negative-ion current density as a function of the RF power*

## 2. ION CYCLOTRON RESONANCE HEATING

ICRH Group

### 2.1 RF Conditioning with Long Pulses and Arcs

W. Becker, F. Wesner

Arcs can be used for conditioning if their burn time is short enough ("spot knocking"). This is usually applied to pressurized coaxial transmission lines. In vacuum-insulated ICRF lines and antennas, the electrical strength is primarily limited by gas discharges, the gas being released from the walls by the RF. For conditioning, this gas is usually removed by multipactor discharges and long high power pulses. Now it has been shown, that the voltage strength in vacuum can be further increased with spot-knocking.

Tests were made with a coaxial vacuum-insulated 6" line. After conditioning with multipactors and 10 s power pulses, first arcs occurred at about 35 kV, clearly increasing the conditioning effect, if the power was cut to zero within 20 µs after arc breakdown. This effect became smaller with increasing burn time until, at 125 µs, no further conditioning effect was seen. Experience from ASDEX Upgrade and W7-AS shows that with long burn times the voltage strength can be severely impaired. Reconditioning is then only possible as long as no arcing channel along an insulating surface is created.

In pressurized lines some 10 pulses were needed for further conditioning, and a small voltage step again resulted in arcs, while in vacuum only few arcs, sometimes only one, were sufficient to allow the next step, which could often be much larger than for pressurized lines. In the test, voltages higher than 60 $kV_{eff}$ were achieved with 1 s pulses. On W7-AS this method resulted in a remarkably improved voltage strength. It will also be applied on ASDEX Upgrade, and the tests will be continued.

### 2.3 Toroidal Transport via Radiative Collisonality

S. Puri

Momentum transfer via Kirchhoff radiation of electrostatic electron and ion cyclotron harmonic waves contributes an enhanced collisionality far in excess of that given by the Fokker-Planck term in the existing neoclassical models. The resultant particle and thermal transport resembles the observed anomalous transport in ohmically heated toroidal plasma. The power radiated per unit volume by a plasma in thermodynamic equilibrium is $\eta_E = (T/\pi^{2)} \iint \Im\,[\omega] k_\perp\, dk_{||}\, dk_\perp$, where $\Im[\omega]$ is the imaginary part of $\omega(\mathbf{k})$. Since the plasmon of energy $\hbar\omega$ carries a momentum $\hbar k$, momentum exchange among the particles via the emission and absorption of radiation gives rise to radiative collisionality. The radiation-induced electron-electron collision frequency $\tilde{\nu}_{ee}$ is about a hundred times larger than the neoclassical value $\nu_{ee}$; *radiative* $\tilde{\chi}_e$ *exceeds neoclassical* $\chi_e$ *by a factor of one hundred,* thereby resolving the most perplexing of the transport anomalies. It is shown that the variation of the radiative particle and thermal diffusivities with magnetic field, isotope mass, plasma temperature, and density is in accord with the experimental observations.

## 3.0 ECRH ON ASDEX UPGRADE

(In cooperation with IPF Stuttgart and IAP Nizhni Novgorod)
H. Brinkschulte, F. Leuterer, M. Münich,
F. Monaco, A.G. Peeters, F. Ryter

A first phase of ECRH experiments using a 140 GHz, 0.5 MW, 0.5 sec gyrotron was completed. Results concerning the evaluation of heat wave propagation are described under ASDEX Upgrade (Sec. 3.2).

The ECRH system is still under construction and will finally use 4 gyrotrons with 0.5 MW, 2 sec each. More details are given under in the ASDEX Upgrade (Sec. 2).

### 3.1 ECRH Power Deposition in ASDEX Upgrade

On ASDEX Upgrade a focused EC wave beam is used. Its geometric optics description leads to an unrealistic focal point with infinite field amplitude. Therefore a formalism which extends the ray equations of geometric optics by including diffraction effects was derived. The resulting equations contain correction terms which lead to a repulsive action between the rays, avoiding thus a focal point. Simple ordinary differential equations describing the propgation of a Gaussian beam can be derived from these equations. The ray tracing code was extended to include the most important terms of the derived equations. It was applied to ASDEX Upgrade shots where ECRH was deposited out of axis by poloidal beam deflection, in which case the deposition profile is primarily determined by the beam geometry. In Fig. 2 we show the radial locations of the 1/e points of the calculated (crosses) and measured (dots) deposition profiles. Their width is about 23 cm. The experimental points were determined by fitting the temperature rise (ECE signals) in the close vicinity of the deposition centre to the solution of a one-dimensional heat diffusion equation with constant coefficients.

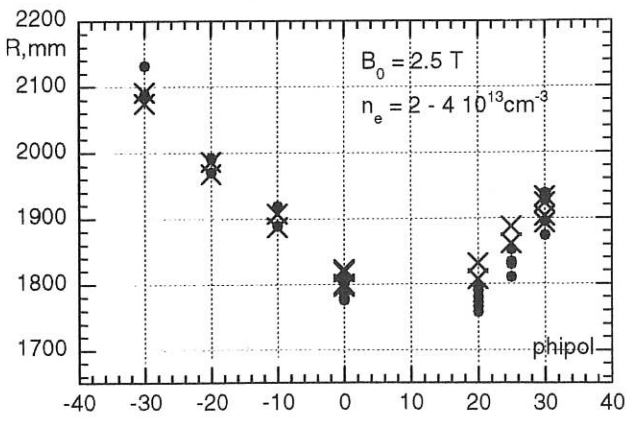


*FIG 2: Calculated (x) and measured (o) location and 1/e-width of the deposition profile*

# PLASMA TECHNOLOGY

(Prof. Dr. Volker Dose

Prof. Dr. Rolf Wilhelm)

The Plasma Technology group is concerned with three tasks: Surface coatings are produced by means of plasma chemical vapor deposition (PCVD) for special applications, mainly in fusion plasma devices. New or improved PCVD procedures or devices are being developed for this purpose. As the scientific part of the activity, plasma, plasma edge, and thin-film diagnostics are employed in order to correlate the discharge parameters with the properties of the resulting coatings and improve understanding of the basic mechanisms of plasma deposition. The third goal is a modeling of the deposition process which allows the discharge conditions to be adjusted in a predictable way in order to optimize a desired property of the growing film.

In 1996, main activities were in-situ characterization of the growth and etching of hydrogenated carbon films, measurement of the particle fluxes onto the substrate from a methane ECR plasma, and deposition and characterization of hydrogenated boron and boron-carbon thin films. In an additional experiment the transition of a multipactor discharge to an HF gas discharge as well as the interaction of multipactor discharges with surfaces were studied.

A. Annen[1], F.-P. Bach[3], U. Bauernschmitt[3], R. Beckmann[2], V. Dose (Division Head)[1], F. Höhn[2], W. Jacob[1], G. Kerkloh[4], A. von Keudell[1], B. Landkammer[1], P. Pecher[1], M. Saß[3], T. Schwarz-Selinger[1], R. Wilhelm (Division Head)[2].

1 Surface Physics Division
2 Technology Division
3 Undergraduate student
4 Technical Staff

## 1. INVESTIGATION OF MULTIPACTOR DISCHARGES

The investigations of multipactor discharges at a frequency of 50 MHz were continued. The transition of a pure electron multipactor at low background pressure (below 0.03 Pa for our setup) to a HF gas discharge was studied in detail. The breakdown of an ordinary HF gas discharge is a function of the HF voltage and the gas pressure. It is described by the well-known Paschen law. In contrast, the pure electron multipactor is independent of the background pressure, and the breakdown voltage is merely a function of the HF frequency, the HF power and the geometry of the setup. In the intermediate pressure region a new regime which we named 'multipactor plasma' was discovered. The electrons of the multipactor collide with background gas atoms, leading to ionization and finally to the breakdown of a gas discharge. This multipactor-supported breakdown happens, however, at a pressure which is about one order of magnitude lower than necessary for an ordinary HF discharge. The electron energy distribution was measured as a function of the background gas pressure. In the multipactor regime almost all electrons arrive at the electrodes with the full HF voltage. Increasing the pressure to values slightly below the multipactor plasma clearly shows the influence of the gas phase collisions. The electron energy distribution broadens significantly, the mean energy shifts to lower values and a large number of low energy electrons appears. With the breakdown of a plasma, the electron current density increases dramatically while the mean energy shifts to very low energies. The existence regions of the multipactor, the multipactor plasma and the ordinary HF gas discharge were determined and characterized by the electron current density, the reflected HF power, and the emitted light. In addition, the current from the electrodes to the chamber walls was measured.

## 2. IN-SITU PLASMA DIAGNOSTICS

### 2.1 Optical Emission Spectroscopy

The collisional-radiative model which was set up the preceding year to calculate the optical emission of low-pressure helium

plasmas was further improved and tested. In general, the optically determined electron temperature is in good agreement with Langmuir probe results. The high sensitivity of the model to reabsorption of resonance lines allows extraction of the neutral gas temperature, which determines the gas density and, therefore, the reabsorption.

### 2.2 Charged and Neutral Particle Fluxes from a Methane ECR Plasma

In continuation of our effort to quantitatively determine the fluxes of plasma species onto the substrate, we determined the mass and energy dependences of our energy-mass analyzer. This now allows the relevant particle fluxes to be quantitatively measured. Calibration was performed by comparing ion-energy distributions measured with the energy-mass analyzer to measurements with a retarding-field analyzer of known transmission for various noble-gas discharges. In methane discharges the ion flux above pressures of about 0.5 Pa is dominated by molecular ions which are formed by ion-molecule reactions in the bulk plasma. These results clearly show the importance of the influence of ion-molecule reactions on the composition of the bulk plasma as well as the flux to the substrate surface.

## 3. THIN FILM DEPOSITION AND EROSION

### 3.1 Erosion of C:H Films in Oxygen, Oxygen/ Hydrogen, and Water Plasmas

The erosion of plasma-deposited hydrogenated carbon (H:C) films by oxygen, hydrogen, and mixed oxygen/hydrogen ECR plasmas was investigated in situ by ellipsometry. Under all applied plasma conditions oxygen plasmas showed the highest erosion rates. In general, oxygen/hydrogen (1:2) mixtures also show higher erosion rates than water plasmas. The erosion rates increase with increasing ion energy and increasing substrate temperature.

### 3.2 Deposition of C:H Films from Various Precursor Gases

The deposition of hydrogenated carbon (H:C) films from ECR plasmas was investigated in situ by spectroscopic ellipsometry. As precursor gases $CH_4$, $C_2H_6$, $C_2H_4$, $C_2H_2$, $C_3H_8$, and $C_4H_{10}$ were used. Furthermore, the deposited films were characterized by ion-beam and infrared analysis. It was found that the precursor gas has a significant influence on the film properties. Films deposited from unsaturated hydrocarbons possess a higher density and higher refractive index than those from saturated hydrocarbons when deposited under comparable conditions. In addition, the growth rate is higher for unsaturated hydrocarbons. However, films deposited from different precursor gases show very similar properties if the resulting hydrogen content is similar.

## 4. THIN FILM CHARACTERIZATION

### 4.1 Hydrocarbon thin films (C:H)

The methods to analyze thin C:H films were continuously improved. For infrared analysis, a new computer-based evaluation formalism which includes interference effects in the thin film and the contribution of absorption bands to the refractive index via the Kramers-Kronig relation was developed. Furthermore, a new experiment was set up to measure the thermally-induced decomposition of thin films by thermal desorption spectroscopy (TDS). A set of C:H films with properties ranging from soft, polymer-like (H/C~0.9, n=1.6) to hard C:H (H/C~0.4, n=2.25) was investigated by TDS, Fourier-transform infrared spectroscopy (FTIR), and ion-beam analysis (IBA). For hard films, $H_2$ is the dominant desorption signal, with desorption maxima at 850 and 1150 K, and contributes about 90% of the total hydrogen desorption. Together with the first maximum at 850 K desorption of $CH_4$ and some higher hydrocarbons is detected. For soft films, desorption starts at about 600 K and is dominated by hydrocarbon species. Films annealed in vacuum to characteristic temperatures were consecutively analyzed by FTIR and IBA. It was found that the integral over the CH vibrational bands around 3000 $cm^{-1}$ shows no simple linear relationship with the hydrogen content, as often assumed in the literature.

### 4.2 Amorphous, Hydrogenated Boron Thin Films (a-B:H)

Investigating the bonding of hydrogen to boron in a-B:H films by FTIR, we found that hydrogen is bonded in two ways, as a terminal B-H and in a B-H-B bridge bond. Comparing the integral over the two IR absorption peaks with the hydrogen content as measured by IBA, we determined the absorption strength for the two peaks. This now allows calculation of the total hydrogen content of the films as well as the fraction of hydrogen in the two bonding types from infrared absorption spectra. Increasing ion energy and substrate temperature during deposition increases the density and reduces the hydrogen content of a-B:H films. It is interesting to note that the hydrogen content is highly correlated to the boron density (correlation coefficient = 0.96). In addition, the amount of hydrogen in the B-H-B bridge bond increases, while H in the terminal B-H bond strongly decreases with increasing boron density. Films with low boron density are chemically unstable. They react with gases from the ambient atmosphere, which leads to an uptake of oxygen and carbon in the films.

# BERLIN DIVISION

(Head of Division: Prof. Dr. G. Fussmann)

The topics of the Berlin Division extend from independent experimental investigations on basic plasma physics, plasma-wall interactions, and diagnostic development (using: PSI plasma generator, UHV laboratory, EBIT source) to the ASDEX Upgrade and WENDELSTEIN 7-AS fusion experiments at Garching. A theory group is involved in various studies of edge physics problems using analytical and computational modelling concepts as well. In support of the development of the WENDELSTEIN 7-X stellarator project, the Berlin branch is engaged in theoretical investigations of magnetic islands and the design of diagnostics.

The work on the fusion experiments at Garching is a continuation of former activities and is described in the ASDEX Upgrade and W7-AS project reports. As to the experimental activities in Berlin, an important event in 1996 was the start-up of the electron beam ion trap (EBIT). First experiments were performed with highly charged ions, including measurements of dielectronic recombination spectra. The PSI plasma generator continues to be used for studies of plasma-wall interactions (e.g. physical and chemical erosion) as well as for measurements of basic plasma properties (e.g. drift and rotation of plasma particles). Development of the two-photon induced $L_\alpha$ fluorescence diagnostic is complete and is now under consideration for possible adaption to a fusion experiment.

M. Akbi[1], P. Bachmann, H. Behrendt, C. Biedermann, W. Bohmeyer, H. Grote, K. Grützmacher[2], A. Herrmann, S. Hesse, D. Hildebrandt, S. Hirsch, B. Jüttner[3], H. Kastelewicz, S. Klose, P. Kornejew, M. Laux, H. Meyer, M. Michailov[4], B. Napiontek, D. Naujoks, E. Pasch, H. Pursch[3], R. Radtke, H.D. Reiner, V. Rohde, M.I. de la Rosa[2], J. Sachtleben, C. Seiser[2], J. Seidel[2], A. Stareprawo, A. Steiger[2], D. Sünder, U. Wenzel, R. Wolf

1 Guest, University Algier, Algeria

2 Physikalisch-Technische Bundesanstalt, Berlin (PTB)

3 Funded by the "Scientists' Integration Programme" (WIP)

4 Guest, Kurchatov Institute, Moscow, Russia

## 1. PSI PLASMA GENERATOR

Chemical erosion measurements were performed for advanced carbon fibre composites (DUNLOP Concept II and Si-doped SEP NS 31) in order to select possible candidates for target materials in ITER. To prevent the samples from being physically sputtered, the electron temperature was kept below 6 eV. The samples were exposed to hydrogen plasmas of $1.2 \cdot 10^{22}$ $m^{-2}s^{-1}$ ion flux density, and heated to include the effect of finite surface temperature. Different methods (weight loss measurements, mass spectrometry, infrared analysis) were employed to obtain chemical erosion yields. The results (FIG. 1) show significant differences as a function of both the material and the surface temperature. The investigations will be complemented by measurements at higher ion flux densities.

To obtain better information on the reflectivities of mirrors exposed to magnetized plasmas, a variety of different samples were tested in the plasma generator (part of ITER cooperation). The experimental conditions were: deuterium plasma of $1.2 \cdot 10^{21}$ $m^{-2}s^{-1}$ ion flux density, temperature and density of the background plasma: $T_e$ = 2-3 eV, $n_e = 10^{16}$ $m^{-3}$, exposure time: 3.5 h, temperature on the backside of the mirrors: < 60°C. As expected, the reflectivity is reduced due to the interaction with the ions. Most striking is the strong deterioration of the regular reflectivity for Al, Cu, and Au at short wavelengths. Mirrors with layers made of molybdenum and rhodium were found to have the longest lifetime.

Active and passive spectroscopy were used to study many specific physics problems in the plasma generator. Spectroscopic and weight loss measurements were combined to measure the S/XB value for tungsten (WI 400.8 nm) sputtered by $D^+$, $He^+$, and $Ar^+$-ions as a function of the electron temperature. To confirm earlier results from passive spectroscopy, measurements of temperature and density profiles as well as rotation and drift velocities were made in an argon plasma using laser-induced fluorescence (LIF). Apart from $T_i$-measurements, there is reasonably good agreement between the LIF measurements and the results of passive spectroscopy.

As part of the cooperation with PTB, Berlin, first quantitative measurements of the two-photon induced $L_\alpha$ fluorescence ($2\gamma$-$L_\alpha$) were made with an improved detection system. Despite the high $L_\alpha$ background of the PSI plasma, the $2\gamma$-$L_\alpha$ signal could be measured with good signal-to-noise ratio (for a single laser pulse: 30 $L_\alpha$ fluorescence photons and 15 $L_\alpha$ background-

photons within a fluorescence time of 10 ns). To enable quantitative measurements, the detection system was calibrated at BESSY, Berlin. From these experiments valuable information for the application of this diagnostic to a fusion device (ITER) were obtained.

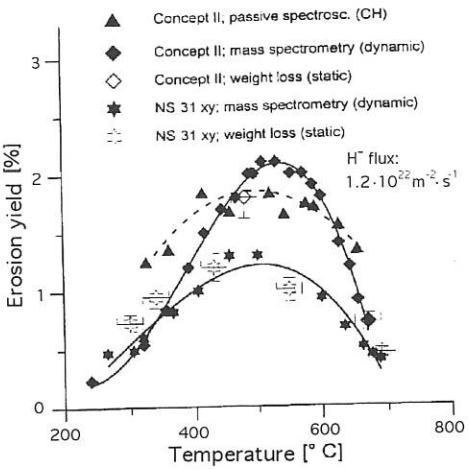


*FIG. 1: Chemical erosion yield as a function of surface temperature.*

## 2. ELECTRON BEAM ION TRAP (EBIT)

In 1996, a new electron beam ion trap (EBIT) was put into operation. EBIT is intended for general atomic physics measurements and applications to fusion relevant hot plasmas. The EBIT technique employs a monoenergetic electron beam, which originates from an electron gun and can be up to 150 mA. The beam is guided into the trap, an assembly of three drift tubes, floating at a potential that can reach 40 kV. A pair of superconducting Helmholtz coils create a 3-tesla magnetic field, which compresses the electron beam to a diameter of about 70 µm as it passes through the trap region. Atoms or low-charged ions are introduced into the trap by injection from an external source. Once the atoms are ionized due to electron collisions, they are radially confined by the space charge of the electron beam and the axial magnetic field. Axial confinement is provided by the two end-drift tubes, which are biased above the centre-drift tube. In addition to ionizing and trapping the ions, the electron beam also serves to excite the ions. A particular ionic stage is produced by appropriate choice of the beam accelerating voltage; exciting and probing of the ions with other electron beam energies is possible by short-time modulation.

First experiments were performed with highly charged Ar, Fe, Kr, Ba, and W ions, including measurements of dielectronic recombination (DR) spectra. The DR process plays an important role in many high-temperature plasmas because it can have dramatic effects on both the ionization balance and the radiation. As an example, FIG. 2 presents spectra for $Kr^{q+}$ ($q \leq 34$) where the electron beam accelerating voltage was repeatedly switched between 12.30 kV (gray spectrum) and 12.51 kV (black spectrum). The spectrum at 12.30 kV corresponds to the case where all lines are exclusively excited by electron impact or are due to radiative recombination (RR) into n = 2, 3, and 4 levels of krypton. For the spectrum at 12.51 kV dielectronic capture of a free electron into a state with n = 5 takes place, resulting in the formation of a doubly excited intermediate state. The decay of the recombined ion is associated with an n = 3-2 transition, corresponding to 13.1 keV X-ray energy (the signature of the DR process) and lower-energy radiative cascades of the spectator electron (n = 5-2 and 4-2 transitions). It is obvious from these results that dielectronic recombination is a significant contributor to line radiation extending over a wide X-ray range. The analysis of dielectronically excited barium ($Ba^{q+}$, $40 \leq q \leq 42$) spectra gave quite similar results with respect to the decay of the doubly excited ions. In addition, an interesting feature which is apparent in these DR spectra is the rearrangement of the charge state distribution with maxima at low and high charge states under conditions where dielectronic recombination dominates the ionization balance.

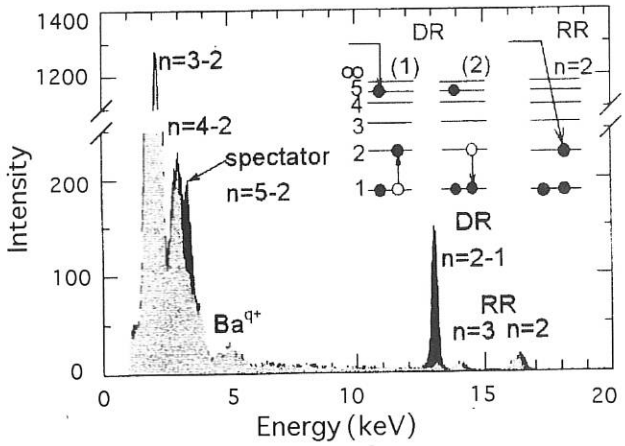


*FIG. 2: X-ray spectra of krypton taken at 80 mA electron beam current and 5.7 % duty cycle. The X-rays at 5 keV originate from a minor barium background in the trap.*

## 3. THE UHV LABORATORY

In the UHV laboratory first analyses were made of $^{13}C$-doped collector probes exposed to the SOL plasma of ASDEX Upgrade. The objective of these investigations is to obtain quantitative results on erosion and deposition. As an example, FIG. 3 shows depth profiles of plasma impurities ($^{11}B$, $^{12}C$, and $^{56}Fe$ isotopes) deposited on graphite samples covered with $^{13}C$ layers (150 nm thick). As to be seen from FIG. 3 the $^{13}C$ layer is only slightly eroded during exposure to the plasma, demonstrating that sputtering was of no importance under the specific conditions.

Time-resolved measurements show that, during start-up of certain discharges, there is enhanced impurity contamination which correlates with high temperatures in the divertor region. During stationary phases, the amount of impurities deposited in the SOL plasma increases with increasing heating power. For example, in discharges with 7.5 MW NBI heating power the amount of carbon collected is more than one order of magnitude larger than in ohmic discharges. Radial impurity profiles were measured for boron and carbon. The decay

lengths show only a weak dependence on the heating power and range from 12 to 18 mm, which is rather close to the decay length of the hydrogen background plasma.

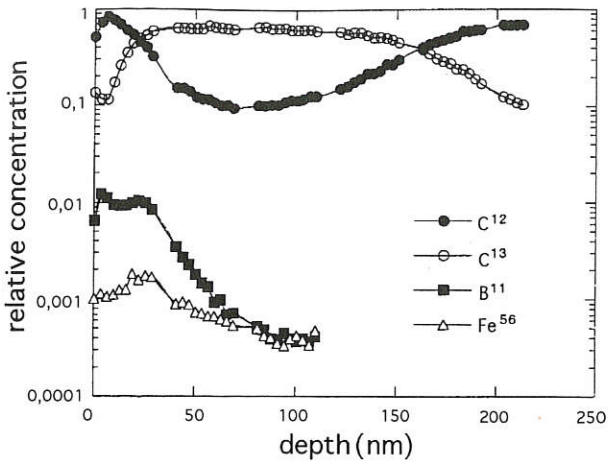


*FIG. 3: Depth profiles of $^{13}C$-doped collector probes.*

## 4. ARCING EFFECTS ON GRAPHITE

The behaviour of electric arcs on graphite cathodes (EK 98) was studied in order to understand specific phenomena observed on inner-wall components of fusion devices. The arcs burned in an atmosphere of deuterium and were exposed to a magnetic field of 0.36 tesla. Two major effects were detected: (i) After extinction of the arcs thermodesorption caused release of deuterium the amount of which is proportional to the current-time integral: about $10^{18}$ molecules per $m^2$ for 1 As arcing. One can project that, for current-time integrals of the order of 100 As, parasitic arcs can considerably contribute to the gas retention of graphite. (ii) Immobile hot spots appeared in the vicinity of arc traces. These spots resemble those which can be observed on the divertor tiles of ASDEX Upgrade. They can be explained by thermoionic emission, reducing the sheath potential which exists between the surface and the arc plasma. Possibly, they are precursors of carbon blooming, occurring in tokamak discharges of high power.

## 5. THEORY AND MODELLING

### 5.1. Monte Carlo Modelling of Impurity Transport

Two Monte Carlo methods were developed, with the complex magnetic field topology being taken into account, to model impurity transport phenomena in the edge plasma of stellarators: (i) A new version of the ERO code where sputtered impurity atoms are followed through successive states of ionization and recombination during their 3D motion in the plasma. (ii) A self-consistent set of 2D hydrodynamic equations describing the edge plasma after injection of impurities into magnetic islands; the magnetic structure is modelled using the Chirikov-Taylor map technique. Titanium was studied in detail, with different cross-diffusion coefficients and conditions of impurity injection being taken into consideration. It is found that injected titanium atoms will be confined in a magnetic island for a longer period of time only if the cross-diffusion coefficient is sufficiently low ($D_{perp} \leq 0.2\ m^2/s$). In this case, noticeable plasma cooling and lowering of the target heat load is possible.

### 5.2. Cross-Field Diffusion by Charge Changing Processes

A new topic is a particular type of transport which is caused by the sequence of ionization and recombination that the particles in a plasma are always subjected to. In this context, most important is the transport of protons due to recombination. Here the occasionally produced atoms can move several centimetres across the magnetic field before they are ionized again or change direction as a result of a charge-exchange collision. The diffusion coefficient associated with this random walk is independent of the magnetic field and has the form $D = f(T_e)T_i/(m_i n_e)$. Its temperature dependence can be expressed in terms of the rate coefficients for ionization, recombination, and charge exchange. For $10\ eV \leq T_e \leq 10^4\ eV$ and $n_e = 10^{19}\ m^{-3}$, for example, D decreases with increasing temperature from about 0.1 to $10^{-3}\ m^2/s$, but is still more than two orders of magnitude larger than the classical diffusion coefficient (for B = 3 tesla) in this temperature range. Of practical importance is the recombinatively induced diffusion in the cooler edge regions and low-temperature divertors ($T_e \leq 5\ eV$).

### 5.3. Bifurcation and Relaxation Oscillations

Low-frequency relaxation oscillations as observed in the divertor of ASDEX Upgrade can be described within the frame of a 0-dimensional model that takes sputtering and radiation of impurities into account. Solution of the related autonomous and parametrically driven model equations yield bifurcations and relaxation oscillations (period of oscillation: 10 - 20 ms). Basically, the bifurcations are due to the non-monotonic behaviour of the radiation characteristics. The model equations represent the special case of a general system of transport equations the stability of which is being analyzed.

### 5.4. Plasma Modelling Calculations for the PSI Generator

The coupled B2-EIRENE code package was adapted to the axisymmetric geometry of the PSI plasma generator (in cooperation with KFA, Jülich). The modelling extends from the exit of the hollow anode to the target plate. The cathode-anode region where the PSI plasma is generated has not yet been considered; because of this the plasma state in the target chamber is governed by the boundary conditions at the anode exit. First modelling calculations for deuterium show that the plasma profile is strongly affected by collisions of charged particles with neutrals. As the mean free path length of the neutrals is much larger than the dimensions of the target chamber, practically the whole plasma is involved in the recycling process. Calculated temperature and density profiles for electrons, ions, and neutrals are in reasonable agreement with the measurements.

# COMPUTER SCIENCE DIVISION

(Prof. Dr. Friedrich Hertweck)

F. Hertweck, Ch. Brosig (until June 1996), G. Czapski (PhD student), R. Dohmen, H. Friedrich, A. Graf (on leave), K. Hallatschek (PhD student), P. Heimann, J. Maier, M.-G. Pacco-Düchs, I. Precht, H. Richter, Ute Schneider-Maxon, D. Stolz, Ch. Tichmann, R. Tisma, M. Zilker

## 1. AMOS/D

Part of the work on AMOS/D is described in the section on ASDEX Upgrade data processing. This includes the commissioning of the last 20 Sbus CAMAC interfaces, the experience gained with the prototype MULTITOP-MX computer, and the status of the Dependence Data Base. Additonal activities are described below.

### 1.1 Mirnov diagnostic

The requirement to extend the Mirnov Diagnostic by eight more channels could be met with the virtually last hardware in stock (one CPU1-board, two FIFO-boards, and a backplane). It is not reasonable to reproduce the existing hardware (the Transputers T800 are not competitive any more), therefore the development of a new generation of high-volume data acquisition systems is becoming urgent.

### 1.2 Design of a new generation of high-speed/ high-volume data acquisiton systems

The very long plasma discharges expected on W7-X and also the growing needs of ASDEX Upgrade call for a new generation of data acquisition systems capable of handling high-volume data streams in real-time (typically a few hundred signals in diagnostics like Mirnov or SoftXray, sampled at rates of a few MHz). This also requires high CPU power to do the analysis. Normally the I/O bandwidth of a processor is limited and it will therefore be necessary to develop parallel systems that are able to cope with the high influx of data. A fast interconnection network is also required because the state of the plasma at any time as reflected by the diagnostic is spread over the parallel processors of the system.

The hardware will be built from available components, such as CPUs (DEC, IBM powerPC, ultraSPARC, etc.) and interconnection components, such as the SCI (Scalable Coherent Interface). Still, substantial software development in the areas of device drivers, data analysis algorithms, and user interfaces is envisaged.

An experimental system is being built with two Motorola powerPC boards.

### 1.3 CD ROM archive for ASDEX Upgrade shot files

In cooperation with the Computing Center a juke box for 500 CDs was installed to keep the ASDEX Upgrade raw data (level-0 shot files). These CD ROMs will be kept outside the Computing Center in a fireproof room. A software package was developed which copies the shot files from the current archive tape onto the CD ROMs. This data migration task is running automatically in the background and will require about another six months to be completed. The juke box is integrated into the system in such a way that data can be accessed from any UNIX workstation or any modern PC.

### 1.4 AMOS/2

The AMOS/2 System is the component of the AMOS/D Data Acquisition System for ASDEX Upgrade that organizes work on the IBM 3090 mainframe. Already two years ago the

mainframe was slated to be taken out of operation as soon as the AFS File System was able to take over the archiving and file migration features of AMOS/2. This could be achieved by mid-1996, when the IBM 3090 was finally shut down.

Along with the shutdown of the AMOS/2 System all remaining components had to be ported to the UNIX server; these include the shot file monitor, the library of data access routines, and the Dependency Data Base DDB. The transition took place in several steps over a period of about one year.

## 2. Parallel computing on the T3D and T3E

All of the work on parallel programs was done in close co-operation with the owners/users of the programs. Some time was spent on comparing performance of the T3D and the T3E, and the investigation of the Portland Group HPF (High Performance Fortran) compiler and the FORGEX parallelizing tool by APR. In December a very successful workshop with the T3E users was organized to exchange experience with the T3D and T3E.

### 2.1 The MHD code HINT

The HINT code (Hayashi and Schwenn) is used for the investigation of stellarator equilibria and was originally written with vector machines as target computers. The code consists of two parts: the solution of the partial differential equations for the magnetic field and the adjustment of the plasma pressure by integrating along the field lines. The latter part was quite difficult to parallelize due to load balancing problems. The solution was to replicate the magnetic field dynamically on all processors and take the starting points of the field lines from a central pool.

### 2.2 Parallelization of Monte Carlo Codes

A first version of the TRIDYN code (Eckstein) was successfully run with results identical to those of the Cray YMP, but the performance was not yet satisfactory and load balancing problems occurred. A new version in Fortran 90 is being prepared.

The PQMC code (Valasek) was parallelized and ported to the T3E.

The TRVMC code (Eckstein) for simulating target sputtering, already parallelized for the T3D, was ported to the T3E.

### 2.3 Parallel algorithms

Parallel algorithms for the FFT in two and three dimensions were developed that are not restricted to linear processor arrays but can handle cuboid topologies; sometimes this is more convenient for the user. On the T3D the performance was better than the available library routines.

Also an algorithm was developed for the solution of a set of tridiagonal systems of linear equations, typically arising in the solution of partial differential equations.

## 3. Neural network computing

The SIEMENS Synapse-1 neurocomputer was used to study the feasibility of using Kohonen feature maps for the classification of Mirnov signals. Work is in progress.

The program to analyze ASDEX Upgrade video films has been enhanced with an interactive user interface and is being implemented on a CNAPS PC board.

## 4. Data processing infrastructure

### 4.1 Fortran 90

Over the past few years the Fortran 90 standard has gained widespread recognition. There are ever more compilers available, including virtually all platforms from supercomputers down do PCs. Tools were developed to smoothly convert Fortran 77 programs to Fortran 90. Though some commercial products are available, more sophisticated programs are needed to convert static f77 programs into f90 programs with dynamic memory allocation and to parallelize existing sequential programs for a parallel computer. An f90 syntax analyzer was developed (based on the f90 syntax in BNF notation) that will produce cross-reference tables showing the kind of usage of all f90 entities in a program.

### 4.2 LIBRIS

LIBRIS is an integrated Library System, used for managing the IPP scientific library and permitting users to enquire about books, reports and journals in the library. It was originally developed by the Computing Center RZG under VM/370 on the IBM mainframe. The bibliographic data were stored in the hierarchical data base system SPIRES, a program designed by Stanford University.

When the central IBM 3090 was scheduled for decommissioning, the LIBRIS system was redesigned for the distributed UNIX environment. The work was undertaken in collaboration with the RZG.

The bibliographic data were ported to the ORACLE data base system, which was already available at the RZG. The interface for accessing the LIBRIS system by the library administration is similar to the old terminal interface, but it is now running in an Xwindow on a PC. The normal library user will access LIBRIS through the WWW. The system has been in operation since May 1996.

# CENTRAL TECHNICAL SERVICES

(Dr.-Ing. Harald Rapp)

The Central Technical Services (ZTE) of Max-Planck-Institut für Plasmaphysik support the experimental divisions with the design, construction and operation of experiments and diagnostics. They also provide and run all kinds of utilities for facility operation and employ approximately 160 workers, technicians and engineers. Task-sharing between the research groups, industry and the Central Technical Services is standard practice for minimizing costs and manpower and for providing technical support according to experimental needs.

## 1. MECHANICAL DESIGN AND CALCULATION
(J. Simon-Weidner)

24 technicians and engineers work in the fields of CAD design and FE calculations for all kind of experimental equipment and diagnostics. The department runs the computer network with software for CAD and FE engineering calculations which consists of 45 workstations, 4 servers and 5 plotters distributed in ZTE and experimental divisions. Major effort was again given to the W7-X design and FE calculations with respect to improvements for the divertor. The diagnostic and NBI requirements have been examined for the improved coil set HS5V10U. First evaluations of the HSR stellarator fusion power plant have been carried out. External fabrication of the W7-X demo cryostat was supervised. The design of ICRH antennae and diagnostic equipment was contineously performed.

## 2. ELECTRONICS DEVELOPMENT
(D. Arz)

The department consists of groups for developing measurement and control techniques and for high-voltage switching and control for NBI and ECRH. Another small group services measurement equipment and personal computers. Programmable logic controls and network development for interaction with PC´s became a major effort. Construction, commissioning and maintenance of 24 high-voltage switchboxes were continued providing a high operational reliability of the NBI and ECRH systems.

## 3. MATERIALS TECHNOLOGY
(S. Deschka)

The department offers technical services for materials development, vacuum testing, plasma welding and surface processing. The latter comprise chemical, galvanic and vapour deposition surface preparation and galvano-plastics. In 1996 the following tasks have been accomplished: browning of the chevrons for the ASDEX cryo pump, process development for tungsten coating, E-beam tests of divertor target plates and failure analysis, characterization of insulating ceramic layers on graphite, transient thermographic investigation for non-destructive test of target elements, stress calculation and shape optimization of coated plasma facing componentes.

## 4. ELECTRIC POWER SUPPLY
(W.R. McGlaun)

The department is responsible for the electric power supply of IPP and the experiments. The staff operates 4 flywheel generators with a total power of 580 MVA, 20 controlled high current rectifiers (462 MVA in total) and 28 high voltage DC modules up to 140 kV supplying the different experimental loads. The partial renewal of the oldest and biggest fly-wheel generator has been started. The work will be ready until april 1997 when ASDEX-Upgrade will start its experimental work with the new divertor. Improvement of the rectifier system has been accomplished as well as power circuit and control adaptions for supplying the additonal heating systems on both experiments.

## 5. FACILITY OPERATION
(H. Rapp)

The department is charged with planning and supervising of all kind of facility installations including cooling of experimental devices. The cooling water wells have been equipped with a modern control for motors and monitoring and a new heat exchanger system for the CRAY T3E has been commissioned. Also a lot of repair work on building installations was carried out. A He gas recovery system was installed together with cryogenic equipment for the W7-X demo cryostat and the ASDEX cryopump.

## 6. WORKSHOPS
(M. Keiner)

More than half of the ZTE personnel work in workshops providing basic capacity for manufactoring experimental and diagnostic devices. Additional capacity is purchased from industry. In the report period the new divertor for ASDEX-Upgrade was a major effort in mechanics. The electric workshops built a variety of control and power supply systems for ECRH and NBI and installed them at the experiments.

# ADMINISTRATION

(Dr. Thomas Köstlin)

The administration and general services of Max-Planck-Institut für Plasmaphysik are organized in six departments:

## PERSONNEL DEPARTMENT

The personnel department is responsible for administrative matters relating to personnel. The personnel figures of the institute for 1996 were as follows:

| | |
|---|---|
| Total personnel (including Greifswald and Berlin) | 1025 |
| Scientists | 308 |
| Technicians | 430 |
| Directorate and Staff Representative Council | 32 |
| General Services | 53 |
| Administration | 74 |
| Other personnel | 128 |
| | 30.01.97 |

## PURCHASING AND CONTRACTS DEPARTMENT

The purchasing and contracts department is responsible for placing survey and follow-up of all contracts and orders placed by IPP. In 1996, approximately 8.900 orders were made. They include complex contracts, many of which were signed after European-wide calls for tender. Furthermore, all export and import formalities are handled within this department: about 135 international and European shipments were carried out in 1996.

## LEGAL AND PATENT DEPARTMENT

This department attends to patent applications and supervision, contracts of cooperation, and licensing of patents in cooperation with Garching Innovation GmbH, a subsidiary of the Max Planck Society. In 1996 the division supervised 113 patents and similar rights.

The legal and patent department is further responsible for looking after for committees. Also it workes out and controls cooperation contracts with German and European Universities and research institutes.

## FINANCIAL AND ACCOUNTING DEPARTMENT

The financial and accounting department is responsible for the financial planning and all financial transactions and fiscal matters of IPP.

| | |
|---|---|
| Total expenses in 1996: | 180,3 MDM |
| This expenses was financed as follows: | |
| Federal Republic of Germany through Federal Ministry of Education, Science, Research and Technology (BMBF) | 97,5 MDM |
| Bavaria | 9.1 MDM |
| Berlin | 0.9 MDM |
| Mecklenburg-Vorpommern | 6.6 MDM |
| EURATOM | 41,9 MDM |
| Other income | 24,3 MDM |

## SITE AND BUILDINGS DEPARTMENT

The site and buildings department is in charge of planning, construction, structural alteration and reconditioning of buildings and main service facilities. Building maintenance is also provided for the neighbouring Max Planck Institutes of Astrophysics and Extraterrestrial Physics, the European Southern Observatory and the Berlin Division of IPP.

## SOCIAL DEPARTMENT

The social department gives assistance to employees seeking housing, provides accommodation for guests in IPP residences, and runs the transport pool, bus and cleaning services.

# Publications

# Publications and Conference Reports


1. *Agarici*, G., J.P. Allibert*, J.M. Ané*, H. Renner* et al.: Towards Long-Pulse, High-Performance Discharges in Tore Supra: Experimental Knowledge and Technological Developments for Heat Exhaust. Fusion Technol. **29**, 417-448 (1996).

2. *Albanese*, R., E. Coccorese*, O. Gruber* et al.: Identification of Plasma Equilibria in ITER from Magnetic Measurements via Functional Parametrization and Neural Networks. Fusion Technol. **30**, 219-235 (1996).

3. *Alexander, M., O. Gruber, H.-U. Fahrbach, O. Gehre, S. de Peña Hempel, K. Lackner, H. Murmann, G. Pereverzev, H. Salzmann, J. Schweinzer, W. Suttrop, ASDEX Upgrade Team* and *NI-Team:* Transport Investigations Using Dimensionally Similar Discharges in ASDEX Upgrade. In: Proc. 23rd Conf. Control. Fusion and Plasma Phys., Kiev 1996, Eds. D.Gresillon, A.Sitenko, A.Zagorodny. ECA 20C. Europ. Phys. Soc., Geneva 1996, 103-106.

4. *Anders*, A., S. Anders*, B. Jüttner* et al.: High-Resolution Imaging of Vacuum Arc Cathode Spots. IEEE Trans. Plasma Sci. **24**, 69-70 (1996).

5. *Annen, A., A. von Keudell* and *W. Jacob:* Erosion of Amorphous Hydrogenated Boron-Carbon Thin Films. J. Nucl. Mater. **231**, 151-154 (1996).

6. *Arndt, S., H. Haberland** and *W.D. Kraeft*:* Two-Particle States in Dense Plasmas - Bound-State Energy and Lifetime. Physica B **228**, 63-71 (1996).

7. *Arndt, S., W.D. Kraeft** and *J. Seidel*:* Two-Particle Energy Spectrum in Dense Electron-Hole Plasmas. Phys. Status Solidi B **194**, 601-617 (1996).

8. *Asp*, S., R. Schuch*, D.R. DeWitt*, C. Biedermann* et al.: Laser-Induced Recombination of $D^+$. Nucl. Instrum. Methods Phys. Res., B **117**, 31-37 (1996).

9. *Aumayr*, F., M. Gieler*, H.P. Winter** and *J. Schweinzer:* Electron Capture by Doubly Charged Ions from Laser Excited Alkali Atoms III. $Ne^{2+}$, $Ar^{2+}$ - Na*(3p) Collisions. J. Phys., B **29**, 1515-1523 (1996).

10. *Bachmann, P., A. Runow*, D. Sünder* and *H. Wobig:* Plasma Cooling due to Impurity Injection into Magnetic Islands. Contrib. Plasma Phys. **36**, 255-259 (1996).

11. *Bachmann, P., D. Sünder* and *U. Wenzel:* Bifurcation and Relaxation Oscillations in Divertor Plasmas. Contrib. Plasma Phys. **36**, 519-539 (1996).

12. *Becker, G.:* Empirical Scaling Law for the Effective Heat Diffusivity in Elmy H Mode Plasmas. Nucl. Fusion **36**, 527-530 (1996).

13. *Becker, G.:* Linear $Z_{eff}$ Scaling of the Anomalous Inward Drift and Enhanced Proportionally Factor during Neon Inflow. Nucl. Fusion **36**, 1751-1758 (1996).

14. *Behrisch, R.:* Materials for Highly Loaded Wall Areas in Fusion Devices (Limiters, Divertor Plates). In: Proc. 6th Workshop Wendelstein 7-X and Helias Reactors, Schloß Ringberg, Tegernsee 1995, Eds. F.Herrnegger, F.Rau. IPP 2/331, IPP, Garching 1996, 130-131.

15. *Behrisch, R., M. Mayer* and *C. García-Rosales:* Composition of the Plasma Facing Material Tokamakium. J. Nucl. Mater. **233-237**, 673-680 (1996).

16. *Behrisch, R., V.M. Prozesky*, H. Huber** et al.: Hydrogen Desorption Induced by Heavy-Ions during Surface Layer Analysis with ERDA. Nucl. Instrum. Methods Phys. Res., B **118**, 262-267 (1996).

17. *Beidler, C.D.:* Neoclassical Transport Properties of HSR. In: Proc. 6th Workshop Wendelstein 7-X and Helias Reactors, Schloß Ringberg, Tegernsee 1995, Eds. F.Herrnegger, F.Rau. IPP 2/331, IPP, Garching 1996, 194-201.

18. *Beidler, C.D., H. Maaßberg* and *A.A. Shishkin*:* Neoclassical Transport in High-Mirror Advanced Stellarators. In: Proc. 23rd Conf. Control. Fusion and Plasma Phys., Kiev 1996, Eds. D.Gresillon, A.Sitenko, A.Zagorodny. ECA 20C. Europ. Phys. Soc., Geneva 1996, 479-482.

19. *Bertel, E.:* The Interaction of Rare Gases with Transition Metal Surfaces. Surf. Sci. Lett. **367**, L61-L65 (1996).

20. *Bertel, E.* and *N. Memmel:* Promoters, Poisons and Surfactants: Electronic Effects of Surface Doping on Metals. Appl. Phys., A **63**, 523-531 (1996).

21. *Bertel, E., P. Sandl, K.D. Rendulic** et al.: Tailoring Surface Electronic Properties to Promote Chemical Reactivity. Ber. Bunsenges. Phys. Chem. **100**, 114-118 (1996).

22. *Bessenrodt-Weberpals, M., H.J. de Blank, M. Maraschek, M. Sokoll, K. Asmussen, ASDEX Upgrade Team* et al.: MHD Activity as Seen in Soft X-Ray Radiation. Plasma Phys. Control. Fusion **38**, 1543-1559 (1996).

23. *Biener, J., C. Lutterloh, A. Schenk*, J. Küppers* et al.: Reaction of Gaseous H(D) Atoms with Physisorbed i-Propanol: Oxidation to Acetone. Surf. Sci. **365**, 255-262 (1996).

24. *Biskamp, D.:* Resistive and Collisionless Reconnection. In: Plasma Astrophysics, Eds. C.Chiuderi, G.Einaudi. Springer, Berlin 1996, 1-30.

25. *Biskamp, D.* and *J.F. Drake*:* Dynamics of the Sawtooth Collapse in Tokamak Plasmas. In: Proc. 15th Conf. Plasma Phys. Control. Nucl. Fusion Res., 3, Seville 1994, IAEA, Vienna 1996, 261-272.

26. *Biskamp, D., E. Schwarz* and *J.F. Drake*:* Two-Dimensional Electron Magnetohydrodynamic Turbulence. Phys. Rev. Lett. **76**, 1264-1267 (1996).

27. *Bleuel, J., G. Theimer, M. Endler, L. Giannone, H. Niedermeyer, ASDEX Upgrade Team* and *W7-AS-Team:* The Edge Turbulence in the W7-AS Stellarator: 2D Characterization by Probe Measurements. In: Proc. 23rd Conf. Control. Fusion and Plasma Phys., Kiev 1996, Eds. D.Gresillon, A.Sitenko, A.Zagorodny. ECA 20C. Europ. Phys. Soc., Geneva 1996, 727-730.

28. *Bohmeyer, W., G. Fußmann, P. Kornejew, H.-D. Rainer* and *H. Grote:* Test of Mirrors for Optical Diagnostics in ITER. In: Proc. 23rd Conf. Control. Fusion and Plasma Phys., Kiev 1996, Eds. D.Gresillon, A.Sitenko, A.Zagorodny. ECA 20C. Europ. Phys. Soc., Geneva 1996, 1128-1131.

29. *Borrass, K., R. Farengo** and *G. Vlases*:* Access Conditions for H-Modes with Detached Divertor Plasmas. Nucl. Fusion **36**, 1389-1394 (1996).

30. *Bosch, H.-S., R. Dux, G. Haas, A. Kallenbach, M. Kaufmann, K. Lackner, V. Mertens, H. Murmann, H. Salzmann, J. Schweinzer,*

*W. Suttrop, M. Weinlich, ASDEX Upgrade Team* and *NI-Team:* Invariance of Divertor Retention on External Particle Flow in Detached ASDEX Upgrade Discharges. Phys. Rev. Lett. **76**, 2499-2502 (1996).

31. *Bosch, H.-S., V. Erckmann, F. Rau, F. Wagner* et al.*:* Summary of the Workshop on Technological Aspects of Steady-State Devices. Plasma Phys. Control. Fusion **38**, 415-449 (1996).

32. *Bosch, H.-S., O. Gruber, G. Haas, A. Kallenbach, M. Kaufmann, K. Lackner, V. Mertens, R. Neu, J. Neuhauser, F. Ryter, J. Schweinzer, H. Zohm, ASDEX Upgrade Team* and *NI-Team:* Compatibility of H-Mode with a Radiating Boundary and Divertor Detachment. Plasma Phys. Control. Fusion **38**, 1493-1496 (1996).

33. *Bowman, J.C.:* On Inertial Scaling Laws. J. Fluid Mech. **306**, 167-181 (1996).

34. *Bowman, J.C.:* A Wavenumber Partitioning Scheme for Two-Dimensional Statistical Closures. J. Sci. Computing **11**, 343-372 (1996).

35. *Bowman, J.C., B.A. Shadwick** and *P.J. Morrison*:* Spectral Reduction for Two-Dimensional Turbulence. In: Proc. Transport, Chaos and Plasma Physics 2, Marseille 1995, Eds. S.Benkadda, F.Doveil, Y.Elskens. World Scientific Publ., Singapore 1996, 58-73.

36. *Bünde, R.:* Reliability and Availability of Fusion Machines. In: Proc. 6th Workshop Wendelstein 7-X and Helias Reactors, Schloß Ringberg, Tegernsee 1995, Eds. F.Herrnegger, F.Rau. IPP 2/331, IPP, Garching 1996, 296-304.

37. *Brakel, R., H. Hacker, D. Hildebrandt, R. Burhenn, A. Elsner, S. Fiedler, L. Giannone, C. Görner, P. Grigull, H.-J. Hartfuß, A. Herrmann, G. Kühner, U. Stroth, A. Weller, R. Wolf, W7-AS-Team, ECRH-Group* and *NI-Group:* Radiative Boundary Studies in the Wendelstein 7-AS Stellarator. In: Proc. 23rd Conf. Control. Fusion and Plasma Phys., Kiev 1996, Eds. D.Gresillon, A.Sitenko, A.Zagorodny. ECA 20C. Europ. Phys. Soc., Geneva 1996, 495-498.

38. *Brañas*, B., M. Hirsch, J. Baldzuhn, T. Geist, H.-J. Hartfuß* et al.*:* Frequency Shift of Reflectometry Signals due to Rotation of Density Turbulence in W7-AS. In: Proc. 23rd Conf. Control. Fusion and Plasma Phys., Kiev 1996, Eds. D.Gresillon, A.Sitenko, A.Zagorodny. ECA 20C. Europ. Phys. Soc., Geneva 1996, 1003-1006.

39. *Camargo* S.J., B.D. Scott* and *D. Biskamp:* The Influence of Magnetic Fluctuations on Collisional Drift-Wave Turbulence. Phys. Plasmas **3**, 3912-3931 (1996).

40. *Campbell*, D.J., A. Bickley*, A. Chankin*, K. McCormick* et al.*:* Studies of Reactor-Relevant H-Mode Regimes in the JET-Pumped Divertor. Plasma Phys. Control. Fusion **38**, 1497-1501 (1996).

41. *Cappello*, S.* and *D. Biskamp:* Reconnection Processes and Scaling Laws in Reversed Field Pinch Magnetohydrodynamics. Nucl. Fusion **36**, 571-581 (1996).

42. *Carlson, A.:* Summary of the First Workshop on Electrical Probes in Magnetized Plasmas. Contrib. Plasma Phys. **36**, 13-18 (1996).

43. *Cattanei, G., D. Hartmann, D.A. Rasmussen*, ICRH-Team, W7-AS-Team* et al.*:* Ion Cyclotron Resonance Heating Experiments on the Stellarator W7-AS. In: Proc. 23rd Conf. Control. Fusion and Plasma Phys., Kiev 1996, Eds. D.Gresillon, A.Sitenko, A.Zagorodny. ECA 20C. Europ. Phys. Soc., Geneva 1996, 499-502.

44. *Chodura, R.:* Probe Diagnostics of Electron Temperature with Steep Gradient. Contrib. Plasma Phys. **36**, 61-66 (1996).

45. *De Blank, H.J., J. Stober, W. Suttrop, ASDEX Upgrade Team* and *NI-Team:* Radial Current Balance in ASDEX Upgrade Discharges in the L- and H-Mode Phases. In: Proc. 23rd Conf. Control. Fusion and Plasma Phys., Kiev 1996, Eds. D.Gresillon, A.Sitenko, A.Zagorodny. ECA 20C. Europ. Phys. Soc., Geneva 1996, 99-102.

46. *Deschka, S., C. García-Rosales, W. Hohenauer** et al.*:* Manufacturing and High Heat Flux Loading of Tungsten Coatings on Fine Grain Graphite for the ASDEX-Upgrade Divertor. J. Nucl. Mater. **233-237**, 645-649 (1996).

47. *Detzel*, T., M. Vonbank*, M. Donath, N. Memmel* and *V. Dose:* Temperature-Dependent Magnetization of fcc Fe/Cu(001) Studied by Spin-Polarized Appearance Potential Spectroscopy. J. Magn. Magn. Mater. **152**, 287-292 (1996).

48. *DeWitt*, D.R., R. Schuch*, H. Gao*, C. Biedermann* et al.*:* Dielectronic Recombination of Boronlike Argon. Phys. Rev., A **53**, 2327-2336 (1996).

49. *Döhrn*, A., P. Nowack*, A. Könies, S. Günter* et al.*:* Stark Broadening and Shift of the First Two Paschen Lines of Hydrogen. Phys. Rev., E **53**, 6389-6395 (1996).

50. *Donath, M., B. Gubanka* and *F. Passek:* Temperature-Dependent Spin Polarization of Magnetic Surface State at Gd(0001). Phys. Rev. Lett. **77**, 5138-5141 (1996).

51. *Dose, V., W. von der Linden* and *A. Garrett*:* A Bayesian Approach to the Global Confinement Time Scaling in W7-AS. Nucl. Fusion **36**, 735-744 (1996).

52. *Dose, V., W. von der Linden* and *A. Garrett*:* Bayesian Parameter Estimation of Nuclear Fusion Confinement Time Scaling Laws. In: Maximum Entropy and Bayesian Methods, Eds. K.M.Hanson, R.N.Silver. Kluwer, Dordrecht 1996, 245-250.

53. *Drake*, J.F., P.N. Guzdar*, S. Novakorskii*, A. Zeiler* and *D. Biskamp:* The L-H Trigger: A Transition from Resistive Ballooning to Toroidal Drift Wave Transport. In: Proc. 15th Conf. Plasma Phys. Control. Nucl. Fusion Res., 3, Seville 1994, IAEA, Vienna, 1996, 561-565.

54. *Drake*, J.F., Y.T. Lau*, P.N. Guzdar*, A. Zeiler* et al.*:* Local Negative Shear and the Formation of Transport Barriers. Phys. Rev. Lett. **77**, 494-497 (1996).

55. *Dryagin*, Y., N. Scalyga** and *T. Geist:* A Notch Filter for 140 GHz Microwave Radiation. Int. J. Infrared Millimeter Waves **17**, 1199-1204 (1996).

56. *Düchs, D.F.* and *H. Weitzner** (Eds.)*:* Proc. 5th Int. Workshop on Plasma Edge Theory in Fusion Devices. Contrib. Plasma Phys. **36**, 93-432 (1996).

57. *Dux, R., A. Kallenbach, K. Behringer, R. Neu, S. de Peña Hempel, M. Sokoll, ASDEX Upgrade Team, NI-Team* and *ICRH-Team:* Measurement and Modelling of Impurity Transport in Radiating Boundary Discharges in ASDEX Upgrade. In: Proc. 23rd Conf. Control. Fusion and Plasma Phys., Kiev 1996, Eds. D.Gresillon, A.Sitenko, A.Zagorodny. ECA 20C. Europ. Phys. Soc., Geneva 1996, 95-98.

58. *Dux, R., A. Kallenbach, M. Bessenrodt-Weberpals, K. Behringer, H.-S. Bosch, J.C. Fuchs, O. Gehre, K.-F. Mast, W. Poschenrieder, H. Murmann, H. Salzmann, J. Schweinzer, W. Suttrop, ASDEX Upgrade Team* and *NI-Team:* Measurement and Modelling of Neon Radiation Profiles in Radiating Boundary Discharges in ASDEX Upgrade Plasma Phys. Control. Fusion **38**, 989-999 (1996).

59. *Eckstein, W., M. Hou** and *V.I. Shulga**: Ion-Induced Alkali-Silicon Interfaces: Atomistic Simulations of Collisional Effects. Nucl. Instrum. Methods Phys. Res., B **119**, 477-486 (1996).

60. *Eckstein, W., E.S. Mashkova**, *V.A. Molchanov** et al.: The Effect of the Fibre Target Structure on the Spatial Distributions of Sputtered Atoms. Nucl. Instrum. Methods Phys. Res., B **115**, 482-484 (1996).

61. *Eckstein, W.* and *V. Philipps**: Physical Sputtering and Radiation-Enhanced Sublimation. In: Physical Processes of the Interaction of Fusion Plasmas with Solids, Eds. W.O.Hofer, J.Roth. Academic Press, San Diego,CA 1996, 93-133.

62. *Endler, M.:* Summary of the Results of the Working Group on 'Statistical Analysis of Turbulence Fluctuation Data'. In: Transport, Chaos and Plasma Physics 2, Eds. S.Benkadda, F.Doveil, Y.Elskens. World Scientific Publ., Singapore 1996, 136-139.

63. *Erckmann, V.:* Electron Cyclotron Current Drive Experiments. In: Heating and Current Drive in Fusion Plasmas, Proc. 7th Workshop on Magnetic Confinement Fusion, Santander 1995. EUR-CIEMAT 32. CIEMAT, Madrid 1996, 323-353.

64. *Erckmann, V.:* Electron Cyclotron Resonance Heating: Experiments. In: Heating and Current Drive in Fusion Plasmas, Proc. 7th Workshop on Magnetic Confinement Fusion, Santander 1995. EUR-CIEMAT 32. CIEMAT, Madrid 1996, 247-289.

65. *Ertl, K., W. von der Linden, V. Dose* and *A. Weller:* Maximum Entropy Based Reconstruction of Soft X Ray Emissivity Profiles in W7-AS. Nucl. Fusion **36,** 1477-1488 (1996).

66. *Feist, J.-H., W. Kraus, E. Speth, M. Ciric, B. Heinemann, F. Probst* and *R. Riedl:* Progress in the Development of a Large-Area EF Plasma Generator. In: Proc. 16th IEEE/NPSS Symp. on Fusion Engineering, Champaign,IL 1995, Eds. H.Miley, C.Elliott. IEEE Service Center, Piscataway,NJ 1996, 976-979.

67. *Feneberg, W.:* Bootstrap Current Derived from Different Model Collision Operators. In: Proc. 23rd Conf. Control. Fusion and Plasma Phys., Kiev 1996, Eds. D.Gresillon, A.Sitenko, A.Zagorodny. ECA 20C. Europ. Phys. Soc., Geneva 1996, 91-94.

68. *Fiedler, S., O. Heinrich, J. Das, K. McCormick* and *W7-AS-Team:* Investigation of the Neutral Gas Distribution on W7-AS Using the Monte-Carlo-Code EIRENE in Combination with the Li-Beam Diagnostic. In: Proc. 23rd Conf. Control. Fusion and Plasma Phys., Kiev 1996, Eds. D.Gresillon, A.Sitenko, A.Zagorodny. ECA 20C. Europ. Phys. Soc., Geneva 1996, 1007-1010.

69. *Field, A.R., C. García-Rosales, G. Lieder, R. Radtke, ASDEX Upgrade Team* et al.: Spectroscopic Measurement of Target Plate Erosion in the ASDEX Upgrade Divertor. Nucl. Fusion **36**, 119-132 (1996).

70. *Fischer, R., T. Fauster, W. von der Linden* and *V. Dose:* Island-Size Distributions of Ag on Pd(111). Surf. Rev. Lett. **3**, 1393-1402 (1996).

71. *Fischer, R., W. von der Linden* and *V. Dose:* On the Importance of $\alpha$ Marginalization in Maximum Entropy. In: Maximum Entropy and Bayesian Methods, Eds. K.M.Hanson, R.N.Silver. Kluwer, Dordrecht 1996, 229-236.

72. *Franzen, P.:* Radiation Enhanced Sublimation of Graphite due to Fast Neutron Irradiation. J. Nucl. Mater. **228**, 1-7 (1996).

73. *Franzen, P., V. Mertens, G. Neu, T. Zehetbauer, G. Raupp, M. Kaufmann, ASDEX Upgrade Team* and *NI-Team:* Online Confinement Regime Identification for the Discharge Control System at ASDEX Upgrade. In: Proc. 23rd Conf. Control. Fusion and Plasma Phys., Kiev 1996, Eds. D.Gresillon, A.Sitenko, A.Zagorodny. ECA 20C. Europ. Phys. Soc., Geneva 1996, 87-90.

74. *Fußmann, G., H. Meyer* and *E. Pasch:* Abel Inversion of Rotating Plasmas. Contrib. Plasma Phys. **36**, 501-517 (1996).

75. *Gafert, J., M. Niethammer, K. Behringer, D.P. Coster, C. Dorn, K. Hirsch, S. de Peña Hempel, ASDEX Upgrade Team, NI-Team* et al.: Investigation of Ion Dynamics in the ASDEX Upgrade Divertor by High Resolution Spectroscopy: First Results on Ion Drift Velocities. In: Proc. 23rd Conf. Control. Fusion and Plasma Phys., Kiev 1996, Eds. D.Gresillon, A.Sitenko, A.Zagorodny. ECA 20C. Europ. Phys. Soc., Geneva 1996, 1015-1018.

76. *García-Rosales, C., P. Franzen, H. Plank, J. Roth* et al.: Re-Emission and Thermal Desorption of Deuterium from Plasma Sprayed Tungsten Coatings for Application in ASDEX Upgrade. J. Nucl. Mater. **233-237**, 803-808 (1996).

77. *Geiger, J., A. Weller, R. Jaenicke, W7-AS-Team* and *NI-Team:* Stability of W7-AS Configurations with Reduced Vacuum Magnetic Well. In: Proc. 23rd Conf. Control. Fusion and Plasma Phys., Kiev 1996, Eds. D.Gresillon, A.Sitenko, A.Zagorodny. ECA 20C. Europ. Phys. Soc., Geneva 1996, 491-494.

78. *Geist, T.* and *H.-J. Hartfuß:* Array of Coupled Phase Locked Oscillators at 160 GHz. IEEE Microwave Guided Wave Lett. **6**, 235-237 (1996).

79. *Geist, T., H.-J. Hartfuß* and *J. Koponen:* Initial Operation of a Multichannel Interferometer at W7-AS. Stellarator News **47**, 6 (1996).

80. *Giannone, L., U. Stroth, J. Köllermeyer* et al.: Combined Analysis of Steady State and Transient Transport by the Maximum Entropy Method. Plasma Phys. Control. Fusion **38**, 477-488 (1996).

81. *Greuner, H., F. Kerl, W. Bitter, R. Holzthüm, O. Jandl, H. Renner* and *J. Kißlinger:* Plasma Facing Components and Cooling Concepts. In: Proc. 6th Workshop Wendelstein 7-X and Helias Reactors, Schloß Ringberg, Tegernsee 1995, Eds. F.Herrnegger, F.Rau. IPP 2/331, IPP, Garching 1996, 120-129.

82. *Grigull, P., R. Behrisch, U. Kreissig** et al.: Simultaneous Analysis of Low-Z Impurities in the Near-Surface Region of Solid Materials by Heavy Ion Elastic Recoil Detection (HIERD). Fresenius' J. Anal. Chem. **353**, 578-581 (1996).

83. *Grigull, P., S. Fiedler, L. Giannone* and *O. Heinrich:* Edge and Divertor Diagnostics for W7-X. In: Proc. Koordinationsgespräche KFA-W7X, Jülich 1996. Ed. J.Winter. KFA, Jülich 1996, 41-74.

84. *Grigull, P., J. Kißlinger* and *H. Niedermeyer:* Plans for the Edge and Divertor Diagnostics at W7-X. In: Proc. 6th Workshop Wendelstein 7-X and Helias Reactors, Schloß Ringberg, Tegernsee 1995, Eds. F.Herrnegger, F.Rau. IPP 2/331, IPP, Garching 1996, 109-114.

85. *Groudeva-Zotova**, *S., W. Jacob* and *A. von Keudell:* Secondary Electron Emission Coefficient of C:H and Si:C Thin Films and Some Relations to their Morphology and Composition. Diamond Related Mater. **5**, 1087-1095 (1996).

86. *Grützmacher**, *K., M.I. de la Rosa**, *J. Seidel**, *G. Fußmann, W. Bohmeyer* et al.: Edge $n_T/n_D$ by Two-Photon Induced $Ly_{-a}$ Fluorescence. In: Diagnostics for Experimental Nuclear Fusion Reactor. Eds. P.E.Stott, G.Gorini, E.Sindoni. Plenum Press, New York,NY 1996, 307-310.

87. *Gubanka, B., M. Donath* and *F. Passek:* Magnetic Phases of fcc-like Fe Films on Cu(001): Answers from the Spin-Dependent Electronic Structure. J. Magn. Magn. Mater. **161**, L11-L16 (1996).

88. *Gubanka, B., M. Donath* and *F. Passek:* Magnetically Split sp-Derived States in fcc-like Fe/Cu(001). Phys. Rev., B **54**, R11153-R11156 (1996).

89. *Günter, S.* and *A. Könies:* Hydrogenic Ion Lines Emitted from Dense Plasmas. In: Proc. Int. Conf. on Phys. of Strongly Coupled Plasmas, Binz/Rügen 1995, Eds. W.D.Kraeft, M.Schlanges. World Scientific Publ., Singapore 1996, 282-285.

90. *Gutdeutsch*, U., U. Birkenheuer*, E. Bertel* et al.: On the Adsorption Site of Ethylene at the Ni(110) Surface: A Combined Experimental and Theoretical Study Involving the Unoccupied Bandstructure. Surf. Sci. **345**, 331-346 (1996).

91. *Haas, G., H.-S. Bosch* and *L. de Kock*:* Neutral Gas Diagnostics for ITER. In: Diagnostics for Experimental Thermonuclear Fusion Reactors, Eds. P.E.Stott, G.Gorini, E.Sindoni. Plenum Press, New York,NY 1996, 571-579.

92. *Häfner*, H.E., K. Heckert*, P. Norajitra*, V. Erckmann, U. Weber* et al.: Kalorimeterversuche zur Verlustbestimmung eines Flüssigstickstoff-gekühlten Millimeterwellen-Fensters an einem Gyrotron in Garching. Forschungszentrum Karlsruhe, Interner Bericht PKF Nr. 066, 1996.

93. *Harmeyer, E.:* Fields, Forces and Stresses in the HSR Coil System. In: Proc. 6th Workshop Wendelstein 7-X and Helias Reactors, Schloß Ringberg, Tegernsee 1995, Eds. F.Herrnegger, F.Rau. IPP 2/331, IPP, Garching 1996, 237-244.

94. *Hartfuß, H.-J.:* Mikrowellendiagnostik. In: Proc. Koordinationsgespräche KFA-W7X, Jülich 1996. Ed. J.Winter. KFA, Jülich 1996, 95-101.

95. *Hartfuß, H.-J., M. Häse, C. Watts** et al.: Temperature Fluctuation Measurements with ECE in W7-AS. Plasma Phys. Control. Fusion **38**, A227-A236 (1996).

96. *Hayes*, P.A., D.H. Yu*, J. Furst*, M. Donath* et al.: Excitation of He $3^3$ P and Ne 3p States by Polarised Electrons. J. Phys., B **29**, 3989-4000 (1996).

97. *Heinrich, O., R. Schneider, H. Verbeek, ASDEX Upgrade Team* et al.: Edge Ion Temperature Profiles in L- and H-Mode Discharges of ASDEX. In: Proc. 23rd Conf. Control. Fusion and Plasma Phys., Kiev 1996, Eds. D.Gresillon, A.Sitenko, A.Zagorodny. ECA 20C. Europ. Phys. Soc., Geneva 1996, 731-734.

98. *Hemsworth*, R.S., J.-H. Feist, M. Hanada*, B. Heinemann* et al.: Neutral Beams for ITER (invited). Rev. Sci. Instrum. **67**, 1120-1125 (1996).

99. *Herrmann, A.:* Optical Surface Temperature Measurement. In: Diagnostics for Experimental Nuclear Fusion Reactor. Eds. P.E.Stott, G.Gorini, E.Sindoni. Plenum Press, New York,NY 1996, 581-589.

100. *Herrmann, A., M. Laux, O. Kardaun, G. Fußmann, V. Rohde, ASDEX Upgrade Team* and *NI-Team:* Characterization of the Power Deposition Profiles in the Divertor of ASDEX Upgrade. In: Proc. 23rd Conf. Control. Fusion and Plasma Phys., Kiev 1996, Eds. D.Gresillon, A.Sitenko, A.Zagorodny. ECA 20C. Europ. Phys. Soc., Geneva 1996, 807-810.

101. *Herrnegger, F.:* Equilibrium Computations for HSR Using the KW-Code. In: Proc. 6th Workshop Wendelstein 7-X and Helias Reactors, Schloß Ringberg, Tegernsee 1995, Eds. F.Herrnegger, F.Rau. IPP 2/331, IPP, Garching 1996, 187-193.

102. *Hirsch, M., H.-J. Hartfuß, T. Geist* et al.: Amplitude Modulated Heterodyne Reflectometer for Density Profile and Density Fluctuation Profile Measurements at W7-AS. Rev. Sci. Instrum. **67**, 1807-1813 (1996).

103. *Hitzschke*, L.* and *S. Günter:* The Influence of Many-Particle Effects beyond the Debye Approximation on Spectral Line Shapes in Dense Plasmas. J. Quant. Spectrosc. Radiat. Transfer **56**, 423-441 (1996).

104. *Hofer*, W.O.* and *J. Roth* (Eds.): Physical Processes of the Interaction of Fusion Plasmas with Solids. Academic Press, London 1996, 389 S.

105. *Hofmann, J.V.:* Requirements for W7-X Diagnostics. In: Proc. 6th Workshop Wendelstein 7-X and Helias Reactors, Schloß Ringberg, Tegernsee 1995, Eds. F.Herrnegger, F.Rau. IPP 2/331, IPP, Garching 1996, 305-312.

106. *Hofmann, J.V.:* Videoauswertung mit IDL. In: Proc. 5th CREASO User Group Conf., Augsburg 1996. CREASO, Gilching 1996, 25-44.

107. *Hofmann, J.V.:* W7-X Spectroscopy. In: Proc. Koordinierungsgespräche KFA-W7-X, Ed. J.Winter. KFA Jülich 1996, 80-94.

108. *Hofmann, J.V., J. Baldzuhn, R. Brakel* et al.: Stellarator Optimization in W7-AS. Plasma Phys. Control. Fusion **38**, A193-A211 (1996).

109. *Hofmann, J.V., H.-J. Hartfuß, H. Ringler, P. Grigull, W7-AS-Team* and *W7-X-Team:* Overview of W7-X Diagnostics. In: Diagnostics for Experimental Nuclear Fusion Reactor. Eds. P.E.Stott, G.Gorini, E.Sindoni. Plenum Press, New York,NY 1996, 607-616.

110. *Holzhauer, E., J. Baldzuhn, S. Fiedler, J. Geiger, M. Hirsch, R. Jaenicke, C. Konrad, A. Weller, W7-AS-Team* and *NI-Team:* Edge Turbulence and Transport Barrier Associated with the H-Mode in the W7-AS Stellarator. In: Proc. 23rd Conf. Control. Fusion and Plasma Phys., Kiev 1996, Eds. D.Gresillon, A.Sitenko, A.Zagorodny. ECA 20C. Europ. Phys. Soc., Geneva 1996, 467-470.

111. *Horvath*, G., J. Schweinzer, H.P. Winter** et al.: Na(3p-3s) Excitation by Impact of Slow Multiply Charged Ions. Phys. Rev., A **54**, 3022-3028 (1996).

112. *Igitkhanov*, Y.* and *D. Naujoks:* Sheath Potential Drop in the Presence of Impurities. Contrib. Plasma Phys. **36**, 67-72 (1996).

113. *Jacob, W.* and *M. Unger*:* Experimental Determination of the Absorption Strength of C-H Vibrations for Infrared Analysis of Hydrogenated Carbon Films. Appl. Phys. Lett. **68**, 475-477 (1996).

114. *Jandl, O.:* Dreidimensionale Thermische Analyse einer Divertorkomponente. In: Proc. 12th Conf. Computational Mechanics, Pernink 1996. Univ. of West Bohemia, Pilsen 1996, 83-90.

115. *Jüttner, B., B. Djakov*, T. Schülke** et al.: Dynamics of Vacuum Arc Spots at a Point Cathode. In: Proc. 17th Int. Symp. Discharges and Electrical Insulation in Vacuum, 1, Berkeley,CA 1996, Eds. S.Anders, A.Anders. IEEE Service Center, New Jersey,NJ 1996, 123-127.

116. *Jüttner, B.* and *A. Förster*:* Evidence and Consequences of Cathode-Spot Substructure in Vacuum Arcs. In: Proc. 17th Int. Symp. Discharges and Electrical Insulation in Vacuum, 1, Berkeley,CA 1996, Eds. S.Anders, A.Anders. IEEE Service Center, New Jersey,NJ 1996, 118-122.

117. *Jüttner, B., V.F. Puchkarev*, E. Hantzsche* et al.: Cathode Spots. In: Handbook of Vacuum Arc Science and Technology, Eds.

R.L.Boxman, P.J.Martin, D.M.Sanders. Noyes Publ., New Jersey,NJ 1996, 73-281.

118. *Kaiser*, R.* and *A. Salat:* Analytic Three-Dimensional Solutions of the Magnetohydrostatic Equations with Twisted Field Lines. Phys. Rev. Lett. **77**, 3133-3136 (1996).

119. *Kallenbach, A.:* Experimental Results of Radiative Cooling in ASDEX Upgrade. In: Proc. 6th Workshop Wendelstein 7-X and Helias Reactors, Schloß Ringberg, Tegernsee 1995, Eds. F.Herrnegger, F.Rau. IPP 2/331, IPP, Garching 1996, 44-55.

120. *Kallenbach, A., R. Dux, H.-S. Bosch, K. Büchl, J.C. Fuchs, O. Gehre, G. Haas, A. Herrmann, W. Herrmann, W. Junker, M. Kaufmann, V. Mertens, K.-F. Mast, J. Neuhauser, S. de Peña Hempel, F. Ryter, J. Schweinzer, K.-H. Steuer, W. Suttrop, H. Zohm, ASDEX Upgrade Team, NI-Team* and *ICRH-Team:* Radiative Boundary Discharges with Impurity Injection and the H-L-Transition in ASDEX Upgrade. Plasma Phys. Control. Fusion **38**, 2097-2112 (1996).

121. *Kallenbach, A., R. Dux, S. de Peña Hempel, G. Becker, H.-S. Bosch, J.C. Fuchs, H. Salzmann, K.-H. Steuer, ASDEX Upgrade Team, NI-Team* and *ICRH-Team:* Optimization of Radiative H-Mode Operation. In: Proc. 23rd Conf. Control. Fusion and Plasma Phys., Kiev 1996, Eds. D.Gresillon, A.Sitenko, A.Zagorodny. ECA 20C. Europ. Phys. Soc., Geneva 1996, 83-86.

122. *Kardaun*, J.Q.P.D.* and *O. Kardaun:* ROC Curves as a Tool in Discriminant Analysis with a View Towards Plasma Fusion Data. In: Proc. 12th Symp. Computational Statistics, Barcelona 1996, Eds. A.Prat, E.Ripoli. Physica-Verl., Heidelberg 1996, 69-70.

123. *Kardaun, O., A. Kus, H-Mode Database Working-Group* and *L-Mode Database Working-Group:* Generalising Regression and Discriminant Analysis: Catastrophe Models for Plasma Confinement and Threshold Data. In: Proc. 12th Symp. Computational Statistics, Barcelona 1996, Eds. A.Prat, E.Ripoli. Physica-Verl., Heidelberg 1996, 313-319.

124. *Kass, T., H.-S. Bosch, F. Hoenen*, K. Lackner, M. Maraschek, H. Zohm, ASDEX Upgrade Team, NI-Team, ICRH-Team* and *ECRH-Team:* The Fishbone-Instability in ASDEX Upgrade. In: Proc. 23rd Conf. Control. Fusion and Plasma Phys., Kiev 1996, Eds. D.Gresillon, A.Sitenko, A.Zagorodny. ECA 20C. Europ. Phys. Soc., Geneva 1996, 79-82.

125. *Kastelewicz, H., D. Reiter*, R. Schneider, D.P. Coster* and *H. Meyer:* B2-EIRENE Simulations for a Deuterium Plasma at PSI-1. In: Proc. 23rd Conf. Control. Fusion and Plasma Phys., Kiev 1996, Eds. D.Gresillon, A.Sitenko, A.Zagorodny. ECA 20C. Europ. Phys. Soc., Geneva 1996, 803-806.

126. *Keudell, A. von* and *W. Jacob:* Growth and Erosion of Hydrocarbon Films Investigated by in situ Ellipsometry. J. Appl. Phys. **79**, 1092-1098 (1996).

127. *Kick, M., H.-J. Hartfuß, J.H. Hofmann* et al.: Overview of W7-X Diagnostics. Stellarator News **47**, 2-5 (1996).

128. *Kick, M.* and *H. Maaßberg:* Ion Heat Transport in W7-AS in the Imfp Regime. Stellarator News **43**, 4-7 (1996).

129. *Kißlinger, J.:* Divertor Aspects in the Helias Reactor In: Proc. 6th Workshop Wendelstein 7-X and Helias Reactors, Schloß Ringberg, Tegernsee 1995, Eds. F.Herrnegger, F.Rau. IPP 2/331, IPP, Garching 1996, 245-248.

130. *Kißlinger, J.:* Modification of the W7-X Modular Coils Improving the Aspect Ratio at High Rotational Transform. In: Proc. 6th Workshop Wendelstein 7-X and Helias Reactors, Schloß Ringberg, Tegernsee 1995, Eds. F.Herrnegger, F.Rau. IPP 2/331, IPP, Garching 1996, 148-153.

131. *Kißlinger, J.:* Simulation of the W7-X Edge Plasma Using the B2-Code. In: Proc. 6th Workshop Wendelstein 7-X and Helias Reactors, Schloß Ringberg, Tegernsee 1995, Eds. F.Herrnegger, F.Rau. IPP 2/331, IPP, Garching 1996, 35-43.

132. *Könies, A., S. Günter* and *G. Röpke*:* On the Time Evolution of the Ionic Microfield in Plasmas. J. Phys., B **29**, 6091-6101 (1996).

133. *Kornejew, P., W. Bohmeyer* and *G. Fußmann:* Thermal Helium Beam for Diagnostic of Electron Density and Temperature. In: Diagnostics for Experimental Nuclear Fusion Reactor. Eds. P.E.Stott, G.Gorini, E.Sindoni. Plenum Press, New York,NY 1996, 599-602.

134. *Küppers, J.:* Interactions of Gaseous H Atoms with Adsorbate Covered Surfaces via Eley-Rideal Reactions. Phys. Chem. **197**, 137-153 (1996).

135. *Kurzan, B., M. Maraschek, A. Silva*, W. Suttrop, H. Zohm, ASDEX Upgrade Team* et al.: Measurement of Fast Density Profile Changes by FM Broadband Reflectometry on ASDEX Upgrade. In: Proc. 23rd Conf. Control. Fusion and Plasma Phys., Kiev 1996, Eds. D.Gresillon, A.Sitenko, A.Zagorodny. ECA 20C. Europ. Phys. Soc., Geneva 1996, 1011-1014.

136. *Lang, P.T.* and *P. Cierpka:* 80 Hz Repetitive Centrifuge Injector for Hydrogen Pellets. Rev. Sci. Instrum. **67**, 619-620 (1996).

137. *Lang, P.T.* and *K.-F. Mast:* Photoresponse of a Miniaturized Ultrabroad-Band Low-Noise Metal-Film Bolometer Detector Array. J. Optics **27**, 25-29 (1996).

138. *Laqua, H.:* Resonant and Nonresonant Electron Cyclotron Heating at Densities above the Plasma Cut-off by O-X-B-Mode Conversion. Stellarator News **44**, 2-4 (1996).

139. *Laqua, H., V. Erckmann, H.-J. Hartfuß, W7-AS-Team* et al.: Resonant and Nonresonant Electron Cyclotron Heating at Densities above the Plasma Cut-off by O-X-B Mode Conversion at W7-AS. In: Proc. 23rd Conf. Control. Fusion and Plasma Phys., Kiev 1996, Eds. D.Gresillon, A.Sitenko, A.Zagorodny. ECA 20C. Europ. Phys. Soc., Geneva 1996, 847-850.

140. *Lehmann, J., P. Roos** and *E. Bertel:* Incorporation of Alkali Metals on Pt(111). Phys. Rev., B **54**, R2347-R2350 (1996).

141. *Lengyel, L.L.:* Fuelling of Fusion Reactors by Pellet Injection. In: Proc. 6th Workshop Wendelstein 7-X and Helias Reactors, Schloß Ringberg, Tegernsee 1995, Eds. F.Herrnegger, F.Rau. IPP 2/331, IPP, Garching 1996, 277-283.

142. *Lengyel, L.L., V.A. Rozhanskij** and *I.Yu. Veselova*:* Electrostatic Shielding of Vaporizing Surfaces Exposed to Hot Plasmas. Nucl. Fusion **36**, 1679-1690 (1996).

143. *Leuterer, F., H. Brinkschulte, F. Monaco, M. Münich, A.G. Peeters, G. Pereverzev, F. Ryter, W. Suttrop, ASDEX Upgrade Team* et al.: First ECRH Experiments in ASDEX Upgrade. In: Proc. 23rd Conf. Control. Fusion and Plasma Phys., Kiev 1996, Eds. D.Gresillon, A.Sitenko, A.Zagorodny. ECA 20C. Europ. Phys. Soc., Geneva 1996, 871-874.

144. *Leuterer, F., H. Brinkschulte, M. Münich, F. Monaco, A.G. Peeters, G. Pereverzev, F. Ryter, M. Zouhar, ASDEX Upgrade Team* et al.: Plans for ECRH in ASDEX Upgrade. In: Proc. 9th Joint Workshop on ECE and ECRH, Borrego Springs,CA 1995. Ed. J.Lohr. World Scientific Publ., Singapore 1996, 529-534.

145. *Linden, W. von der, M. Donath* and *V. Dose:* Application of MaxEnt to Inverse Photoemission Spectroscopy. In: Maximum Entropy and Bayesian Methods, Ed. G.R.Heidbreder. Kluwer, Dordrecht 1996, 343-350.

146. *Linden, W. von der, K. Ertl* and *V. Dose:* Bayesian Consideration of the Tomography Problem. In: Maximum Entropy and Bayesian Methods, Eds. J.Skilling, S.Sibisi. Kluwer, Dordrecht 1996, 41-49.

147. *Linden, W. von der, R. Fischer* and *V. Dose:* Evidence Integrals. In: Maximum Entropy and Bayesian Methods, Eds. K.M.Hanson, R.N.Silver. Kluwer, Dordrecht 1996, 443-448.

148. *Linsmeier, C., H. Knözinger** and *E. Taglauer:* Depth Profile Analysis of Strong Metal-Support Interactions on $Rh/TiO_2$ Model Catalysts. Nucl. Instrum. Methods Phys. Res., B **118**, 533-540 (1996).

149. *Lutterloh, C., J. Biener, K. Pöhlmann, J. Küppers* et al.: Modification of the Benzene-Metal Interaction by C and H Monolayers at Pt(111) Surfaces. Surf. Sci. **352-354**, 133-137 (1996).

150. *Lutterloh, C., J. Biener, A. Schenk** and *J. Küppers:* Interaction of D(H) Atoms with Physisorbed Benzene and (1,4)-Dimethyl-Cyclohexane: Hydrogenation and H Abstraction. J. Chem. Phys. **104**, 2392-2400 (1996).

151. *Maaßberg, H.:* Need of Density Profile Control? In: Proc. 6th Workshop Wendelstein 7-X and Helias Reactors, Schloß Ringberg, Tegernsee 1995, Eds. F.Herrnegger, F.Rau. IPP 2/331, IPP, Garching 1996, 202-214.

152. *Maaßberg, H., C.D. Beidler, M. Kaiser* and *E.E. Simmet:* Neoclassical Transport Predictions for Stellarators in the Long-Mean-Free-Path Regime. In: Proc. 23rd Conf. Control. Fusion and Plasma Phys., Kiev 1996, Eds. D.Gresillon, A.Sitenko, A.Zagorodny. ECA 20C. Europ. Phys. Soc., Geneva 1996, 487-490.

153. *MacDonald*, R.J., E. Taglauer* and *K.R. Wandelt** (Eds.): Surface Science - Principles and Current Applications. Springer, Berlin 1996, 372 S.

154. *Maingi*, R., G.L. Jackson*, M.R. Wade*, G. Haas* et al.: Control of Wall Particle Inventory with Divertor Pumping on DIII-D. Nucl. Fusion **36**, 245-253 (1996).

155. *Marushchenko*, N., U. Gasparino, H. Maaßberg* and *M. Romé:* Bounce Averaged Fokker-Planck Code for the Simulation of ECRH at W7-AS. In: Proc. 23rd Conf. Control. Fusion and Plasma Phys., Kiev 1996, Eds. D.Gresillon, A.Sitenko, A.Zagorodny. ECA 20C. Europ. Phys. Soc., Geneva 1996, 950-953.

156. *Mashkova*, E.S., V.A. Molchanov*, I.M. Fayazov** and *W. Eckstein:* Angular Characteristics of Sputtering of Polycrystalline Au. Istvestia Akademia Nauk **60**, 131-137 (1996).

157. *Mashkova*, E.S., V.A. Molchanov*, V.I. Shulga*, W. Eckstein* et al.: Interface Formation in Silicon by Cesium Bombardment. Nucl. Instrum. Methods Phys. Res., B **115**, 519-522 (1996).

158. *Mashkova*, E.S., V.A. Molchanov*, V.I. Shulga*, W. Eckstein* et al.: Modification of Near-Surface Layers of Silicon under Cesium Ion Bombardment. Poverkhnost **8**, 90-104 (1996).

159. *Mayer, M., R. Behrisch, H. Plank, J. Roth,* et al.: Codeposition of Hydrogen with Be, C and W. J. Nucl. Mater. **230**, 67-73 (1996).

160. *Memmel, N.* and *V. Dose:* Low-Dimensional States on Metal Surfaces. In: Surface Science - Principles and Current Applications, Eds. R.J.MacDonald, E.C.Taglauer, K.R.Wandelt. Springer, Berlin 1996, 64-75.

161. *Mertens, V., P.T. Lang, K. Büchl, R. Dux, J.C. Fuchs, O. Gruber, G. Haas, A. Kallenbach, M. Kaufmann, R.S. Lang, K.-F. Mast, H.W. Müller, R. Neu, J. Neuhauser, F. Ryter, H. Salzmann, J. Schweinzer, W. Suttrop, M. Weinlich, H. Zohm, ASDEX Upgrade Team* and *NI-Team:* High Density Operation in Auxiliary Heated ASDEX Upgrade Discharges. In: Proc. 23rd Conf. Control. Fusion and Plasma Phys., Kiev 1996, Eds. D.Gresillon, A.Sitenko, A.Zagorodny. ECA 20C. Europ. Phys. Soc., Geneva 1996, 15-18.

162. *Meyer-Spasche, R.:* A Free Boundary Eigenvalue Problem. In: Proc. 1st World Congress of Nonlinear Analysts, Tampa,FL 1992, Ed. V.Lakshmikantham. De Gruyter, Berlin 1996, 911-924.

163. *Milch, I.:* Um Haaresbreite. ELRAD Magazin für Elektronik und techn. Rechneranwendungen **6**, 11 (1996).

164. *Müller*, G.A., V. Erckmann, H.-J. Hartfuß* et al.: Shear Modification by ECCD and Related Confinement Phenomena in W7-AS. In: Proc. 11th Top. Conf. Radio Frequency Power in Plasmas, Palm Springs,CA 1995. Eds. R.Prater, V.S.Chan. AIP Conf. Proc. 355, AIP Press, New York,NY 1996, 133-142.

165. *Müller, H.W., P.T. Lang, K. Büchl, M. Kaufmann, P. McCarthy, V. Mertens, W. Schneider, H. Zohm, ASDEX Upgrade Team* et al.: On the Possibility of q-Probe Measurements by Observation of Pellet Ablation by a Fast-Framing Camera at ASDEX Upgrade. In: Proc. 23rd Conf. Control. Fusion and Plasma Phys., Kiev 1996, Eds. D.Gresillon, A.Sitenko, A.Zagorodny. ECA 20C. Europ. Phys. Soc., Geneva 1996, 1019-1022.

166. *Murtagh*, F., A. Aussem** and *O. Kardaun:* The Wavelet Transform in Multivariate Data Analysis. In: Proc. 12th Symp. Computational Statistics, Barcelona 1996, Eds. A.Prat, E.Ripoli. Physica-Verl., Heidelberg 1996, 397-403.

167. *Naujoks, D.* and *W. Eckstein:* Non-Linear Erosion Effects in Plasma Experiments. J. Nucl. Mater. **230**, 93 -100 (1996) .

168. *Naujoks, D., K. Asmussen, M. Bessenrodt-Weberpals, S. Deschka, R. Dux, W. Engelhardt, A.R. Field, G. Fußmann, J.C. Fuchs, C. García-Rosales, S. Hirsch, K.-F. Mast, R. Neu, R. Radtke, J. Roth, U. Wenzel, ASDEX Upgrade Team* et al.: Tungsten as Target Material in Fusion Devices. Nucl. Fusion **36**, 671-687 (1996).

169. *Neu, R., K. Asmussen, G. Fußmann, P. Geltenbort, G. Janeschitz, K. Schönmann, G. Schramm, ASDEX Upgrade Team* et al.: Monitor for the Carbon and Oxygen Impurities in the ASDEX Upgrade Tokamak. Rev. Sci. Instrum. **67**, 1829-1833 (1996).

170. *Neu, R., K. Asmussen, K. Krieger, A. Thoma, H.-S. Bosch, S. Deschka, R. Dux, W. Engelhardt, C. García-Rosales, O. Gruber, A. Herrmann, A. Kallenbach, M. Kaufmann, V. Mertens, F. Ryter, V. Rohde, J. Roth, M. Sokoll, A. Stäbler, W. Suttrop, M. Weinlich, H. Zohm, M. Alexander, G. Becker, K. Behler, K. Behringer, R. Behrisch, A. Bergmann, M. Bessenrodt-Weberpals, M. Brambilla, H. Brinkschulte, K. Büchl, A. Carlson, R. Chodura, D.P. Coster, H.J. de Blank, S. de Peña Hempel, R. Drube, H.-U. Fahrbach, J.-H. Feist, W. Feneberg, S. Fiedler, P. Franzen, J.C. Fuchs, G. Fußmann, J. Gafert, O. Gehre, J. Gernhardt, G. Haas, G. Herppich, W. Herrmann, S. Hirsch, M. Hoek, F. Hofmeister, H. Hohenöcker, D. Jacobi, W. Junker, O. Kardaun, T. Kass, H. Kollotzek, W. Köppendörfer, B. Kurzan, K. Lackner, P.T. Lang, R.S. Lang, M. Laux, L.L. Lengyel, F. Leuterer, M. Maraschek, K.-F. Mast, P. McCarthy, D. Meisel, R. Merkel, H.W. Müller, M. Münich, H. Murmann, B. Napiontek, G. Neu, J. Neuhauser, J.-M. Noterdaeme, E. Pasch, G. Pautasso, A.G. Peeters, G. Pereverzev, C.S. Pitcher, W. Poschenrieder, G. Raupp, K. Reinmüller, R. Riedl, H. Röhr, H. Salzmann, W. Sandmann, H.-B. Schilling, D. Schlögl, H. Schneider, R. Schneider, W. Schneider, G.*

*Schramm, J. Schweinzer, B.D. Scott, U. Seidel, E. Speth, K.-H. Steuer, J. Stober, B. Streibl, W. Treutterer, M. Troppmann, M. Ulrich, H. Verbeek, P. Verplancke, O. Vollmer, H. Wedler, U. Wenzel, F. Wesner, R. Wolf, R. Wunderlich, D. Zasche, T. Zehetbauer, H.-P. Zehrfeld* et al.: The Tungsten Divertor Experiment at ASDEX Upgrade. Plasma Phys. Control. Fusion **38**, A165-A179 (1996).

171. *Neuhauser, J.* et al.: Conclusions for the W7-X Divertor Based on Tokamak Experience. In: Proc. 6th Workshop Wendelstein 7-X and Helias Reactors, Schloß Ringberg, Tegernsee 1995, Eds. F.Herrnegger, F.Rau. IPP 2/331, IPP, Garching 1996, 70-75.

172. *Niedermeyer, H., P. Grigull, D. Dorst, F.-W. Hoffmann, E. Katzmarek* and *J. Kißlinger:* Relevance of Future Edge Studies at W7-AS for W7-X. In: Proc. 6th Workshop Wendelstein 7-X and Helias Reactors, Schloß Ringberg, Tegernsee 1995, Eds. F.Herrnegger, F.Rau. IPP 2/331, IPP, Garching 1996, 115-119.

173. *Noterdaeme, J.-M., W. Becker, F. Braun, H. Faugel, J.C. Fuchs, W. Herrmann, F. Hofmeister, R. Neu, W. Suttrop, J. Schweinzer, P. Verplancke, F. Wesner, ICRF-Team, ASDEX Upgrade Team* and *NI-Team:* Achievement of the H-Mode with a Screenless ICRF Antenna in ASDEX Upgrade. In: Proc. 11th Top. Conf. Radio Frequency Power in Plasmas, Palm Springs,CA 1995. Eds. R.Prater, V.S.Chan. AIP Conf. Proc. 355, AIP Press, New York,NY 1996, 47-50.

174. *Noterdaeme, J.-M., M. Brambilla, F. Hofmeister, J. Schweinzer, W. Schneider, P. Verplancke, ICRF-Group* and *ASDEX Upgrade Team:* Mutual Influence between the ICRF Antennas and the Edge Density on ASDEX Upgrade. In: Proc. 23rd Conf. Control. Fusion and Plasma Phys., Kiev 1996, Eds. D.Gresillon, A.Sitenko, A.Zagorodny. ECA 20C. Europ. Phys. Soc., Geneva 1996, 723-726.

175. *Nührenberg, C.:* Global Ideal Magnetohydrodynamic Stability Analysis for the Configurational Space of Wendelstein 7-X. Phys. Plasmas **3**, 2401-2410 (1996).

176. *Nührenberg, C., Y. Nakamura*, J.L. Johnson** et al.: Comparison of the Calculations of the Stability Properties of a Specific Stellarator Equilibrium with Different MHD Stability Codes. J. Comput. Phys. **128,** 43-57 (1996).

177. *Nührenberg, J., S. Gori, C. Nührenberg, E. Strumberger* and *R. Zille:* W7-X Physics Assessment of a Fusion Coil Set. In: Proc. 6th Workshop Wendelstein 7-X and Helias Reactors, Schloß Ringberg, Tegernsee 1995, Eds. F.Herrnegger, F.Rau. IPP 2/331, IPP, Garching 1996, 172-177.

178. *Passek, F., M. Donath* and *K. Ertl:* Spin-Dependent Electron Attenuation Lenghts and Influence on Spectroscopic Data. J. Magn. Magn. Mater. **159**, 103-108 (1996).

179. *Pautasso, G., K. Büchl, J.C. Fuchs, O. Gruber, A. Herrmann, K. Lackner, P.T. Lang, K.-F. Mast, M. Ulrich, H. Zohm* and *ASDEX Upgrade Team:* Use of Impurity Pellets to Control Energy Dissipation during Disruption. Nucl. Fusion **36**, 1291-1297 (1996).

180. *Peeters, A.G.:* Extensions of the Ray Equations of Geometric Optics to Include Diffraction Effects. In: Proc. 23rd Conf. Control. Fusion and Plasma Phys., Kiev 1996, Eds. D.Gresillon, A.Sitenko, A.Zagorodny. ECA 20C. Europ. Phys. Soc., Geneva 1996, 851-854.

181. *Peeters, A.G.:* Extension of the Ray Equations of Geometric Optics to Include Diffraction Effects. Phys. Plasmas **3**, 4386-4395 (1996).

182. *Peeters, A.G.* and *E. Westerhof*:* Impact of Radial Transport on the Quasilinear Plateau Formation due to Electron Cyclotron Waves. Phys. Plasmas **3**, 1628-1633 (1996).

183. *Penningsfeld, F.-P., J. Geiger, W. Ott, E. Speth, W7-AS-Team* and *NI-Team:* 3 MW Neutral Injection into the Stellarator Wendelstein 7-AS - Heating Efficiency at High-Beta Operation. In: Proc. 23rd Conf. Control. Fusion and Plasma Phys., Kiev 1996, Eds. D.Gresillon, A.Sitenko, A.Zagorodny. ECA 20C. Europ. Phys. Soc., Geneva 1996, 483-486.

184. *Penningsfeld, F.-P.* and *E. Speth:* High-Energy NBI with Negative Ions. In: Proc. 6th Workshop Wendelstein 7-X and Helias Reactors, Schloß Ringberg, Tegernsee 1995, Eds. F.Herrnegger, F.Rau. IPP 2/331, IPP, Garching 1996, 313-319.

185. *Pfirsch, D.* and *D. Correa-Restrepo:* Collisional Drift Fluid Equations and Implications for Drift Waves. Plasma Phys. Control. Fusion **38**, 71-101 (1996).

186. *Pfirsch, D.* and *R.N. Sudan*:* Stability of Force-Free Taylor States in a New Version of Magnetic Flux-Averaged Magnetohydrodynamics. Phys. Plasmas **3**, 29-34 (1996).

187. *Pinkau, K.:* The Early Days of Gamma-Ray Astronomy. Astron. Astrophys., Suppl. Ser. **120**, 43-47 (1996).

188. *Plank, H., R. Schwörer* and *J. Roth:* Erosion Behaviour and Surface Composition Modifications of SiC under $D^+$ Ion Bombardment. Nucl. Instrum. Methods Phys. Res., B **111**, 63-69 (1996).

189. *Plank, H., R. Schwörer* and *J. Roth:* Surface Composition Modifications of Carbides and Doped Graphites due to $D^+$ Ion Bombardment. Surf. Coat. Technol. **83**, 93-98 (1996).

190. *Post*, D., A. Kukushkin*, R. Schneider, H.-S. Bosch, D.P. Coster, K. Lackner, J. Neuhauser* et al.: ITER Divertor Modelling: Predictions and Experimental Validation. In: Proc. 15th Conf. Plasma Phys. Control. Nucl. Fusion Res., 2, Seville 1994, IAEA, Vienna 1996, 561-565.

191. *Prozesky*, V.M., H. Huber*, W. Assmann** and *R. Behrisch:* Evaluation of Spectra of Energetic Ions not Fully Stopped in $\Delta E$-$E_{rest}$ Telescopes. Nucl. Instrum. Methods Phys. Res., B **118**, 327-331 (1996).

192. *Pursch*, H.* and *B. Jüttner:* The Behaviour of the Ion Current at the Extinction of High Current Vacuum Arcs. In: Proc. 17th Int. Symp. Discharges and Electrical Insulation in Vacuum, 1, Berkeley,CA 1996, Eds. S.Anders, A.Anders. IEEE Service Center, New Jersey,NJ 1996, 169-172.

193. *Rangelov, G.* and *T. Fauster:* Thermally-Induced Evolution of Codeposited Co-Si Layers on Si(100) Surfaces. Surf. Sci. **365**, 403-410 (1996).

194. *Rau, F.* and *J. Kißlinger:* On Maintenance Aspects for HSR. In: Proc. 6th Workshop Wendelstein 7-X and Helias Reactors, Schloß Ringberg, Tegernsee 1995, Eds. F.Herrnegger, F.Rau. IPP 2/331, IPP, Garching 1996, 284-295.

195. *Reiter, S.* and *E. Taglauer:* Oxygen-Induced Faceting on Cu(115). Surf. Sci. **367**, 33-39 (1996).

196. *Renner, H., J. Nührenberg, E. Strumberger, P. Merkel, J. Kißlinger, H. Wobig, F. Rau* and *H. Greuner:* W7-X Divertor Design and Development Program In: Proc. 6th Workshop Wendelstein 7-X and Helias Reactors, Schloß Ringberg, Tegernsee 1995, Eds. F.Herrnegger, F.Rau. IPP 2/331, IPP, Garching 1996, 3-22.

197. *Rohde, V.* and *ASDEX Upgrade Team:* Langmuir Probe Measurements in the Midplane of ASDEX Upgrade. Contrib. Plasma Phys. **36**, 109-116 (1996).

198. *Rohde, V., M. Laux, A. Herrmann, D. Hildebrandt, B. Napiontek, M. Weinlich* and *ASDEX Upgrade Team:* Scrape-off Layer Behaviour in ASDEX Upgrade Ohmic and L-Mode Density Scan. In: Proc. 23rd Conf. Control. Fusion and Plasma Phys., Kiev 1996, Eds. D.Gresillon, A.Sitenko, A.Zagorodny. ECA 20C. Europ. Phys. Soc., Geneva 1996, 811-814.

199. *Romé, M., U. Gasparino, H.-J. Hartfuß, H. Maaßberg* et al.: Effect of the Radial Drift of Trapped Suprathermal Electrons on the ECRH Power Deposition Profile. In: Proc. 23rd Conf. Control. Fusion and Plasma Phys., Kiev 1996, Eds. D.Gresillon, A.Sitenko, A.Zagorodny. ECA 20C. Europ. Phys. Soc., Geneva 1996, 867-870.

200. *Roos*, W.D., J. du Plessis*, G.N. van Wyk*, E. Taglauer* and *S. Wolf:* Surface Structure and Composition of NiAl(100) by Low-Energy Ion Scattering. J. Vac. Sci. Technol., A **14**, 1648-1651 (1996).

201. *Roth, J., W. Eckstein, H. Plank* and *R. Schwörer:* Plasma Facing Materials in View of Erosion. In: Proc. 6th Workshop Wendelstein 7-X and Helias Reactors, Schloß Ringberg, Tegernsee 1995, Eds. F.Herrnegger, F.Rau. IPP 2/331, IPP, Garching 1996, 132-136.

202. *Roth, J.* and *C. García-Rosales:* Analytic Description of the Chemical Erosion of Graphite by Hydrogen Ions. Nucl. Fusion **36**, 1647-1659 (1996).

203. *Roth, J., H. Graupner*, S.P. Withrow*,* et al.: Chemical Interaction of Si, Ti, and Mo with Graphite Surfaces. J. Appl. Phys. **79**, 7695-7702 (1996).

204. *Roth, J., H. Plank* and *R. Schwörer:* Erosion of Si- and Ti Doped Graphites due to Deuterium Irradiation. Phys. Scr. T **64**, 67-70 (1996).

205. *Ryter, F., M. Alexander, W. Suttrop, J. Köllermeyer, F. Leuterer, A.G. Peeters, G. Pereverzev, ECRH-Team, ASDEX Upgrade Team* and *NI-Team:* Perturbative Transport from Sawtooth Propagation and ECRH Modulation in ASDEX Upgrade. In: Proc. 23rd Conf. Control. Fusion and Plasma Phys., Kiev 1996, Eds. D.Gresillon, A.Sitenko, A.Zagorodny. ECA 20C. Europ. Phys. Soc., Geneva 1996, 11-14.

206. *Ryter, F.* and *H-Mode Database Working Group:* H-Mode Power Threshold Database for ITER. Nucl. Fusion **36**, 1216-1264 (1996).

207. *Ryter, F.* and *H-Mode Database Working Group:* Results from the ITER H-Mode Threshold Database. Plasma Phys. Control. Fusion **38**, 1279-1282 (1996).

208. *Sapper, J.:* Design Steps for Wendelstein 7-X. In: Proc. 6th Workshop Wendelstein 7-X and Helias Reactors, Schloß Ringberg, Tegernsee 1995, Eds. F.Herrnegger, F.Rau. IPP 2/331, IPP, Garching 1996, 320-324.

209. *Sardei, F., Y. Feng* and *J. Kißlinger:* 3D Modelling of the Island Divertor. In: Proc. 6th Workshop Wendelstein 7-X and Helias Reactors, Schloß Ringberg, Tegernsee 1995, Eds. F.Herrnegger, F.Rau. IPP 2/331, IPP, Garching 1996, 96-108.

210. *Schauer, F.:* Cooling System for Wendelstein 7-X. In: Proc. Symp. Cryog. Syst. for Large Scale Supercond. Appl., Toki 1996, Ed. T.Mito. NIFS-PROC-28, Nat. Inst. for Fusion Science, Nagoya 1996, 61-64.

211. *Schauer, F.:* Optimization and Stability of a Cable-in-Conduit Superconductor. IEEE Trans. Magn. **32**, 2760-2763 (1996).

212. *Schittenhelm, M., H. Zohm* and *ASDEX Upgrade Team:* Interpretation of Mirnov Measurements in ASDEX Upgrade. In: Proc. 23rd Conf. Control. Fusion and Plasma Phys., Kiev 1996, Eds. D.Gresillon, A.Sitenko, A.Zagorodny. ECA 20C. Europ. Phys. Soc., Geneva 1996, 1027-1030.

213. *Schneider, R., D.P. Coster, J. Neuhauser, H.-S. Bosch, M. Kaufmann, K. Lackner, ASDEX Upgrade Team* et al.: SOL Modelling of the Tokamak. In: Proc. 6th Workshop Wendelstein 7-X and Helias Reactors, Schloß Ringberg, Tegernsee 1995, Eds. F.Herrnegger, F.Rau. IPP 2/331, IPP, Garching 1996, 56-69.

214. *Schuch*, R., S. Asp*, C. Biedermann* et al.: Reactions of Cooled Ions with Cold Electrons in CRYRING. Acta Phy. Pol., B **27**, 307-322 (1996).

215. *Schumacher*, U., K. Asmussen, G. Fußmann, R. Neu* et al.: Investigations on Calibration Sources for Soft-X-Ray Plasma Spectroscopy and Impurity Monitors. Rev. Sci. Instrum. **67**, 2826-2830 (1996).

216. *Schweinzer, J., O. Gehre, G. Haas, H. Murmann, J. Neuhauser, H. Salzmann, W. Sandmann, W. Schneider, W. Suttrop, M. Weinlich, ASDEX Upgrade Team* and *NI-Group:* Scaling of Edge Parameters for High Confinement, High Density ASDEX Upgrade Discharges. In: Proc. 23rd Conf. Control. Fusion and Plasma Phys., Kiev 1996, Eds. D.Gresillon, A.Sitenko, A.Zagorodny. ECA 20C. Europ. Phys. Soc., Geneva 1996, 719-722.

217. *Schwenn, U., R. Dohmen* and *T. Hayashi*:* Performance of the 3D Plasma Equilibrium Code HINT on Vector and MPP Systems. In: Proc. 8th Joint EPS-APS Int. Conf. on Physics Computing, Krakow 1996, Eds. P.Borcherds, M.Bubak, A.Maksymowicz. Academic Computing Centre Cyfronet, Krakow 1996, 410-411.

218. *Schwörer, R., H. Plank* and *J. Roth:* Surface Modifications and Erosion Yields of Silicon and Titanium Doped Graphites due to Low Energy $D^+$ Bombardment. J. Nucl. Mater. **230**, 208-213 (1996).

219. *Scott, B.:* Three Dimensional Computation of Collisional Drift Wave Turbulence and Transport in Tokamak Geometry. In: Proc. 23rd Conf. Control. Fusion and Plasma Phys., Kiev 1996, Eds. D.Gresillon, A.Sitenko, A.Zagorodny. ECA 20C. Europ. Phys. Soc., Geneva 1996, 51-54.

220. *Selberg*, N., A. Bárány*, C. Biedermann* et al.: Slow Collisions between Highly-Charged Ions and C60: Absolute DE Values and Cross Sections. Phys. Rev., A **53**, 874-879 (1996).

221. *Selberg*, N., C. Biedermann* and *H. Cederquist*:* Semi-empirical Scaling Laws for Electron Capture at Low Energies. Phys. Rev., A **54**, 4127-4135 (1996).

222. *Shishkin*, A.A., O. Motojima*, A.V. Zolotukhin* et al.: Progress in the Reactor Heliotron/Torsatron Physics Study. In: Proc. 23rd Conf. Control. Fusion and Plasma Phys., Kiev 1996, Eds. D.Gresillon, A.Sitenko, A.Zagorodny. ECA 20C. Europ. Phys. Soc., Geneva 1996, 551-558.

223. *Shishkin*, A.A., A.V. Zolotukhin, M.S. Smirnova** et al.: Some Aspects of Heliotron/Torsatron Reactor Physics. In: Proc. 6th Workshop Wendelstein 7-X and Helias Reactors, Schloß Ringberg, Tegernsee 1995, Eds. F.Herrnegger, F.Rau. IPP 2/331, IPP, Garching 1996, 227-236.

224. *Silva*, A., M.E. Manso*, L. Cupido*, M. Albrecht, A. Kallenbach, B. Kurzan, W. Suttrop* and *ASDEX Upgrade Team:* Ultrafast Broadband Frequency Modulation of a Continuous Wave Reflectometry System to Measure Density Profiles on ASDEX Upgrade. Rev. Sci. Instrum. **67**, 4138-4145 (1996).

225. *Simmet, E.E.:* Statistical Analysis of the Global Energy Confinement Time in Ohmic Discharges in the ASDEX Tokamak. Plasma Phys. Control. Fusion **38**, 689-704 (1996).

226. *Stober, J., D.P. Coster, H.-U. Fahrbach, R. Fischer, G. Haas, W. Herrmann, O. Kardaun, S. de Peña Hempel, R. Schneider, H. Verbeek, ASDEX Upgrade Team, NI-Team* et al.*:* Profiles of Ion Temperature an Neutral Density from the Simulation of Charge Exchange Measurements and Additional Experimental Data. In: Proc. 23rd Conf. Control. Fusion and Plasma Phys., Kiev 1996, Eds. D.Gresillon, A.Sitenko, A.Zagorodny. ECA 20C. Europ. Phys. Soc., Geneva 1996, 1023-1026.

227. *Stroth, U., L. Giannone, H.-J. Hartfuß, ECH-Group* and *W7-AS-Team:* Fast Transport Changes and Power Degradation in the W7-AS Stellarator. Plasma Phys. Control. Fusion **38**, 611-618 (1996).

228. *Stroth, U., M. Murakami*, R.A. Dory** et al.*:* Energy Confinement Scaling from the International Stellarator Database. Nucl. Fusion **36**, 1063-1077 (1996).

229. *Strumberger, E.:* SOL Studies for Finite-b Helias Equilibria. Contrib. Plasma Phys. **36**, 171-176 (1996).

230. *Strumberger, E.:* SOL Studies for Finite-b Helias Equilibria. In: Proc. 6th Workshop Wendelstein 7-X and Helias Reactors, Schloß Ringberg, Tegernsee 1995, Eds. F.Herrnegger, F.Rau. IPP 2/331, IPP, Garching 1996, 23-34.

231. *Strumberger, E.:* SOL Studies for W7-X Based on the Island Divertor Concept. Nucl. Fusion **38**, 891-908 (1996).

232. *Suttrop, W., K. Büchl, H.J. de Blank, J. Schweinzer, H. Zohm, ASDEX Upgrade Team, NI-Group* and *ICRH-Group:* Characteristics of Edge Localized Modes in ASDEX Upgrade. Plasma Phys. Control. Fusion **38**, 1407-1410 (1996).

233. *Suttrop, W., H.J. de Blank, G. Haas, H. Murmann, O. Gehre, H. Reimerdes, F. Ryter, H. Salzmann, J. Schweinzer, J. Stober, H. Zohm, ASDEX Upgrade Team, NI-Team* and *ICRH-Team:* The Role of Edge Parameters for L-H Transition and ELM Behaviour on ASDEX Upgrade. In: Proc. 23rd Conf. Control. Fusion and Plasma Phys., Kiev 1996, Eds. D.Gresillon, A.Sitenko, A.Zagorodny. ECA 20C. Europ. Phys. Soc., Geneva 1996, 47-50.

234. *Taglauer, E., J. du Plessis** and *G.N. van Wyk*:* Surface Segregation and Preferential Sputtering of Binary Alloys. In: Surface Science - Principles and Current Applications, Eds. R.J.MacDonald, E.C.Taglauer, K.R.Wandelt. Springer, Berlin 1996, 136-145.

235. *Taglauer, E., S. Reiter, A. Liegl** et al.*:* Ion Scattering and Scanning Tunneling Microscopy Studies of Stepped Cu Surfaces. Nucl. Instrum. Methods Phys. Res., B **118**, 456-461 (1996).

236. *Tasso, H.:* Energy Methods in Magnetohydrodynamics. In: Proc. Workshop on Energy Methods in Continuum Mechanics, Oviedo 1996, Eds. S.N.Antonsev, J.I.Diaz, S.I.Shmarev. Kluwer, Dordrecht 1996, 158-174.

237. *Tasso, H.:* Hamiltonian Formulation of Odd Burgers Hierarchy. J. Phys. A **29**, 7779-7784 (1996).

238. *Tasso, H.:* Hamiltonians and Fluctuations of Continuous Plasma Models. Nuovo Cim., B **111**, 343-354 (1996).

239. *Tasso, H.:* Hamiltonians and Statistics of Continuous Plasma Models. ZAMM Suppl. **4**, 241-244 (1996).

240. *Tasso, H.:* On Magnetized Parallel Flows. Phys. Lett. A **222**, 97-100 (1996).

241. *Tasso, H.* and *W. Horton*:* Statistical Properties of the Drift Wave Fluctuations. Plasma Phys. Rep. **22**, 701-713 (1996).

242. *Thannhäuser, G.:* Rechtsfragen partnerschaftlicher Infrastrukturprojekte. Wirtschaftsrechtl. Beratung **3**, 336-340 (1996).

243. *Theimer, G., M. Endler, L. Giannone, H. Niedermeyer* et al.*:* Individual Event Analysis: A New Tool for the Investigation of Structures in Turbulence. In: Transport, Chaos and Plasma Physics 2, Eds. S.Benkadda, F.Doveil, Y.Elskens. World Scientific Publ., Singapore 1996, 89-92.

244. *Thomson, K.* and *H-Mode Database Working-Group:* Scaling Studies of Plasma Energy Confinement and of H-Mode Power Threshold. In: Proc. 12th Symp. Computational Statistics, Barcelona 1996, Eds. A.Prat, E.Ripoli. Physica-Verl., Heidelberg 1996, 123-124.

245. *Throumoulopoulos, G.N.* and *D. Pfirsch:* Negative-Energy Perturbations in Circularly Cylindrical Equilibria within the Framework of Maxwell-Drift Kinetic Theory. Phys. Rev., E **53**, 2767-2777 (1996).

246. *Verplancke, P.:* Characteristics of a Langmuir Probe in a Magnetic Field with High Sweep Frequencies. Contrib. Plasma Phys. **36**, 145-150 (1996).

247. *Weinlich, M.* and *A. Carlson:* Flush Mounted Probes in ASDEX Upgrade - Can they be Operated as Triple Probes? Contrib. Plasma Phys. **36**, 53-60 (1996).

248. *Weinlich, M., A. Carlson, R. Chodura, C.S. Pitcher, V. Rohde, U. Wenzel, ASDEX-Upgrade Team* and *NI-Team:* Electron Temperature in Front of the Target Plates in Various Divertor Scenarios in ASDEX Upgrade. In: Proc. 23rd Conf. Control. Fusion and Plasma Phys., Kiev 1996, Eds. D.Gresillon, A.Sitenko, A.Zagorodny. ECA 20C. Europ. Phys. Soc., Geneva 1996, 715-718.

249. *Weisen*, H., V. Piffl*, A. Weller* et al.*:* Measurement and Modelling of Light Impurity Behaviour in TCV. In: Proc. 23rd Conf. Control. Fusion and Plasma Phys., Kiev 1996, Eds. D.Gresillon, A.Sitenko, A.Zagorodny. ECA 20C. Europ. Phys. Soc., Geneva 1996, 111-114.

250. *Wenzel, U., B. Napiontek, G. Fußmann, H. Kastelewicz, M. Laux* and *A. Thoma:* Interpretation of the Carbon Line Emission in the ASDEX Upgrade Divertor. In: Proc. 23rd Conf. Control. Fusion and Plasma Phys., Kiev 1996, Eds. D.Gresillon, A.Sitenko, A.Zagorodny. ECA 20C. Europ. Phys. Soc., Geneva 1996, 799-802.

251. *Werthmann, H.* and *M. Brambilla:* On the Efficiency of Ion Bernstein Wave Launching. Nucl. Fusion **36**, 1357-1367 (1996).

252. *Wesner, F., W. Becker, F. Braun, H. Faugel, F. Hofmeister, R. Neu, J.-M. Noterdaeme, M. Schittenhelm, T. Sperger, P. Verplancke, ICRF-Group, ASDEX Upgrade Team, NI-Team* et al.*:* Recent Results from ICRF Experiments on ASDEX Upgrade. In: Proc. 11th Top. Conf. Radio Frequency Power in Plasmas, Palm Springs,CA 1995. Eds. R.Prater, V.S.Chan. AIP Conf. Proc. 355, AIP Press, New York,NY 1996, 15-22.

253. *Westerhof*, E., G. Giruzzi*, R.W. Harvey*, A.G. Peeters* et al.*:* Comments on 'Analysis of Electron Cyclotron Current Drive Using Neoclassical Fokker-Planck Code without Bounce-Average Approximation'. Phys. Plasmas **3**, 2827-2828 (1996).

254. *Westerhof*, E.* and *A.G. Peeters:* A Model for Bootstrap Current Calculations with Bounce Averaged Fokker-Planck Codes. Comput. Phys. Commun. **95**, 131-138 (1996).

255. *Wittmann*, M.* and *J. Küppers:* A Model of Hydrogen Impact Induced Chemical Erosion of Carbon Based on Elementary Reaction Steps. J. Nucl. Mater. **227**, 186-194 (1996).

256. *Wobig, H.:* On Rotation of Multi-Species Plasmas in Toroidal Systems. Plasma Phys. Control. Fusion **38**, 1053-1081 (1996).

257. *Wobig, H., C.D. Beidler, G. Grieger, E. Harmeyer, J. Kißlinger, J. Nührenberg, F. Rau, J. Sapper* et al.*:* Helias Reactor Studies. In: Proc. 6th Workshop Wendelstein 7-X and Helias Reactors, Schloß Ringberg, Tegernsee 1995, Eds. F.Herrnegger, F.Rau. IPP 2/331, IPP, Garching 1996, 154-171.

258. *Wolf, R., A. Herrmann, R. Brakel, Y. Feng, A. Elsner, L. Giannone, P. Grigull, D. Hildebrandt, F. Sardei* and *W7-AS-Team:* Study of the Power Balance in the W7-AS Stellarator by Means of 2-Dimensional Limiter Thermography and Bolometry. In: Proc. 23rd Conf. Control. Fusion and Plasma Phys., Kiev 1996, Eds. D.Gresillon, A.Sitenko, A.Zagorodny. ECA 20C. Europ. Phys. Soc., Geneva 1996, 583-586.

259. *Wolle*, B., Y. Feng, S. Koch** et al.*:* Measurement of Neutron Emission Profiles and Neutron Spectra by Means of Nuclear Emulsions. Nucl. Instrum. Meth. Phys. Res., A **368**, 425-430 (1996).

260. *Zeiler, A., D. Biskamp* and *J.F. Drake*:* Three-Dimensional Collisional Drift-Wave Turbulence: Role of Magnetic Shear. Phys. Plasmas **3**, 3947-3956 (1996).

261. *Zeiler, A., D. Biskamp, J.F. Drake** et al.*:* Three-Dimensional Fluid Simulations of Tokamak Edge Turbulence. Phys. Plasmas **3**, 2951-2960 (1996).

262. *Zeiler, A., J.F. Drake** and *D. Biskamp:* Electron Temperature Fluctuations in Drift-Resistive Ballooning Turbulence. In: Proc. 23rd Conf. Control. Fusion and Plasma Phys., Kiev 1996, Eds. D.Gresillon, A.Sitenko, A.Zagorodny. ECA 20C. Europ. Phys. Soc., Geneva 1996, 3-6.

263. *Zohm, H.:* Edge Localized Modes (ELMs). Plasma Phys. Control. Fusion **38**, 105-128 (1996).

264. *Zohm, H.:* The Physics of Edge Localized Modes (ELMs) and their Role in Power and Particle Exhaust. Plasma Phys. Control. Fusion **38**, 1213-1223 (1996).

265. *Zohm, H., M. Alexander, R. Buttery*, S. de Peña Hempel, O. Gruber, T. Kass, M. Maraschek, W. Sandmann, S. Sesnic, M. Sokoll, A. Stäbler, H.-P. Zehrfeld, ASDEX Upgrade Team, NI-Team* et al.*:* Beta-Limiting Phenomena in ASDEX Upgrade. In: Proc. 23rd Conf. Control. Fusion and Plasma Phys., Kiev 1996, Eds. D.Gresillon, A.Sitenko, A.Zagorodny. ECA 20C. Europ. Phys. Soc., Geneva 1996, 43-46.

266. *Zolotukhin, A.V., C.D. Beidler, F. Herrnegger, J. Kißlinger* and *H. Wobig:* Guiding Center Motion of Collisionless $\alpha$–Particles in a Helias Reactor Configuration. In: Proc. 23rd Conf. Control. Fusion and Plasma Phys., Kiev 1996, Eds. D.Gresillon, A.Sitenko, A.Zagorodny. ECA 20C. Europ. Phys. Soc., Geneva 1996, 475-478.

267. *Zolotukhin, A.V., F. Herrnegger* and *H. Wobig:* Guiding Center Studies for $\alpha$-Particles in HSR. In: Proc. 6th Workshop Wendelstein 7-X and Helias Reactors, Schloß Ringberg, Tegernsee 1995, Eds. F.Herrnegger, F.Rau. IPP 2/331, IPP, Garching 1996, 178-186.

268. *Zvonkov*, S., G. Igonkina*, A. Stefanovskij** and *A. Herrmann:* Wall Conditioning in T-15: Investigations of Wall Surface State by WASA II. In: Proc. 23rd Conf. Control. Fusion and Plasma Phys., Kiev 1996, Eds. D.Gresillon, A.Sitenko, A.Zagorodny. ECA 20C. Europ. Phys. Soc., Geneva 1996, 747-750.

## Diploma Theses

269. *Bach, F.-P.:* Charakterisierung von amorphen Kohlenwasserstoffschichten. Univ. Bayreuth 1996.

270. *Bauernschmitt, U.:* Bestimmung der Elektronentemperatur in Niederdruckplasmen mittels optischer Emissionsspektroskopie. Univ. Bayreuth 1996.

271. *Fuchs, T.:* Bestimmung des Energiehaushaltes und des Leistungseintrages in Targets am Plasmagenerator PSI-1. Humboldt-Univ. Berlin 1996.

272. *Grote, K.:* Dynamische Eigenschaften von Einschrittverfahren. Techn. Univ. München 1996.

273. *Müller, H.W.:* Studie zur q-Profil Bestimmung mittels Pelletablation an ASDEX Upgrade. Univ. Bayreuth 1996.

274. *Murtfeld, U.:* Untersuchung der NiAl(100)-Oberfläche mit LEED und niederenergetischer Ionenstreuung. Univ. München 1996.

275. *Pöhlmann, K.:* Wechselwirkungen von H-Atomen mit physisorbierten Kohlenwasserstoffen. Univ. Bayreuth 1996.

276. *Reimerdes, H.:* Bestimmung lokaler Transportkoeffizienten während Edge Localized Modes am Tokamakexperiment ASDEX Upgrade. Techn. Univ. München 1996.

277. *Saß, M.:* Deposition und Charakterisierung amorpher hydrogenisierter Bor-Schichten. Techn. Univ. München 1996.

278. *Schwarz-Selinger, T.:* Einfluß der Quellgase auf die plasmagestützte Deposition von Kohlenwasserstoff-Schichten. Techn. Univ. München 1996.

279. *Ullrich, W.:* Messung sekundärer Fusionsreaktionen in ASDEX Upgrade. Univ. Augsburg 1996.

280. *Wölfl, F.:* Der Effekt von Edge Localized Modes auf den Einschluß von Teilchen und Energie im Tokamak. Univ. Augsburg 1996.

281. *Zecho, T.:* Wechselwirkungen thermischer Wasserstoffatome mit einer Monolage Graphit unter katalytischem Einfluß von Pt(100). Univ. Bayreuth 1996.

## Doctoral Theses

282. *Asmussen, K.:* Untersuchungen zum Verhalten von Wolfram in Tokamakplasmen. Techn. Univ. München 1996.

283. *Gubanka, B.:* Magnetische Oberflächeneffekte in Dünnschichtsystemen: Untersuchungen der spinabhägigen elektronischen Struktur. Univ. Bayreuth 1996.

284. *Hanesch, P.:* Die Pt(110)-Oberfläche und die Adsorption von Brom: mikroskopische und mesoskopische Struktur, Bindungsverhältnisse. Univ. Bayreuth 1996.

285. *Kass, T.:* Untersuchungen zum Verhalten hochenergetischer Ionen in magnetisch eingeschlossenen Plasmen. Techn. Univ. München 1996.

286. *Keudell, A. von:* Wachstumsmechanismen bei der plasmagestützten Abscheidung von Kohlenwasserstoffschichten, eine in-situ Ellipsometriestudie. Bayreuth Univ. 1996.

287. *Kornejew, P:* Bestimmung der Elektronenparameter in Randschichtplasmen unter Verwendung eines thermischen Heliumstrahls. Humboldt-Univ. Berlin 1996.

288. *Napiontek, B.:* Untersuchung der Strahlungsbilanz im Divertor von ASDEX Upgrade. Humboldt-Univ. Berlin 1996.

289. *Unverzagt, M.:* Bedeutung der Energie dynamischer, zugänglicher linearer Störungen eines Gleichgewichts für dessen Stabilität angewandt auf quasineutrale elektrostatische oder magnetodynamische Driftstörungen. Techn. Univ. München 1996.

290. *Verplancke, P.:* Langmuirsondes bij hoge frequenties in een gemagnetiseerd plasma: een theoretische en experimentele studie. Univ. Gent 1996.

## Habilitation

291. *Günter, S.:* Optische Eigenschaften dichter Plasmen. Univ. Rostock 1996.

## Patents

292. *Braun, F.:* Hochleistungsdämpfungsglied. Deutschland P 4301583, Freigabe: 27.11.1996.

293. *Gehringer, K.:* Vorrichtung zum Eindrücken von Dichtungsringen in Flansche. Deutschland Gbm 29519353.0, Gebrauchsmustereintragung: 25.1.1996.

294. *Haas, G.:* Heißkathoden-Ionisationsmanometer. Japan Gbm 2139214, Patenterteilung: 15.10.1996.

295. *Heinemann, B., R. Riedl, M. Busch** et al.: Vakuumgefäß. Deutschland 196 35 136.7, Anmeldung: 26.8.1996.

296. *Kotzlowski, H.:* Aktiv gekühlte Einrichtung. Japan Nr. 60-502223, Erteilungsbeschluß: 23.1.1996.

297. *Kraus, W.:* Isolierte Antenne für Hochfrequenz-Plasmageneratoren. Deutschland P 42 41 927, Freigabe: 30.9.1996, Europaanmeldung Nr. 93119967.3, Aufgabe.

298. *Liebl, H.:* Kompaktes Massenspektrometer. US-Patent Nr. 4,843,239, Freigabe: 24.10.1996.

299. *Liebl, H.* and *B. Senftinger:* Elektronenmikroskop. Japan Patent Nr. 1883108, Freigabe: 19.11.1996.

300. *Mukherjee, S.B.:* Wärmeschutzschild. Japan Patentanmeldung Nr. HEI I-212834, Freigabe: 22.7.1996.

301. *Richter, H.:* Modulares Koppelnetz. US-Patent Nr. 5,175,539, Freigabe: 7.5.1996.

302. *Schauer, F.:* Gasdurchlässige Hochspannungsisolation. Deutschland DE 19504 857A1, Offenlegung: 22.8.1996, PCT-Anmeldung Europa/USA/Japan: 9.2.1996, Nr. PCT/EP96/00559.

303. *Schäftner, J.:* Dichtringabziehvorrichtung. Deutschland Gbm 296 01 651.9, Gebrauchsmusteranmeldung: 31.1.1996, Gebrauchsmustereintragung: 23.5.1996.

304. *Schneider, F.:* Hybrider Regler. Europa (EP-DE, FR, NL, CH, GB) Nr. 0418832, Patenterteilung: 28.8.1996.

305. *Weichselgartner, H.:* TARA-System. US-Patent Nr. 4,490,228, Freigabe: 7.5.1996.

306. *Wilhelm, R.:* Mikrowellenplasmaverfahren zur PCVD-Innenbeschichtung metallischer Rohre. Japan Patentanmeldung Nr. 149764/89, Freigabe: 2.7.1996.

307. *Wilhelm, R., W. Möller* and *R. Hytry:* Verfahren und Einrichtung zur PECVD-Innenbeschichtung. Europa (EP-DE, CH, FR, GB, IT, Lichtenstein) Nr. 0568049, Patenterteilung: 24.1.1996.

# Lectures

308. *Annen, A., A. von Keudell, R. Beckmann* and *W. Jacob:* Deposition und Charakterisierung amorpher hydrogenisierter Bor-Kohlenstoff-Schichten (a-B/C:H). Verhandl. DPG (VI) **31**, 1180, DS12.2 (1996).

309. *Annen, A., A. von Keudell, R. Beckmann* and *W. Jacob:* Erosion von amorphen hydrogenisierten Bor-Kohlenstoff-Schichten (a-B/C:H) in Wasserstoffplasmen unter gleichzeitigem Ionenbeschuß. Verhandl. DPG (VI) **31**, 705, P4.2 (1996).

310. *Asmussen, K., W. Engelhardt, R. Neu, K. Behringer, M. Bessenrodt-Weberpals, R. Dux, J.C. Fuchs, S. Hirsch, K. Krieger, K.-F. Mast, A. Thoma, U. Wenzel, ASDEX Upgrade Team, NI-Team, ICRH-Team* and *ECRH-Team:* Erste spektroskopische Untersuchungen zum Verhalten des Wolfram-Divertors an ASDEX Upgrade. Verhandl. DPG (VI) **31**, 757, P15.42 (1996).

311. *Bach, F.-P., R. Beckmann* and *W. Jacob:* Untersuchung der Struktur und chemischen Zusammensetzung von a-C:H-Schichten. Verhandl. DPG (VI) **31**, 1235, DS39.48 (1996).

312. *Bauernschmitt, U., R. Beckmann, W. Jacob* and *V. Dose:* Läßt sich die Elektronentemperatur in Niederdruckplasmen mittels optischer Emissionsspektroskopie bestimmen? Verhandl. DPG (VI) **31**, 708, P5.6 (1996).

313. *Bauernschmitt, U., R. Beckmann, W. Jacob* and *V. Dose:* Stoß-Strahlungsmodell zur optischen Bestimmung der Elektronentemperatur in Niederdruckplasmen. Verhandl. DPG (VI) **31**, 775, P20.17 (1996).

314. *Beckmann, R., U. Bauernschmitt, W. Jacob* and *V. Dose:* Läßt sich die Elektronentemperatur in Niederdruckplasmen mittels optischer Emissionsspektroskopie bestimmen? 7. Bundesdt. Fachtagung Plasmatechnologie, Bochum 1996.

315. *Behringer, K.:* Aktuelle Fragen der Plasmaphysik. Seminar, Univ. Augsburg, SS 1996.

316. *Behringer, K.:* Aktuelle Fragen der Plasmaphysik. Seminar, Univ. Augsburg, WS 1996/97.

317. *Behringer, K.:* Einführung in die Plasmaspektroskopie. Vorlesung, Univ. Augsburg, WS 1996/97.

318. *Behringer, K.:* Experimental Observations and Analysis Techniques. Workshop on Atomic Physics and Astrophysics and its Implementation in the Atomic Data and Analysis Structure, Oak Ridge,TN 1996.

319. *Behringer, K.:* Experimental Observations and Analysis Techniques for the Main Plasma. Workshop on Atomic Physics and Astrophysics and its Implementation in the Atomic Data and Analysis Structure, Oak Ridge,TN 1996.

320. *Behringer, K.:* Extracting Data from ADAS for Fusion. Workshop on Atomic Physics and Astrophysics and its Implementation in the Atomic Data and Analysis Structure, Oak Ridge,TN 1996.

321. *Behringer, K.:* Hydrogen Opacity Effects in Fusion Plasmas. 2nd ADAS Workshop in Astrophys. and Lab. Fusion Plasmas, Abingdon 1996.

322. *Behringer, K.:* Measurement of NI and NII Excitation Rate Coefficients in Low Pressure Arc Discharges. 2nd ADAS Workshop in Astrophys. and Lab. Fusion Plasmas, Abingdon 1996.

323. *Behringer, K.:* Moleküle in Fusionsexperimenten und reaktiven Plasmen - Grundlagen und Ergebnisse spektroskopischer Diagnostikmethoden. Seminar, Univ. Bochum 1996.

324. *Behringer, K.:* Spektroskopie von Nichtgleichgewichtsplasmen. Vorlesung, Univ. Augsburg, SS 1996.

325. *Behringer, K.:* Spektroskopische Diagnostik an NI and NII mit ADAS. Seminar, Univ. Stuttgart 1996.

326. *Behrisch, R.:* Beitrag der Gefäßwände zur Wasserstoffteilchenbilanz bei Fusionsexperimenten. Kolloquiumsvortrag, Hahn-Meitner-Inst. Berlin 1996.

327. *Behrisch, R.:* Elementarprozesse der Plasma-Wand-Wechselwirkung. Plasmakolloquium, IPF Stuttgart 1996.

328. *Behrisch, R.:* Surface Layer Characterisation by High Energy Heavy-Ion Elastic Recoil Detection. Gordon Res. Conf. on Particle Solid Interactions, Plymouth State College, New Hampshire 1996.

329. *Beidler, C.D., G. Grieger, E. Harmeyer, F. Herrnegger, J. Kißlinger, J. Nührenberg, F. Rau, J. Sapper, H. Wobig, A.V. Zolotukhin* et al.: The Helias Reactor. 16th IAEA Fusion Energy Conf., Montreal 1996.

330. *Beidler, C.D.* and *H. Maaßberg:* Neoclassical Transport in Advanced Stellarators. Workshop on Theory of Fusion Plasmas, Varenna 1996.

331. *Beilis*, I., B. Djakov*, B. Jüttner* et al.: Number and Dynamics of Arc Cathode Spots in High Current Vacuum Discharges. Verhandl. DPG (VI) **31**, 702, P2.2 (1996).

332. *Bertel, E.:* Electronic Surface States and the Hydrogen Dissociation Barrier. WE-Heraeus Seminar, Ilmenau 1996.

333. *Bertel, E.:* Promoters, Poisons and Surfactants: Electronic Effects of Surface Doping on Metals. 15th Gen. Conf. of the Cond. Matter Div. of the EPS, Baveno 1996.

334. *Bertel, E.:* Promotoren, Inhibitoren und Surfactants: Oberflächendotierung von Metallen in Katalyse und Epitaxie. Univ. Innsbruck 1996.

335. *Bertel, E.:* Promotoren, Inhibitoren und Surfactants: Zum Wirkungsmechanismus der Oberflächendotierung von Metallen. Univ. Kassel 1996.

336. *Bertel, E.:* Promotoren, Inhibitoren und Surfactants: Zum Wirkungsmechanismus der Oberflächendotierung von Metallen. Verhandl. DPG (VI) **31**, 1758, OV (1996).

337. *Bertel, E.:* Stress und mesoskopische Oberflächenmorphologie von Pt(110). SFB-338 Seminar, Filzmoos 1996.

338. *Bertel, E.:* Stress-induzierter Einbau von Alkalimetallen in Pt(111)? Univ. Marburg 1996.

339. *Bessenrodt-Weberpals, M.:* Hochtemperatur-Plasmaphysik. Vorlesung, Univ. Düsseldorf, WS 1996/97.

340. *Bessenrodt-Weberpals, M.:* Plasmatechnologie. Vorlesung, Univ. Düsseldorf, WS 1996/97.

341. *Biedermann, C., A. Förster*, G. Fußmann* and *R. Radtke:* First Results from the Berlin EBIT. 8th Conf. Physics of Highly Charged Ions, Omiya, Saitama, Japan 1996.

342. *Biskamp, D.:* Electron Magnetohydrodynamic Turbulence. 2nd Workshop on Nonlinear Dynamics, New York,NY 1996.

343. *Biskamp, D.:* Studies in Collisionless Magnetic Reconnection. APS-DDP Meeting, Denver,CO 1996.

344. *Bleuel, J., M. Endler, H. Niedermeyer* and *G. Theimer:* Investigation of Plasma Edge Turbulence in W7-AS with Langmuir Probe Arrays. EU-US Transport Task Force Workshop, Varenna 1996.

345. *Bleuel, J., M. Endler, H. Niedermeyer* and *G. Theimer:* Korrelationsmessungen in der Abschälschicht von W7-AS. Verhandl. DPG (VI) **31**, 758, P15.46 (1996).

346. *Borrass, K., D.P. Coster, D. Reiter** and *R. Schneider:* Study of Recombining Gas Targets. 12th Int. Conf. on Plasma Surface Interactions in Controlled Fusion Devices, St. Raphael 1996.

347. *Bosch, H.-S.:* Helium Transport in ASDEX Upgrade. Kolloquium, IPF Stuttgart 1996.

348. *Bosch, H.-S.:* Nuclear Fusion - Energy Source in the Stars and also on Earth? ESO Astronomy Course, ESO, Garching 1996.

349. *Bosch, H.-S.:* Review on Recent Experiments on Tungsten, Erosion and Wall Sources. 5th ITER Divertor Expert Group Meeting, Montreal 1996.

350. *Bosch, H.-S., D.P. Coster, R. Dux, J.C. Fuchs, G. Haas, A. Herrmann, S. Hirsch, A. Kallenbach, J. Neuhauser, R. Schneider, J. Schweinzer, M. Weinlich, ASDEX Upgrade Team* and *NI-Team:* Particle Exhaust in Radiative Divertor Experiments. 12th Int. Conf. on Plasma Surface Interactions in Controlled Fusion Devices, St. Raphael 1996.

351. *Bosch, H.-S., D.P. Coster, R. Dux, G. Haas, A. Kallenbach, W. Poschenrieder* and *R. Schneider:* Heliumtransport in der Plasmarandschicht von ASDEX Upgrade. Verhandl. DPG (VI) **31**, 765, P17.7 (1996).

352. *Bosch, H.-S., A. Kallenbach, D.P. Coster, R. Dux, G. Haas, M. Kaufmann, K. Lackner, J. Neuhauser, S. de Peña Hempel, R. Schneider, ASDEX Upgrade Team, NI-Team* and *ICRH-Team:* Impurity Transport and Exhaust in Radiative Edge Experiments in ASDEX Upgrade. 16th IAEA Fusion Energy Conf., Montreal 1996.

353. *Bosch, H.-S., J. Neuhauser, W. Sandmann, J. Schweinzer:* ITER Edge Database Contributions of ASDEX Upgrade. 4th ITER Divertor Expert Group Meeting, San Diego,CA 1996.

354. *Bowman, J.C.:* Spectral Reduction for Two-Dimensional Turbulence. Univ. Düsseldorf 1996.

355. *Bowman, J.C.:* Spectral Reduction for Two-Dimensional Turbulence. Workshop on Non-Conservative Processes, Cambridge 1996.

356. *Brakel, R., W7-AS-Team, W7-X-Team, NI-Team* et al.: Experimentelle Ergebnisse des Stellarators W7-AS und ihre Bedeutung für W7-X. Verhandl. DPG (VI) **31**, 763, P17.1 (1996).

357. *Braun, F.:* An Arc Detection Method for ICR-Heating Sytems. 19th Symp. on Fusion Technology, Lisbon 1996.

358. *Brinkschulte, H., F. Leuterer, F. Monaco, M. Münich* et al.: The 140 GHz/2MW/2 sec ECRH System for ASDEX Upgrade. 19th Symp. on Fusion Technology, Lisbon 1996.

359. *Brinkschulte, H., F. Leuterer, M. Münich, F. Monaco, A.G. Peeters, F. Ryter* and *W. Suttrop:* ECRH in ASDEX Upgrade - Description of the RF System and First Results. 3rd Int. Workshop on Strong Microwaves in Plasmas, Moscow 1996.

360. *Burhenn, R.:* Investigations on the Transport of Injected Impurity Tracers at the Stellarator Wendelstein 7-AS. Southwestern Inst. of Physics, Leshan,China 1996.

361. *Burhenn, R.:* Measurement of Edge Density and Temperature Using LBO-Technique (Review). Southwestern Inst. of Physics, Leshan,China 1996.

362. *Burhenn, R.:* Stellarators W7-AS and W7-X: Features and Capabilities of the Low-Shear Modular Stellarator Concept. Southwestern Inst. of Physics, Leshan,China 1996.

363. *Burtseva*, T., V. Barabash*, I. Mazul*, C. García-Rosales, S. Deschka, R. Behrisch* and *A. Herrmann:* Performance of the Ti Doped Carbon Rg-Ti 91 at the Divertor of the Tokamak ASDEX Upgrade. 12th Int. Conf. on Plasma Surface Interactions in Controlled Fusion Devices, St. Raphael 1996.

364. *Carlson, A.:* How Turbulence Can Determine a Langmuir Probe Characteristic. PPPL, Princeton 1996.

365. *Carlson, A., R. Chodura, A. Herrmann, M. Weinlich* and *ASDEX Upgrade Team:* The Credibility of Flush Mounted Langmuir Probes in ASDEX Upgrade. 12th Int. Conf. Plasma Surface Interactions in Controlled Fusion Devices, St. Raphael 1996.

366. *Carlson, A., V. Rohde, M. Weinlich* and *ASDEX Upgrade Team:* The Separation of Angle and Size Effects on Langmuir Probe Characteristics. 12th Int. Conf. on Plasma Surface Interactions in Controlled Fusion Devices, St. Raphael 1996.

367. *Cattanei, G., D. Hartmann* and *J.F. Lyon*:* Plasma Heating and Sustainment with ICRH on W7-AS. 38th Annual Meeting of the Div. of Plasma Physics, Denver,CO 1996.

368. *Coster D.P., R. Schneider, J. Neuhauser, H.-S. Bosch, R. Wunderlich, J.C. Fuchs, K.-F. Mast, A. Kallenbach, R. Dux, G. Becker, ASDEX Upgrade Team* et al.: B2-Eirene Modelling of ASDEX Upgrade. 12th Int. Conf. on Plasma Surface Interactions in Controlled Fusion Devices, St. Raphael 1996.

369. *De Blank, H.J., J. Schweinzer, W. Suttrop, H. Zohm* and *ASDEX Upgrade Team:* Local Stability Criteria and Type I Edge Localized Modes. 23rd EPS Conf. on Controlled Fusion and Plasma Physics, Kiev 1996.

370. *Deschka, S., S. Schweizer, B. Streibl, C. García-Rosales, G. Hofmann, ASDEX Upgrade Team* et al.: Divertor II Plasma Facing Components for ASDEX Upgrade. 19th Symp. on Fusion Technol., Lisbon 1996.

371. *Donath, M.:* Elektronische Oberflächenzustände in magnetischen Systemen mit itineranten und lokalisierten Momenten. Festkörperphysik-Seminar, Univ. Zürich-Irchel 1996.

372. *Donath, M.:* Elektronische Oberflächenzustände in magnetischen Systemen mit itineranten und lokalisierten Momenten. Kolloquium zur Festkörpertheorie, Humboldt-Univ. Berlin 1996.

373. *Donath, M.:* Ferromagnetismus und spinabhängige elektronische Struktur in niedrigdimensionalen Systemen. Phys. Kolloquium, Univ. Münster 1996.

374. *Donath, M.:* Oberflächenuntersuchungen mit spinpolarisierten Elektronen. Plasmakolloquium, IPF Stuttgart 1996.

375. *Donath, M.:* Spin-Dependent Electronic Structure in Magnetic Systems of Reduced Dimension. Seminar Festkörperphysik, Univ. de Fribourg 1996.

376. *Donath, M., B. Gubanka, F. Passek* and *V. Dose:* Magnetic Order of fcc-Like Fe Films on Cu(001): New Insight Gained from the Spin Dependence of Electronic States. 15th Gen. Conf. of the Cond. Matter Div. of the EPS, Baveno 1996.

377. *Dose, V.:* How to Separate the Signal from the Background. Conf. MaxEnt and Bayesian Methods, Bergendaal 1996.

378. *Dose, V.:* Nuclear Fusion. Univ. of Bloemfontein 1996.

379. *Dose, V.:* Physikalische Prinzipien der Kernfusion. Univ. Kassel 1996.

380. *Dose, V.:* Spline-Based Adaptive Resolution Image Reconstruction. Conf. MaxEnt and Bayesian Methods, Bergendaal 1996.

381. *Dose, V.:* Spline Theory and the Bayesian Connection. Nat. Accelerator Center and the Univ. of Cape Town 1996.

382. *Dose, V.:* Surface Physics at IPP. Nat. Accelerator Center and the Univ. of Cape Town 1996.

383. *Dose, V.:* Wavelets. Plasmakolloquium, IPF Stuttgart 1996.

384. *Dose, V.:* Wavelets. Univ. of Bloemfontein 1996.

385. *Dose, V.:* Wege und Irrwege zur Inversen Photoemission. Ehrenpromotion, Univ. Kassel 1996.

386. *Drevlak, M., R. Brinkmann** and *R. Wanzenberg**: Improved Beam Stability with New Parameter Set for the S-Band Linear Collider. LINAC-96, Geneva 1996.

387. *Drevlak, M., M. Timm** and *T. Weiland**: Simulation of Linac Operation Using the Tracking Code L. LINAC-96, Geneva 1996.

388. *Düchs, D.F.:* Energie aus kontrollierter Kernfusion. Vorlesung, Univ. Bochum, WS 1996/97.

389. *Düchs, D.F.:* Theorie zum Transport in heißen magnetisierten Plasmen. Vorlesung, Univ. Bochum, SS 1996.

390. *Düchs, D.F.:* Zur Theorie der Diagnostiken und Datenauswertung bei Fusionsplasmen. Vorlesung, Univ. Bochum, WS 1996/97.

391. *Dux, R.:* Plasmaphysik und Fusionsforschung. Vorlesung, Univ. Augsburg, WS 1996/97.

392. *Dux, R., K. Behringer, M. Bessenrodt-Weberpals, J.C. Fuchs, A. Kallenbach, K.-F. Mast, ASDEX Upgrade Team, NI-Team* and *ICRH-Team:* Messung und Modellierung der Hauptraumstrahlung bei Experimenten mit strahlender Randschicht an ASDEX Upgrade. Verhandl. DPG (VI) **31**, 764, P17.5 (1996).

393. *Eckstein, W.:* Computer Simulation of Isotope Effect on Sputtering. Univ. of Science, Okayama 1996.

394. *Eckstein, W.:* Dynamische Änderungen eines Festkörpers durch Ionenbeschuß. ETH Zürich 1996.

395. *Eckstein, W.:* Isotope Sputtering. Moscow State Univ. 1996.

396. *Eckstein, W.:* Isotope Sputtering. Osaka Electro-Communication Univ., Osaka 1996.

397. *Eckstein, W.:* Physical Sputtering and Reflection in Plasma-Wall Interaction. Nat. Inst. for Fusion Science, Nagoya 1996.

398. *Eckstein, W.:* Physical Sputtering and Reflection Processes in Plasma-Wall Interactions. Int. Workshop on Interfacial Effects in Quantum Engineering Systems, Mito 1996.

399. *Eckstein, W.:* Sputtering of Multicomponent Systems. Nat. Inst. of Metals, Tsukuba 1996.

400. *Ehrenberg**, *J.K., D.J. Campbell**, *P.J. Harbour**, *K. McCormick* et al.: Neutral Particle Compression in the JET Mk I Divertor. 12th Int. Conf. on Plasma Surface Interactions in Controlled Fusion Devices, St. Raphael 1996.

401. *Empacher**, *L., W. Förster**, *G. Gantenbein**, *V. Erckmann, T. Geist, H. Laqua* et al.: Conceptual Design of the 140 GHz/10 MW CW ECRH System for the Stellarator W7-X. 19th Symp. on Fusion Technology, Lisbon 1996.

402. *Erckmann, V.:* Overview on Recent Experiments with ECRH and ECCD at W7-AS. 8th Joint Russian-German Meeting on ECRH and Gyrotrons, Nizhny Novgorod 1996.

403. *Erckmann, V.:* Physics Experiments with ECRH and ECCD at W7-AS. Kurchatov Inst. of Atomic Energy Plasma Physics Dept., Moscow 1996.

404. *Erckmann, V.:* Shear Related Confinement with ECCD and Inductive Current Drive in W7-AS. EU-US Transport Task Force Workshop, Varenna 1996.

405. *Erckmann, V.:* Das W7-X Projekt in Greifswald. Fa. Spinner GmbH, München 1996.

406. *Erckmann, V., H. Laqua, U. Gasparino* et al.: High Density ECRH and Shear Related Confinement with ECCD in W7-AS. 16th IAEA Int. Conf. on Plasma Physics and Controlled Nuclear Fusion Research, Montreal 1996.

407. *Erckmann, V., M. Romé, A. Borschegovsky** et al.: Overview on ECRH and ECCD Experiments at the W7-AS Stellarator. 3rd Int. Workshop on Strong Microwaves in Plasmas, St. Petersburg 1996.

408. *Fantz**, *U., B. Heger** and *K. Behringer:* Besetzung der Vibrations- und Rotationszustände von $H_2$ und $N_2$ in Niederdruckplasmen. Verhandl. DPG (VI) **31**, 775, P20.18 (1996).

409. *Fantz** *U., B. Heger** and *K. Behringer:* Untersuchungen zur chemischen Erosion von Kohlenstoffschichten durch $H_2$- und $D_2$-Plasmen. Verhandl. DPG (VI) **31**, 783, P20.42 (1996).

410. *Feng, Y., F. Sardei, J. Kißlinger* and *P. Grigull:* A 3D Monte Carlo Code for Plasma Transport in Island Divertors. 12th Int. Conf. on Plasma Surface Interactions in Controlled Fusion Devices, St. Raphael 1996.

411. *Frank, P., J.-H. Feist, W. Kraus, E. Speth* et al.: Status of BATMAN. Joint Development Comm. Meeting, CEA, Cadarache 1996.

412. *Franzen, P.:* Thermische Desorption von Wasserstoff aus Graphit. Seminar, Univ. Magdeburg 1996.

413. *Franzen, P., C. García-Rosales, H. Plank* et al.: Hydrogen Trapping in and Release from Tungsten: Modelling and Comparison with Graphite with Regard to its Use as Fusion Reactor Material. 12th Int. Conf. on Plasma Surface Interactions in Controlled Fusion Devices, St. Raphael 1996.

414. *Fuchs, J.C., K. Büchl, E. Berger, V. Dose* and *ASDEX Upgrade Team:* Rekonstruktion der Lage von toroidal symmetrischen Strukturen aus CCD-Bildern an ASDEX Upgrade. Verhandl. DPG (VI) **31**, 747, P15.12 (1996).

415. *Fußmann, G.:* Forschungsaktivitäten im IPP-Berlin. Kolloquium, KFA Jülich 1996.

416. *Fußmann, G.:* Transport of Highly Charged Particles in Magnetized Plasmas. Int. Conf. Physics of Dusty Plasmas, Goa,Indien 1996.

417. *Geist, T.:* 160 GHz Interferometer zur Messung der linienintegrierten Elektronendichte in einem Plasma. Seminar, Techn. Univ. München 1996.

418. *Geist, T., E. Würsching* and *H.-J. Hartfuß:* 160 GHz Interferometer for Measurements of the Line Integrated Electron Density in Plasma Experiments. 4th Int. Workshop on Terahertz Electronics, Erlangen 1996.

419. *Giannone, L., A. Elsner, K. Ertl* et al.: Tomography by the Maximum Entropy Method for the W7-AS and W7-X Multichannel Bolometer Systems. 11th Topical Conf. on High Temperature Plasma Diagnostics, Monterey,CA 1996.

420. *Gori, S., W. Lotz* and *J. Nührenberg:* Quasi-Isodynamic Stellarators. Int. Workshop on Theory of Fusion Plasmas, Varenna 1996.

421. *Greuner, H., W. Bitter, R. Holzthüm, O. Jandl, F. Kerl, J. Kißlinger* and *H. Renner:* Divertor Engineering for the Stellarator Wendelstein 7-X. 19th Symp. on Fusion Technology , Lisbon 1996.

422. *Greuner, H., T. Huber*, J. Kißlinger* and *H. Renner:* Design, Manufacturing and Testing of the W7-X Target Element Prototypes. 19th Symp. on Fusion Technology, Lisbon 1996.

423. *Grieger, G.:* Aufgaben und Ziele für das in Greifswald zu errichtende Fusionsexperiment: Stellarator 'Wendelstein 7-X'. Hahn-Meitner-Inst., Berlin, 1996.

424. *Grieger, G.:* Ein europäisches Kernforschungsprojekt für Greifswald. Der Stellarator Wendelstein 7-X in Greifswald. Außenstellentagung der MPG, Beilngries 1996.

425. *Grieger, G.:* Fusion Power Coordinating Committee. - Report to CERT 6/96 - IEA, Paris 1996.

426. *Grieger, G.:* Das Fusionsexperiment Wendelstein 7-X in Greifswald. Öffentl. Abendvortrag, Arndt-Schule, Greifswald 1996.

427. *Grieger, G.:* News from Wendelstein 7-X. Nat. Inst. for Fusion Science, Nagoya 1996.

428. *Grieger, G.:* Stationary Operation of Wendelstein 7-X - The W7-X Superconducting Magnet. Fusion Evaluation Board, Garching 1996.

429. *Grieger, G.:* Der Stellarator Wendelstein 7-X in Greifswald. Humboldt-Univ. Berlin 1996.

430. *Grieger, G.:* Der Stellarator Wendelstein 7-X in Greifswald. Verhandl. DPG (VI) **31**, 513, PV3 (1996).

431. *Grieger, G.:* Der Stellarator Wendelstein 7-X in Greifswald. Univ. Greifswald 1996.

432. *Grieger, G.:* The Stellarator Wendelstein 7-X at Greifswald. Dt.-ital. Wissenschaftstag, Greifswald 1996.

433. *Grieger, G.* and *W7-X-Team:* The Wendelstein 7-X Project. 19th Symp. on Fusion Technology, Lisbon 1996.

434. *Grigull, P., J. Baldzuhn, R. Brakel* et al.: High Recycling in Island Divertor Configurations. 4th Europ. Fusion Physics Workshop, Stockholm 1996.

435. *Grigull, P., R. Brakel, Y. Feng, G. Herre, D. Hildebrandt, F. Sardei* and *W7-AS-Team:* High Recycling in Island Divertor Configurations. 4th Europ. Fusion Physics Workshop, Stockholm 1996.

436. *Grigull, P., Y. Feng, D. Hildebrandt, F. Sardei, G. Herre, O. Heinrich, A. Elsner, S. Fiedler, J.V. Hofmann, J. Kißlinger, G. Kühner, H. Niedermeyer, R. Schneider, H. Verbeek, F. Wagner, A. Weller, R. Wolf* and *W7-AS-Team:* High Recycling in W7-AS Island Divertor Configurations. 16th Int. Conf. Plasma Physics and Controlled Nuclear Fusion Research, Montreal 1996.

437. *Grigull, P., D. Hildebrandt, F. Sardei, Y. Feng, S. Fiedler, G. Herre, R. Brakel, J.V. Hofmann, J. Kißlinger, G. Kühner, H. Ringler, W7-AS-Team* and *NI-Group:* Experimental Study on Highly Collisional Edge Plasmas in W7-AS Island Divertor Configurations. 12th Int. Conf. Plasma Surface Interactions in Controlled Fusion Devices, St. Raphael 1996.

438. *Grote, H., W. Bohmeyer, H.-D. Reiner, H. Behrendt, G. Fußmann, H. Meyer, D. Naujoks, E. Pasch:* Comparison of Chemical Sputtering Yields for Different Graphites at High Ion Flux Densities. 12th Int. Conf. Plasma Surface Interaction in Controlled Fusion Devices, St. Raphael 1996.

439. *Gruber, O.:* Expert Group Comments on Beta Limit. Joint TAC&IPC Informal Technical Assessment on Physics (ITER DDR), Montreal 1996.

440. *Gruber, O.:* Report from the Subgroup on 'Interpretation of Events'. Tripartite Exchange Agreement Workshop on Effects of Plasma Behaviour on Tokamak Structural Components, JET, Abingdon 1996.

441. *Gruber, O.:* Summary on Disruption Mitigation by Killer Pellets. 4th ITER Physics R&D Expert Group Meeting on Disruption, Plasma Control and MHD, Naka 1996.

442. *Gruber, O., M. Alexander, F. Ryter, H.-U. Fahrbach, S. de Peña Hempel, H. Murmann, G. Pereverzev, J. Schweinzer, W. Suttrop, ASDEX Upgrade Team, NI-Team* et al.: ρ S Experiments in L and H Mode in ASDEX Upgrade. EU-US Transport Task Force Workshop, Varenna 1996.

443. *Gruber, O.* and *ASDEX Upgrade Team:* Asymmetries during Disruptions and Interaction with the Structures in ASDEX Upgrade. Tripartite Exchange Agreement Workshop on Effects of Plasma Behaviour on Tokamak Structural Components, JET, Abingdon 1996.

444. *Gruber, O.* and *ASDEX Upgrade Team:* The Control System of ASDEX Upgrade. 3rd ITER Plasma Control Task Force Meeting, Naka 1996.

445. *Gruber, O.* and *ASDEX Upgrade Team:* Disruptions and VDEs in ASDEX Upgrade - Disruption Mitigation by Impurity Pellets. 4th ITER Physics R&D Expert Group Meeting on Disruption, Plasma Control and MHD, Naka 1996.

446. *Gruber, O.* and *ASDEX Upgrade Team:* Disruptions and VDEs in ASDEX Upgrade - Halo Currents and Stress Forces. 4th ITER Physics R&D Expert Group Meeting on Disruption, Plasma Control and MHD, Naka 1996.

447. *Gruber, O.* and *ASDEX Upgrade Team:* Disruptions and VDEs in ASDEX Upgrade - Power Balance and Target Heat Load. 4th ITER Physics R&D Expert Group Meeting on Disruption, Plasma Control and MHD, Naka 1996.

448. *Gruber, O.* and *ASDEX Upgrade Team:* Disruptions and VDEs in ASDEX Upgrade - Reactions to Plasma Disturbancies. 4th ITER Physics R&D Expert Group Meeting on Disruption, Plasma Control and MHD, Naka 1996.

449. *Gruber, O.* and *ASDEX Upgrade Team:* Online Plasma Regime Identification for Discharge Control at ASDEX Upgrade. 3rd ITER Plasma Control Task Force Meeting, Naka 1996.

450. *Gruber, O., ASDEX Upgrade Team* and *NI-Team:* MHD Stability and Disruption Studies in ASDEX Upgrade: 16th IAEA Fusion Energy Conf., Montreal 1996.

451. *Gubanka, B., M. Donath, F. Passek* and *V. Dose:* Magnetische Ordnung von fcc-artigen Eisenfilmen auf Cu(100): Neue Einsichten gewonnen aus der Spinabhängigkeit elektronischer Zustände. Dreikönigstreffen über 'Struktur und Magnetismus', Physikzentrum, Bad Honnef 1996.

452. *Gubanka, B., M. Donath, F. Passek* and *V. Dose:* Magnetische Ordnung von fcc-artigen Eisenfilmen auf Cu(001): Neue Einsichten gewonnen aus der Spinabhängigkeit elektronischer Zustände. Verhandl. DPG (VI) **31**, 1910, O38.6 (1996).

453. *Gubanka, B., M. Donath, F. Passek* and *V. Dose:* Surface as Magnetic Driver in fcc-Like Fe Films on Cu(001). 16th Europ. Conf. on Surface Science, Genova 1996.

454. *Günter, S.:* Spektrallinien unter dem Einfluß äußerer Magnetfelder. Seminar, Univ. Kiel 1996.

455. *Günter, S.* and *A. Könies:* Linienprofile wasserstoffähnlicher Ionen. Verhandl. DPG (VI) **31**, 761, P16.7 (1996).

456. *Günter, S.* and *A. Könies:* Shifted and Asymmetric Profiles of Hydrogen and Hydrogenic Ions. 13th Int. Conf. on Spectral Lines Shapes, Florence 1996.

457. *Haas, G., M. Bessenrodt-Weberpals, H.-S. Bosch, K. Büchl, O. Gruber, V. Mertens, U. Seidel* and *ASDEX Upgrade Team:* Particle Balance and Particle Control during Start up Phase of Tokamak Discharges in ASDEX Upgrade. 12th Int. Conf. on Plasma Surface Interactions in Controlled Fusion Devices, St. Raphael 1996.

458. *Hanesch, P., P. Sandl* and *E. Bertel:* Brom-induzierte Umrekonstruktion von Pt(110). Verhandl. DPG (VI) **31**, 1858, O25.5 (1996).

459. *Harmeyer, E., N. Jaksic* and *J. Simon-Weidner:* On Modular Coils of a Helias Reactor. 19th Symp. on Fusion Technology, Lisbon 1996.

460. *Hartfuß, H.-J.:* Detektion von mm- und submm-Wellen. Vorlesung, Univ. Regensburg, SS 1996.

461. *Hartfuß, H.-J.:* Diagnostics for W7-X. 11th Topical Conf. on High Temperature Plasma Diagnostics, Monterey,CA 1996.

462. *Hartfuß, H.-J.:* ECE Fluctuation Measurements at the W7-AS Stellarator. 23rd EPS Conf. on Controlled Fusion and Plasma Physics, Kiev 1996.

463. *Hartfuß, H.-J.:* Mikrowellenmeßtechnik I. Vorlesung, Univ. Regensburg, WS 1996/97.

464. *Häse, M.* and *H.-J. Hartfuß:* Elektronentemperatur-Fluktuationsmessungen an Wendelstein 7-AS. Verhandl. DPG (VI) **31**, 735, P10.6 (1996).

465. *Häse, M., H.-J. Hartfuß, C. Watts** et al.: Temperature Fluctuation Measurements on the W7-AS Stellarator. EU-US Transport Task Force Workshop, Varenna 1996.

466. *Heinemann, B., J.-H. Feist, W. Kraus, F. Probst, R. Riedl* and *E. Speth:* Development of a Novel Compact RF-Source. 19th Symp. on Fusion Technology, Lisbon 1996.

467. *Heinemann, B., JAERI-NBI-Group** and *NISSIN Electric Co.*:* Negative Ion Source and 1 MeV Accelerator for ITER NBI. Joint Development Comm. Meeting, JET, Abingdon 1996.

468. *Herre, G., R. Schneider, D.P. Coster* et al.: A 2D Approach to Island Divertor Modelling for Wendelstein 7-AS. 12th Int. Conf. on Plasma Surface Interactions in Controlled Fusion Devices, St. Raphael 1996.

469. *Hildebrandt, D., R. Brakel, A. Elsner* et al.: Plasma Response on Impurity Injection in W7-AS. 12th Int. Conf. on Plasma Surface Interactions in Controlled Fusion Devices, St. Raphael 1996.

470. *Hildebrandt, D., R. Brakel, P. Grigull, J. Baldzuhn, R. Burhenn, A. Elsner, S. Fiedler, L. Giannone, H. Hacker, R. Jaenicke, H.-J. Hartfuß, A. Herrmann, J.V. Hofmann, G. Kühner, D. Naujoks, F. Sardei, A. Weller, R. Wolf, W7-AS-Team, ECRH-Group* and *NI-Group:* Plasma Response on Impurity Injection in W7-AS. 12th Int. Conf. Plasma Surface Interactions in Controlled Fusion Devices, St. Raphael 1996.

471. *Hildebrandt, D.* and *V. Rohde:* Lokale und temporäre Verunreinigungsinjektion in AUG und W7-AS. Ringberg 1996.

472. *Hirsch, M.:* H-Mode Investigations in the W7-AS Stellarator. JET, Abingdon 1996.

473. *Hirsch, M.:* Reflektometrie zur gleichzeitigen Messung von Dichteprofilen und Dichtefluktuationsprofilen. Seminar, KFA Jülich 1996.

474. *Hirsch, M., E. Holzhauer, J. Baldzuhn* et al.: Edge Transport Barrier and Edge Turbulence During H-Mode Operation in the W7-AS Stellarator. 16th IAEA Int. Conf. on Plasma Physics and Controlled Nuclear Fusion Research, Montreal 1996.

475. *Hoenen*, F., J. Stein*, G. Degenhardt*, H.-S. Bosch, T. Kass* et al.: Digitale Pulsverarbeitung mit sphärischen Ionisationskammern. Verhandl. DPG (VI) **31**, 744, P15.1 (1996).

476. *Hofmann, J.V.:* Spektroskopie - eine kurze Übersicht. Besucher-Vortrag, IPP, Garching 1996.

477. *Hofmann, J.V.:* Stand der Kernfusionsforschung. Johann-Gottfried-Herder-Gymnasium, Greifswald 1996.

478. *Hofmann, J.V.:* Stand der Kernfusionsforschung. Hansa-Gymnasium, Stralsund 1996.

479. *Hofmann, J.V.:* Stand der Kernfusionsforschung. Herder-Gymnasium, Stralsund 1996.

480. *Hofmann, J.V., W7-AS-Team, ECRH-Group* and *NI-Group:* Stellarator Optimization Studies in W7-AS. 23rd EPS Conf. on Controlled Fusion and Plasma Physics, Kiev 1996.

481. *Hofmeister, F.* and *ICRH-Team:* Matching Fast ICRF Antenna Coupling Variations by Frequency Change. 19th Symp. on Fusion Technology, Lisbon 1996.

482. *Höhn, F., R. Beckmann, W. Jacob, F. Wesner* and *R. Wilhelm:* Untersuchungen zum Übergang von der Multipaktorentladung zur HF-Gasentladung. Verhandl. DPG (VI) **31**, 703, P2.4 (1996).

483. *Höhn, F., R. Beckmann, W. Jacob, F. Wesner* and *R. Wilhelm:* Untersuchungen zur Wechselwirkung von Multipaktorentladungen mit den Oberflächen von Edelstahlelektroden. Verhandl. DPG (VI) **31**, 788, P11.6 (1996).

484. *Jacob, W.:* Oberflächenmechanismen bei Deposition und Erosion. Kolloquiumsvortrag, Univ. Greifswald 1996.

485. *Jacob, W.:* Quantitative Analysen an amorphen Kohlenwasserstoffschichten. Seminarvortrag, Univ. Greifswald 1996.

486. *Jacob, W.* and *M. Unger*:* Experimentelle Bestimmung der Dipolstärke von C-H Vibrationsschwingungen für die Infrarotanalyse

von C:H-Schichten. 7. Bundesdt. Fachtagung Plasmatechnologie, Bochum 1996.

487. *Jacob, W.* and *M. Unger*:* Experimentelle Bestimmung der Dipolstärke von C-H Vibrationsschwingungen für die Infrarotanalyse von C:H-Schichten. Verhandl. DPG (VI) **31**, 1181, DS12.4 (1996).

488. *Jaksic, N., J. Simon-Weidner* and *J. Sapper:* Buckling Analysis of the W7-X, Inner Vacuum Vessel. 19th Symp. on Fusion Technol., Lisbon 1996.

489. *Jaksic, N., J. Simon-Weidner* and *J. Sapper:* Local Stress Analysis of the W7-X Superconducting Winding Pack. 19th Symp. on Fusion Technology, Lisbon 1996.

490. *Jüttner, B.:* Nichtstationäre Brennfleckplasmen. Verhandl. DPG (VI) **31**, 702, P2.1 (1996).

491. *Jüttner, B.* and *G. Fußmann:* Plasmaphysik und Plasmatechnologie. Vorlesung, Humboldt-Univ. Berlin, WS 1995/96.

492. *Kallenbach, A.:* H- and CDH-Modes with Radiating Boundary. 4th Europ. Fusion Physics Workshop, Stockholm 1996.

493. *Kallenbach, A., H.-S. Bosch, S. de Peña Hempel, R. Dux, M. Kaufmann, V. Mertens, J. Neuhauser, W. Suttrop, H. Zohm, ASDEX Upgrade Team, NI-Team* and *ICRH-Team:* Possible Divertor Solutions for a Fusion Reactor. 19th Symp. on Fusion Technology, Lisbon 1996.

494. *Kammler*, T., M. Scherl** and *J. Küppers:* Abstraktion von adsorbiertem Sauerstoff auf Ni(100) Oberflächen mit thermischen H(D) Atomen. Verhandl. DPG (VI) **31**, 1769, O3.7 (1996).

495. *Kappel*, M., J. Biener* and *J. Küppers:* Chemische Erosion von HOPG mit thermischen H Atomen: eine UHV-STM/AFM Studie. Verhandl. DPG (VI) **31**, 1888, O32.4 (1996).

496. *Kardaun, O.:* Consistency between Energy Measurements, Database Conditioning, and Prediction Reliability. 4th Meeting of the ITER Confinement Database and Modelling Expert Group, Moscow 1996.

497. *Kardaun, O.:* Interval Estimates for the Confinement Time in ITER. 1st Joint Meeting of the ITER Confinement and Transport Expert Group and the ITER Confinement Database and Modelling Expert Group, Montreal 1996.

498. *Kass, T., H.-S.Bosch, F. Hoenen*, K. Lackner, M. Maraschek, A. Weller, H. Zohm, ASDEX Upgrade Team* and *W7-AS-Team:* Das Verhalten hochenergetischer injizierter Teilchen im Tokamak ASDEX Upgrade und im Stellarator Wendelstein 7-AS. Verhandl. DPG (VI) **31**, 710, P6.1 (1996).

499. *Kastelewicz, H., D. Reiter*, R. Schneider, D.P. Coster* and *H. Meyer:* B2-EIRENE-Rechnungen für den Plasmagenerator PSI 1. Verhandl. DPG (VI) **31**, 780, P20.32 (1996).

500. *Kaufmann, M.:* Aktuelle Themen der Fusionsforschung. Kolloquium, Univ. Greifswald 1996.

501. *Kaufmann, M.:* Edge Density and Global Performance. 4th Europ. Fusion Physics Workshop, Stockholm 1996.

502. *Kaufmann, M.:* Einführung in die Plasmaphysik und Fusionsforschung I. Vorlesung, Univ. Bayreuth, WS 1996/97.

503. *Kaufmann, M.:* Stand der Fusionsforschung und Beispiele von aktuellen Forschungsthemen. Kolloquium, Univ. Gießen 1996.

504. *Kaufmann, M., J. Schweinzer, M. Albrecht, M. Alexander, K. Asmussen, G. Becker, K. Behler, K. Behringer, R. Behrisch, E. Berger, A. Bergmann, M. Bessenrodt-Weberpals, K. Borrass, H.-S. Bosch, M. Brambilla, F. Braun, H. Brinkschulte, C. Brosig, K. Büchl, A. Buhler, A. Carlson, R. Chodura, D.P. Coster, H.J. de Blank, S. de Peña Hempel, S. Deschka, V. Dose, C. Dorn, R. Drube, R. Dux, W. Engelhardt, J. Engstler, H.-U. Fahrbach, J.-H. Feist, S. Fiedler, A.R. Field, P. Franzen, J.C. Fuchs, G. Fußmann, J. Gafert, C. García-Rosales, O. Gehre, J. Gernhardt, T. Grossmann, O. Gruber, S. Günter, G. Haas, K. Hallatschek, J. Hartmann, B. Heinemann, P. Heimann, A. Herrmann, W. Herrmann, G. Herppich, F. Hertweck, K. Hirsch, S. Hirsch, M. Hoek, F. Hofmeister, E. Holzhauer, H. Hohenöcker, P. Ignacz, D. Jacobi, B. Jüttner, W. Junker, A. Kallenbach, O. Kardaun, T. Kass, H. Kastelewicz, C. Klepper, H. Kollotzek, W. Köppendörfer, W. Kraus, K. Krieger, B. Kurzan, K. Lackner, P.T. Lang, R.S. Lang, M. Laux, L.L. Lengyel, F. Leuterer, G. Lieder, J. Maier, M. Maraschek, K.-F. Mast, D. Meisel, H. Meister, R. Merkel, V. Mertens, H.W. Müller, F. Münich, H. Murmann, B. Napiontek, D. Naujoks, G. Neu, R. Neu, J. Neuhauser, J.-M. Noterdaeme, M. Pacco-Düchs, E. Pasch, G. Pautasso, A.G. Peeters, G. Petravich, W. Poschenrieder, I. Precht, F. Puri, G. Raupp, K. Reinmüller, H. Reimerdes, R. Riedl, V. Rohde, H. Röhr, J. Roth, F. Ryter, H. Salzmann, W. Sandmann, W. Schärich, H.-B. Schilling, M. Schittenhelm, D. Schlögl, H. Schneider, R. Schneider, U. Schneider, W. Schneider, K. Schönmann, G. Schramm, T. Schütte, S. Schweizer, R. Schwörer, B. Scott, U. Seidel, S. Sesnic, M. Sokoll, E. Speth, A. Stäbler, K.-H. Steuer, J. Stober, B. Streibl, W. Suttrop, A. Thoma, C. Tichmann, R. Tisma, W. Treutterer, M. Troppmann, M. Ulrich, H. Verbeek, P. Verplancke, O. Vollmer, H. Wedler, U. Wenzel, F. Wesner, M. Weinlich, H. Werthmann, R. Wilhelm, R. Wolf, R. Wunderlich, D. Wutte, D. Zasche, H.-P. Zehrfeld, T. Zehetbauer, M. Zilker, H. Zohm, M. Zouhar* et al.*:* Overview of ASDEX Upgrade Results. 16th IAEA Fusion Energy Conf., Montreal 1996.

505. *Keudell, A. von:* Antisynergism during Etching of Amorphous Carbon Films by Hydrogen Plasmas Investigated by in-situ Ellipsometry. Seminarvortrag, Univ. of Illinois, Chicago,IL 1996.

506. *Keudell, A. von:* Elementary Surface Reactions during PEVCD of C:H Films. Seminarvortrag, Techn. Univ. Eindhoven 1996.

507. *Keudell, A. von:* Plasma-Surface-Interactions: Deposition of Amorphous Carbon. ERASMUS Summer School, Techn. Univ. Eindhoven 1996.

508. *Keudell, A. von:* Surface Reactions during PECVD of Amorphous Carbon Films, Investigated by in-situ Ellipsometry. Seminarvortrag, Univ. of Illinois, Urbana,IL 1996.

509. *Keudell, A. von:* Surface Reactions during PECVD of Amorphous Carbon Films, Investigated by in-situ Ellipsometry. 11th Workshop on Inelastic Ion-Surface Collisions, Wangerooge 1996.

510. *Keudell, A. von:* Wachstumsmechanismen bei der plasmagestützten Abscheidung von Kohlenwasserstoffschichten. Seminarvortrag, Techn. Univ. München 1996.

511. *Keudell, A. von* and *W. Jacob:* Erosion von a-C:H-Schichten mit Wasserstoffplasmen: in situ Beobachtung der Erosionsmechanismen mittels Ellipsometrie. Verhandl. DPG (VI) **31**, 1174, DS8.1 (1996).

512. *Keudell, A. von* and *W. Jacob:* Infrarotspektroskopie an dünnen Filmen: Vergleich der unterschiedlichen Auswerteverfahren. 7. Bundesdt. Fachtagung Plasmatechnologie, Bochum 1996.

513. *Keudell, A. von* and *W. Jacob:* Oberflächenreaktionen bei der plasmagestützten Herstellung von a-C:H-Schichten: Vergleich der Quellgase Methan und Acetylen. 7. Bundesdt. Fachtagung Plasmatechnologie, Bochum 1996.

514. *Kick, M., J. Baldzuhn, J. Geiger* et al.: High Ion Temperatures and High Beta in W7-AS. 16th IAEA Int. Conf. on Plasma Physics and Controlled Nuclear Fusion Research, Montreal 1996.

515. *Koch*, T., R. Richter** and *J. Küppers:* Charakterisierung dünner AG-Schichten auf Ir(111)-Oberflächen. Verhandl. DPG (VI) **31**, 1810, O13.2 (1996).

516. *Könies, A.:* Die Zeitentwicklung des ionischen Mikrofeldes. Seminarvortrag, Univ. Kiel 1996.

517. *Könies, A.* and *S. Günter:* Asymmetrische und verschobene Profile von Wasserstofflinien. Verhandl. DPG (VI) **31**, 748, P15.16 (1996).

518. *König*, R.W.T., K.D. Lawson*, P.J. Lomas*, K. McCormick* et al.: Recycling in JET High Performance Hot-Ion H-Modes. 38th Annual Meeting of the Div. of Plasma Physics, Denver,CO 1996.

519. *Konrad, C., H.-J. Hartfuß, E. Holzhauer* and *W7-AS-Team:* Dichtefluktuationsmessung mittels kohärenter Mikrowellenstreuung am Stellarator Wendelstein 7-AS. Verhandl. DPG (VI) **31**, 735, P10.8 (1996).

520. *Kornejew, P.:* Heliumstrahldiagnostik am Plasmagenerator PSI-1. KFA Jülich 1996.

521. *Kraus, W., J.-H. Feist, M. Ciric* and *E. Speth:* Optimization of a Large-Area RF Plasma Generator. 19th Symp. on Fusion Technology, Lisbon 1996.

522. *Krieger, K., K. Asmussen, R. Neu, V. Rohde, J. Roth, R. Schwörer, A. Thoma, ASDEX Upgrade Team, NI-Team* and *ICRH-Team:* Erosion and Transport of Tungsten in ASDEX Upgrade. 16th Int. Conf. Plasma Physics and Controlled Nuclear Fusion Research, Montreal 1996.

523. *Krieger, K., K. Behler, A. Herrmann*, G. Raupp* and *ASDEX Upgrade Team:* Remote Participation Activities at ASDEX Upgrade. IAEA Meeting on Telecommunication for Remote Participation in Fusion Research, Montreal 1996.

524. *Krieger, K., J. Roth, A. Annen, W. Jacob, B. Napiontek, M. Weinlich* et al.: Study of Gross and Net Erosion in the ASDEX Upgrade Divertor. 12th Int. Conf. on Plasma Surface Interactions in Controlled Fusion Devices, St. Raphael 1996.

525. *Krieger, K., J. Roth, ASDEX Upgrade Team* and *NI-Team:* Targetplattenerosion im Divertor von ASDEX Upgrade. Verhandl. DPG (VI) **31**, 736, P11.1 (1996).

526. *Kronhardt*, H., K.-D. Herrmann*, W. Broocks** and *M. Pillsticker:* Determination of Compound Properties for Superconducting Magnets by Combined Theoretical and Experimental Methods. 19th Symp. on Fusion Technology, Lisbon 1996.

527. *Kühner, G., J. Knauer* and *H. Ringler:* Probing $f_e$ (v) by Thomson Scattering on W7-X. 11th Topical Conf. on High Temperature Plasma Diagnostics, Monterey,CA 1996.

528. *Küppers, J.:* Reactions of Gaseous H Atoms with Adsorbates at Solid Surfaces. Int. Symp. on Surface Chemistry, Atomic Scale Surface Science Res. Center, Yonsei Univ., Seoul 1996.

529. *Küppers, J.:* Reactions of H Atoms with Adsorbed Molecules. Surface Science Center, Pittsburgh Univ. 1996.

530. *Küppers, J.:* Surface Chemistry of Undoped and Boron Doped a-C:H Films. Dept. of Chemistry, Pohan Inst. of Science and Technology, Pohan 1996.

531. *Küppers, J.:* Surface Reactions with H Atoms. WE-Heraeus Seminar, Ilmenau 1996.

532. *Kurzan, B., M. Albrecht, M.E. Manso*, W. Suttrop, ASDEX Upgrade Team* et al.: Messung von Elektronendichteprofilen auf der Hochfeldseite von ASDEX Upgrade durch Mikrowellenreflektometrie. Verhandl. DPG (VI) **31**, 733, P10.1 (1996).

533. *Kurzan, B., K.-H. Steuer* and *W. Suttrop:* Runaway Electrons in a Tokamak - A Free-Electron Maser. 11th Top. Conf. on High-Temperature Plasma Diagnostics, Monterey,CA 1996.

534. *Küstner, M., W. Eckstein, J. Roth* and *V. Dose:* Zerstäubung rauher Oberflächen. Verhandl. DPG (VI) **31**, 1817, O16.3 (1996).

535. *Labich, S.:* Rhodium-Katalysatoren, Oberflächenanalytische Untersuchungen an Modellsystemen. SFB-338 Seminar, Filzmoos 1996.

536. *Labich, S.:* Untersuchungen zur Metall-Träger-Wechselwirkung an Modellkatalysatoren. SFB-Tag, Univ. München 1996.

537. *Labich, S., E. Taglauer* and *H. Knözinger*:* Investigation of SMSI Effects on a $Rh/TiO_2$ Model Catalyst by Surface Spectroscopies. ⇔ Chemisorption and Reactivity on Supported Clusters and Thin Films. NATO ASI, Erice 1996.

538. *Labich, S., E. Taglauer* and *H. Knözinger*:* LEIS Investigation of SMSI Effects on a $Rh/TiO_2$ Model Catalyst Supported by Surface Spectroscopies. 11th Int. Workshop on Inelastic Ion-Surface Collisions, Wangerooge 1996.

539. *Lang, P.T., M. Bessenrodt-Weberpals, K. Büchl, O. Gruber, V. Mertens, H. Salzmann, H. Zohm, ASDEX Upgrade Team* and *NI-Team:* Hochdichte H-Mode Plasmen in ASDEX Upgrade. Verhandl. DPG (VI) **31**, 711, P6.4 (1996).

540. *Lang, P.T., P. Cierpka* and *P. Kupschus*:* High Repetitive Pellet Injectors for Plasma Density Control. 19th Symp. on Fusion Technology, Lisbon 1996.

541. *Lang, P.T., B.V. Kuteev*, K. Büchl, H.W. Müller* and *ASDEX Upgrade Team:* Neon Pellet Ablation in Hot Plasmas. Verhandl. DPG (VI) **31**, 745, P15.5 (1996).

542. *Lang, R.S., P.T. Lang, S.M. Ergorov*, W. Beck, P. Cierpka, J. Perchermeier, M. Ulrich, H. Vetter* and *G. Weber:* Pelletinjector Development and Application at IPP. Verhandl. DPG (VI) **31**, 746, P15.7 (1996).

543. *Laqua, H.:* Neue Elektronzyklotronheizszenarien am W7-AS Stellarator. Plasmakolloquium, IPF Stuttgart 1996.

544. *Laqua, H.:* Resonant and Nonresonant Electron Cyclotron Heating at Densities above the Plasma Cut-off by O-X-B-Mode Conversion at W7-AS. 8th Joint Russian-German Meeting on ECRH and Gyrotrons, Nizhny Novgorod 1996.

545. *Laqua, H.:* Resonant and Nonresonant Electron Cyclotron Heating at Densities above the Plasma Cut-off by O-X-B-Mode Conversion at W7-AS. Kurchatov Inst. of Atomic Energy Plasma Physics Dept., Moscow 1996.

546. *Lehmann, J.:* Incorporation of Alkali Metals on Pt(111). 16th Europ. Conf. on Surface Science, Genova 1996.

547. *Lehmann, J.:* Quantum-Size-Effekte auf dem Weg von der Zwei- zur Ein-Dimensionalität. SFB-338 Seminar, Filzmoos 1996.

548. *Lehmann, J.* and *E. Bertel:* Stress-induzierter Einbau von Alkalimetallen in Pt(111)? Verhandl. DPG (VI) **31**, 1892, O34.2 (1996).

549. *Leuterer, F.:* ECRH in ASDEX Upgrade. Institutskolloquium, École Polytechnique Fédérale de Lausanne 1996.

550. *Leuterer, F.:* Plasma Waves. Summer Univ. for Plasma Physics, IPP, Garching 1996.

551. *Leuterer, F., H. Brinkschulte, F. Monaco, M. Münich* et al.: Impact of the ASDEX Upgrade Stray Magnetic Field on Electron Beam Deposition in the Toriy Dummy Tube. 8th Joint Russian-German Meeting on ECRH and Gyrotrons, Nizhny Novgorod and Moscow 1996.

552. *Leuterer, F., A.G. Peeters, G. Pereverzev, F. Ryter* and *W. Suttrop:* ECRH Power Deposition Profiles in ASDEX Upgrade. 8th Joint Russian-German Meeting on ECRH and Gyrotrons, Nizhny Novgorod and Moscow 1996.

553. *Leuterer, F., F. Ryter, J. Köllermeyer, A.G. Peeters, G. Pereverzev, W. Suttrop, ASDEX Upgrade Team, ECRH-Group* and *NI-Group:* Heat Wave Experiments in ASDEX Upgrade. 8th Joint Russian-German Meeting on ECRH and Gyrotrons, Nizhny Novgorod and Moscow 1996.

554. *Lingertat*, J., A. Tabasso*, S. Ali-Arshad*, K. Borrass* et al.: Studies of Giant ELM Interaction with the Divertor Target in JET. 12th Int. Conf. on Plasma Surface Interactions in Controlled Fusion Devices, St. Raphael 1996.

555. *Linsmeier, C., N. Freed** and *I.S.T. Tsong*:* Dual Ion Beam System for the Deposition of Wide Bandgap Semiconductors. March Meeting of the APS, St. Louis,MO 1996.

556. *Lomas*, P.J.* and *K. McCormick:* High Fusion Performance ELM-Free H-Modes and the Approach to Steady Operation. 16th IAEA Int. Conf. on Plasma Physics and Controlled Nuclear Fusion Research, Montreal 1996.

557. *Lortz, D.* and *G.O. Spies:* Interface Localized Instability in Resistive Magnetohydrodynamics. Int. Conf. on Plasma Physics, Nagoya 1996.

558. *Lortz, D.* and *G.O. Spies:* Interface Localized Instability in Resistive Magnetohydrodynamics. Univ. of Texas, Austin,TX 1996.

559. *Lutterloh*, C., K. Pöhlmann, J. Biener* and *J. Küppers:* Wechselwirkung einer Graphitmonolage auf Pt(111) mit thermischen H Atomen. Verhandl. DPG (VI) **31**, 1887, O32.3 (1996).

560. *Maingi*, R., B. Terreault*, G. Haas, H.-S. Bosch* et al.: Comparison of Wall/Divertor Deuterium Retention and Plasma Fueling Requirements on the DIII-D, TdeV and ASDEX Upgrade Tokamaks. 12th Int. Conf. on Plasma Surface Interactions in Controlled Fusion Devices, St. Raphael 1996.

561. *Maraschek, M., T. Kass* and *H. Zohm:* Beobachtung von TAE Moden an ASDEX Upgrade. Verhandl. DPG (VI) **31**, 710, P6.2 (1996).

562. *Matthews*, G.F., S. Allen*, N. Asakura*, A. Kallenbach, K. McCormick* et al.: Scaling Radiative Plasmas to ITER. 12th Int. Conf. on Plasma Surface Interactions in Controlled Fusion Devices, St. Raphael 1996.

563. *Mayer, M.:* Codeposition of Hydrogen with Be, C and W. 3rd Int. Workshop on Tritium Effects in Plasma Facing Components, Ispra 1996.

564. *Mayer, M., R. Behrisch, P. Andrew** et al.: Erosion at the Vessel Walls of JET. 12th Int. Conf. on Plasma Surface Interactions in Controlled Fusion Devices, St. Raphael 1996.

565. *Mayer, M., R. Behrisch, H. Plank, J. Roth* et al.: Kodeponierung von Wasserstoff mit Beryllium, Kohlenstoff und Wolfram. Verhandl. DPG (VI) **31**, 738, P11.4 (1996).

566. *McCormick, K.:* Correlation of Core Plasma Parameters with Neutral Pressure and ELM Frequency. JET Divertor Task Force Seminar, Abingdon 1996.

567. *McCormick, K.:* An Introduction to Two ASDEX Edge Databases. ITER Edge Database Workshop, Montreal 1996.

568. *McCormick, K.:* Particle Balances for the Hot Ion H-Mode in the Mark IIa Divertor. JET High-Performance Task Force Seminar, Abingdon 1996.

569. *McCormick, K., A. Chankin*, S. Clement** et al.: Derivation of SOL Transport Coefficients Using 2D Modelling for Hot-Ion ELM-Free H-Modes in JET. 12th Int. Conf. on Plasma Surface Interactions in Controlled Fusion Devices, St. Raphael 1996.

570. *Memmel, N.:* Niederdimensionale elektronische Zustände an Metalloberflächen - Ursachen und Bedeutung. Kolloquium, Univ. Bayreuth 1996.

571. *Merkel, P., C. Nührenberg* and *W.A. Cooper*:* Free-Boundary Ideal MHD Modes in W7-AS. Int. Workshop on Theory of Fusion Plasmas, Varenna 1996.

572. *Mertens, V., A. Herrmann, A. Kallenbach, J. Neuhauser, J. Schweinzer, K. Behringer, A. Carlson, R. Dux, G. Haas, M. Kaufmann, P.T. Lang, R.S. Lang, K.-F. Mast, B. Napiontek, M. Weinlich, ASDEX Upgrade Team* and *NI-Team:* Edge and Divertor Physics in ASDEX Upgrade with Emphasis on Density Limit Characteristics. 16th IAEA Fusion Energy Conf., Montreal 1996.

573. *Meyer-Spasche, R.:* Dynamische Eigenschaften von Differenzenverfahren. Seminar der Gruppe 'Nichtlineare Dynamik', Techn. Univ. München 1996.

574. *Meyer-Spasche, R.:* Gleichgewichte und Stabilität: Nichtlineare Fluiddynamik. Vorlesung, Techn. Univ. München, SS 1996.

575. *Meyer-Spasche, R.:* Perfurkationsprobleme in Anwendungen. Vorlesung, Techn. Univ. München, WS 1996/97.

576. *Miethke *, F., A. Sonnenfeld *, H. Strobel* et al.: Vergleichende kinetische und thermodynamische Charakterisierung der $CO_2$-Zerlegung in anisothermen Plasmen. Verhandl. DPG (VI) **31**, 754, P15.33 (1996).

577. *Milch, I.:* Energie aus dem Sternenfeuer. Kernfusionsforschung. Frauen führen Frauen. Deutsches Museum München 1996.

578. *Miller, S., H. Plank, G. Berning** and *J. Roth:* Untersuchung der chemischen Wechselwirkung von Titanschichten auf Graphit mittels Röntgenstrahl-induzierter Photoelektronen-Spektroskopie. Verhandl. DPG (VI) **31**, 1172, DS7.1 (1996).

579. *Müller, H.W., K. Büchl, T. Henningsen, M. Kaufmann, P.T. Lang, V. Mertens, W. Schneider, H. Zohm, ASDEX Upgrade Team* et al.: Analyse der q-Profil Messung mittels Pelletablation an ASDEX Upgrade. Verhandl. DPG (VI) **31**, 745, P15.4 (1996).

580. *Müller*, M., T. Schimmel*, R. Schaller*, J. Küppers* et al.: Zweidimensionale stick-slip-Prozesse bei der Rasterkraftmikroskopie auf atomarer Skala: Untersuchungen auf $WSe_2$ als Modellsystem. Verhandl. DPG (VI) **31**, 1898, O35.6 (1996).

581. *Murakami*, S., N. Nakajima*, U. Gasparino* et al.: Monte Carlo Simulation Study of ECR Heating in Non-Axisymmetric Devices. Joint Numerical Tokamak and US-Japan Workshop on

Plasma Simulation Including Electron Dynamics, Philadelphia,PA 1996.

582. *Murakami*, S., N. Nakajima*, S. Okamura*, U. Gasparino* et al.: Orbit Effects of Energetic Particles on the Reachable β-Value and the Radial Electric Field in NBI and ECR Heated Heliotron Plasmas. 16th IAEA Int. Conf. on Plasma Physics and Controlled Nuclear Fusion Research, Montreal 1996.

583. *Murakami*, S., N. Nakajima*, M. Okamoto*, U. Gasparino, H. Maaßberg, M. Romé* et al.: Orbit Effects on the ECRH Deposition Profile in Stellarator-Devices. 8th Int. Conf. on Plasma Physics, Nagoya 1996.

584. *Murtfeld, U., E. Taglauer, H. Knözinger** et al.: Untersuchung der NiAl(100)-Oberfläche mit LEED und Ionenstreuung. Verhandl. DPG (VI) **31**, 1928, O42.2 (1996).

585. *Naujoks, D., B. Bachmann, A. Runow** and *D. Sünder:* Monte Carlo Modelling of the Transport in the Stellarator Pheripery with Magnetic Islands. 12th Int. Conf. Plasma Surface Interactions in Controlled Fusion Devices, St. Raphael 1996.

586. *Naujoks, D., J. Steinbrink, U. Wenzel* and *PSI-Group:* Spatial Distributions of Neutral Atoms in the Near-Target Plasma: Theory and Experiment. 12th Int. Conf. Plasma Surface Interactions in Controlled Fusion Devices, St. Raphael 1996.

587. *Neu, R., ASDEX Upgrade Team, NI-Team, ICRH-Team* and *ECRH-Team:* Hoch Z Metalle als Wandmaterial in Fusionsanlagen. Kolloquium, IPF Stuttgart 1996.

588. *Neu, R., ASDEX Upgrade Team, NI-Team, ICRH-Team* and *ECRH-Team:* The Tungsten Divertor Experiment at ASDEX Upgrade. Seminar, MIT, Cambridge,MA 1996.

589. *Neu, R., K. Asmussen, K. Behringer, M. Bessenrodt-Weberpals, K. Büchl, S. Deschka, R. Dux, W. Engelhardt, J.C. Fuchs, C. García-Rosales, A. Herrmann, S. Hirsch, A. Kallenbach, M. Kaufmann, K. Krieger, K.-F. Mast, A. Thoma, U. Wenzel, ASDEX Upgrade Team, NI-Team, ICRH-Team* and *ECRH-Team:* ASDEX Upgrade Divertorverhalten mit Hoch- und Niedrig-Z Materialien. Verhandl. DPG (VI) **31**, 764, P17.4 (1996).

590. *Neu, R., K. Asmussen, S. Deschka, A. Thoma, M. Bessenrodt-Weberpals, R. Dux, W. Engelhardt, J.C. Fuchs, J. Gafert, C. García-Rosales, A. Herrmann, K. Krieger, K.-F. Mast, J. Roth, V. Rohde, M. Weinlich, U. Wenzel, ASDEX Upgrade Team* and *NI-Team:* The Tungsten Divertor Experiment at ASDEX Upgrade. 12th Int. Conf. on Plasma Surface Interactions in Controlled Fusion Devices, St. Raphael 1996.

591. *Neu, R., K. Asmussen, K. Krieger, A. Thoma, H.-S. Bosch, S. Deschka, R. Dux, W. Engelhardt, C. García-Rosales, O. Gruber, A. Herrmann, A. Kallenbach, M. Kaufmann, V. Mertens, F. Ryter, V. Rohde, J. Roth, M. Sokoll, A. Stäbler, W. Suttrop, M. Weinlich, H. Zohm, M. Alexander, G. Becker, K. Behler, K. Behringer, R. Behrisch, A. Bergmann, M. Bessenrodt-Weberpals, M. Brambilla, H. Brinkschulte, K. Büchl, A. Carlson, R. Chodura, D.P. Coster, H.J. de Blank, S. de Peña Hempel, R. Drube, H.-U. Fahrbach, J.-H. Feist, W. Feneberg, S. Fiedler, P. Franzen, J.C. Fuchs, G. Fußmann, J. Gafert, O. Gehre, J. Gernhardt, G. Haas, G. Herppich, W. Herrmann, S. Hirsch, M. Hoek, F. Hofmeister, H. Hohenöcker, D. Jacobi, W. Junker, O. Kardaun, T. Kass, H. Kollotzek, W. Köppendörfer, B. Kurzan, K. Lackner, P.T. Lang, R.S. Lang, M. Laux, L.L. Lengyel, F. Leuterer, M.E. Manso, M. Maraschek, K.-F. Mast, D. Meisel, R. Merkel, H.W. Müller, M. Münich, H. Murmann, B. Napiontek, G. Neu, J. Neuhauser, J.-M. Noterdaeme, E. Pasch, G. Pautasso, A.G. Peeters, G. Pereverzev, C.S. Pitcher, W. Poschenrieder, G. Raupp, K. Reinmüller, R. Riedl, H. Röhr, H. Salzmann, W. Sandmann, H.-B. Schilling, D. Schlögl, H. Schneider, R. Schneider, W. Schneider, G. Schramm, J. Schweinzer, B.D. Scott, U. Seidel, E. Speth, K.-H. Steuer, J. Stober, B. Streibl, W. Treutterer, M. Troppmann, M. Ulrich, H. Verbeek, P. Verplancke, O. Vollmer, H. Wedler, U. Wenzel, F. Wesner, R. Wolf, R. Wunderlich, D. Zasche, T. Zehetbauer, H.-P. Zehrfeld* et al.: The Tungsten Divertor Experiment at ASDEX Upgrade. 23rd EPS Conf. on Controlled Fusion and Plasma Physics, Kiev 1996.

592. *Neuhauser, J.:* Edge Models and Operational Limits. 4th Europ. Fusion Physics Workshop, Stockholm 1996.

593. *Niedermeyer, H., R. Balbin*, J. Bleuel* et al.: Fluctuations, Turbulent Transport and Analysis Tools. EU-US Transport Task Force Workshop, Varenna 1996.

594. *Niedermeyer, H., J. Bleuel, M. Endler* et al.: Correlation Properties of Turbulent Fluctuations at the Edge of W7-AS. Transport Task Force, Turbulence Working Group Meeting, Jülich 1996.

595. *Niedermeyer, H., J. Bleuel, M. Endler* et al.: Fluctuations in High Temperature Fusion Plasmas. EPS 10, Europ. Phys. Society, Trends in Physics, Seville 1996.

596. *Noda*, N., V. Philipps** and *R. Neu:* A Review of Recent Experiments on W and High-Z Materials as Plasma-Facing Components in Magnetic Fusion Devices. 12th Int. Conf. on Plasma Surface Interactions in Controlled Fusion Devices, St. Raphael 1996.

597. *Noterdaeme, J.-M.:* New ICRF Results on ASDEX Upgrade. ITER Joint Working Meeting, Garching 1996.

598. *Noterdaeme, J.-M.:* Nuclear Fusion: A Long-Term Energy Option? Status and Perspectives. Nat. Energy Board of Thailand, Bangkok 1996.

599. *Noterdaeme, J.-M.:* Status of ICRF on ASDEX Upgrade and W7-AS. Europ. Coord. Comm. on Fast Waves, Stockholm 1996.

600. *Noterdaeme, J.-M., S. Wukitch, D. Hartmann, M. Brambilla, F. Braun, G. Cattanei, J. Gafert, R. Neu, W. Suttrop, J. Schweinzer, W. Schneider, P. Verplancke, F. Wesner, ICRF-Group, NI-Team, ASDEX Upgrade Team, W7-AS-Team* et al.: ICRF Heating Results in ASDEX Upgrade and W7-AS. 16th IAEA Fusion Energy Conf., Montreal 1996.

601. *Nührenberg, J.:* The Optimized Stellarator W7-X. Fusion Evaluation Board, Garching 1996.

602. *Ott, W., W. Melkus, F.-P. Penningsfeld, F. Probst, E. Speth, R. Süss* and *W7-AS-Team:* Upgrading of the Injection Power of the W7-AS Neutral Beam System. 19th Symp. on Fusion Technology, Lisbon 1996.

603. *Pasch, E., W. Bohmeyer, H. Grote, H. Meyer, H.-D. Reiner* and *G. Fußmann:* Temperatur und Driften der schweren Teilchen im Plasmagenerator PSI-1. Verhandl. DPG (VI) **31**, 726, P8.30 (1996).

604. *Pautasso, G.:* Mechanical and Thermal Loads during Disruptions in ASDEX Upgrade. Seminar, Karlsruhe 1996.

605. *Pecher, P.* and *W. Jacob:* Energieverteilungen verschiedener Ionen aus einem Methan-ECR-Plasma. Verhandl. DPG (VI) **31**, 743, P13.6 (1996).

606. *Pecher, P.* and *W. Jacob:* Massenaufgelöste Ionenenergieverteilungen, $CH_3$-Radikalen- und Neutralgasflüsse aus einem Methan-ECR-Plasma. 7. Bundesdt. Fachtagung Plasmatechnologie, Bochum 1996.

607. *Pecher, P.* and *W. Jacob:* Massenspektrometrische Bestimmung der $CH_3$-Radikal- und Neutralgasflüsse aus einem Methan-ECR-Plasma. Verhandl. DPG (VI) **31**, 743, P13.5 (1996).

608. *Peeters, A.G.:* Description of Wave Propagation Including Refraction and Diffraction in an Anisotropic Dispersive Medium. 3rd Int. Workshop on Strong Microwaves in Plasmas, Moscow 1996.

609. *Peeters, A.G.:* Extensions of the Ray Equations of Geometric Optics to Include Diffraction Effects. FOM Inst. for Plasma Physics, Rijnhuizen 1996.

610. *Peeters, A.G.:* Neues im Bereich ECRH und Transport. Graduiertenkolleg, Univ. Düsseldorf 1996.

611. *Perkins*, F.W., D. Post, M. Rosenbluth*, K. Borrass, D.J. Campbell*, V. Mertens, J. Neuhauser, H. Zohm* et al.: ITER Operational Limits. 16th IAEA Fusion Energy Conf., Montreal 1996.

612. *Pernreiter, W.* and *H.-J. Hartfuß:* Zyklotronemission bei nicht-thermischer Elektronenenergieverteilung an Wendelstein 7-AS. Verhandl. DPG (VI) **31**, 735, P10.7 (1996).

613. *Pfirsch, D:* Drift-Waves Re-Examined. Colloquium, Lab. of Plasma Studies, Cornell Univ., Ithaca,NY 1996.

614. *Pfirsch, D.:* Some Critical Remarks Concerning Present-Day Drift-Wave Theories. 2nd Workshop on Nonlinear Dynamics, Chaos, Transport, Turbulence, and Magnetic Fusion. Courant Inst, New York Univ. 1996.

615. *Pinkau, K.:* Basic Research in Astrophysics and the Energy Problem. Alexander-von-Humboldt-Stiftung, Bonn 1996.

616. *Pinkau, K.:* Das Energieproblem - eine unbewältigte Gefahr. Techn. Univ. Berlin 1996.

617. *Pinkau, K.:* Die Erforschung der kontrollierten Kernfusion und das Energieproblem. DPG, Frankfurt am Main 1996.

618. *Pinkau, K.:* Freiheit der Forschung insbesondere bei den Zukunftstechnologien. Ev. Akademie, Tutzing 1996.

619. *Pinkau, K.:* Die Fusion, ITER und der Stellarator in Greifswald. Dt. Atomforum, Bonn 1996.

620. *Pinkau, K.:* Das internationale Fusionsprojekt ITER - Kommentare zur Haltung der Bundesregierung. Rotary Club, München 1996.

*621. Pinkau, K.:* Internationale Großprojekte, ihre Begründung, Entstehung, Arbeitsweise und Auswirkungen. MPG, Schloß Ringberg, Tegernsee 1996.

622. *Pinkau, K.:* Internationale Kooperation in der Wissenschaft. Karl-Heinz-Beckurts Stiftung, Bonn 1996.

623. *Pinkau, K.:* Ist Fusionsforschung wichtig? Oder die Verfremdung des Zuschauers zum Betroffenen. DPG, Berlin 1996.

624. *Pinkau, K.:* Kernfusion - Alternative zur fossilen Energieversorgung im 21. Jahrhundert. Stiftung Wissenschaft und Politik, Ebenhausen 1996.

625. *Pinkau, K.:* Klima, Energieverbrauch und Wirtschaftsstandort im globalen Wettbewerb. Kath. Kreisbildungswerk Miesbach, Fischbachau 1996.

626. *Pinkau, K.:* Kontrollierte Kernfusion. Urania, Berlin 1996.

627. *Pinkau, K.:* Motivation für Fusionsforschung und der gegenwärtigen Stand der weltweiten Forschung. Informationsseminar Kernfusion, Darmstadt 1996.

628. *Pinkau, K.:* Present Status and Perspectives of Nuclear Fusion. ESA, Estec 1996.

629. *Pinkau, K.:* Stand der Kernfusion. Die Insel, Marl 1996.

630. *Pinkau, K.:* Stand und Perspektiven der Fusionsforschung. DPG, Jena 1996.

631. *Pinkau, K.:* Stand und Perspektiven der Fusionsforschung. Ev. Studentengemeinde, Greifswald 1996.

632. *Pinkau, K.:* Stand und Perspektiven der Fusionsforschung. MNU Tagung, Düsseldorf 1996.

633. *Pinkau, K.:* Stand und Perspektiven der Fusionsforschung - Das Fusionsexperiment Wendelstein. Christus-Kirche, Greifswald 1996.

634. *Pinkau, K.:* Stand und Perspektive der Fusionsforschung. Ges. Dt. Naturforscher und Ärzte, Regensburg 1996.

635. *Pinkau, K.:* Strom aus Fusion. Hannover-Messe, Hannover 1996.

636. *Pinkau, K.:* Worin gründen die heutigen Vorbehalte gegenüber der Technik? Techn. Univ. München, Freising 1996.

637. *Pitcher, C.S., A. Carlson, J.C. Fuchs, G. Haas, A. Herrmann, S. Hirsch, V. Rohde, W. Suttrop, J. Schweinzer* and *M. Weinlich:* Routes to Divertor Detachment in ASDEX-Upgrade. 12th Int. Conf. Plasma Surface Interactions in Controlled Fusion Devices, St. Raphael 1996.

638. *Raupp, G., K. Lüddecke*, G. Neu, W. Treutterer, D. Zasche, T. Zehetbauer* and *ASDEX Upgrade Team:* Structure for Next Generation Discharge Control Systems. 19th Symp. on Fusion Technology, Lisbon 1996.

639. *Reichle*, R., J.K. Ehrenberg*, N.A.C. Gottardi*, K. McCormick* et al.: Low Energy Neutral Fluxes in the JET Divertor. 12th Int. Conf. on Plasma Surface Interactions in Controlled Fusion Devices, St. Raphael 1996.

640. *Reinmüller, K., A. Bergmann* and *K. Lackner:* Entstehung von 'Hot Spots' in mikroskopischen PIC-Simulationen. Verhandl. DPG (VI) **31**, 766, P15.12 (1996).

641. *Reinmuth, J., F. Passek, M. Donath* and *V. Dose:* Appearance Potential Spectroscopy an $FeNi_3$. Verhandl. DPG (VI) **31**, 1910, O38.7 (1996).

642. *Reiter, S.:* Sauerstoffinduzierte Rekonstruktion vizinaler Kupferoberflächen. SFB-338 Seminar, Filzmoos 1996.

643. *Reiter, S.* and *E. Taglauer:* Surface Faceting on Cu(115) Induced by Oxygen Adsorption. 5th Int. Conf. on the Structure of Surfaces, Aix-en-Provence 1996.

644. *Reiter, S., S. Wolf* and *E. Taglauer:* Sauerstoffinduzierte Facettierung und Rekonstruktion auf gestuften Cu-Oberflächen. Verhandl. DPG (VI) **31**, 1814, O14.7 (1996).

645. *Renner, H.:* Advanced Stellarator W7-X: Divertor Design and Engineering. US-Japan Workshop P279 on High Heat Flux Components and Plasma Surface Interactions for Next Fusion Devices, JAERI, Naka 1996.

646. *Renner, H.:* Divertor for W7-X - Diagnostics. Kolloquium, Nat. Inst. for Fusion Science, Toki-Shi 1996.

647. *Renner, H.:* Divertor for W7-X - Modelling of W7-X Boundary. Kolloquium, Nat. Inst. for Fusion Science, Toki-Shi 1996.

648. *Renner, H.:* Divertor for W7-X - Physics and Engineering, Design. Kolloquium, Nat. Inst. for Fusion Science, Toki-Shi 1996.

649. *Renner, H.:* Divertor for W7-X - Vessel and In-Vessel Components. Kolloquium, Nat. Inst. for Fusion Science, Toki-Shi 1996.

650. *Renner, H.:* Prospects of W7-X Stellarator. Kolloquium, Nat. Inst. for Fusion Science, Toki-Shi 1996.

651. *Renner, H., E. Strumberger, J. Kißlinger, J. Nührenberg* and *H. Wobig:* Boundary Modelling of the Stellarator Wendelstein 7-X. 12th Int. Conf. on Plasma Surface Interactions in Controlled Fusion Devices, St. Raphael 1996.

652. *Rohde, V., M. Laux, P. Bachmann, A. Herrmann, M. Weinlich* and *ASDEX Upgrade Team:* Direct Measurement of the Plasma Potential in the Edge of ASDEX Upgrade Using a Self Emitting Probe. 12th Int. Conf. Plasma Surface Interactions in Controlled Fusion Devices, St. Raphael 1996.

653. *Romé, M., U. Gasparino, H. Maaßberg* et al.: Kinetic Description of Low Density ECRH Discharges at W7-AS. Joint Varenna-Lausanne Int. Workshop on Theory of Fusion Plasmas, Varenna 1996.

654. *Roth, J.:* The ASDEX-Upgrade Tungsten Divertor Experiment. Sandia Labs., Albuquerque,NM 1996.

655. *Roth, J.:* High-Z Materials for First Wall Application. Sandia Labs., Livermore,CA 1996.

656. *Roth, J.* and *Arbeitsgruppe Plasma-Wand-Wechselwirkung:* Recent Results on Sputtering Erosion and D/T Codeposition. ITER Working Meeting on Materials for In-Vessel Components, Garching 1996.

657. *Rust, N., B. Wolle*, G. Beikert, M. Kick, U. Stroth* et al.: Simulation und Analyse von Neutralteilchen-Spektren bei W7-AS. Verhandl. DPG (VI) **31**, 763, P17.2 (1996).

658. *Ryter, F., M. Alexander, J. Köllermeyer, F. Leuterer, A.G. Peeters, G. Pereverzev, W. Suttrop, ECRH-Team, ASDEX Upgrade Team* and *NI-Team:* Perturbative Transport from Sawtooth Propagation and ECRH Modulation in ASDEX Upgrade. EU-US Workshop on Transport in Fusion Plasmas, Varenna 1996.

659. *Ryter, F.* and *ASDEX Upgrade Team:* Improved Confinement in ASDEX Upgrade. 5th Workshop of the ITER Expert Group on Database and Modelling, Montreal 1996.

660. *Ryter, F., ASDEX Upgrade Team* and *NI-Team:* The 1st Contribution from ASDEX Upgrade to the ITER H-Mode Confinement DB. 4th Workshop of the Database and Modelling Expert Group, Moscow 1996.

661. *Ryter, F., A. Kallenbach, ASDEX Upgrade Team* and *NI-Team:* Status of the H-L Studies in ASDEX Upgrade. 4th Workshop of the Database and Modelling Expert Group, Moscow 1996.

662. *Ryter, F., V. Mertens* and *ASDEX Upgrade Team:* Operation above Greenwald Limit in ASDEX Upgrade. 3rd Workshop of the ITER Expert Group on Confinement and Transport, Montreal 1996.

663. *Salat, A.* and *J.A. Tataronis*:* The Shear Alfvén Wave in a Three-Dimensional Ideal MHD Equilibrium. 38th Annual Meeting of the Div. of Plasma Physics, Denver,CO 1996.

664. *Sapper, J.:* The Superconducting Magnet System for the Wendelstein 7-X Stellarator. 12th Topical Meeting on the Technology of Fusion Energy, ANS, Reno,NV 1996.

665. *Sardei, F., Y. Feng, P. Grigull* et al.: Island Divertor Studies on W7-AS. 12th Int. Conf. on Plasma Surface Interactions in Controlled Fusion Devices, St. Raphael 1996.

666. *Sardei, F., P. Grigull, R. Brakel, Y. Feng, S. Fiedler, G. Herre, D. Hildebrandt, J.V. Hofmann, J. Kißlinger, G. Kühner, H. Niedermeyer, H. Ringler, F. Wagner, W7-AS-Team* and *NI-Group:* Island Divertor Studies on W7-AS. 12th Int. Conf. Plasma Surface Interactions in Controlled Fusion Devices, St. Raphael 1996.

667. *Saß, M., A. Annen, R. Beckmann* and *W. Jacob:* Bindungsstruktur PECVD-deponierter amorpher hydrogenisierter Bor-Schichten. Verhandl. DPG (VI) **31**, 1235, DS39.49 (1996).

668. *Schauer, F.:* Cooling of the W7-X Superconducting Coils. 16th Cryog. Eng. Conf., Kitakyushu 1996.

669. *Schauer, F.:* Demountable and Gas Permeable High Voltage Insulation for Superconducting Coil Connections. Meeting of CIGRE TF 15.06-01 'Cryogenic Insulation Materials and Technology', Paris 1996.

670. *Schauer, F.:* Das Stellarator-Fusionsexperiment Wendelstein 7-X. Chem.-Phys. Gesellschaft, Wien 1996.

671. *Schimmel*, T., U. von Toussaint*, J. Küppers* and *M. Lux-Steiner:* Der Übergang von stetiger Abtastung zu atomarem Stick-Slip: Untersuchungen mit dem Rasterkraftmikroskop auf $WSe_2$. Verhandl. DPG (VI) **31**, 1868, O28.2 (1996).

672. *Schleußner*, D., D. Rösler*, J. Becker*, R. Behrisch* et al.: Temperature Controlled Outgassing of Divertor Materials. 3rd Int. Workshop on Tritium Effects in Plasmafacing Components, Ispra 1996.

673. *Schleußner*, D., D. Rösler*, M. Ehrt*, R. Behrisch* et al.: Meßverfahren und Versuchsanlagen zur zerstörungsfreien quantitativen Untersuchung von Graphitproben hinsichtlich der Abgabe von Gasen. Verhandl. DPG (VI) **31**, 2100, VA1.8 (1996).

674. *Schneider, R.:* Randschichtphysik: Experiment und Modellierung. Graduiertenkolleg, Düsseldorf/Jülich 1996.

675. *Schneider, R., H.-S. Bosch, J. Neuhauser, D.P. Coster, K. Lackner* and *M. Kaufmann:* Divertor Geometry Optimization for ASDEX Upgrade. 12th Int. Conf. on Plasma Surface Interactions in Controlled Fusion Devices, St. Raphael 1996.

676. *Schneider, R., D.P. Coster, K. Borrass, H.-S. Bosch, J. Neuhauser, K. Lackner, M. Kaufmann, A. Kallenbach, K. Behringer, K. Büchl, R. Dux, J.C. Fuchs, G. Haas, A. Herrmann, K.-F. Mast, J. Schweinzer, ASDEX Upgrade Team* et al.: Modelling of Radiation Distribution and Impurity Divertor Compression in ASDEX Upgrade. 16th IAEA Fusion Energy Conf., Montreal 1996.

677. *Schwenn, U.:* Computer Simulation of Plasmas. Summer Univ. for Plasma Physics, IPP, Garching 1996.

678. *Schwenn, U.:* Parallelization and Visualization of HINT Code and Results (W7-X). Nat. Inst. for Fusion Science, Nagoya 1996.

679. *Schwenn, U.:* Performance of the 3D Plasma Equilibrium Code HINT on Vector and MPP Systems. 6. Interdisziplinäre Jahrestagung 'Nichtlineare Dynamik, Chaos und Strukturbildung', Techn. Univ. München 1996.

680. *Schwörer, R., J. Roth, K. Asmussen, C. García-Rosales, D. Hildebrandt, K. Krieger, R. Neu, V. Rohde, W. Schneider* and *ASDEX Upgrade Team:* Migration of Tungsten Eroded from Divertor Tiles in ASDEX Upgrade. 12th Int. Conf. Plasma Surface Interactions in Controlled Fusion Devices, St. Raphael 1996.

681. *Scott, B., S. Camargo** and *F. Jenko:* Self-Consistent Computation of Transport by Fluid Drift Turbulence in Tokamak Geometry. 16th IAEA Fusion Energy Conf., Montreal 1996.

682. *Sergeev*, V.Yu., O.A. Sineva*, P.T. Lang, K. Büchl* and *ASDEX Upgrade Team:* Ablation Rate Oscillations of Carbon Pellets Injected into ASDEX Upgrade. Verhandl. DPG (VI) **31**, 745, P15.6 (1996).

683. *Simmet, E.E.* and *U. Stroth:* Statistical Analysis of the Density and the Energy Confinement Time at the Transition from Linear to Saturated Ohmic Confinement. 23rd EPS Conf. on Controlled Fusion and Plasma Physics, Kiev 1996.

684. *Simon-Weidner, J., N. Jaksic* and *J. Sapper:* Buckling Analysis of the W7-X Inner Vacuum Vessel. 19th Symp. on Fusion Technology, Lisbon 1996.

685. *Sokoll, M., M. Bessenrodt-Weberpals* and *ASDEX Upgrade Team:* Tomographische Rekonstruktion von MHD-Instabilitäten am Tokamak ASDEX Upgrade. Verhandl. DPG (VI) **31**, 712, P6.6 (1996).

686. *Speth, E.:* Comments on JENIPHER. Joint Development Comm. Meeting, JET, Abingdon 1996.

687. *Speth, E.:* Further Comments on JENIPHER. Joint Development Comm. Meeting, CEA, Cadarache 1996.

688. *Speth, E.:* Neutralteilchenheizung von Fusionsplasmen. Festvortrag, Univ. Frankfurt 1996.

689. *Speth, E.:* Neutralteilchenheizung von Fusionsplasmen. Kolloquium, Univ. Frankfurt 1996.

690. *Speth, E.:* Status of BATMAN and the 2nd AUG-Injector. Joint Development Comm. Meeting, JET, Abingdon 1996.

691. *Steuer, K.-H.:* Fusionsreaktoren, schnelle Brüter und Sonnenkraftwerke - Stand und Perspektiven bei der Erschließung neuer Energiequellen. 3 Schulvorträge, MPG Hauptversammlung, Saarbrücken 1996.

692. *Steuer, K.-H.:* Kernfusion - Forschung für die Energie der Zukunft. Fachhochschule Saarbrücken 1996.

693. *Stork*, D.* and *K. McCormick:* Optimisation of JET Steady-State ELMy Discharges with ITER-Relevant Divertor Conditions. 16th IAEA Int. Conf. on Plasma Physics and Controlled Nuclear Fusion Research, Montreal 1996.

694. *Streibl, B., S. Deschka, O. Gruber, B. Jüttner, P.T. Lang, K. Mattes, G. Pautasso, J. Perchermeier, H. Schneider, U. Seidel, W. Suttrop, M. Weißgerber* et al.: In-Vessel Cryo Pump for ASDEX Upgrade Divertor II. 19th Symp. on Fusion Technology, Lisbon 1996.

695. *Stroth, U.:* Bayes'sche Statistik zur Analyses Experimenteller Daten. Antrittsvorlesung, Univ. Heidelberg 1996.

696. *Stroth, U.:* Comparison of Stellarator and Tokamak Transport. EU-US Transport Task Force Workshop, Varenna 1996.

697. *Stroth, U.:* Confinement Modes in Stellarators. Europ. Fusion Program Workshop, Stockholm 1996.

698. *Stroth, U.:* Einführung in die Plasmaphysik II. Fachvorlesung, Univ. Heidelberg, WS 1996/97.

699. *Stroth, U.:* Experimental Results from Stellarators. Summer Univ. for Plasma Physics, IPP, Garching 1996.

700. *Stroth, U.:* Vergleichende Transportstudien in Stellaratoren und Tokamaks. Seminar, Univ. Heidelberg 1996.

701. *Stroth, U., R. Burhenn, J. Geiger* et al.: Comparative Studies of Stellarator and Tokamak Transport. 16th IAEA Int. Conf. on Plasma Physics and Controlled Nuclear Fusion Research, Montreal 1996.

702. *Sun*, G., M. Fiedrich*, R. Grötzschel*, R. Behrisch* et al.: Tritium Depth Profiling in Carbon by Accelerator Mass Spectrometry. 3rd Int. Workshop on Tritium Effects in Plasmafacing Components, Ispra 1996.

703. *Suttrop, W.:* MHD-Phänomene in Tokamakplasmen. Verhandl. DPG (VI) **31**, 698, PII (1996).

704. *Suttrop, W.:* Tokamak Operational Range Restrictions Imposed by Edge Phenomena. Kolloquium, EPFL-CRPP, Lausanne 1996.

705. *Suttrop, W.:* Untersuchung von MHD-Phänomenen im Tokamak ASDEX Upgrade durch Beobachtung der Elektronen-Zyklotronresonanz Emission. Kolloquium, IPF Stuttgart 1996.

706. *Taglauer, E.:* Adsorbat-induzierte Rekonstruktion vizinaler Kupfer-Oberflächen. Univ. Osnabrück 1996.

707. *Taglauer, E.:* Struktur und Zusammensetzung von NiAl(100). Techn. Univ. Wien 1996.

708. *Takizuka, T.* and *ITER Confinement Database and Modelling Expert-Group:* Threshold Power and Energy Confinement for ITER. 16th Int. Conf. on Plasma Physics and Controlled Nuclear Fusion Research, Montreal 1996.

709. *Taroni*, A., A. Cherubini*, G. Corrigan*, K. McCormick* et al.: Simulation of JET Plasmas with Combined Core and Edge Transport Codes. 23rd EPS Conf. on Controlled Fusion and Plasma Physics, Kiev 1996.

710. *Taroni*, A.* and *K. McCormick:* Energy and Particle Transport Modelling with a Time-Dependent Combined Core and Edge Transport Code. 16th IAEA Int. Conf. on Plasma Physics and Controlled Nuclear Fusion Research, Montreal 1996.

711. *Tasso, H.:* Hamiltonians and Fluctuations of Continuous Plasma Models. Groupe Physique et Statistique des Plasmas, Univ. Libre de Bruxelles 1996.

712. *Toussaint*, U. von, T. Schimmel** and *J. Küppers:* Computersimulation des Abbildungsproszesses auf atomarer Skala beim Rasterkraftmikroskop. Verhandl. DPG (VI) **31**, 1898, O35.5 (1996).

713. *Treutterer, W., J. Gernhardt, O. Gruber, G. Raupp, U. Seidel, ASDEX Upgrade Team* et al.: Plasma Shape Control Design in ASDEX Upgrade. 19th Symp. on Fusion Technology, Lisbon 1996.

714. *Ullrich, W., H.-S. Bosch, F. Hoenen*, T. Kass* and *ASDEX Upgrade Team:* Messung des Tritonen Burnup in ASDEX Upgrade. Verhandl. DPG (VI) **31**, 733, P10.2 (1996).

715. *Vlases*, G.* and *K. McCormick:* Effect of Divertor Configuration on Plasma Performance in JET. 16th IAEA Int. Conf. on Plasma Physics and Controlled Nuclear Fusion Research, Montreal 1996.

716. *Wagner, F.:* Energie aus dem Sternenfeuer - Fusionsforschung in Greifswald. Volkshochschule, Greifswald 1996.

717. *Wagner, F.:* Experimentelle Plasmaphysik I. Vorlesung, Techn. Univ. München, WS 1996/97.

718. *Wagner, F.:* Experimentelle Plasmaphysik II. Vorlesung, Techn. Univ. München, SS 1996.

719. *Wagner, F.:* H-Mode Studies in W7-AS. Seminar, Kyushu Univ., Kasuga-shi 1996.

720. *Wagner, F.:* Kernfusion: Stand und Perspektiven. Vortrag, Wissenschaftszentrum, Bonn 1996.

721. *Wagner, F.:* Physics in Stellarators. Seminar, CIEMAT, Madrid 1996.

722. *Wagner, F.:* The Physics of W7-AS in Relation to W7-X. 8th Joint Russian-German Meeting on ECRH and Gyrotrons, Nizhny Novgorod 1996.

723. *Wagner, F.:* Physikalische Grundlagen des Wendelstein 7-X. Journal Club, Walther-Meisner-Inst., Garching 1996.

724. *Wagner, F.:* Stand und Perspektive. Seminar, Fa. Siemens, Erlangen 1996.

725. *Wagner, F.:* Topics in Toroidal Confinement. 8th Int. Conf. on Plasma Physics, Nagoya 1996.

726. *Wagner, F.:* Die wesentlichen wissenschaftlichen Ergebnisse der Kernfusionsforschung der letzten 10 Jahre. Info-Seminar Kernfusion, Techn. Hochschule Darmstadt 1996.

727. *Wang, W., J. Roth* and *W. Jacob:* Isotopic Exchange in a-C:H. Workshop on Tritium Effects in Plasmafacing Components, Ispra 1996.

728. *Weinlich, M., A. Carlson, M. Laux, C.S. Pitcher* and *V. Rohde:* Abhängigkeit des Stroms zu einer Langmuirsonde von der Geometrie der umgebenden Strukturen. Verhandl. DPG (VI) **31**, 759, P15.47 (1996).

729. *Wenzel U., A. Kallenbach, S. Hirsch, R. Dux, T. Thoma, B. Napiontek, J.C. Fuchs, K.-F. Mast* and *H. Kastelewicz:* Spatial Radiation Profiles in the ASDEX Upgrade Divertor for Attached and Detached Plasmas. 12th Int. Conf. on Plasma Surface Interactions in Controlled Fusion Devices, St. Raphael 1996.

730. *Wesner, F.:* ICRF Operation during H-Mode with ELMs - Development Status at ASDEX Upgrade. 19th Symp. on Fusion Technology, Lisbon 1996.

731. *Wesner, F.:* Plasma Heating. Summer Univ. for Plasma Physics, IPP, Garching 1996.

732. *Wilhelm. R.:* Einsatz von nicht-thermischen Niedertemperaturplasmen in der Oberflächen- und Dünnschichttechnologie. Univ. Wuppertal 1996.

733. *Wilhelm, R.:* Plasma-Applications in Surface- and Thinfilm Technology. Univ. Gent 1996.

734. *Wilhelm, R.:* Plasma Technology. Summer Univ. for Plasma Physics, IPP, Garching 1996.

735. *Wilhelm, R.:* Plasmatechnologie in Deutschland: Stand und Perspektiven. Univ. Bochum 1996.

736. *Wilhelm, R.:* Stand und Aussichten der Kernfusion. Univ. Oldenburg 1996.

737. *Wilhelm, R.* and *W. Jacob:* 'Running' Waveguide Discharges. Univ. of Sofia 1996.

738. *Wobig, H.:* Introduction to Stellarator Physics. Summer Univ. for Plasma Physics, IPP, Garching 1996.

739. *Wobig, H.:* Theoretische Plasmaphysik I. Vorlesung, Techn. Univ. München, WS 1996/97.

740. *Wobig, H.:* Theoretische Plasmaphysik II. Vorlesung, Techn. Univ. München, SS 1996.

741. *Wobig, H.:* Vom Nördlinger Ries, vom Chaos oder der Schwierigkeit ein Plasma einzuschließen. Humboldt-Univ. Berlin 1996.

742. *Zebisch, P., P. Grigull, V. Dose, E. Taglauer* and *W7-AS-Team:* Mass Spectroscopic Measurements in the Plasma Edge of the W7-AS Stellarator. 12th Int. Conf. on Plasma Surface Interactions in Controlled Fusion Devices, St. Raphael 1996.

743. *Zehetbauer, T., P. Franzen, G. Neu, V. Mertens, G. Raupp, W. Treutterer, D. Zasche* and *ASDEX Upgrade Team:* Plasma Regime Guided Discharge Control at ASDEX Upgrade. 19th Symp. on Fusion Technology, Lisbon 1996.

744. *Zeiler, A.:* 3D Simulationen zur Tokamak Randschicht Turbulenz. Kolloquium, IPF Stuttgart 1996.

745. *Zeiler, A.:* Electron and Ion Temperature Fluctuations in Three-Dimensional Drift-Resistive Ballooning Turbulence. Workshop on Transport in Fusion Plasmas, Varenna 1996.

746. *Zeiler, A., D. Biskamp, J.F. Drake** et al.: Three-Dimensional Plasma-Edge Turbulence Including Electron and Ion Temperature Fluctuations. 16th IAEA Fusion Energy Conf., Montreal 1996.

747. *Zohm, H.:* The H-Mode Operational Window in Local Parameters. 4th Europ. Fusion Physics Workshop, Stockholm 1996.

748. *Zohm, H.:* Plasmaphysik und Fusionsforschung II. Vorlesung, Univ. Augsburg, SS 1996.

749. *Zohm, H., W. Suttrop, H.J. de Blank, W. Herrmann, A. Kallenbach, T. Kass, M. Kaufmann, B. Kurzan, M. Maraschek, H. Reimerdes, F. Ryter, H. Salzmann, J. Schweinzer, J. Stober, ASDEX Upgrade Team, ECRH-Team, ICRH-Team, NI-Team* et al.: Study of H-Mode Physics in ASDEX Upgrade. 16th IAEA Fusion Energy Conf., Montreal 1996.

# Internal Laboratory Reports

IPP 1/293 *Wölfl, F.:* Der Effekt von Edge Localized Modes auf den Einschluß von Teilchen und Energie im Tokamak.

IPP 1/294 *Ullrich, W.:* Messung sekundärer Fusionsreaktionen in ASDEX Upgrade.

IPP 1/296 *Lang, P.T., H. Zohm, K. Büchl, J.C. Fuchs, O. Gehre, O. Gruber, R.S. Lang, V. Mertens, J. Neuhauser, H. Salzmann, ASDEX Upgrade Team* and *NI-Team:* Pellet Injection into ASDEX Upgrade Plasmas.

IPP 1/297 *Maraschek, M., J.C. Fuchs, K.-F. Mast, V. Mertens* and *H. Zohm:* Online Determination of Total Radiated Power by Bolometric Cameras with Statistical Methods.

IPP 1/298 *Kass, T.:* Untersuchungen zum Verhalten hochenergetischer ionen in magnetisch eingeschlossenen Plasmen.

IPP 1/300 *Reimerdes, H.:* Bestimmung lokaler Transportkoeffizienten während Edge Localized Modes am Tokamakexperiment ASDEX Upgrade.

IPP 1/301 *Gayer, T.* and *H. Zohm:* MHD.PRO - Ein Programm zur Stabilitätsanalyse von MHD-Gleichgewichten im Screw-Pinch.

IPP 1/302 *Köppendörfer, W.:* Die Eisenabschirmung um ASDEX Upgrade.

IPP 1/303 *Müller, H.W.:* Studie zur q-Profil Bestimmung mittels Pelletablation an ASDEX Upgrade.

IPP 1/304 *Lang, P.T., K. Büchl, M. Kaufmann, R.S. Lang, V. Mertens, H.W. Müller, J. Neuhauser* et al.: Pellet Injection into ASDEX Upgrade Plasmas with Improved Szenario from the Magnetic High-Field Side.

IPP 1/305 *Bosch, H.-S.* and *B. Frohwitter (Eds.):* ASDEX Upgrade Results - Publications and Conference Contributions. Period 10/96 to 12/96.

IPP 1/306 *Suttrop, W., A.G. Peeters, ASDEX Upgrade Team* and *NI-Group:* Practical Limitations to Plasma Edge Temperature Measurements by Radiometry of Electron Cyclotron Emission.

IPP 1/307 *Pitcher*, C.S., A.H. Boozer*, H. Murmann, J. Schweinzer* and *W. Suttrop:* The Relation of Edge Confinement to Global Confinement in ASDEX Upgrade.

IPP 2/331 *Herrnegger, F.* and *F. Rau (Eds.):* Proceedings of the 6. Workshop on WENDELSTEIN 7-X and Helias Reactors, Schloss Ringberg, Tegernsee (DE), 20.11.95 - 24.11.95.

IPP 2/332 *Schauer, F.:* Demontierbare, gasdurchlässige Hochspannungsisolation für die W7-X-Supraleiterverbindungen.

IPP 2/333 *Strumberger, E.* and *R. Zille:* Magnetic Field Structures and Plasma Properties of High-Iota High-Mirror W7-X Configurations.

IPP III/208 *Feng, Y., F. Sardei, J. Kißlinger* and *P. Grigull:* A 3D Monte Carlo Code for Plasma Transport in Island Divertors.

IPP III/210 Max-Planck-Institut für Plasmaphysik, Garching(DE): W7-AS Contributions to the 7th Toki Conference, Toki (JP), 28.11.95 - 1.12.95.

IPP III/211 *McCormick, K., S. Fiedler, G. Kocsis*, J. Schweinzer* et al.: Edge Density Measurement with a Fast Li-Beam Probe on Tokamak and Stellarator Experiments.

IPP III/212 Max-Planck-Institut für Plasmaphysik, Garching(DE): W7-AS Contributions to the 11th Topical Conference High-Temperature Plasma Diagnostics. W7-AS Contributions to the 12th International Conference on Plasma Surface Interactions. W7-AS Contributions to the 23rd EPS Conference on Controlled Fusion and Plasma Physics.

IPP III/213 *Zoletnik*, S., G. Kocsis*, S. Fiedler, K. McCormick, J. Schweinzer* et al.: Observations with the Li-Beam Diagnostic on W7-AS.

IPP III/214 *Teubel, A.:* Orbit Calculations for Determination of Heavy Ion Beam Probe Ports on W7X.

IPP III/215 *Simmet, E.E., H.-U. Fahrbach, W. Herrmann* and *U. Stroth:* Analysis of the Ion Energy Transport in Ohmic Discharges in the ASDEX Tokamak.

IPP III/216 *Stroth, U.:* A Comparative Study of Stellarator and Tokamak Transport.

IPP 4/270 *Knobloch, A.F.:* Equations for Conceptual Tokamak Fusion Reactor Design.

IPP 4/273 *Puri, S.:* Radiative Transport in Toroidal Plasmas.

IPP 4/274 *Girka*, I.O.:* How Ripples of the Steady Magnetic Field in Tokamaks Influence Propagation, Conversion and Absorption of Alven and Fast Magnetosonic Waves.

IPP 5/66 *Brambilla, M.:* A Full Wave Code for Ion Cyclotron Waves in Toroidal Plasmas.

IPP 5/67 *Günter, S.:* Optische Eigenschaften dichter Plasmen.

IPP 5/68 *Kardaun, O.* and *A. Kus:* Basic Probability Theory and Statistics for Experimental Plasma Physics.

IPP 5/69 *Zeiler, A., J.F. Drake** and *D. Biskamp:* Electron Temperature Fluctuations in Drift-Resistive Balooning Turbulence.

IPP 5/70 *Borrass, K., R. Schneider* and *R. Farengo*:* A Scrape-off Layer Based Model for Hugill-Greenwald Type Density Limits.

IPP 5/71 *Brambilla, M.:* The Physics of Ion Cyclotron Heating in Tokamaks.

IPP 5/72 *Bosch, H.-S.* and *B. Frohwitter (Eds.):* ASDEX Upgrade Results - Publications and Conference Contributions. Period 10/96 to 12/96.

IPP 5/73 *Kristof, G.:* Two-Fluid Simulation of Expansion and Confinement of Pellet-Produced Hydrogen Clouds in Hot Magnetized Plasmas.

IPP 6/334 *Meyer-Spasche, R.* and *D.F. Düchs:* A General Method for Obtaining Unconventional and Nonstandard Difference Schemes.

IPP 6/337 *Throumoulopoulos*, G.N.* and *D. Pfirsch:* Negative-Energy Perturbations in Circularly Cylindrical Equilibria within the Framework of Maxwell-Drift Kinetic Theory.

IPP 6/338 *Tasso, H.:* An Exercise Motivated by Dissipative Magnetohydrodynamic Stability.

IPP 6/339 *Zeiler, A., D. Biskamp* and *J.F. Drake*:* 3D Collisional Drift-Wave Turbulence, Role of Magnetic Shear.

IPP 6/340 *Tasso, H.:* On Magnetized Parallel Flows.

IPP 6/341 *Kaiser*, R.* and *A. Salat:* Analytic Three-Dimensional Solutions of the Magnetohydrostatic Equations with Twisted Field Lines.

IPP 6/342 *Croci, R.:* Non Local Effects of ICRH on the Singularities of the E.M. Field.

IPP 6/343 *Throumoulopoulos*, G.N.* and *H. Tasso:* Cylindrical Ideal Magnetohydrodynamic Equilibria with Incompressible Flows.

IPP 6/344 *Pfirsch, D.* and *D. Correa-Restrepo:* Lagrangians for Plasmas in Drift-Fluid Approximation.

IPP 6/345 *Tasso, H.:* A Nonlinear Equation for Drift Waves.

IPP 8/10 *Kornejew, P.:* Bestimmung der Elektronenparameter in Randschichten unter Verwendung eines thermischen Heliumstrahls.

IPP 9/110 *Keudell, A. von:* Wachstumsmechanismen bei der plasmagestützten Abscheidung von Kohlenwasserstoffschichten, eine in situ Ellipsometriestudie.

IPP 10/1 *Dux, R., A. Kallenbach* and *ASDEX Upgrade Team:* Characteristics and Modelling of Radiative Boundary Discharges in ASDEX Upgrade.

IPP 10/2 *Asmussen, K.:* Untersuchungen zum Verhalten von Wolfram in Tokamakplasmen.

IPP 10/3 *Napiontek, B.:* Untersuchung der Strahlungsbilanz im Divertor von ASDEX Upgrade.

IPP 10/4 *Bosch, H.-S.* and *B. Frohwitter (Eds.):* ASDEX Upgrade Results - Publications and Conference Contributions. Period 10/96 to 12/96.

## External Laboratory Reports


EUR FU/XII-012/108/96 — *Heinemann B.:* Preliminary Design Status of the Ion Source and Accelerator of the ITER NBI-System. In: Engineering and Physics Design of the ITER NBI 1 MeV, 12.5 MW Module. NET Next Europ. Torus, Garching.

EUR FU/XII-012/108/96 — *Feist, J.-H.:* Magnetic Shielding for ITER NBI. In: Engineering and Physics Design of the ITER NBI 1 MeV, 12.5 MW Module. NET Next Europ. Torus, Garching.

IFSR 746 — *H. Tasso* and *W. Horton:* Statistical Properties of the Drift Wave Fluctuations. Inst. For Fusion Studies, Austin,TX.

JET-R(96)06 — *Huysmans*, G.T.A., R. Schneider* and *K. Borrass:* SOL-One, A One-D Scrape-off-Layer Transport Code. JET Joint Europ. Torus, Abingdon.

NIFS-450 — *Biskamp, D.* and *D. Sato*:* Partial Reconnection in the Sawtooth Collapse. Nat. Inst. for Fusion Science, Nagoya.

# Author Index

# Teams

**ASDEX Upgrade-Team:**, M.Albrecht, M.Alexander, K.Asmussen, G.Becker, K.Behler, K.Behringer, A.Bergmann, M.Bessenrodt-Weberpals, K.Borrass, H.-S.Bosch, M.Brambilla, F.Braun, H.Brinkschulte, K.Büchl, A.Buhler, A.Carlson, R.Chodura, D.Coster, L.Cupidol*, H.-J.De Blank, S.De Peña Hempel, S.Deschka, C.Dorn, R.Drube, R.Dux, W.Engelhardt, J.Engstler, H.-U.Fahrbach, J.-H.Feist, S.Fiedler, P.Franzen, J.C.Fuchs, G.Fußmann, J.Gafert, O.Gehre, J.Gernhardt, O.Gruber, S.Günter, G.Haas, K.Hallatschek, J.Hartmann, , B.Heinemann, G.Herppich, A.Herrmann, W.Herrmann, S.Hirsch, M.Hoek, F.Hofmeister, F.Hoenen*, H.Hohenöcker, P.Ignacz, D.Jacobi, W.Junker, A.Kallenbach, O.Kardaun, T.Kass, M.Kaufmann, A.Khutoretski*, H.Kollotzek, W.Köppendörfer, W.Kraus, K.Krieger, B.Kurzan, B.Kuteev*, K.Lackner, P.T.Lang, R.S.Lang, M.Laux, L.L.Lengyel, F.Leuterer, M.Maraschek, M.Markoulaki*, K.-F.Mast, P.McCarthy*, D.Meisel, R.Merkel, V.Mertens, H.W.Müller, F.Münich, H.Murmann, B.Napiontek, G.Neu, R.Neu, J.Neuhauser, J.-M.Noterdaeme, E.Pasch, G.Pautasso, A.G.Peeters, G.Pereverzev, G.Petravich*, C.S.Pitcher, W.Poschenrieder, G.Raupp, K.Reinmüller, R.Riedl, V.Rohde, H.Röhr, J.Roth, F.Ryter, H.Salzmann, W.Sandmann, H.-B.Schilling, M.Schittenhelm, D.Schlögl, H.Schneider, R.Schneider, W.Schneider, G.Schramm, S.Schweizer, J.Schweinzer, R.Schwörer, B.D.Scott, U.Seidel, S.Sesnic, I.Shustov*, A.Silva*, M.Sokoll, E.Speth, A.Stäbler, K.-H.Steuer, J.Stober, B.Streibl, W.Suttrop, A.Thoma, W.Treutterer, M.Troppmann, N.Tsois*, M.Ulrich, P.Varela*, H.Verbeek, P.Verplancke, O.Vollmer, Z.Wang*, H.Wedler, M.Weinlich, U.Wenzel, F.Wesner, R.Wolf, R.Wunderlich, N.Xantopoulus*, Q.Yu*, D.Zasche, H.-P.Zehrfeld, T.Zehetbauer, H.Zohm, M.Zouhar.

**ICRH-Group:** W.Becker, F.Braun, H.Faugel, R.Fritsch, D.Hartmann, F.Hofmeister, J.-M.Noterdaeme, S.Puri, P.Verplancke, F.Wesner.

**ITER Confinement Database and Modelling Expert Group:** D.Boucher*, G.Bracco*, T.N.Carlstrom*, J.G.Cordey*, J.W.Connor*, A.N.Chudnovskii*, J.C.DeBoo*, W.Dorland*, Yu.V.Esipchuk*, S.J.Fielding*, T.Fukuda*, R.S.Granetz*, M.Greenwald*, T.Hirayama*, G.T.Hoang*, W.Houlberg*, Y.Kamada*, O.Kardaun, S.M.Kaye*, M.Kikuchi*, A.Kus, Y.Martin*, T.Matsuda*, Y.Miura*, O.Naito*, Y.Ogawa*, J.Ongena*, M.Ossipenko*, F.Perkins*, E.Righi*, F.Ryter, D.P.Schissel*, J.A.Snipes*, U.Stroth, H.Tamai*, T.Takizuka*, K.Thomsen*, M.Valovic*.

**ITER H- and L-Mode Database-Working-Group:** J.A.Snipes*, R.S.Granetz*, M.Greenwald*, F.Ryter, O.Kardaun, U.Stroth, A.Kus, M.Valovic*, S.J.Fielding*, J.C.DeBoo*, T.Carlstrom*, D.P.Schissel*, K.Thomson*, D.J.Campbell*, J.P.Christiansen*, J.G.Cordey*, E.Righi*, Y.Miura*, N.Suzuki*, M.Mori*, T.Matsuda*, H.Tamai*, T.Fukuda*, Y.Kamada, T.Matsuda, M.Sato*, T.Takizuka*, K.Tsuchiya*, S.M.Kaye*.

**NI-Group:** M.Ciric, J.-H.Feist, B.Heinemann, W.Kraus, W.Melkus, S.Obermayer; W.Ott, F.-P.Penningsfeld, F.Probst, R.Riedl, W.Schärich, E.Speth, A.Stäbler, R.Süß, O.Vollmer, K.Wittenbecher.

**NI-Team(W7-AS):** W.Melkus, W.Ott, F.-P.Penningsfeld, F.Probst, E.Speth, R.Süß, A.Teubel.

**W7-AS-Team:** R.Balbin, J.Baldzuhn, K.Behringer, B.Bomba, R.Brakel, R.Büchse, R.Burhenn, G.Cattanei, A.Dodhy, D.Dorst, K.Dyabilin, A.Elsner, M.Endler, K.Engelhardt, V.Erckmann, U.Gasparino, J.Geiger, T.Geist, S.Geissler, L.Giannone, P.Grigull, G.Grünwald, H.Hacker, H.-J.Hartfuß, O.Heinrich, G.Herre, C.Hidalgo, M.Hirsch, J.V.Hofmann, J.Hofner, E.Holzhauer, R.Isler, R.Jänicke, J.Junker, F.Karger, M.Kick, A.Kislyakov, J.Kißlinger, C.Konrad, H.Kroiss, G.Kühner, N.F.Larinova, A.Lazaros, T.Luce, P.Luttner, H.Maaßberg, C.Mahn, W.Mandl, K.McCormick, H.Niedermeyer, W.Ohlendorf, F.Rau, H.Renner, H.Ringler, A.Rudyj, N.Ruhs, J.Saffert, J.Sapper, F.Sardei, S.Sattler, F.Schneider, U.Schneider, G.Siller, U.Stroth, G.Theimer, M.Tutter, E.Unger, F.Wagner, R.Waltz, U.Weber, A.Weller, H.Wobig, E.Würsching, S.Wurdack, D.Zimmermann, M.Zippe, S.Zöpfel.

**W7-X-Team:** S.Arndt, C.D.Beidler, R.Bünde, M.Drevlak, S.Gori, H.Greuner, G.Grieger, E.Harmeyer, C.Henning, F.Herrnegger, F.-W.Hoffmann, J.Junker, J.Kißlinger, A.Könies, P.Merkel, H.Münch, A.Nitsche, C.Nührenberg, J.Nührenberg, I.Ott, M.Pillsticker, F.Rau, H.Renner, J.Sapper, F.Schauer, I.Schönewolf, U.Schwenn, H.Strobel, E.Strumberger, M.Wanner, S.Weber, H.Wobig, R.Zille, A.V.Zolotukhin.

# University Contributions to IPP Programme

# LEHRSTUHL FÜR EXPERIMENTELLE PLASMAPHYSIK DER UNIVERSITÄT AUGSBURG

(Prof. Dr. Kurt Behringer)

## PLASMA EDGE DIAGNOSTICS

(K.Behringer, U. Fantz, H. Paulin)

### 1 Molecular Spectroscopy

Vibrational excitation of the $H_2$ molecular ground state ($X\ ^1\Sigma_g^+$) is of importance for reactive plasmas and the divertors of fusion experiments. A method is being developed to determine this population from emission spectroscopy of the Fulcher bands ($d\ ^3\Pi_u$). As shown in the Annual Report 1995, the appearance of these bands changes with plasma conditions. If heavy-particle collisions are negligible, conclusions can be drawn on the ground-state vibrational population on the basis of the Franck-Condon principle. The Franck-Condon factors for the singlet and triplet vibrational levels involved were calculated from the overlap integrals of the molecular wave functions. In contrast to the $N_2$ molecule, the ground-state vibrational temperature in $H_2$ does not project into the upper state as another Boltzmann distribution and, therefore, there is no simple correlation of vibrational temperatures in ground and excited states. The vibrational population normalized to v=0 was calculated for $H_2$ as a function of the ground-state vibrational temperature on the basis on the Franck-Condon principle ( Fig. 1).

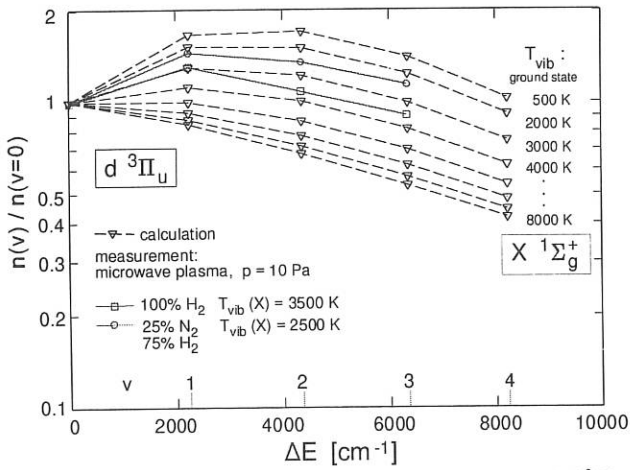


*FIG .1: Relative vibrational population of the $H_2$ level $d\ ^3\Pi_u$ as a function of the vibrational temperature of the ground state.*

Measurements of the Fulcher band vibrational distribution in a microwave plasma confirm the behaviour expected for $T_{vib} \approx 3500$ K in the ground state. To gain confidence in this method, attempts were made to change the hydrogen vibrational temperature by adding other gases to the discharge. In a $H_2/N_2$ plasma mixture $T_{vib}$ is lower (2500 K, Fig.1), probably due to a resonance phenomenon in the vibrational spacing of the two molecular ground states, which is about 0.5 eV for $H_2$ and 0.25 eV for $N_2$. According to measurements in the second positive system the vibrational temperature of the $N_2$ ground state in a $N_2$ plasma is $T_{vib} \approx 5500$ K. Another method for investigating vibrational excitation consists in analyzing the $H_2/D_2$ UV continuum radiation (transition from the binding triplet a state to the repulsive b state). First measurements of this continuum in the 200 - 300 nm wavelength range have been carried out and appear promising.

In ASDEX Upgrade the $CH/CH^+$ band ratio was recorded during methane gas injection and an intensity ratio of 2.5 was found. During $CD_4$ injection the $CD^+$ band (v′- v′′ = 0 - 0 or others) could not be detected at all. These investigations are part of the ongoing study on prompt redeposition of impurity ions in the divertor.

### 2 Chemical Erosion

The chemical erosion yield of carbon by cold H or D atoms was investigated as a function of the substrate temperature. The optical system for measuring CH/CD and $C_2$ Swan bands as well as Balmer lines and $H_2$ bands (to measure the degree of dissociation) is now equipped with a CCD camera. It therefore allows recording of time- and space-resolved spectra. The surface temperature of the investigated materials (EK98, CFC, a-C:H) was varied between 300K and 1000K (± 50K). For a flux of hydrogen atoms of about $10^{21}$ $m^{-2}s^{-1}$ the yield is of the order of one per cent. Above 800K it decreases and is a factor 2.5 lower at 1000K. For D, the yield is about three times higher than for H. Fig.2 demonstrates these results in $D_2/H_2$/He plasmas in contact with EK98 by means of the CH/CD band intensities. Investigations with a mass spectrometer confirm the relevance of the band intensities to the methane yield.

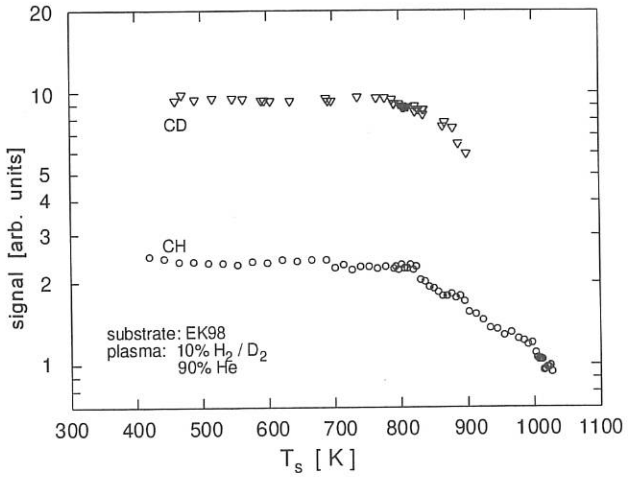


*FIG. 2: Chemical carbon erosion (EK98) by cold neutral hydrogen and deuterium atoms as a function of substrate temperature.*

Additional spectroscopic criteria are being employed for a more extensive study of carbon erosion and the formation of higher hydrocarbons. In laboratory plasmas, Swan and Mulliken bands (231.2 nm) were recorded and will be used to calibrate the $C_2$ flux derived from the Swan bands in the $C_2$ metastable system. $C_2$ Swan bands at 516.5 nm were investigated in high spectral resolution. Neutral carbon lines at 247.8 and 193 nm were recorded in laboratory plasmas by means of a VUV spectrometer and were found to be very intense. These measurements will eventually form the basis of advanced diagnostics of chemical carbon erosion.

# LEHRSTUHL FÜR EXPERIMENTALPHYSIK VI DER UNIVERSITÄT BAYREUTH

(Prof. Dr. Jürgen Küppers)

## ELEMENTARY STEPS OF CHEMICAL EROSION OF GRAPHITE BASED MATERIALS BY HYDROGEN.

(J. Biener, M. Wittmann, C. Lutterloh, K. Horn, M. Kappel)

IPP-University of Bayreuth cooperation activities concentrate on the investigation of fusion relevant plasma-wall interaction processes. Accordingly, the surface chemistry of hydrogen on possible reactor wall materials (C, C/B, metals) is the primary research topic.

Previously, we have identified two processes which govern the surface chemistry of the hydrogen atom/surface interaction:

1. Hydrogenation: H(gas) + A(ad) → AH(ad)
2. Abstraction: H(gas) + A(ad) → AH(gas)

Reaction (1) is responsible for the buildup of a hydrogen inventory in carbon based wall materials which are in contact with a plasma. Reaction (2) provides a means to exchange this inventory, e.g. H, by a different isotope, e.g. D.

The above reactions exhibit characteristics which are a consequence of the potential energy associated with the gaseous H atom. The reactions are primarily driven by the reaction energy and do not exhibit big activation barriers. And the reactions occur only in a small range restricted to the immediate vicinity of the point of impact of the atom.

In order to confirm these general attributes, the reactions of H atoms with adsorbed benzene and dimethyl-cyclohexane (DMC) was studied. These molecules are well suited as models for the C-H configurations typical for hydrogenated carbon produced by plasma/carbon-wall interaction.

As expected from the exothermicity argument, benzene hydrogenation was observed as an efficient process. The experiments confirmed the whole sequence of six hydrogenation steps, including the role of special situations present if double bonds need to be broken. The initial cross section for the $C_6H_6 + H \rightarrow C_6H_7$ reaction, about 8 $Å^2$, seems to be very big for an atom/adsorbate reaction, however, one has to consider that the delocalized $\pi$ system of the benzene molecule acts as a reaction center.

Conversely, the abstraction of H from the saturated DMC molecule is much less efficient, indicating that the reaction centers, $CH_3$ or $CH_2$ groups, have a much more localized character. Abstraction cross sections of about 1 $Å^2$ are in line with the fact that product hydrogen molecules can only be generated at a close encounter.

A model for chemical erosion of carbon under impact of H atoms was developed in which the reaction cross sections determined from studies at hydrogenated carbon and hydrocarbon molecules were used as input parameters. A further parameter was the thermal decomposition activation energy of radical centers which are generated by hydrogenation at C-C double bonds. The model predicts a flux dependence of the erosion efficiency, which is simply a consequence of the competition between hydrogenation and thermal decomposition of the radical centers.

To test the role of the exothermicity in H atom/adsorbate reactions, the interaction of H with adsorbed $(CH_3)_2CHOH$ was studied. This molecule exhibits two hydrogens which can be abstracted (neglecting the H's at the methyl groups): a H at the C, and a H at the OH group. The energy argument would favor the former as the abstraction object. It was confirmed this H gets abstracted first, followed by abstraction from the OH group, which leaves acetone, $(CH_3)_2CO$, as the final reaction product.

Studies of the interaction of H atoms with adsorbate covered metal surfaces are very scarce. Due to the fact that metals (Be, W) are still considered as first wall materials, there is a need for these investigations. Experiments in which H atom beams were directed at clean and adsorbate covered Ni(100) surfaces revealed that the above-mentioned processes, hydrogenation and abstraction, also play the key role in that type of reactions. The kinetics of atom/surface reactions were determined by monitoring gaseous reaction products simultaneously with atom exposure from a heated atom source. Reaction products remaining at the surface were collected via thermal desorption. Variation of the surface temperature allowed to discriminate between direct and surface reactions. As an example, the interaction of H atoms with oxygen covered Ni(100) surface involves the steps:

1. $H(gas) + O(ad) \rightarrow OH(ad)$
2. $H(gas) + OH(ad) \rightarrow H_2O(ad)$
3. $H_2O(ad) \rightarrow H_2O(gas)$
4. $H(gas) + OH(ad) \rightarrow H_2O(gas)$

As expected, the first step, hydrogenation of oxygen to hydroxyl, is rate determining. Its cross section of about 0.3 $Å^2$ identifies this markedly exothermic step as a direct process. Hydrogenation of hydroxyl groups to water has a cross section of 4.5 $Å^2$ and can proceed via two competing pathways. One pathway, step 2, leads to adsorbed water, which desorbes thermally activated above 180 K via step 3. Step 4 leads directly to gaseous water, even at low temperatures, 120 K, indicating that the energy released at reaction is responsible for the desorption event. Competition between steps 2 and 4 is suggested by the fact that a considerable fraction of the water molecules remain at the surface after completion of the hydrogenation reaction. Hydrogen bonding between water molecules may play a substantial role in the energy release required for the exothermic step 2.

Hydrogen atom impact induced clean-off reactions of that type are expected to be of importance for adsorbate covered metal surfaces. Further investigations are needed to study the effect of surface structure and composition on these reactions.

## Publications and Conference Reports

C. Lutterloh, J. Biener, A. Schenk, and J. Küppers: Interaction of D(H) Atoms with Physisorbed Benzene and (1,4)-dimethylcyclohexane: Hydrogenation and H Abstraction. J. Chem. Phys. **104** (1996) 2392.

M. Wittmann and J. Küppers: A Model of Hydrogen Impact Induced Chemical Erosion of Carbon based on Elementary Reaction Steps. J. Nucl. Mater. **227** (1996) 186.

C. Lutterloh, J. Biener, K. Pöhlmann, A. Schenk, and J. Küppers: Modification of the Benzene-Metal Interaction by C and H Monolayers at Pt(111) Surfaces. Surf. Sci. **352-354** (1996) 133.

J. Biener, C. Lutterloh, A. Schenk, K. Pöhlmann, and J. Küppers: Reaction of Gaseous H(D) Atoms with Physisorbed i-Propanol: Oxidation to Acetone. Surf. Sci. **365** (1996) 255.

J. Küppers: Interactions of Gaseous H Atoms with Adsorbate Covered Surfaces via Eley-Rideal Reactions Z. Phys. Chem. **197** (1996) 137.

J. Küppers: Spektroskopie an Festkörperoberflächen, in: Spektroskopie amorpher und kristalliner Festkörper, Eds. D.Haarer, H.W.Spiess, Steinkopf, Darmstadt, 1995.

J. Küppers: Reactions of Gaseous H Atoms with Adsorbates at Solid Surfaces Proc. International Symposium on Surface Chemistry, Atomic-scale Surface Science Research Center, Yonsei University, Seoul, Korea, Nov. 1996.

## Oral Presentations

C. Lutterloh, K. Pöhlmann, J. Biener and J. Küppers: Wechselwirkung einer Graphitmonolage auf Pt(111) mit thermischen H Atomen. Frühjahrstagung der Deutschen Physikalischen Gesellschaft, Regensburg, März 1996.

M. Kappel, J. Biener and J. Küppers: Chemische Erosion von HOPG mit thermischen H Atomen: eine UHV-STM/AFM Studie. Frühjahrstagung der Deutschen Physikalischen Gesellschaft, Regensburg, März 1996.

J. Küppers: Surface Reactions with H Atoms. WE-Heraeus Seminar: Hydrogen in Solids and at Solid Surfaces: Present Status and Future Trends, Ilmenau, 30.5.1996.

J. Küppers: Reactions of H Atoms with Adsorbed Molecules. Surface Science Center, Pittsburgh University, Pittsburgh, Pa., USA, 9.10.1996.

J. Küppers: Surface Chemistry of Undoped and Boron Doped a-C:H films. Dept. of Chemistry, Pohan Institute of Science and Technology, Pohan, Korea, 30.10.1996.

J. Küppers: Reactions of Gaseous H Atoms with Adsorbates at Solid Surfaces. International Symposium on Surface Chemistry, Atomic-scale Surface Science Research Center, Yonsei University, Seoul, Korea, 1.11.1996.

## Diploma Thesis:

K. Pöhlmann: Wechselwirkungen von H Atomen mit physisorbierten Kohlenwasserstoffen. Universität Bayreuth, 1996.

M. Scherl: Wechselwirkung von thermischen Wasserstoff-atomen mit adsorbiertem Sauerstoff auf Ni(100). Universität Bayreuth, 1996.

T. Zecho: Wechselwirkungen thermischer Wasserstoffatome mit einer Monolage Graphit unter katalytischem Einfluß von Pt(100). Universität Bayreuth 1996.

# INSTITUT FÜR ANGEWANDTE PHYSIK DER UNIVERSITÄT HEIDELBERG

(Prof. Dr. Klaus Hübner)

Cooperation with IPP in the fields of CX and neutron diagnostics was continued in 1996. This comprises CX and neutron measurements at W7-AS, numerical simulation of neutron transport as well as neutron diagnostics for W7-X.

## 1. DESIGN OF A DETECTOR SYSTEM FOR COLLIMATED D-D NEUTRON FLUX MEASUREMENTS ON W7-X

(T. Baloui, B. Wolle)

At a given measurement position on fusion experiments any measured neutron flux or spectrum consists of an unscattered 'direct' contribution and a scattered background which can be substantial and extends down to thermal velocities.

Our new concept is to detect moderated neutrons rather than the original 2.5 MeV neutrons. This offers the possibility to use a detector which is insensitive to the fraction of penetrating unwanted high-energetic neutrons. We are using Bonner spheres, which are neutron detectors with isotropic and in a wide energy range slowly varying response function[1]. The Bonner sphere is placed inside a compact shielding arrangement which moderates and absorbs incident neutrons from outside the line-of-sight of the collimator. Then, a dedicated moderator plate is introduced behind the collimator and a Bonner sphere is placed aside from this moderator target. The dimension of this target or moderator in direction of the neutron emission is optimized such that only for the initially high-energetic neutrons in the line-of-sight the scattering probability is approximately one. Thus, these incident neutrons are being moderated down into the energy range where the Bonner sphere is sensitive.

By using the Monte Carlo neutron transport code MCNP and a simulation of the neutron emission profile for a realistic fusion plasma the response function of the new compact detector system can be calculated. Based on these simulation calculations the properties of the detector system and the design concept can be optimized for measurements.

## 2. ERROR ANALYSIS FOR NEUTRON YIELD MEASUREMENT BY SAMPLE ACTIVATION

(G. Beikert)

Sample activation has recently become the standard technique for the absolute determination of neutron yields from fusion devices. The technique requires a measurement of the sample activation and a Monte Carlo calculation of the ratio of sample activation and neutron yield. However, even in the most recent works few attention has been paid to the error analysis of the measurement result. Specifically, the effects from simplifications in the model used for Monte Carlo calculation of the response coefficients have not yet been appropriately investigated.

In support of activation measurements carried out at W7-AS, we have performed a detailed error analysis. We have investigated the sensitivity of the Monte Carlo result on parameters of the neutron source distribution such as mean neutron energy, spectral width, Shafranov shift, neutron emission profile, and anisotropy of neutron emission. The error introduced by simplifications of the complicated W7-AS stellarator geometry has been determined by special purpose Monte Carlo calculations. Benchmark measurements at the Physikalisch-Technische Bundesanstalt have allowed us a to make a reliable estimation of the error contribution due to uncertainties in the neutron scattering cross-section libraries.

1) B. Wiegel, A. V. Alvera, and B. R. L. Siebert, Report PTB-N-21 (1994), Physikalisch-Technische Bundesanstalt Braunschweig

# LEHRSTUHL FÜR MESSTECHNIK (LMT) DER UNIVERSITÄT DES SAARLANDES

(Prof. Dr. Alexander W. Koch)

## 1. SPECKLE MEASUREMENT OF THERMAL DEFORMATION OF GRAPHITE TILES

M. Ruprecht, M. Jakobi

### 1.1 Introduction

The aim of the cooperation between the IPP and University of Saarland is to develop a suitable speckle measurement system for detecting surface changes during plasma exposure in an experimental fusion reactor. Besides the erosion caused by sputtering, the thermal deformation of the first wall is of interest.

### 1.2 Phase-shifting Speckle Interferometry

The measurement of surface changes is being performed by two different methods of speckle interferometry. The use of speckle interferometry permits measurement at nearly all kinds of surfaces. One method is to analyze an intensity interference. The other, more accurate method, is to calculate a phase pattern. The visible fringe pattern represents a contour line plot of the investigated surface. The resolution is in the range of some 1/10 µm. The two images clearly exhibit the advantages of the phase-evaluating technique. In order to measure the phase change of the reflected light caused by deformation of a random rough surface, it is necessary to take four images of each surface state. These single images are taken by an interferometer, e.g. the Michelson type. The intensity difference of the images depends on shifting of the reference surface in the interferometer in steps of a fixed phase angle. The resulting interferograms are captured by means of a CCD camera with a computer interface for image analysis. The measured intensities in the undeformed state are given by

$$I_k = I_0^1 \cdot \left[1 + \beta_1 \cdot \cos\left(\Phi_1 - (k - \tfrac{5}{2}\alpha_1)\right)\right] ,$$

where k=1,2,3,4. In the deformed state the intensities

$$I_k = I_0^2 \cdot \left[1 + \beta_2 \cdot \cos\left(\Phi_2 - (k - \tfrac{5}{2}\alpha_1)\right)\right]$$

are obtained for k=5,6,7,8. The calculation of the phase angle representing the height value of the surface can be calculated according to the simple formula

$$\Phi = \tan^{-1} \frac{I_4 - I_2 + I_5 - I_7}{I_1 - I_3 + I_8 - I_6}$$

Better results were obtained by using the Carré algorithm for the calculation of the phase.

### 1.3 Measurement on Graphite Tiles

Figure 1 shows the deformation of a graphite tile under thermal load. This sample measurement example clearly shows the ability of the phase-shifting technique to detect surface variations even on surfaces with a very low reflection index like graphite. The measurement was performed with an argon ion laser and a standard CCD camera.

*FIG. 1: Surface deformation of a graphite tile during thermal load*


[1] Berger, E., W. von der Linden, V. Dose , M. Ruprecht, A.W. Koch: A New Approach for the Evaluation of Speckle Deform. Measurements by Application of the Wavelet Transformation, Applied Optics (subm. 1996).

[2] Jakobi, M.: Aufbau und Integration eines Phase-Shifting-Moduls in einen rechnergesteuerten Oberflächenmeßplatz, Dipl. Thesis, Lehrstuhl für Meßtechn.,1996.

[3] Ruprecht, M., A. Trunzler, A.W. Koch: Anwendung von CCD-Kameras in der Oberflächenprüfung mittels Speckle-Verfahren, Proc. 97. Tagung der Deutschen Gesellschaft für angewandte Optik (DGaO), Neuchâtel/Schweiz, Mai 1996, 46.

[4] Ruprecht M.: Zweidimensionale Oberflächenprüfung mittels Speckleverfahren, Tagungsband Kolloquium „Trends in der industriellen Meßtechnik", Saarbrücken, Eds. A.W.Koch, M.Ruprecht and O.Toedter, Univ. des Saarlandes, Juni 1996, 22-28.

# INSTITUT FÜR PLASMAFORSCHUNG (IPF) DER UNIVERSITÄT STUTTGART

(Prof. Dr. U. Schumacher)

Developments, measurements and interpretations in connection with the electron cyclotron resonance (ECRH) systems and with the microwave and spectroscopy systems for the stellarator and tokamak are the basis for the close collaboration of Institute for Plasma Research (IPF) at Stuttgart University with MPI of Plasma Physics at Garching. Contributions to the ECRH system of W7-X are of increasing importance. Bulk and divertor plasma diagnostics are supported by microwave measurements and high resolution spectroscopy, respectively.

## 1. PLASMA HEATING AND MILLIMETER-WAVE DIAGNOSTICS

(H. Z o h m , L. Empacher, W. Förster, G. Gantenbein, W. Kasparek, H. Kumrić, G.A. Müller, P.G. Schüller, K. Schwörer, D. Wagner)

### 1.1 Electron cyclotron resonance heating (ECRH)

The studies on ECRH in fusion plasmas were continued. In addition to the contributions to the ECRH systems on the two fusion experiments W7-AS and ASDEX Upgrade in Garching, contributions to the design work for the ECRH system of W7-X, the new stellarator of IPP to be built in Greifswald, were made. Also, a conceptual design for an ECRH startup system on ITER was proposed.

#### *1.1.1 ECRH on W7-AS*

In 1996, two of the new 140 GHz long-pulse gyrotrons were put into operation. During commissioning of the system, the large content of high-order modes of the gyrotron beams led to breakdown and high losses in the transmission lines. The reason was an imperfect matching optics, which was designed on the basis of data supplied by the manufacturer.

With the help of a new IR-camera, and using a PVC-plate as target, the power distribution of the beams was measured and recorded digitally with high accuracy. Based on these distributions measured at several cross sections, the phase information was reconstructed numerically. An example is given in **Fig. 1.1**, where the measured power distribution at one cross section is shown together with a reconstructed beam pattern.

In a second step, a pair of phase correcting mirrors, which convert most of the power into the suitable transmission mode, was designed. The calculated profile of the second matching mirror is shown in **Fig. 1.2**.

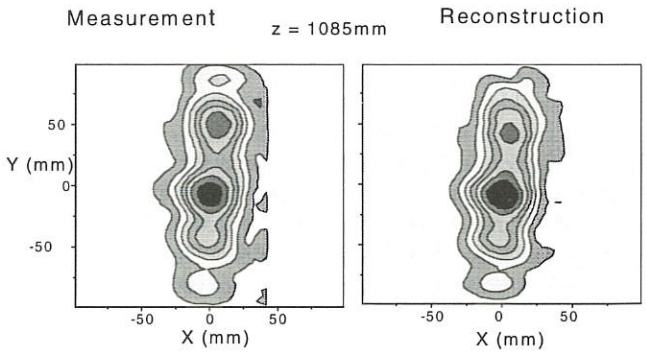


*FIG. 1.1: Comparison of a measured and a reconstructed power distribution of the gyrotron beam.*

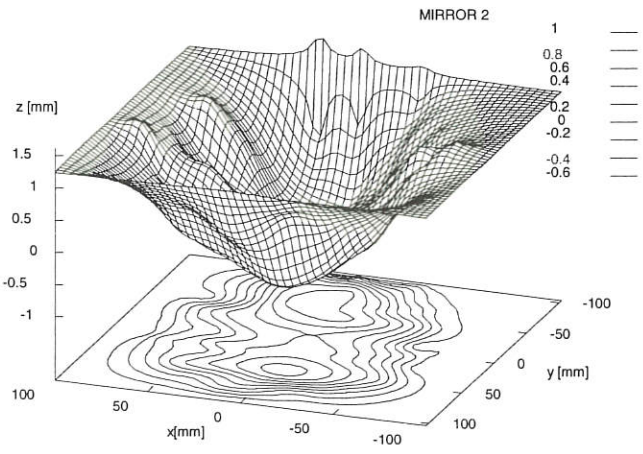


*FIG. 1.2: Calculated profile of a beam matching mirror.*

In parallel, Russian scientists from IAP Nizhny Novgorod manufactured new mirrors based on these measurements. After alignment of the mirrors both gyrotrons could be operated with long pulses (typically 2 s) at a power level of about 500 kW.

Exact measurements of the total power as function of time with the mitre bend directional couplers are still a problem, as these can only be calibrated with short pulses due to the limitations of the calorimetric loads. The long-pulse signals of these couplers are somewhat disturbed by interference with spurious modes in the corrugated lines. Improvements of this situation by increasing the mode selectivity of the couplers are under way.

### *1.1.2 ECRH system for ASDEX Upgrade*

An important aim of the ASDEX Upgrade divertor tokamak is directed towards transport studies including H-mode physics and dynamic phenomena such as stability control of the plasma. Since ECRH heating allows the power to be deposited in the plasma with well defined localization, it constitutes an optimal tool to perform such investigations. In addition, electron cyclotron current drive (ECCD) allows to influence the MHD mode activity and will be used in experiments to study the active control of these instabilities.

#### *1.1.2.1 Transmission lines*

In 1996, design and construction of the 2 MW, 140 GHz ECRH system for ASDEX Upgrade was continued. In its final stage, this system will consist of four gyrotrons with individual transmission lines which are a combination of beam waveguide and corrugated $HE_{11}$ waveguide sections (I.D. 87 mm). Along the beam path the transmission lines are equipped with two grooved mirrors which allow to adjust any polarization of the beam between linear and circular to obtain optimum accessibility to the plasma.

In first plasma experiments with a short pulse gyrotron (output power 0.5 MW, pulse length 0.5 s) the transmission line No. 2, Sector 6, was operated routinely with high stability and reliability (see ASDEX Upgrade section of this Annual Report). After conditioning of the beam line, no problems with arcing occurred.

The pulse length of the gyrotrons ordered from the Russian company GYCOM will be 2 s at 0.5 MW or, alternatively, 1 s at 0.75 MW output power. One main limitation of the pulse length is the thermal loading of the BN windows at the gyrotron and the torus ports. To reduce the power density at the torus window, the transmission line was upgraded with a special non-linear taper (I.D. 87 mm $\rightarrow$ 123 mm) which transforms the $HE_{11}$ mode into a $HE_{11}/HE_{12}$ mode mixture with a more homogeneous radial power distribution. For this diameter, a mitre bend coupler was constructed to measure forward and backward travelling power in the waveguide. In the vacuum vessel, a fixed focusing and a steerable mirror allow poloidal and toroidal scans of the microwave beam.

The first gyrotron from GYCOM (Zodiac) was installed (transmission line No. 2, Sector 6) and acceptance tests were performed with the specified parameters using a dummy load. The design and construction of special parts for this transmission line (waveguide sections, mitre bend couplers, flexible parts for compensation of thermal expansion, diagnostic equipment, focusing mirrors, motor-driven polarizers) were completed.

The design of the transmission lines No. 3 and 4 (Sector 14) up to the launching mirrors was finished. The optical components were manufactured on the basis of the expected beam parameters given by the manufacturer of the gyrotrons. An improved system for coupling the free space beam to the corrugated waveguide was developed and standard waveguide sections with I.D. 87 mm for transmission of the microwave power from the gyrotron to the torus port ($\approx$ 2×15 m), special waveguide sections and diagnostic elements were delivered to IPP. Waveguide components for I.D. 123 mm, including those which will be installed in the vacuum vessel, were manufactured.

#### *1.1.2.2 Electronic equipment for the ASDEX Upgrade ECRH system*

In 1996, the development of electronic equipment for the gyrotrons focused on sweep generators and cathode heater supplies. To prevent local overheating of the collector surface of the gyrotron, the electron beam has to be swept over a large area during the pulse. This is performed with an additional solenoid put on the collector and driven with a sawtooth current generator. Four power supplies were tested sucessfully with the Zodiac gyrotron and adapted to the special requirements of the particular solenoid. One of these power supplies was integrated in the existing control system and is routinely running with the gyrotron.

Four computer controlled cathode heater supplies were adapted to the Zodiac gyrotron. Tests of the hard- and software were performed successfully. The software was extended to allow interactive test of the fibre optic communication line and simple check and control of the power supply. Further improvements of this software, which will take into account the nonlinear characteristics of particular system components, are under way.

### *1.1.3 ECRH system for W7-X*

In cooperation with IPP Garching, and in close contact with the team planning the building, the design work for the transmission system of the ECRH facility on W7-X was continued. The conceptual design was finalized. Wherever possible, a modular design was adopted. Top and side views of the ECRH system are shown in **Fig. 1.3**.

The generator consists of 10 gyrotrons at 140 GHz (1 MW, CW, each), situated in a separate building next to the stellarator hall. Two further gyrotrons at lower frequency (e.g. 70 GHz for low-field experiments) are foreseen. The ECRH building also contains the water- and cryocooling system, part of the high-voltage supply as well as control and laboratory rooms. The transmission is achieved completely by mirrors which are mounted in a concrete duct connecting the ECRH hall to the torus hall. Near to the gyrotrons matching and polarizing mirrors are installed which allow individual conditioning of the gyroton beams. The main part of the transmission is accomplished by two multi-beam waveguides, each combining 5 beams at 140 GHz (and, optionally, an additional beam at 70 GHz) on common mirrors. Near to the stellarator, the beams are split again and guided to six ports in total equipped with steerable launchers for each beam. Movable mirrors allow to switch the beams to calorimetric loads or to a CW dummy load.

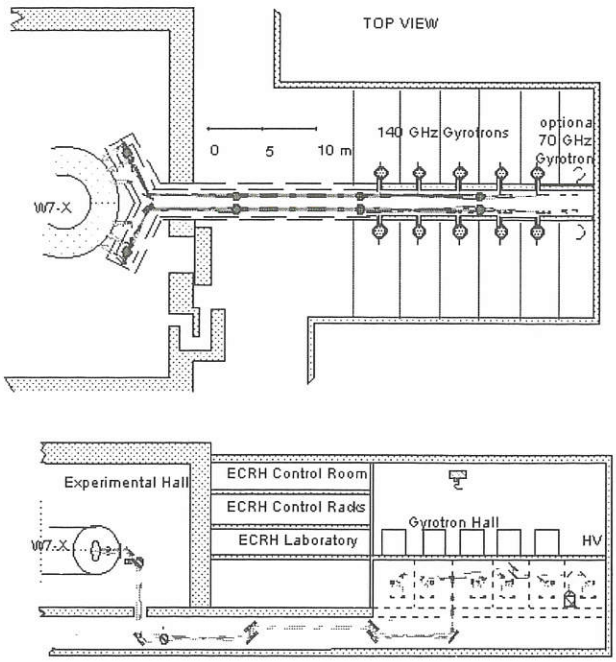


*FIG. 1.3: Top view and side view of the ECRH system planned for W7-X.*

To guarantee high efficiency of the transmission, both gaussian beam propagation and techniques of geometrical optics (to simplify alignment and to increase stability) have been used for the design. Diffraction calculations were started with the goal to optimize the surfaces of the multibeam mirrors. First results show a sufficiently high performance, i.e. large bandwidth, low mode conversion and good imaging quality for the preliminary mirror design chosen for the W7-X system. Furthermore, phase-correct multimode transmission was investigated to avoid the problem of beam pattern modifications behind the gyrotron window and in front of the torus window.

To check the alignment of the mirrors, a control system is being developed which is based on autocollimation of the beam by gratings in Littrow mount milled on the reflector surface. Design studies for the cooling of mirrors and for dummy loads were continued.

Experiments simulating a multibeam waveguide on a small scale were started the results of which will be compared with the numerical results. Additionally, a test facility for the whole transmission system is currently under construction at IPF. This installation will consist of one complete line using components of weight and size identical to those foreseen for W7-X. It will help to verify the numerical results as well as thermomechanical properties of the cooled mirrors, polarizers and loads for CW operation and to identify possible problems of stability and alignment. In a later phase, it can be used to test components prior to installation in Greifswald.

### *1.1.4 Loads for high-power microwaves*

Calorimetric and dummy loads were built for high-power microwave measurements and tests of the Russian gyrotrons at W7-AS and ASDEX Upgrade. By an improved distribution of the microwave energy in these loads the tests could be performed with full pulse lengths of the gyrotrons installed in Garching which up to now were limited to 2 s at a power of 500 kW.

From the experiments with the existing loads the conclusion was drawn that for near future gyrotrons with longer pulses and/or higher power absorbing materials with larger microwave penetration length and thus increased absorbing volume will have to be applied. Cold and hot measurements of customary light-weight firebricks with varied mixtures of alumina and silica and high porosity were performed. The results are promising owing to the fact that the energy loading capacity of these bricks can be at least tripled compared with the sand lime bricks used so far.

For quick calorimetric measurements of the microwave power at various positions of the transmission line a simple load was built which will be able to perform ballistic single pulse measurements up to 50 ms. This load will be used on ASDEX Upgrade during the next experimental period in 1997.

### *1.1.5 ITER contributions*

#### *1.1.5.1 ECR startup system*

A conceptual design of an ECR startup system for ITER was worked out. To provide outside wall limited startup over a range of central magnetic fields between 4.0 T and 5.7 T, at least two frequencies in the range of 90 GHz to 140 GHz will be required. Robust and reliable startup requires approximately 3 MW of power to be applied to the plasma in a short pulse (< 1 s).

An assessment of the present technology as well as future developments was done relevant for the ITER startup system (source, transmission, launcher) with special emphasis on the broadband characteristics of the components and tunability of gyrotrons. Additional constraints arise from the requirement of robustness (e.g. through relative motions of the system due to mechanical stresses).

Based on this assessment, two possible solutions of the system can be proposed: a separate startup system especially designed for this purpose and a version that can be integrated into the ITER ECR heating and current drive system. The startup system can be completely realised with presently available technology, but will profit from further developments, such as step-tunable gyrotrons.

## 1.2 Millimeter wave diagnostics

In addition to collective Thomson scattering described below work on reflectometry was done both on W7-AS and ASDEX Upgrade. The latter as well as contributions to the modification of the interferometer on ASDEX Upgrade can be found in the respective IPP sections of this Annual Report. Another study was concerned with the introduction of methods developed for transmission of high power millimeter waves to the problems of low power transmission in diagnostic applications.

### *1.2.1 Collective Thomson scattering on W7-AS*

The frequency spectra of thermal fluctuations of the electron density are measured via collective Thomson scattering (CTS) on W7-AS. Heating gyrotrons at 140 GHz (ECRH) are used as source of the probing radiation. The aim is to obtain the ion temperature from thermal scattering spectra and to extrapolate the results with respect to possible measurement of the energy distribution of alpha particles in fusion plasmas. In addition, the propagation of plasma waves in the frequency window of the ion spectra are studied, e.g. at the lower-hybrid frequency and at ion cyclotron harmonics. These investigations are carried out in collaboration with the Institute for Applied Physics (IAP), Nizhny Novgorod.

In 1996, successful scattering experiments were performed using a newly developed antenna (90° geometry), to achieve a spatial resolution of $\leq 4$ cm and a very low stray radiation level of $< 2\times10^{-7}$. At low plasma densities, a sharp resonance line around 200 MHz is seen, the assignment of which requires further investigation. At the full magnetic field of 2.4 T (second harmonic ECE ), it is possible to measure scattering spectra down to the thermal level, provided the resonance zone lies outside the line-of-sight of the receiver antenna.

At present, high temperatures above 1 keV cannot be achieved with heating methods compatible with the CTS diagnostic, since the other gyrotrons used for heating operate at the same frequency. Owing to the low ion temperatures achieved up to now, the scattering spectra remain relatively narrow (200 MHz). The central part cannot be measured due to the notch-filter used to suppress the gyrotron line. Thus, absolute calibration of the spectra cannot be obtained. Fit procedures for the measured spectra yield values for the ion temperature in reasonable agreement with independent diagnostic methods.

It should be noted, that in certain operating regimes of the W7-AS stellarator, the scattering spectra are clearly nonthermal. This is believed to be a problem central to the future application of this diagnostic method to measure routinely ion temperatures in fusion experiments.

### *1.2.2 Design studies for ITER millimeter-wave diagnostics*

The application of oversized corrugated $HE_{11}$ waveguides in low power diagnostic systems on ITER was studied. Up to now such waveguides (corrugation depth $\lambda/4$) are mainly used in ECRH high power transmission lines at a fixed frequency. They offer the advantages of low ohmic losses, inherent filtering of spurious modes and the possibility of using compact mitre bends. For highly oversized corrugated waveguides, these characteristics also hold for a wider frequency range.

In existing diagnostic systems using smooth oversized waveguides, ohmic losses and mode conversion in mitre bends are a serious problem for precise amplitude and phase measurements, e.g. for ECE or reflectometry. Here, oversized corrugated waveguides are very good candidates for low loss broadband operation with a smooth transmission characteristic both in amplitude and phase. In such waveguides high order spurious modes can be suppressed by including gaps into the transmission line which cause only very low losses for the main $HE_{11}$ mode, but have a high efficiency in filtering the higher

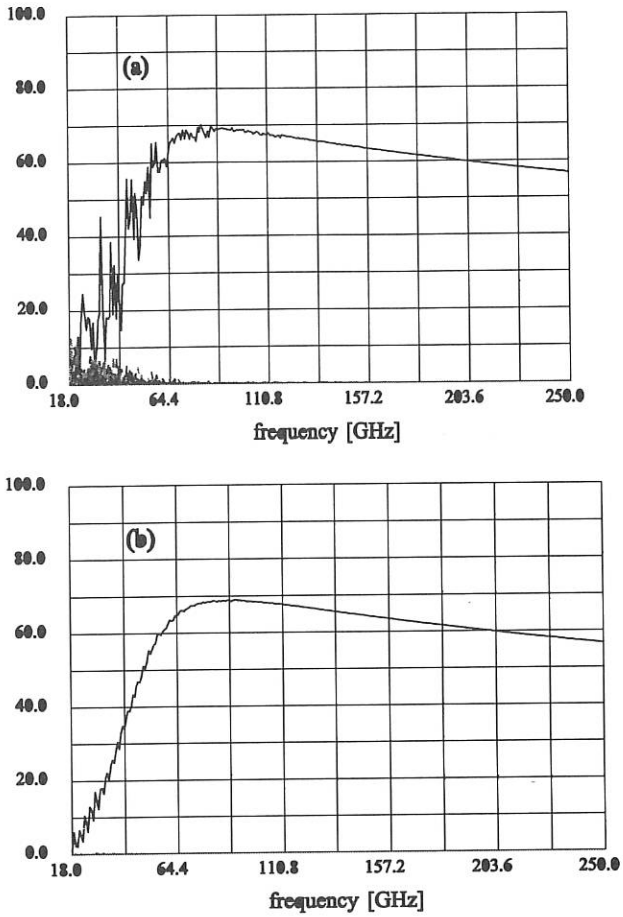


*FIG. 1.4: Estimated transmitted power through a complete transmission line of 100 m length (I.D. = 63.mm) including 10 mitre bends (a) and 10 mitre bends and 10 gaps for mode filtering (b).*

order modes. Calculations for a 100 m long transmission line including 10 mitre bends demonstrate this behaviour. The results are shown in **Fig. 1.4**.

The transmission line without gaps (**Fig. 1.4a**) shows a rather erratic amplitude and phase characteristic, whereas for the line including 10 gaps (**Fig. 1.4b**) the frequency characteristic is almost smooth without noticeable additional damping. Due to the almost linear polarization of the $HE_{11}$ mode, broadband Brewster angle windows can be applied. Two combined Brewster angle windows serve as an effective polarization splitter.

Experiments were performed with a highly oversized corrugated waveguide system. A transmission line with a length of 13.9 m including 3 mitre bends with plane mirrors was built. An effective overall length of approximately 27.8 m was obtained by inserting a plane mirror at the end of the transmission line and analyzing the reflected signal. The inner diameter of the corrugated waveguide is 87 mm. In order to achieve a frequency independent excitation of the $HE_{11}$ waveguide mode a quasi-optical coupler, mainly consisting of mirrors in a confocal arrangement, was used. A partially reflecting dielectric plate used as a beam splitter together with an additional focusing mirror allows the detection of the reflected signal from the transmission line. The numerically evaluated bandwidth of the $HE_{11}$ mode using a scattering matrix code could be confirmed experimentally. Broadband excitation of the $HE_{11}$ mode was

demonstrated over the frequency range 45-170 GHz. Broadband Brewster angle windows were included in the transmission line. The introduction of gaps into the transmission line lead to a smoothening of the frequency characteristic, both, in amplitude and phase and also resulted in a reduced sensitivity to misalignments.

## 2. PLASMA EDGE DIAGNOSTICS

(U. Schumacher, M. Bross, G. Dodel, J. Gafert, K. Hirsch, H. Jentschke, E. Holzhauer, M. Niethammer[1)], H. Schmidt, G. Volk[2)], M. Wiese[3)])

[1)] until July 12, 1996
[2)] until April 14, 1996
[3)] until August 31, 1996

### 2.1 Erosion measurements

The interaction of materials (C/C-SiC, SiC and graphite) with plasmas is investigated within the framework of the "Sonderforschungsbereich" SFB 259. Besides spectroscopic investigations of spectral line radiation of Si I and C I from erosion products the molecular bands of CN are of most interest. Additional measurements of the relatively weak, but important absorption of Si I resonance lines (at wavelengths of 251 nm and 288 nm) yield absorption coefficients of up to about $k = 50\ m^{-1}$ near to the target which is exposed to the plasma jet. This corresponds to an average Si concentration of $4.2\times10^{18}\ m^{-3}$ in front of the C/C-SiC target, assuming that the radial absorption profile is approximately equal to the measured emission profile. Altering the plasma parameters only slightly towards lower temperatures (-15%) and consequently lower electron densities changes the measured absorption by a factor of 2. This result is in agreement with data from modelling the erosion of the C/C-SiC target plates, under the assumption of $T_e >> T_{gas} = T_{rot}$ and assuming the erosion products being released with surface temperatures of about 1900 K from the hot target. Moreover, it agrees with the gravimetric losses of the target. Corresponding results were obtained from spectroscopic measurements of the absolute line intensities of the Si I triplet 251 nm using a simplified collisional radiative model for silicon and taking into account that these resonance lines are partially optically thick at these population densities.

The Si I emission lines, which are slightly modified by self absorption, show very strong intensity changes for small variations of the parameters of the eroding plasma. This plasma in front of the target has two successive influences on the emission of erosion products: firstly, it effects the surface via plasma wall interaction which releases thermally ($T_e \leq 1$ eV, no sputtering) the Si and C atoms as erosion products from reactions next to the surface (molecules between the air-like plasma and target material), and, secondly, the plasma excites these eroded molecules and atoms which subsequently leads to the measured emission spectra. Therefore this method is extremely sensitive to variations of the plasma parameters, especially of the temperatures $T_e$ and $T_{gas}$ due to the exponential dependence of the emission on the temperature. Measurements show that changes of the electron temperature of only about 15% (including the respective change of the electron density) produce a variation of the emission line intensity of Si I by a factor of 4. It is intended to verify this change of plasma parameters by varying the plasma arc current between 1400 A and 1650 A (corresponding power range 150 kW to 186 kW) and by evaluating the rotational temperature of $N_2^+$ molecules and the electron temperature and density measured by laser Thomson scattering.

The sensitive probing method (Si I emission measurements) may also be applied when C/C-SiC compound material with fibres of high thermal conductivity (>100 W/Km) will be tested at W7-AS as a candidate for blanket material in fusion devices.

### 2.2 High resolution spectroscopy in the divertor of ASDEX Upgrade

Detailed analysis of the ion dynamics in the divertor of ASDEX Upgrade is necessary for optimizing the divertor with respect to plasma power dispersion, impurity retention and gas control. For the investigation of ion dynamics high resolution emission spectroscopy is applied. While from the measured Doppler shift of the emission line the flow velocity of the respective ions can be deduced, the Doppler broadening contains information on the thermal (Maxwellian) energy distribution and thus allows to determine the ion temperature.

For these ion temperature and ion velocity distribution measurements an optical spectroscopic system with high spectral, temporal, and spatial resolution was brought into operation. Integrated along 74 lines of sight, which are differently oriented with respect to the magnetic field lines, emission spectra of atoms and ions were highly resolved by an Echelle spectrometer and recorded by a 2D-CCD camera. The lines of sight are realized by the installation of three versatile fiberoptical systems. One of these, consisting of 30 lines of sight, is aligned in a poloidal plane, which is mainly perpendicular to the magnetic field, while the other two, consisting of 22 lines of sight each, are oriented roughly toroidally, one tangentially to the magnetic field direction and the other opposite to it. These toroidally oriented systems are designed in a special matrix-like pattern in order to achieve spatial resolution for ion dynamics investigations in the outer as well as in the inner divertor fan.

The highly resolved emission spectra measured have to be evaluated taking into account the Zeeman effect, the instrumental function of the spectroscopic system and the Doppler broadening. In addition, the spatial distribution of the plasma parameters and hence the ion emissivity along the line of sight has to be considered by an appropriate weighting procedure.

The spectra of He I as an example for neutrals do not show a Doppler shift in accordance with the fact that neutral helium has an isotropic velocity distribution. The magnetic field strength deduced from the Zeeman splitting is identical for observation parallel and perpendicular to the magnetic field lines and agrees well with the magnetic probe measurements.

However, spectral lines of impurity ions show pronounced Doppler shifts for toroidal observation conditions. The shifts are opposite for parallel and antiparallel toroidal observation and result in (chord averaged) flow velocities of the order of $1.1\times10^4$ m/s. From the Doppler width of the ion spectra the ion temperature is determined to be in the range of 5 eV for $C^{2+}$ ions. An example for an ASDEX Upgrade discharge starting in L-mode

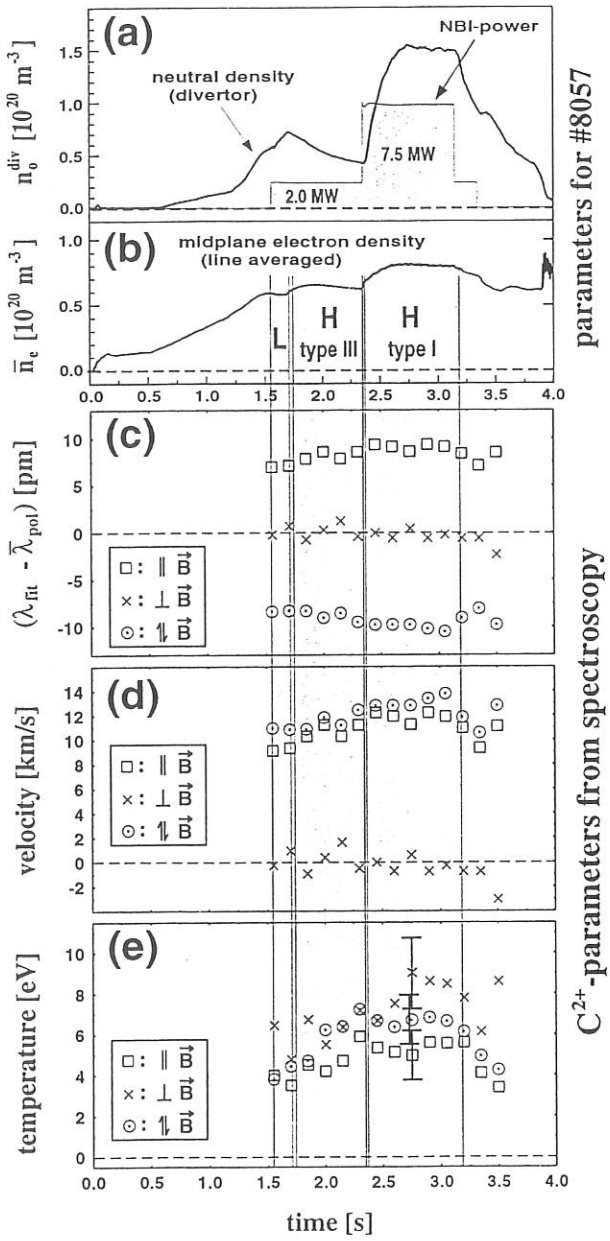


*FIG. 2.1:* *Time behaviour of some plasma parameters for the ASDEX Upgrade discharge number 8057 as the neutral density in the divertor and the neutral beam injection power (a) and the line averaged electron density (b) in comparison to the results of the high resolution spectroscopy on $C^{2+}$ ions : the Doppler shifts (c), the resulting flow velocities towards the outer divertor plates (d) and the temperatures of the $C^{2+}$ ions (e).*

and turning to two ELMy H-mode phases is given in **Fig. 2.1**. It demonstrates the opposite Doppler shifts for the toroidal observations compared to the unshifted lines for the poloidal direction, such that the flow velocities turn out to be of equal amount.

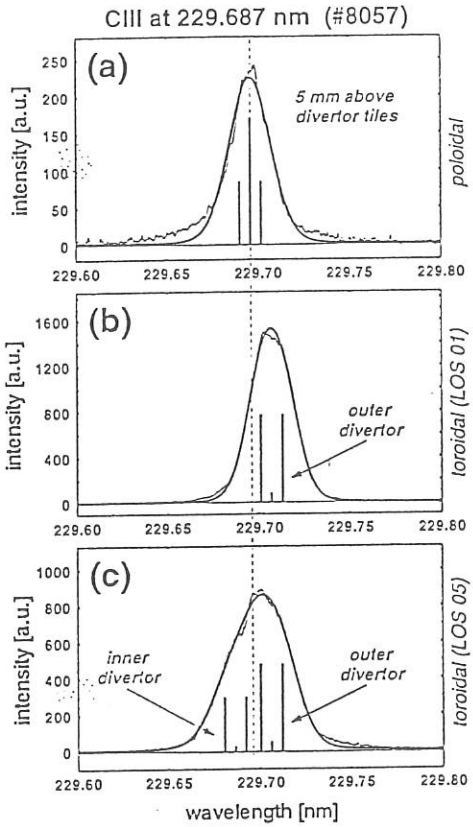


*FIG. 2.2:* *Comparison of spectra of $C^{2+}$ ions for the CIII singlet line taken for poloidal (a) and two toroidal chords, one of them collecting only $C^{2+}$ emission from the outer divertor (b), and one of them collecting $C^{2+}$ emission from both the outer and the inner divertor (c), which allows flow velocity determination in the inner as well as in the outer divertor region.*

Moreover, the ion temperatures deduced from these spectra are found to be equal within the error margin. These experimentally determined values agree within about 50% with the results of calculations using the B2-EIRENE code.

The matrix-like arrangement of the toroidal lines of sight allows to determine flow velocities and ion temperatures in the outer as well as in the inner divertor region. Therefore, comparison of the ion dynamics in both divertor areas is possible. As an example **Fig. 2.2** depicts the spectra of a poloidal line of sight which shows no Doppler shift (a), in comparison with spectra from the toroidal lines of sight for the outer divertor alone (b) and for the superposition of contributions from the outer and inner divertor (c). From numerical fits to the measured spectra the flow velocities are found to be of equal amount ($1.1 \times 10^4$ m/s) for the inner as well as for the outer divertor, the speeds being always directed towards the divertor plates.

These results demonstrate that high resolution spectroscopy is well suited to analyse the ion dynamics in the ASDEX Upgrade divertor. On the basis of the experience acquired substantial improvements in the layout and arrangement of the line of sight system for the new divertor II in ASDEX Upgrade were performed.

# PUBLICATIONS, CONFERENCE REPORTS, DOCTORAL THESES, DIPLOMA THESES, LABORATORY REPORTS, AND SEMINAR TALKS

## PUBLICATIONS

Denisov, G.G., D.A. Lukovnikov, W. Kasparek, and D. Wagner:
"On the resonant scattering at guide dielectric windows".
Int. J. Infrared and Millimeter Waves **17** (1996) 933-945.

Neu, R., K. Asmussen, G. Fussmann, P. Geltenbort, G. Janeschitz, K. Krieger, K. Schönmann, G. Schramm, and U. Schumacher:
" A monitor for the carbon and oxygen impurities in the ASDEX Upgrade tokamak".
Rev. Sci. Instrum. **67** (1996) 1829 - 1833.

Schumacher, U., K. Asmussen, G. Fussmann, T. Liebsch, and R. Neu:
"Investigations on calibration sources for soft x-ray plasma spectroscopy and impurity monitors".
Rev. Sci. Instrum. **67** (1996) 2826 - 2830.

Wagner, D., M. Thumm, W. Kasparek, G.A. Müller, and O. Braz:
"Prediction of TE-, TM-, and hybrid-mode transmission losses in gaps of oversized waveguides using a scattering matrix code".
Int. J. Infrared and Millimeter Waves **17** (1996) 1071-1081.

## CONFERENCE REPORTS

Frühjahrstagung der Deutschen Physikalischen Gesellschaft, Fachausschuß Plasmaphysik, Rostock, Germany,
March 18 - 21, 1996

Hirsch, K., G. Bauer, M. Bross, H. Jentschke, G. Volk, and M. Wiese:
"Spektroskopie und Laser-Thomson-Streuung am Plasmawindkanal".
Verhandl. DPG (VI) **31** (1996) P8.33.

8th Joint Russian-German Meeting on ECRH and Gyrotrons, Nizhny Novgorod and Moscow, Russia,
June 10 - 15, 1996

Empacher, L., W. Förster, G. Gantenbein, W. Kasparek, H. Kumric, G.A. Müller, P.G. Schüller, K. Schwörer, U. Schumacher, and D. Wagner:
"Recent activities on transmission of high-power microwaves".

Empacher, L., G. Gantenbein, W. Kasparek, V. Erckmann, and H.P. Laqua:
"Calculations and experiments for transformation of gyrotron output beams".

23rd EPS Conference on Controlled Fusion and Plasma Physics, Kiev, Ukraine, June 24 - 28, 1996

Gafert, J., M. Niethammer, K. Behringer, D.Coster, C. Dorn, K. Hirsch, S. de Pena-Hempel, U. Schumacher, NI Group, and ASDEX Upgrade Team:
"Investigation of ion dynamic in the ASDEX Upgrade divertor by high resolution spectroscopy: first results of ion drift velocities".
Proc. ECA **20C** (1996).

Holzhauer, E., J. Baldzuhn, S. Fiedler, J. Geiger, M. Hirsch, R. Jaenicke, Ch. Konrad, A . Weller, W7-AS Team, and NBI Team:
"Edge turbulence and transport barrier associated with the H-mode in the W7-AS stellarator".
Proc. ECA **20C** (1996).

21st International Conference on Infrared and Millimeter Waves, Berlin, Germany, July 14 - 19, 1996

Thumm, M., A. Möbius, and D. Wagner:
"Advanced quasi-optical mode converter for a step-tunable 118-162 GHz, 1 MW gyrotron".
Proc., M. von Ortenberg, H.U. Mueller, Edts., ISBN 3-00-000800-4.

Thumm, M., C.T. Iatrou, A. Möbius, and D. Wagner:
"Built-in mode converters for coaxial gyrotrons".
Proc., M. von Ortenberg, H.U. Mueller, Edts., ISBN 3-00-000800-4.

Wagner, D., W. Kasparek, and G. Gantenbein:
"Broadband characteristics of $HE_{11}$-transmission lines" .
Proc., M. von Ortenberg, H.U. Mueller, Edts., ISBN 3-00-000800-4 (1996).

3rd Int. Workshop on Strong Microwaves in Plasmas, Nizhny Novgorod, Russia, August 7 - 14, 1996

Suvorov, E.V., A.B. Burov, Y.A. Dryagin, S.E. Filchenkov, A.A. Fraiman, L.V. Lubyako, D.A. Ryndyk, N.K. Skalyga, O.B. Smolyakova, V. Erckmann, H. Laqua, T. Geist, M. Kick, E. Holzhauer, W. Kasparek, ECRH Group, W7-AS Team, and CX-Diagnostic Team:
"Lower hybrid turbulence excited by a transverse ion beam in a magnetized plasma".

9th Symposium on Fusion Technology (SOFT), Lisbon, Portugal, September 16 - 20, 1996

Empacher, L., W. Förster, G. Gantenbein, W. Kasparek, H. Kumric, G. A. Müller, P.G. Schüller, K. Schwörer, U. Schumacher, D. Wagner, V. Erckmann, T. Geist, and H. Laqua:
"Conceptual design of the 140 GHz/10MW cw ECRH system for the stellarator W7-X".
To be published in Fusion Technology.

Empacher, L., G. Gantenbein, W. Kasparek, V. Erckmann, and H. Laqua:
"Matching a nongaussian gyrotron beam to a transmission line using thermographic measurements".

16th IAEA Fusion Energy Conference, Montreal, Canada, October 7 - 11, 1996

Hirsch, M., E. Holzhauer, J. Baldzuhn, B. Branas, S. Fiedler, J. Geiger, T. Geist, P. Grigull, H. J..Hartfuß, J. Hofmann, R. Jaenicke, C. Konrad, J. Koponen, G. Kuhner, W. Pernreiter, A. Weller, F. Wagner, H. Wobig, and the W7-AS Team:
"Edge transport barrier and edge turbulence during H-mode operation in the W7-AS stellarator".

## DOCTORAL THESIS

Wagner, D.:
"Analyse und Entwurf von korrugierten überdimensionierten Hochleistungsmillimeterwellensystemen".

## DIPLOMA THESIS

Wiese, M.:
"Laser-Thomson-Streuung am Plasmawindkanal".

## SEMINAR TALKS

Hirsch, K.:
"Spektroskopie und Laser-Thomson-Streuung am Plasmawindkanal".
Institut für Niedertemperatur-Plasmaphysik e.V., Greifswald, March 3, 1996

Schumacher, U.:
"Probleme und Perspektiven der Plasma-Wand-Wechselwirkung".
Physikalisches Kolloquium der Universität Basel,
January 8, 1996

Schumacher, U.:
"Astrophysik und Plasmaforschung".
Studium Generale Astronomie, Stuttgart, January 10, 1996

Schumacher, U.:
"Die Kernfusion - Lösung aller Energieprobleme?"
AK Ringvorlesung, Universität Stuttgart, January 31, 1996.

# How to reach
# Max-Planck-Institut für Plasmaphysik (IPP)

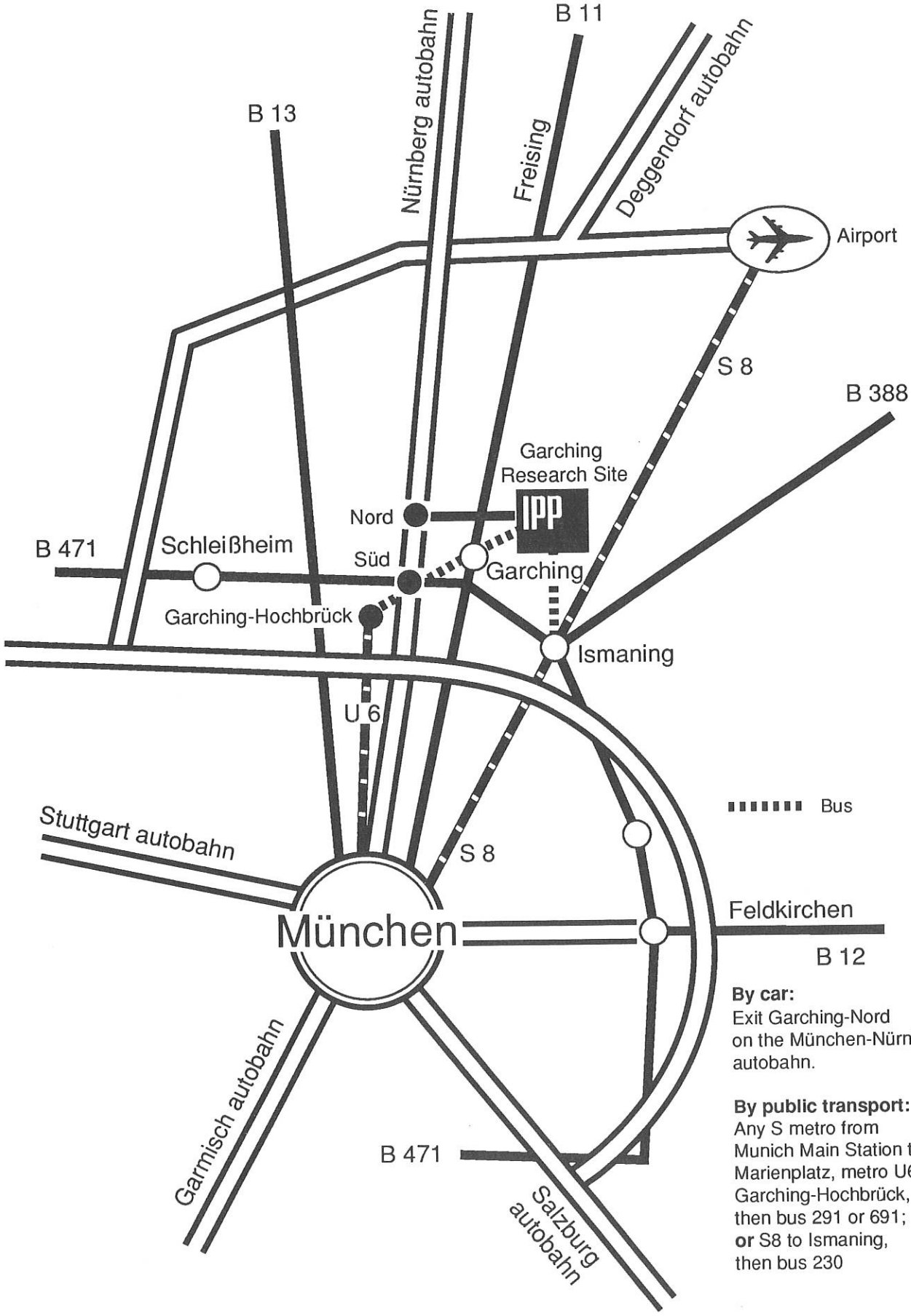


**By car:**
Exit Garching-Nord
on the München-Nürnberg
autobahn.

**By public transport:**
Any S metro from
Munich Main Station to
Marienplatz, metro U6 to
Garching-Hochbrück,
then bus 291 or 691;
**or** S8 to Ismaning,
then bus 230

ANNUAL REPORT 1996

Max-Planck-Institut für Plasmaphysik (IPP) • 85748 Garching bei München
Telephone (0 89) 32 99-01 • Telefax (0 89) 32 99-22 00

Printing: Oldenbourg Graphische Betriebe GmbH, Kirchheim

Printed in Germany
ISSN 0179-9347

This work was performed under the terms of the agreement between Max-Planck-Institut für Plasmaphysik and the European Atomic Energy Community to conduct joint research in the field of plasma physics.

IPP

Max-Planck-Institut
für Plasmaphysik